Actin network architecture and dynamics studied in vitro and in vivo

Majdouline Abou-Ghali

Sorbonne Université

Ecole doctorale Complexité Du Vivant
Laboratoire Physico Chimie Curie — Institut Curie

Actin network architecture and dynamics studied *in vitro* and *in vivo*

Par Majdouline Abou-Ghali
Thèse de doctorat de Biologie

Dirigée par Julie Plastino

Présentée et soutenue publiquement le 29 mars 2019

Devant un jury composé de :

Rajaa	Boujemaa-Paterski	Maitre de conférence	Rapportrice
Olivia	Du Roure	Directrice de recherche	Examinatrice
Antoine	Jégou	Chargé de recherche	Examinateur
Christophe	Le Clainche	Directeur de recherche	Rapporteur
Julie	Plastino	Directrice de recherche	Directrice de thèse
François	Robin	Chargé de recherche	Examinateur

Acknowledgements

« Wear gratitude like a cloak and it will feed every corner of your life" Rumi

The acknowledgments are the last thing I write of this manuscript, yet the most difficult in my sense. Many people have accompanied me throughout this journey and showed their support at different level, for that I will eternally be grateful.

The biggest share of thanks goes to Julie. Thank you believing in me; you literally taught me everything! Thank you for being honest, considerate, helpful whenever needed, and always present. Thank you for the long hours spent in your office or in a hallway discussing all kinds of topics from science to life issues, politics, travel, books, vampires, and latest songs. Thank you for being a real mentor who taught me how to be rigorous, attentive to details, and use all my senses when doing an experiment, for pushing me when needed, comforting and helping me come up with solutions when things were not working (aka: most of the time!), and teaching me when to stop trying. Most importantly, thank you for showing me that science is not only about experiments, it is as well about human interaction. A good PI is the one who listens, understands, and exchange as a human not only as a boss, you were the best PI in that sense. Thank you for treating me like an equal rather than an inferior, for giving me so many chances to travel with you and be part of some really cool experiences. Thank you for everything.

For the Sykes/Plastino team: Cécile, Julie, Karine, Clement, Rodrigo, Antoine, Camille, Darine, Hanane, Patricia, Wylie, Valentina, Fabrice, I enjoyed every single moment we shared. You all taught me things beyond my expectations. It was truly enriching to interact with each one of you on a scientific and personal level. Cécile: Thank you for running (along with Julie) the team like you do, always making us feel part of a big family and always standing up for us. For giving me advice on how to overcome my fear of public speaking, for being an example on how to fight for what we want and never give up on what we believe in. For all the dinners/lunches you organized for us where we talked about everything but science. Karine: the best thing that happened to this team. Thank you for being a fun person with a big smile on your face and spreading positive energy. For always reminding me that things will be okay. Clément: Thank you for being the cool researcher that never failed to give advice on experiments along with music, for spreading your good vibes and love for broccoli.

Many thanks go to my major support system on a daily basis: Antoine, Camille, Darine, and Hanane, you guys have been the best team mates anyone could ever ask for. Thank you for all the laughter we have shared and all the fun times we've had around a coffee doing crosswords, a meal, or in a park enjoying the sun. You are the most awesome "normal guys" on the planet. Darine: thank you for being you, my twin as I feel a lot of the times. The best thing that happened during my PhD was you joining the lab.

To the CAMs: Antoine and Camille, you are more than amazing. I really don't know how my life would have been without you! Thank you for helping me with the experiments when things were not working, for sharing your proteins and your advice, for making Pyrene and Bradford much more fun than what they really are, for teaming up to aliquot because it is never fun to aliquot alone! For being there every step of the way supporting me even through my writing phase, for sharing amazing music and singing out loud in the lab or in the office. For bringing joy to my life and making me want to come to the lab everyday even when it was difficult to find motivation. We have an indescribable bond that I never had with anyone, so thank you for being true friends and not only my lab mates. Special thanks to Camille, for all the late evening talks about literally everything! Thank you for being my sunshine.

UMR168 has a unique atmosphere, my thanks go to everyone who made this place feel like home. Thank you Laura for being a friend I could count on who shared my route since the beginning of this journey, the tough times and the good times. For being such a good listener who had my back, was ready to punch someone for me, always found the right words and never failed to make me laugh. Fahima for being the soul of the lab who never failed to make me laugh and showed me real friendship. Thank you for always reminding me to stay real and humble, and of course for taking me out of my shell and making me interact with everyone in the lab. Thank you Joanna and Julien (along with Camille) for being the most adorable office mates who shared joy, food, and music and made us the coolest office in the building. Aude for always being the positive, heartwarming person who gives me faith in humanity. Michael for being the sweetest, most caring person I have ever met. Thanh for being kind, caring, funny, for making me discover so many restaurants and always amazing me with how much you can eat! Thank you Brigitte and Laurence for the administrative help and the big smile you always had.

Thank you for my beloved market group: Remy, John, Alicia, Gert-jan, and occasional Efe. You made my saturday something to look forward to! Thank you for the lovely company between tomatoes and avocadoes, for the amazing brunches (mainly John's), and for proving that scientists can be so much fun in a market or at a lake. Special thanks goes to Remy, thank you for turning into a best friend even though I was not looking for one! For always finding a positive side to any situation, for cooking for me while discussing existential issues or jut random places to visit on weekends.

For my Palestinian friends, Maha, Layla, Maria, Haneen, Bisan, Majd S, Fawzya, Baraa, Ramz, Majd and Muna, thank you for being supportive all the way and always showing interest in what I do. For always being there and surrounding me even though we are miles apart. For my friends in Jordan, Ahmad R, Ahmad B, Moha, Rasha, and Yousef, for always taking the time even if it is a few hours to catch up and fill me with positive energy. Maha, my best friend, thank you for believing in me even when I did not believe in myself! For running with me around Ramallah to send my master application on time, for supporting me during my PhD as long as my life moments, the good and the bad ones. For keeping my feet on the ground and telling me to get real whenever I complain too much. Thank you for being my person.

Last but not least, the biggest thank you for my family (mum, dad, Ismail): you are my rock. Along with my grandma and uncle, you all believed in me all along and pushed me towards my goals and dreams, and gave me all possible means to achieve them, thank you for always making me a priority. Thank you for absorbing all my stress, taking all my complains and sometimes breakdowns. You are a true blessing and I will never be thankful enough for having you. True unconditional love means helping the other spread their wings and fly even if it means flying away. Thank you for helping me spread my wings instead of cutting them, and lifting me higher and higher each time I fell.

Table of Contents

Preface

Cell shape changes are crucial for different cell processes such as cell motility, cell division, wound healing and organ development, and are involved in pathologies like cancer. Cell shape is established by the cellular cytoskeleton. A key component of the cytoskeleton is actin, a biopolymer which interacts with many partners providing a high diversity of structures. Much effort has been made to understand actin cytoskeleton assembly and dynamics, however, the way it orchestrates some processes is still only partly understood. During my PhD I studied actin network architecture and dynamics both *in vitro* and *in vivo*. For the *in vitro* part, I used a reconstituted system of actin assembly to examine the role of the barbed end elongation enhancement protein, Ena/VASP. Specifically, I probed the interplay between Ena/VASP, the Arp2/3 complex (an actin polymerization nucleator) and capping protein in defining actin network polarity and growth. I also used this reconstituted system to test the effect of photoswitchable Arp2/3 complex inhibitors, in view to developing these reagents for general use in the actin field. These molecules, based on CK-666, can isomerize upon illumination with different wavelengths of light, giving active and inactive forms. Such drugs would give excellent spatial and temporal control over Arp2/3 complex activity in biological settings. For the *in vivo* part of my PhD studies, I investigated actin cytoskeleton architecture and rheological properties of the cytoplasm of the early embryo of evolutionarily distant nematode species. The goal of this project was to understand how all nematode embryos undergo a similar first asymmetric cell division, despite differences in cell shape changes and cytoplasmic characteristics.

This thesis is organized into six chapters: the first two are introductory chapters, the third is a methods chapter to accompany results chapters four and five, and chapter six is another results chapter including methods pertaining to that chapter. A co-authored review article and two co-authored research articles are in the annexes. In the first chapter cell shape changes and more particularly cell motility is introduced, as well as the main actin structures used for motility. Actin, actin-binding proteins and their roles, polymerization activating proteins and the biomimetic approach are also described. The second chapter focuses on Ena/VASP protein, and reviews its role in different processes including cell motility, as well as what is known about its mode of action. The fourth, fifth and sixth chapters detail the results I obtained during my PhD. The fourth chapter shows the effect of Ena/VASP on actin network polarity establishment. The second chapter details the assessment of a series of putative photoswitchable Arp2/3 complex inhibitors and the validation of one of them. The sixth and last chapter is an exploratory chapter focused on actin network architecture *in vivo* in nematode embryos. The results of the first study will make up my first author publication which will be submitted soon. The other two studies are being continued by co-workers in the lab.

Chapter 1: General Introduction to Cell Motility and the Actin Cytoskeleton

1.1 Cell shape changes and motility

Cell shape changes are required for essential life processes, such as cell division, and cell motility during wound healing and morphogenesis. However, cell motility is also key for the development of certain pathologies, most notably cancer metastasis.

How cells move is a complicated process, which can occur by different mechanisms, triggered by many different factors and involving the action of numerous proteins. One of the main motility modes involves the formation of a protrusion in the direction of movement with adhesions to the substrate and de-adhesion at the back of the cell, called mesenchymal cell motility (Figure 1.1). This process depends on the assembly of the biopolymer actin, and on the contractile activity of the molecular motor myosin.

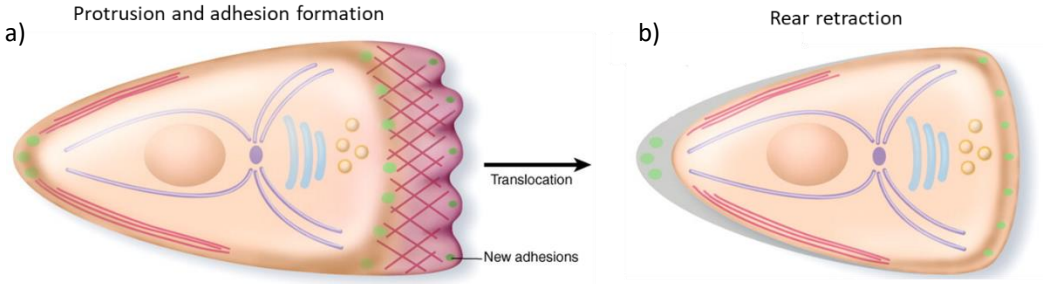

Figure 1.1 – Schematic representation of mesenchymal cell motility. a) In order to migrate, cells form protrusions in the direction of migration, and adhesions are formed to stabilize these protrusions. b) Adhesion disassembly and contraction at the rear of the cell lead to rear retraction. From (Ridley et al., 2003).

1.2 Structures of cell motility

Cells tightly control actin dynamics to produce structures that are unique both morphologically and functionally. Lamellipodia and filopodia are actin-dependent membrane protrusions at the front of the cell implicated in mesenchymal cell motility, while the cell cortex is the layer of actin interspersed with molecular motors, juxtaposed with the membrane at the back of the moving cell (Figure 1.2). Ventral stress fibers are contractile actin bundles that end in focal adhesions (Blanchoin et al., 2014).

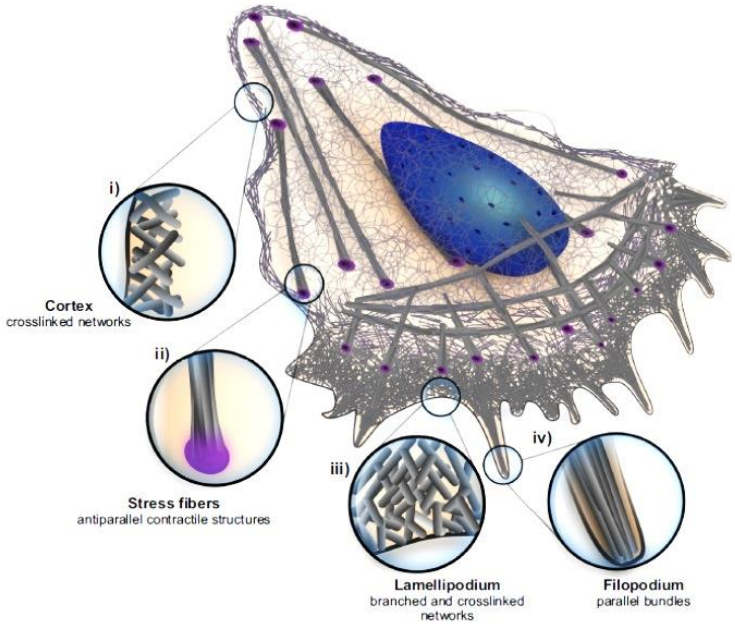

Figure 1.2 – Schematic representation of different actin architectures in a moving cell: the lamellipodium, filopodia, the cell cortex and stress fibers ending in focal adhesions (purple). The different structures are circled and zoomed in to see the details of the actin networks. From (Blanchoin et al., 2014).

1.2.1 Lamellipodia

The lamellipodium is a quasi-two-dimensional cellular protrusion with a thickness of about 200 nm and a depth of several microns, which forms at the front of a migrating cell, tens of microns wide (Small and Resch, 2005). The lamellipodium is considered as the major force driving mesenchymal cell migration in both 2D and 3D environments since it is what adheres to the substrate and pulls the cell forward (Caswell and Zech, 2018; Petrie et al., 2012).

This protrusion is filled with a dense actin network mainly composed of branched filaments entangled with each other (Svitkina and Borisy, 1999) (Figure 1.3). For many years this structure was at the center of a debate as to whether it was really branched biochemically via a branching protein, the Arp2/3 complex, which will be described in the next section, or just appeared branched due to the crisscrossing of straight filaments (Urban et al., 2010). The debate was settled not long ago when a study reanalyzed electron microscopy data originally used to justify the crisscross/unbranched theory, and demonstrated the presence of branched actin filaments (Yang and Svitkina, 2011).

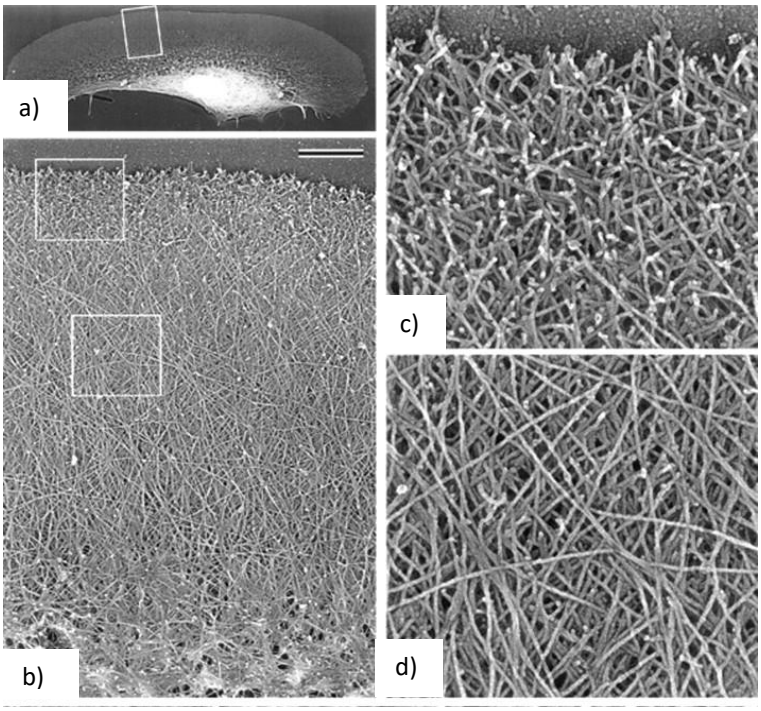

Figure 1.3 – Electron microscopy images of the lamellipodium of a moving keratocyte. a) View of the actin network in the lamellipodia. b) The network is denser at the cell front (zoomed image shown in c) compared to the back (zoomed image shown in d). Scale bar is 1 μm. From (Svitkina et al., 1997).

1.2.2 Filopodia

Filopodia are finger-like protrusions of bundled unbranched actin filaments at the front of the cell, several micrometers long and around 200 nm wide (Mogilner and Rubinstein, 2005) (Figure 1.4). Filopodia are widely considered as a sensor of the environment of the cell as they extend and retract with a speed of several μm per minute (Mallavarapu and Mitchison, 1999). These structures form the first focal adhesions with the matrix and contacts between neighboring cells (Jacquemet et al., 2015).

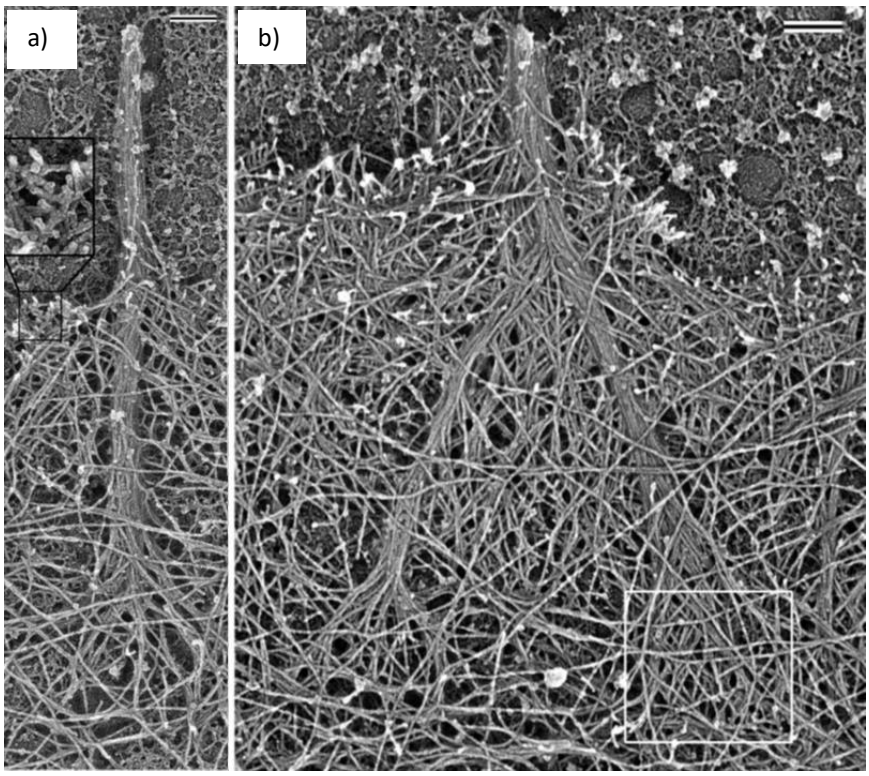

Figure 1.4 - Electron microscopy images of filopodia. a) A filopodium contains a tight bundle of actin filaments that separates at its root and becomes a part of the surrounding network. Filaments in the roots are long compared with the branching network of the adjacent lamellipodium (inset). b) Recently fused filopodium consists of two sub-bundles. Scale bar is 0.2 µm. From (Svitkina et al., 2003).

1.2.3 The cell cortex

The cell cortex is a layer of actin underneath the plasma membrane at the back of the cell that is highly contractile due to the presence of myosin motors. It is several hundred nanometers thick and is composed of a mixture of bundled and branched filaments, resulting in a mesh size in the range of 100 nm (Chugh and Paluch, 2018; Salbreux et al., 2012).

1.2.4 Stress fibers and focal adhesions

In the migrating cell, there are three types of stress fibers: ventral stress fibers, transverse arcs, and dorsal stress fibers (Hotulainen and Lappalainen, 2006) (Figure 1.5). Ventral stress fibers are the most important for cell motility. They are made of bundled unbranched actin filaments, containing myosin motors along with various cross-linking proteins (Naumanen et al., 2008; Pellegrin and Mellor, 2007; Tojkander et al., 2011). Ventral stress fibers terminate in focal adhesions, sites of cell-substrate adhesion rich in actin and actin binding proteins (Ciobanasu et al., 2013). Ventral stress fibers play an important role in cellular

contractility and provide force for cell adhesion and migration (Ridley and Hall, 1992; Tojkander et al., 2012).

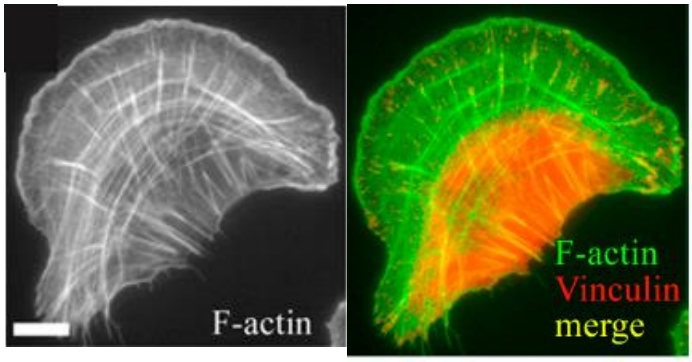

Figure 1.5 – Stress fibers in osteosarcoma cells. Actin is fluorescently labeled and ventral stress fibers are observed as bright bundles terminating in focal adhesions as visualized with vinculin staining. Bar, 10 µm. From (Hotulainen and Lappalainen, 2006).

1.3 Actin polymerization and dynamics

1.3.1 Actin in general

To grasp how cells produce the actin structures described in the previous sections, we need to understand basic actin dynamics. Actin is one of the most abundant proteins in the cell: it represents around 5% of the total protein in eukaryotic cells and it can attain 10% in specific types of cells like muscle and microvilli-containing cells (Lodish et al., 2000). In addition to giving cells their shape and driving movement, actin is essential for other processes like muscle contraction, cell division and gene transcription, which explains its abundance in many cell types.

Actin is highly conserved through evolution (Gunning et al., 2015; Hanukoglu et al., 1983). From small unicellular eukaryotes, like yeast, that have only one gene encoding for actin to humans that have six genes encoding for several isoforms, few changes have occurred in the actin amino acid sequence (> 94% identity) (Vedula and Kashina, 2018). The six mammalian isoforms of actin are arranged into three families: α-actin (skeletal, smooth muscle and cardiac) is found in muscle cells, as is γ-smooth muscle actin, while β-actin and γ-actin are found in non-muscle cells (Vedula and Kashina, 2018). Although very similar in amino acid sequence and overall 3D fold, actin isoforms play divergent roles in cells for reasons that are not entirely clear (Vedula and Kashina, 2018).

1.3.2 From monomers to filaments

Monomeric actin (G-actin)

Actin in its monomeric form is a globular protein of 42 kDa, roughly 5.5 nm in diameter (Kabsch et al., 1985). Composed of one polypeptide chain of 375 amino acids, actin is slightly acidic. Actin has two domains separated by a cleft, which binds two cofactors: a nucleotide, which can be either ATP or ADP, and a cation which can be either calcium (Ca^{+2}) or magnesium (Mg^{+2}) (Figure 1.6). Each of the two domains contain two other subdomains: subdomains I, II, III and IV. The accessible side of subdomains I and III are called the barbed end of the monomer, and the accessible side of subdomains II and IV are called the pointed end of the monomer (Figure 1.6). Monomers can assemble spontaneously to form filaments when placed in presence of nucleotide and a divalent cation at physiological salt concentrations. The dynamic of formation and the stability of filaments is highly dependent on the nucleotide state and the identity of the metal ion (Carlier, 1991).

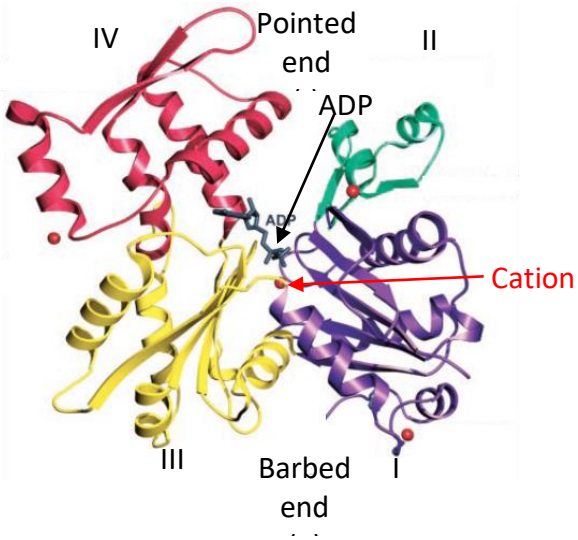

Figure 1.6 – Representation of an ADP-bound actin monomer. Cation is in red and a molecule of ADP is in black. The monomer is composed of 2 lobes separated by a cavity that contains the ATP and the cation. Each lobe has two domains. Adapted from (Otterbein et al., 2001).

Filamentous actin (F-actin)

F-actin is a linear chain of actin monomers arranged in a helix composed of two parallel protofilaments with a step size of 37 nm (Figure 1.7). Actin monomers assemble in a polar manner with barbed faces pointing in the same direction. As a result, the two ends of the filament expose different sides of the ultimate actin monomer, thus giving the filament a polarity with a pointed and a barbed monomer face exposed at each end. In fact, the nomenclature is inspired by the appearance of the filaments by transmission electron

microscope. When actin filaments are decorated with a fragment of the myosin II protein, myosin organizes into an arrowhead-type structure (Figure 1.7).

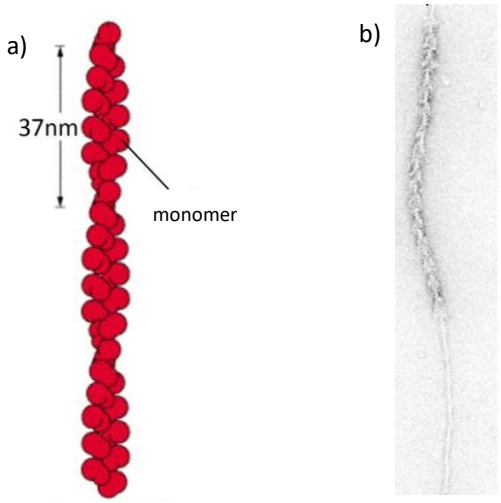

Figure 1.7 – a) Schematic representation of an actin double helix, adapted from (Alberts et al., 2002). b) Electron microscopy image of an actin filament decorated with myosin II heads. From (Pollard and Borisy, 2003).

1.3.3 Assembly dynamics

Actin polymerization has been reproduced *in vitro* using purified actin in order to study kinetics independently from other proteins. These studies revealed that the polymerization of actin takes place in three phases: the nucleation phase, the elongation phase, and the stationary phase (Figure 1.8).

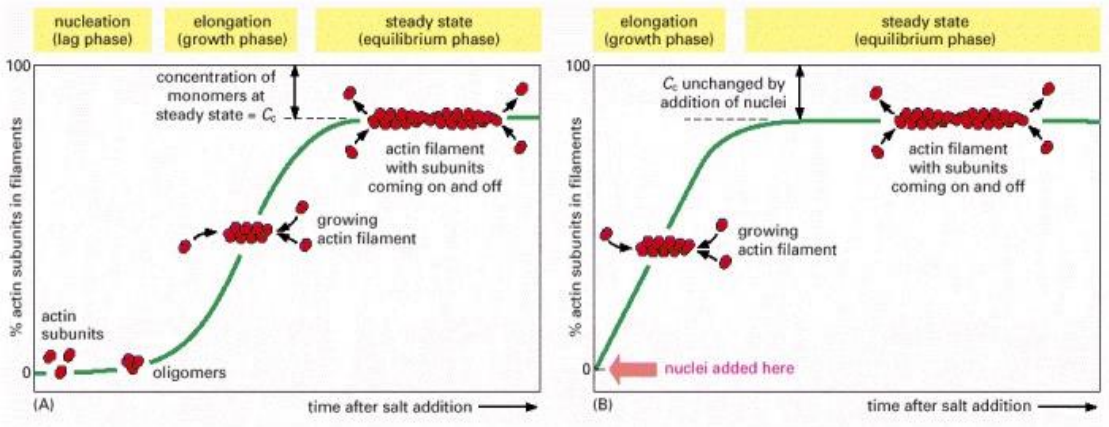

Figure 1.8 - Actin polymerization over time. Polymerization is triggered by the addition of salt to the monomer solution. The formation of seeds or nuclei, composed of three actin monomers, is a kinetically slow step that can be avoided if the polymerization is started from a solution that already contains oligomers. Elongation from trimers to make filaments is rapid and occurs at both ends of the filament until the steady state is reached. From (Alberts et al., 2002).

The nucleation phase is the stable association of three actin monomers to form an oligomer (also known as a nucleus or a seed), and this is the rate limiting step of the polymerization process. This oligomer serves as a nucleus to which monomers of actin will bind, rapidly elongating the filament. This phase can be bypassed by adding preformed actin oligomers in the solution.

The elongation phase describes the addition of G-actin monomers to the oligomers, elongating the filament. Monomer association and dissociation rates at the two ends of the filament are not equal (see next subsection "Critical concentration and ATP hydrolysis"), and the elongation of the pointed and barbed ends are thus described by different equations where $k_{on,b}$ and $k_{off,b}$ pertain to monomer association and dissociation rate constants, respectively, at the barbed end, and $k_{on,p}$ and $k_{off,p}$ pertain to the same constants at the pointed end. C is the concentration of monomeric actin.

$$Growth\ barbed\ end\text{:}\ \frac{dn_b}{dt} = k_{on,b} * C - k_{off,b}$$

$$Growth\ pointed\ end\text{:}\ \frac{dn_p}{dt} = k_{on,p} * C - k_{off,p}$$

These equations indicate that elongation of the barbed and pointed ends is the difference between assembly, which depends on the instantaneous actin monomer concentration, and disassembly, which is constant. At high actin monomer concentration at the beginning of the elongation phase, actin filaments elongate from both ends more rapidly than monomers dissociate. Over time the actin monomer pool becomes depleted, and at the "critical concentration" where $C_{c,\,b} = k_{off,\,b} / k_{on,\,b}$ for the barbed end and $C_{c,\,p} = k_{off,\,p} / k_{on,p}$ for the pointed end, the ends stop elongating. In other words, the critical concentration is the monomer concentration at which association and dissociation are equal.

The stationary phase. Once the critical concentration is reached, the concentration of F-actin plateaus and the net growth of the filament is zero. In ADP actin this is a true equilibrium, where monomers continue to dissociate from both ends, transiently increasing the actin monomer concentration and allowing repolymerization. However, the presence of ATP monomers coupled with ATP hydrolysis in the filament produces a situation where the critical concentration of the barbed end is lower than that of the pointed end. In this case the barbed end will grow concomitant with shrinking of the pointed end, and filaments will turnover with no net change in the quantity of F-actin. This occurs with consumption of ATP, and is therefore a steady state not an equilibrium (Figure 1.8). This phenomenon, called "treadmilling", was first illustrated by polymerization experiments with radioactively labelled G-actin (Wegner, 1976), and has been confirmed more recently by TIRF microscopy imaging of dynamic actin filaments (Fujiwara et al., 2002).

Critical concentration and ATP hydrolysis

As mentioned, the presence of ATP in the polymerization assay changes the rate constants of monomer association and dissociation at both the barbed and pointed ends, and creates critical concentration differentials (Figure 1.9). Putting numbers to it, the critical concentration in ATP actin for the barbed end it is 0.12 µM, and for the pointed end 0.62 µM, whereas in ADP-actin, both ends have critical concentrations of 0.5 µM. The rate constants used to calculate these critical concentrations were originally measured by electron microscopy of elongating filaments, fixed at different time points (Pollard, 1986). In the past 20 years, new techniques to study unfixed filaments, such as TIRF microscopy, have confirmed these pioneering studies (Kuhn and Pollard, 2005). Overall the barbed end of the filament is more dynamic than the pointed end: the rate constants are higher for both polymerization and depolymerization (Figure 1.9). The nucleotide state of the monomer also alters association and dissociation constants. In particular ATP-actin dissociates from the barbed end of a filament slower than ADP-actin, but both of them dissociate slowly at the pointed end (Pollard, 1986). Although ADP-actin and even non-nucleotide bound actin can polymerize and assemble into filaments (De La Cruz et al., 2000), the polymerization rate of ATP-actin is much higher.

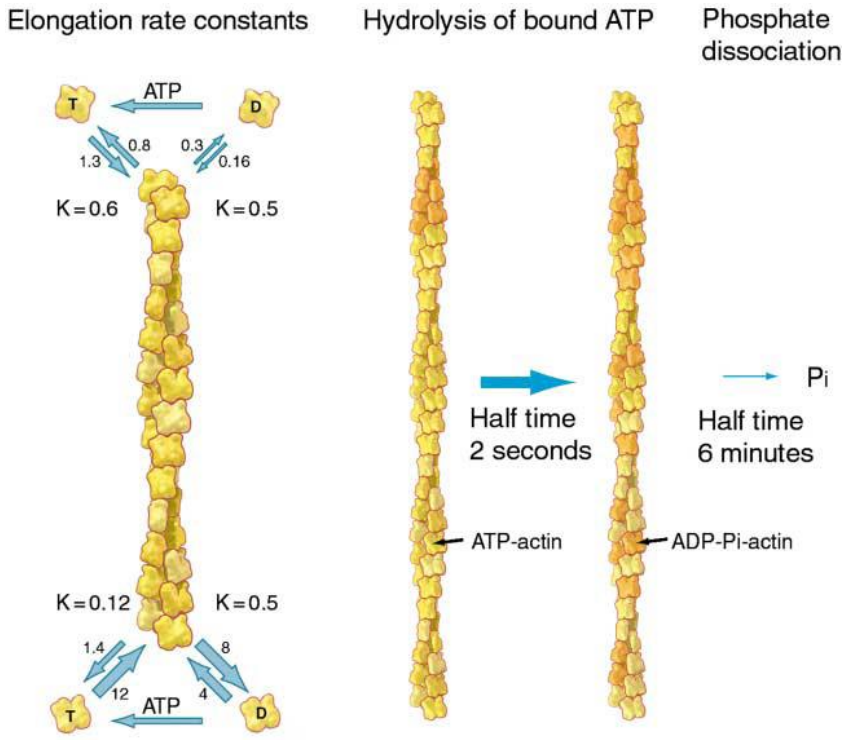

Figure 1.9 – Actin filament dynamics. Left: On rate constants ($\mu M^{-1}s^{-1}$), off rate constants (s^{-1}) and critical concentrations (K, expressed in µM) in ATP and ADP actin at the barbed end (bottom) and pointed end (top). Middle and right: the time needed to hydrolyze ATP into ADP- Pi in an actin filament, and the time needed for phosphate to dissociate. From (Pollard and Borisy, 2003).

Once in the filament, actin acts as an ATPase, hydrolyzing ATP to ADP and phosphate (Figure 1.9). This hydrolysis happens as filaments age, and triggers filament disassembly. ATP hydrolysis is a fast process, with a half-time of about 2 seconds (Blanchoin and Pollard, 2002), and irreversible (Carlier et al., 1988). ADP-P_i is a long-lasting intermediate as phosphate dissociation is slow (half-time of about 350 seconds) (Carlier and Pantaloni, 1986). If an actin monomer is followed over time, first it will incorporate into the barbed end of a filament in its ATP form, then ATP will be hydrolyzed to ADP-P_i, and after a while, phosphate will be released, allowing monomer to dissociate from the filament at the pointed end.

From these *in vitro* studies of pure actin dynamics, if we assume that the cell is at steady state, motility is determined by the dissociation at the pointed end to replenish the actin monomer pool, so approximately 18 events per minute in ADP-actin. With each monomer addition contributing about 2.5 nm to filament length (5.5 diameter, but staggered because of the helix), cell speeds of 0.05 μm/min would be expected (Pollard and Borisy, 2003). This number is much slower than actual cells like keratocytes, which can move at 10 μm/min. On the other hand, actin monomer concentrations in some highly motile cells are on the order of hundreds of μM (Pollard et al., 2000). Given barbed end elongation dynamics, one could expect, before steady state establishment, protrusion speeds of hundreds of μm/min. This is also never observed. The main explanation for such inconsistencies between *in vitro* estimations and *in vivo* observations is the activity of regulatory proteins.

1.4 Actin polymerization regulatory proteins

Actin regulatory proteins play key roles in the control of actin polymerization dynamics by directly binding either monomeric or filamentous actin and influencing the stability, nucleation, network formation and depolymerization of F-actin, or controlling monomer sequestering and delivery to barbed ends (Goley and Welch, 2006). There are hundreds of actin binding proteins that generate a vast panel of diverse structures that are essential for cellular functions (Figure 1.10)

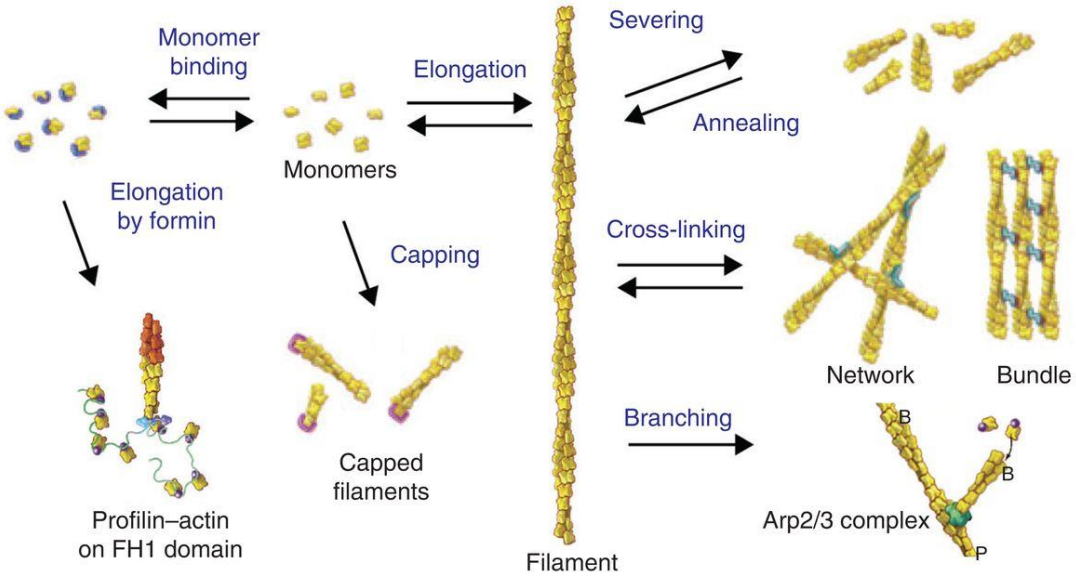

Figure 1.10 – Overview of different actin binding protein families and their functions. Schematic illustrating monomer binding, filament severing, capping by capping protein, elongation, branching by Arp2/3 complex, cross-linking and bundling. From (Pollard, 2016).

1.4.1 G-actin binding proteins

In cells, the concentration of G-actin in the cytosol can be a thousand-fold more than the critical concentration of barbed ends in ATP-actin *in vitro*, depending on cell type (Pollard et al., 2000). This pool of actin is kept in monomeric form by monomer-binding proteins that are capable of binding globular actin and changing its interaction with filament ends and/or sequestering it and preventing it from polymerizing (Skruber et al., 2018).

Profilin is a 14 kDa protein that binds monomeric actin, stimulating the exchange of ADP for ATP on actin monomers by increasing the rate of nucleotide dissociation by a 1000 fold (Goldschmidt-Clermont et al., 1991). Profilin also inhibits spontaneous nucleation in solution. In some cell types, it is sufficient to sequester all the free monomers in the cell (Kaiser et al., 1999). Profilin can also bind proline-rich domains of certain proteins that are partners of actin, like Ena/VASP proteins and formins (discussed later in the manuscript). Profilin complexes with actin by binding to the barbed face of the monomer leaving the side containing the nucleotide binding site free (Plastino and Blanchoin, 2018). Consequently, profilin favors polymerization at the barbed end of a filament and inhibits pointed end assembly. By the same mechanism profilin prevents formation of the actin trimer thus shutting down spontaneous nucleation of actin filaments.

Thymosin-β4 is the most abundant actin sequestering protein in mammals. It is a 43 amino acid (~5 kDa) protein that forms a 1:1 complex with G-actin, and competes with profilin

for binding (Pollard et al., 2000). Thymosin-β4 inhibits actin nucleation, but unlike profilin, also inhibits polymerization and the exchange of nucleotide on monomers (Goldschmidt-Clermont et al., 1992; Xue et al., 2014) . Since its affinity for ATP-actin is 50 to 100 times higher than its affinity for ADP-actin (Carlier et al., 1993; Jean et al., 1994), nucleotide exchange presumably occurs before thymosin-β4 binds to recycling actin monomers (Plastino and Blanchoin, 2018).

1.4.2 F-actin regulating proteins

Just as monomeric actin dynamics is tightly controlled by actin-binding proteins, so F-actin-binding proteins modulate the dynamics and growth of filaments. One of the most important of these is **capping protein,** a heterodimer of structurally similar α- and β-subunits that bind with high affinity to the barbed end of actin filaments (Kd 0.1- 1 nM) and prevent their polymerization (Schafer et al., 1996). Capping is virtually irreversible with barbed ends remaining capped for a long time (half-time for dissociation is 30 minutes). Capping proteins thus limit the number of growing barbed ends and regulate filament length, generating short filaments more suitable for producing force to protrude the membrane during cell movement. (Iwasa and Mullins, 2007) (Kawska et al., 2012).

ADF/cofilin or actin depolymerizing factor, is a 15 kDa protein that interacts with both actin monomers and filaments (Blanchoin and Pollard, 1998). Bound to actin monomers, ADF/cofilin inhibits nucleotide exchange (Nishida, 1985), but profilin can overcome this inhibition (Blanchoin and Pollard, 1998). ADF/cofilin binds the side of actin filaments, preferentially to ADP-actin rather than ATP-actin or ADP-P_i actin (Cao et al., 2006). ADF/cofilin changes the structure and the mechanical properties of filaments (Blanchoin and Pollard, 1999; McCullough et al., 2011; McGough et al., 1997). Due to the differential in mechanical properties, a filament partially decorated with ADF/cofilin is severed at the boundary between naked and decorated parts of the filament (Suarez et al., 2011). Recently, it was shown that Aip1, a small actin-interacting protein, cooperates with ADF/cofilin to induce severing of fully decorated actin filaments, the situation *in vivo* where ADF/cofilin concentrations can be high (Nadkarni and Brieher, 2014). Along with fragmenting the filament, binding of ADF/cofilin near barbed ends induces the dissociation of capping protein and blocks monomer addition while allowing dissociation, leading to filament depolymerization (Tanaka et al., 2018; Wioland et al., 2017).

1.4.3 Cross-linkers of actin networks

Physical connections between actin filaments are induced by cross-linkers, resulting in a variety of different kinds of networks (Figure 1.11). To name the main cross-linkers, fascin, α-actinin and fimbrin are actin filament bundlers. Fascin tightly links parallel actin filaments to form polar bundles important for filopodia (Svitkina et al., 2003; Vignjevic et al., 2006), fimbrin is similar, but makes a looser bundle, while α-actinin can crosslink both parallel and anti-parallel filaments into loose bundles (Revenu et al., 2004; Stevenson et al., 2012). Filamin cross-links

disordered actin filaments into orthogonal arrays and spectrin binds several actin filaments at once, forming loose actin networks.

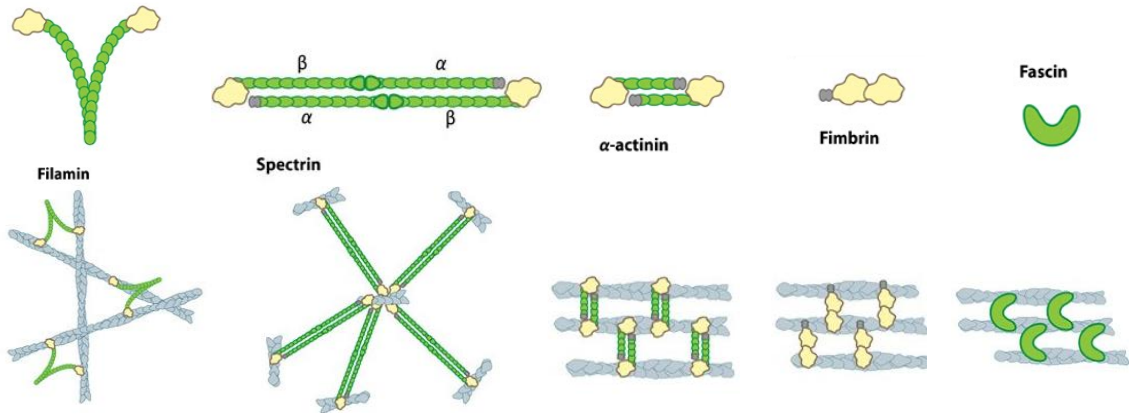

Figure 1.11 - Some actin cross-linking proteins and the network structures they form. Yellow represents actin binding domains, green the rest of the protein and actin filaments are shown in grey. Barbed and pointed ends are visible. Adapted from https://www.mechanobio.info/.

1.4.4 Molecular motors

The family of myosin motors contains about 25 different classes of proteins. Myosins use energy resulting from ATP hydrolysis to generate forces. Each attachment/hydrolysis cycle is coupled with a conformational change of the myosin heads that translates to the movement of the myosin motor along the filament when the catalytic cycle of the heads of the myosin dimer are coordinated. Myosins sense the polarity of actin filaments and move directionally.

One member of this family is non-muscle myosin II present in the cortex of cells and essential for cell motility. Myosin II assembles into small, bipolar mini filaments of 10 to 30 myosins arranged in an anti-parallel manner. The heads at the mini filament extremities bind to anti-parallel oriented actin filaments and pull them together. Filaments slide past each other, giving a contraction of the network (Aguilar-Cuenca et al., 2014; Levayer and Lecuit, 2012; Vicente-Manzanares et al., 2009).

1.4.5 Actin nucleating proteins

In vivo, the spontaneous formation of actin filaments from monomers is suppressed due to the activity of profilin and thymosin-β4, as described in previous sections. Instead in cells filaments are nucleated by specific proteins leading to the formation of different kinds of actin networks.

Formins are a homodimeric family of proteins that have a formin homology 2 (FH2) domain capable of interacting with barbed ends of actin filaments and an FH1 domain that

interacts with profilin and recruits profilin-bound actin monomers (Goode and Eck, 2007). Formins not only nucleate the formation of new filaments (Pruyne et al., 2002), but they subsequently track the barbed end of the polymerizing filament through their FH2 domain, while accelerating elongation by adding monomers to the barbed end using their FH1 domain in a processive fashion (Pring et al., 2003; Romero et al., 2004; Watanabe et al., 1997). Due to the interaction of its FH2 domain with barbed ends, formin protects them from capping protein, and is thus known as a leaky capper (Harris et al., 2004). Formins have been shown to be implicated in the formation and maintenance of filopodia (Schirenbeck et al., 2005) and also lamellipodia (Block et al., 2012).

The Arp2/3 complex

The Actin Related Protein complex, or Arp2/3 complex, is composed of 7 subunits of which the subunits Arp2 and Arp3 show 45% identity to actin (Machesky et al., 1994). To efficiently nucleate new filament formation, the Arp2/3 complex must be activated by the WASP/WAVE/Scar family of proteins (next section), and also requires the presence of a pre-existing filament (Machesky et al., 1999). Activated Arp2/3 complex binds laterally to the side of a pre-existing actin filament and nucleates another filament to which it stays bound at its pointed end, creating a branch at 70° (Blanchoin et al., 2000; Machesky et al., 1999; Mullins et al., 1998; Rouiller et al., 2008) (Figure 1.12). The new barbed end grows until capped, generating force and movement such as for lamellipodial extension (Pollard and Borisy, 2003; Svitkina et al., 2003). In mammals, there exist Arp2/3 complexes with different properties, and this affects actin filament nucleation and dynamics (Abella et al., 2016).

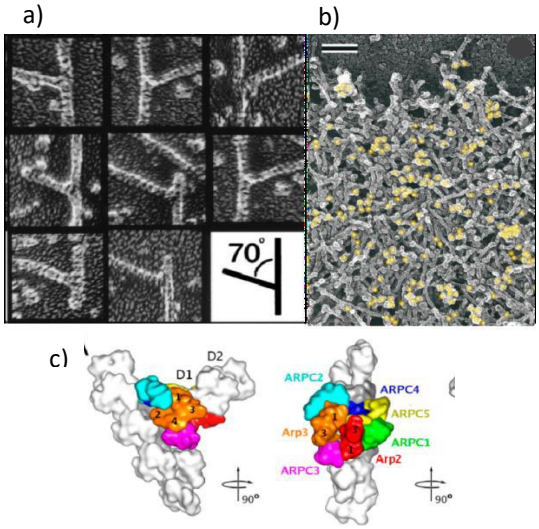

Figure 1.12 - The Arp2/3 complex creates branches. a) Electron microscopy images of branches occurring at a 70° angle via the Arp2/3 complex. b) Electron microscopy image of the lamellipodium, gold beads coupled with antibodies decorate the Arp2/3 complex, scale bar 10 µm. c) Model of the structure of branches formed by the Arp2/3 complex. a) and b) adapted from (Mullins et al., 1998) and c) from (Rouiller et al., 2008).

1.4.6 Activators of actin polymerization

Activators of the Arp2/3 complex are also called nucleation promoting factors (NPFs). NPFs are numerous and diverse, but they all have in common a highly conserved carboxy-terminal domain, VCA (also called WA), which is the domain that binds and activates the Arp2/3 complex (Higgs and Pollard, 1999). The VCA domain consists of the V portion, which is a WH2 domain that binds monomeric actin, the C portion or cofilin homology sequence, and an acidic portion (A) that binds the Arp2/3 complex and promotes a conformational change to stimulate its nucleating activity (Espinoza-Sanchez et al., 2018; Higgs et al., 1999; Marchand et al., 2001; Symons et al., 1996). N-terminal to the VCA domain, NPFs contain a proline rich domain (PRD) that binds profilin-actin and delivers profilin-actin to adjacent growing barbed ends and/or to the WH2 domain (Bieling et al., 2018). The N-terminal part of NPFs have a role in the interaction with Rho family GTPases and lipids.

The first NPF identified as an activator of Arp2/3 complex was the ActA protein, from *Listeria* (next section). ActA contains a VCA-like domain and a proline-rich domain, but these domains are organized differently: the VCA domain makes up the N-terminus of the protein (Skoble et al., 2000). The most important mammalian NPFs are WASP (Wiskott- Aldrich syndrome protein), and Scar (Suppressor of cyclic AMP repressor), similar to WAVE (WASP-family verprolin-homologous protein), which will be described in the following (Machesky and Insall, 1998; Machesky et al., 1999).

WASP and N-WASP family

WASP is expressed in hematopoietic cells and contains several domains at its N-terminus that regulate its activity: a WASP homology domain (WH1), a basic region and a GTPase binding domain (GBD). WASP in its basal state is in a folded inactive conformation, autoinhibited by binding of the GBD to the VCA domain, preventing the interaction with and activation of Arp2/3 complex (Kim et al., 2000; Symons et al., 1996). This autoinhibition is released by the binding of Cdc42 to the GBD (Symons et al., 1996). The PRD of WASP has been shown to interact with Ena/VASP proteins (Chapter 2) (Castellano et al., 2001).

N-WASP, or Neural WASP, is a ubiquitous protein present in a variety of cells (Miki et al., 1996). Highly similar to WASP, the particularity of N-WASP is its slightly modified VCA domain that contains two verprolin homology domains (VVCA) (Miki et al., 1996; Yamaguchi et al., 2000). The double V domain was originally thought to be at the origin of N-WASP's increased Arp2/3 complex activating capacity as compared to WASP, but this was later shown to be incorrect, and to instead be due to the increased acidity of the A domain of N-WASP as compared to WASP (Zalevsky et al., 2001). Like WASP, N-WASP is autoinhibited via the interaction of the GBD and VCA domains. This inhibition is relieved differently that WASP: binding of either Cdc42 or phosphatidyl-inositol (4,5)- bisphosphate (PIP_2) is sufficient to loosen

the inhibiting conformation and for the activation of the Arp2/3 complex (Prehoda et al., 2000; Rohatgi et al., 2000).

WAVE/Scar family

WAVE was discovered as a *Dictyostelium discoideum* homologue of WASP (Bear et al., 1998; Miki et al., 1998). In mammals there are three isoforms of WAVE: WAVE1 and WAVE3 are expressed mainly in the brain, while WAVE2 has ubiquitous expression. All three isoforms have a common structure, similar to WASPs: a basic domain, a proline rich region, and a VCA domain. Unlike WASPs, WAVEs have a basal actin nucleation activity (Machesky et al., 1999), and an N-terminal WAVE homology domain (WHD) instead of a GBD. WAVE is important in motility structures such as lamellipodia. It has been shown that it can interact, through its proline rich region, with partner proteins like Ena/VASP (Chapter 2) to enhance actin assembly and motility (Havrylenko et al., 2015).

The basal activity of WAVE is regulated by a protein complex called the WAVE Regulatory Complex. This complex is composed of ABI1 (Abelson-interacting protein), NPA1 (Nck associated protein 1), SRA1 (specifically Rac associated 1), and HSPC300 (known as BRICK). In this complex, HSPC and ABI1 bind WAVE while NAP1 interacts with ABI1 and SRA1 (Gautreau et al., 2004). *In vitro* studies of the complex proved that it inhibits WAVE activity by masking its binding site to the Arp2/3 complex (Derivery et al., 2009; Ismail et al., 2009). Moreover, SRA1 sequesters the VCA domain of WAVE and prevents it from interacting with monomeric actin (Chen et al., 2010). Downstream of extracellular stimuli, active Rho GTPase Rac1 binds WAVE at the SRA1 subunit inducing a conformational change that liberates the VCA domain and enables it to interact with the Arp2/3 complex (Chen et al., 2010). Membrane localization of the WAVE Regulatory Complex is driven by its interaction with Rac1 (Chen et al., 2017). New studies revealed that the role of WAVE goes beyond its NPF function; it can also tether the branched actin network to the plasma membrane and accelerate filament elongation (Bieling et al., 2018).

1.4.7 Putting all the ingredients together

The actin-binding proteins and their activities described in the preceding sections can be put together to describe a cell motility event like lamellipodial protrusion (Figure 1.13). External stimuli activate receptors on the cell membrane that signal to Rho family GTPases and PIP_2, which activate, in their turn, the WASP/WAVE/Scar proteins. Active NPFs bind the Arp2/3 complex at the membrane, activate its nucleation activity to create branches off the sides of mother filaments with a 70^o angle. Due to local activation at the membrane of NPFs, nucleation of new filaments happens exclusively at the leading edge of the moving cell. Filaments grow in the system until capping proteins bind their barbed ends and terminate their polymerization. ADF/cofilin and profilin then work together, along with other proteins mentioned in text but

not pictured in Figure 1.12, to replenish the ATP-actin monomer pool for subsequent rounds of Arp2/3 complex-driven nucleation. In this scenario, all branches are depicted as pointing forward, with barbed ends oriented toward the cell membrane.

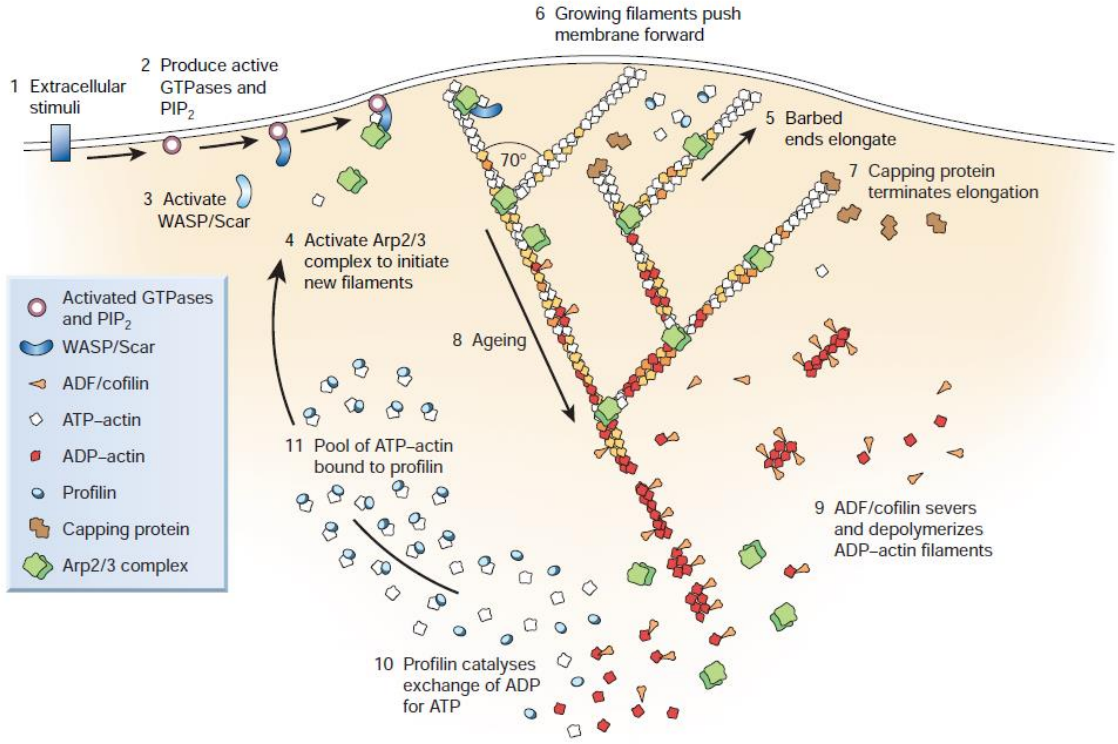

Figure 1.13 - Actin binding proteins at the front of a migrating lamellipodium. The schematic represents the dendritic model of actin polymerization. From (Pollard and Borisy, 2003).

In fact, branches are randomly oriented, and filaments therefore grow in all directions in the absence of capping protein (Achard et al., 2010). However, in the presence of capping protein, filaments are quickly capped, and the actin network away from the surface can therefore be described as a “dead zone” (Figure 1.14). New material is introduced into the network mostly by nucleation events at the surface, and this increase in material between the dead zone and the surface exerts forces on the plasma membrane thus pushing forward and generating motility.

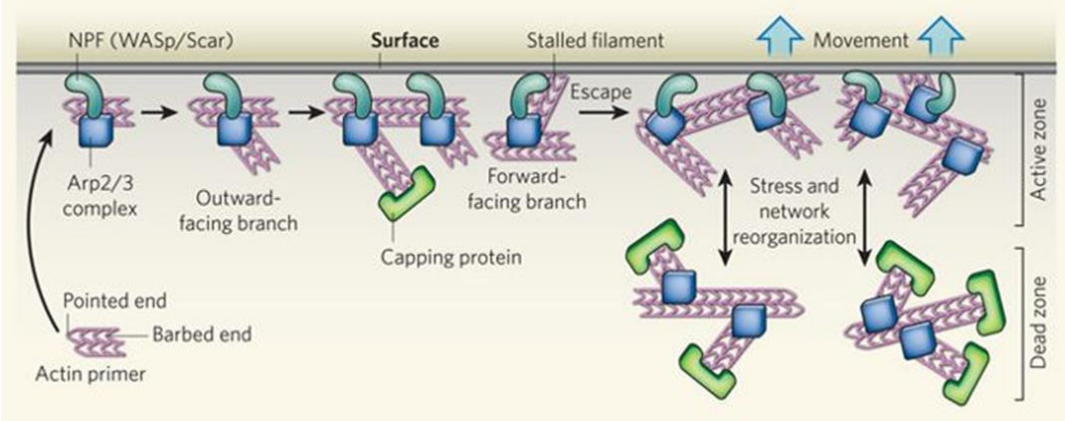

Figure 1.14 - Nucleation by primer model proposed by (Achard et al., 2010), giving random filament orientations leading to incorporation of new material in the form of branches beneath the membrane thus pushing it forward. From (Sykes and Plastino, 2010).

Several polymerization activating factors are involved in lamellipodia formation, but for a long time it was thought to be mainly activated by WAVE complex through Rac activation pathway (Chen et al., 2010). Relatively recently, WASP family proteins have been implicated; studies showed that Rac-independent N-WASP is the major polymerization regulator during cell motility in 3D (Petrie et al., 2012; Tang et al., 2013). This suggests that lamellipodia is mainly initiated by WAVE but that WASP can play that role as well. Other proteins are involved in regulating the dynamics of lamellipodia, like Ena/VASP (Krause and Gautreau, 2014).

1.5 Biomimetic approaches to study actin dynamics and actin-based motility

Living systems are diverse and structurally and biochemically complex as explained in the previous sections of this chapter. In cells, hundreds of protein-protein interactions are involved in cellular movement, rendering it difficult to perform controlled experiments and generate quantitative measurements. To tackle this complexity, both top-down and bottom-up approaches are used. The top-down approach starts with the cell and simplifies it by removing different proteins believed to be involved in the process of interest in order to better understand it. The bottom-up approach starts from purified components and proteins and recreates a target process. With this method, the minimal essential elements that are necessary and sufficient for a given function can be determined. This is also called a biomimetic approach. Biomimetic approaches have been extensively used to study how actin dynamics produces cell motility.

1.5.1 *Listeria monocytogenes* motility

The intracellular bacterial pathogen, *Listeria*, was the inspiration of the first biomimetic systems reconstituting actin-based motility. *Listeria* infects cells through an internalization process and then propels itself in the host cytosol by forming an actin structure known as a comet (Figure 1.15). This actin comet pushes the *Listeria* forward with enough force to deform the plasma membrane, and invade a neighboring cell (Figure 1.15).

Listeria expresses several virulent factors on its surface. One of these agents is the ActA protein (Actin Assembly-inducing protein), distributed in a polarized manner and capable of activating the Arp2/3 complex (Boujemaa-Paterski et al., 2001a; Kocks et al., 1993; Welch et al., 1997). Once ActA activates the Arp2/3 complex, a network of actin forms at the surface of the pathogen making a comet. The structure of actin in the comet resembles the network that forms beneath the membrane in moving cells. In particular actin filaments have their barbed ends oriented in the direction of motion, towards the surface of the bacteria (Tilney et al., 1992) similar to that observed in the lamellipodium (Svitkina et al., 1997). ActA remained for a long time the only known activator of the Arp2/3 complex until WASP family proteins came into the picture (Welch et al., 1998). ActA is sufficient to produce movement in *Listeria*, it possesses all the essential elements to start the polymerization, and all other components for motility are hijacked from the host cytosol (Skoble et al., 2000).

.

a)

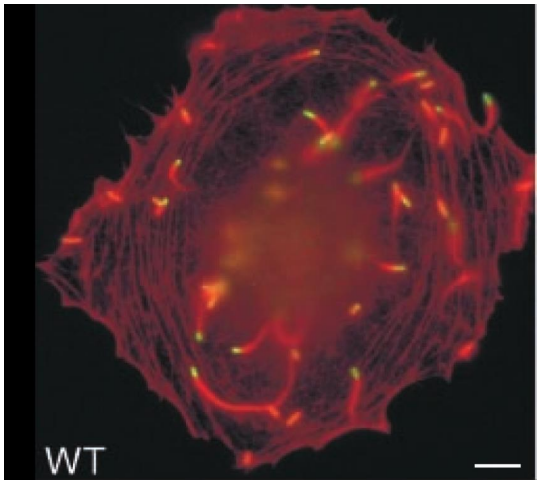

b)

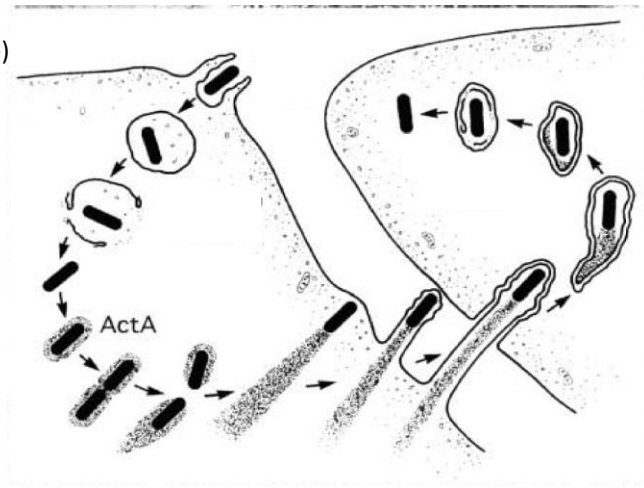

Figure 1.15 - *Listeria monocytogenes* motility. a) Fluorescent microscopy image of *Listeria* propelled by an actin comet in an infected cell. Actin is labelled in red using phalloidin and the bacteria is in green. Scale bar 10 µm (Skoble et al., 2001). b) Schematic representation of the infection cycle of *Listeria* showing the role of ActA in initiatin actin polymerization around the *Listeria*, comet formation and the deformation of the plasma membrane to invade a neighboring cell. From (Tilney and Portnoy, 1989).

1.5.2 Reconstitution of actin polymerization

From *Listeria* to beads

Listeria can move using actin comets in the host cell cytoplasm, and this movement can also be reproduced in cellular extracts where membranes and organelles have been removed (Gouin et al., 1999; Kocks et al., 1995). From this observation emerged the idea of finding a minimal composition of proteins that could support *Listeria* movement. Mixing various purified actin-binding proteins in different amounts led to the definition of a minimal motility mix: actin, the Arp2/3 complex, ADF/cofilin, and capping protein (Loisel et al., 1999). Ena/VASP proteins and profilin were found to be not essential for motility, but increased the speed of *Listeria* movement.

The system can be simplified further by replacing the bacteria with a polystyrene bead coated with the polymerization activator ActA (Figure 1.16). In this way the geometry and the coating of the surface can be controlled (Cameron et al., 1999; Carlier et al., 2003; Noireaux et al., 2000). Complete control of the motility mix protein composition, and the geometry and coating of the propelled object make the bead system a powerful system to understand cellular movement. Replacing ActA by mammalian Arp2/3 complex activators like WASP/WAVE/Scar makes the system more directly relevant for the moving cell, and shows that these activators are sufficient for the formation of branched Arp2/3 complex-dependent actin network that induces motility (Bernheim-Groswasser et al., 2002; Fradelizi et al., 2001). It has been shown in recent studies that these *in vitro* networks not only produce movement, but can sense force and adapt to it, similar to what has been observed in cells (Bieling et al., 2016; Mueller et al., 2017).

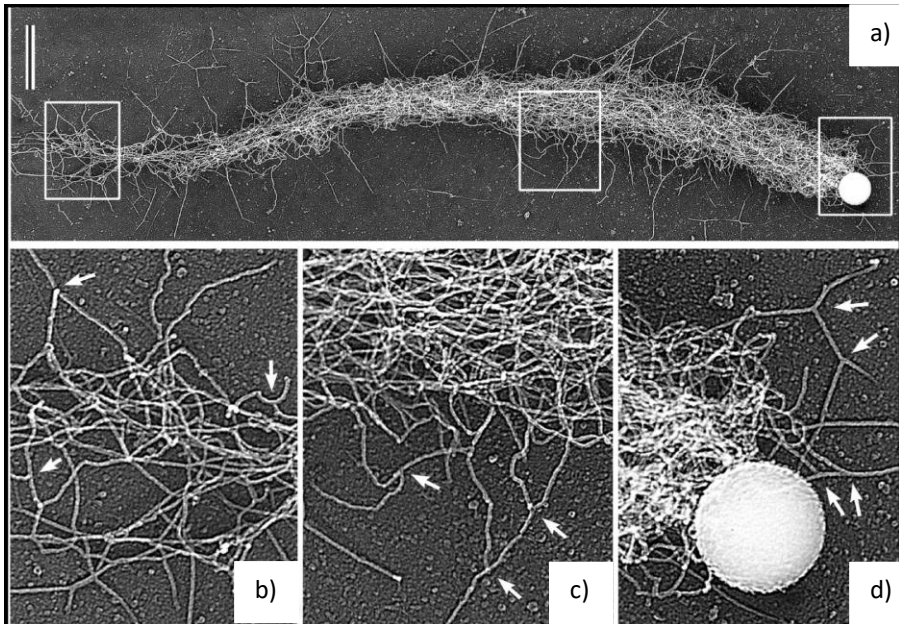

Figure 1.16 - Actin comets on beads. a) Electron microscopy images of an actin comet assembled on a bead coated with ActA and placed in a *Xenopus* egg extract. b-d) Zoom on the boxed regions in a). Tarrows point the Y shaped junctions present in the comet. This dendritic network is similar to the one observed at the leading edge of migrating cells. Scale 1 µm. From (Cameron et al., 2001).

1.5.3 Symmetry breaking and movement generation

In order to produce actin comets from the surface of a bead that has been uniformly coated with activator, a symmetry breaking process has to occur. The steps are as follows:

1) Actin filaments polymerize uniformly from a bead surface coated with polymerization activator, forming an entangled network. Nucleation takes place only at the surface as the activator is present there, and barbed ends are rapidly capped, so growth of new actin is confined to the bead surface. As actin polymerizes, the old actin network is pushed away from the bead surface by the formation of the new network.
2) This stretches the old actin network and stress builds up (van der Gucht et al., 2005). This produces a break in the actin network, and it relaxes away from the site of rupture, giving rise to a comet (Figure 1.17) (van der Gucht et al., 2005).

Many studies on actin based motility and actin network assembly have been conducted using the bead system. This system allows for the modulation of actin-binding proteins in the motility mix and on the bead surface, and for the quantification of the effect of these changes

on actin network growth, architecture and mechanics, and/or the effects on comet formation and bead speed.

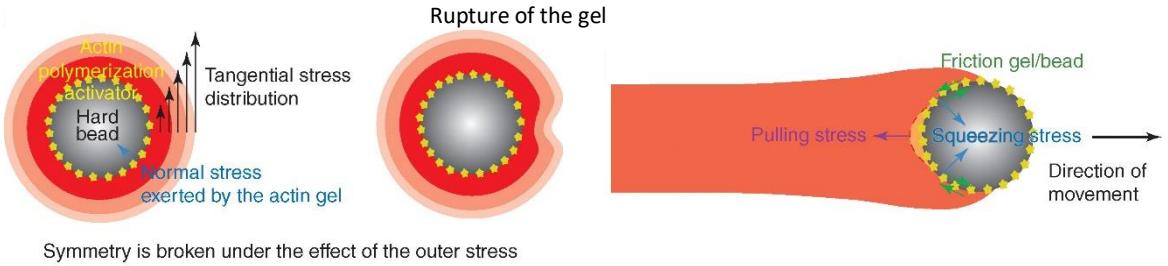

Figure 1.17 - Scheme illustrating steps of growth of the network on the surface of a bead leading to the symmetry breaking event and the formation of an actin comet that propels the bead forward. From (Plastino and Sykes, 2005).

1.5.4 Diversity of biomimetic systems

Beads have been useful, but during the past two decades, biomimetic systems to study actin polymerization have diversified in order to answer different questions (Figure 1.18). Glass rods coated with polymerization activators, and more recently, micro-patterning of activators on surfaces have been used to more closely mimic the quasi-2D lamellipodium (Achard et al., 2010; Boujemaa-Paterski et al., 2017; Carlier et al., 2003). Oil droplets coated with activators have been used to study mechanical deformation produced by the actin network (Boukellal et al., 2004; Trichet et al., 2007) . Liposomes coated with activators are also used to study mechanical parameters like forces exerted by an actin network on the plasma membrane and acto-myosin tension (Caorsi et al., 2016; Simon et al., 2018). Liposomes or water-in-oil emulsions encapsulating motility mixes and activators are also used to study actin network properties under geometrical and confinement conditions more like the cell (Abu Shah and Keren, 2014; Dürre et al., 2018; Pontani et al., 2009). As mentioned above, micro-patterning of activators has found its way into the field, and is being used to print actin polymerization in different motifs to see how geometry controls actin network organization, actin-binding protein activity and myosin motor function (Boujemaa-Paterski et al., 2017; Reymann et al., 2012; Reymann et al., 2010).

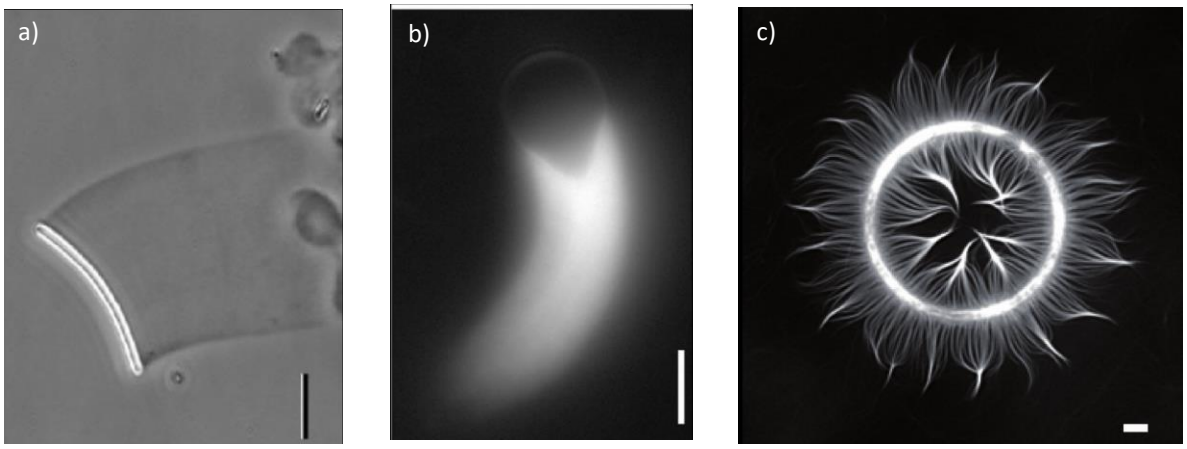

Figure 1.18 - Diversity of biomimetic systems to study actin polymerization a) A glass rod (30 µm diameter) coated with an activator of actin polymerization. The flat, broad actin network mimics a lamellipodium. Phase contrast microscopy. Scale far 10 µm. From (Carlier et al., 2003). b) Oil droplet coated with a polymerization activator, placed in HeLa cell extract. The droplet deforms due to the stress generated by actin growth. Fluorescent microscopy; actin is fluorescently labelled. Scale bar 4 µm. From (Boukellal et al., 2004). c) Activator micropatterned in a ring shape in order to create bundles of actin. Fluorescent microscopy; actin is fluorescently labeled. Scale 10 µm. From (Reymann et al., 2010).

These different biomimetic systems are presented here only to provide a context for the bead system, and to show the activity in the field. In fact, for the experimental *in vitro* work that will be presented in Chapter 4 and 5 of this manuscript, the original bead system was used as it is still the simplest way to assess certain properties, including network polarity and actin-based motility.

Chapter 2: Ena/VASP Proteins

2.1 Ena/VASP proteins in general

Ena/Vasodilator-stimulated phosphoprotein (Ena/VASP) proteins are actin-binding proteins that were one of the main subjects of study during my PhD, so I will describe them in detail in this chapter. Ena/VASP proteins have been variously attributed to have nucleation activity, the capacity to compete with capping protein for barbed ends (called anti-capping) and barbed end elongation enhancement activity (Trichet et al., 2008) (Krause and Gautreau, 2014). These activities will be explained more fully at the end of this chapter, along with a description of the controversies surrounding the mechanisms of Ena/VASP protein action.

The first member of this family to be discovered was *Drosophila* Enabled (Ena), the gene for which was discovered as a dominant suppressor of lethal mutations in the tyrosine kinase gene *abl*, involved in axon guidance (Gertler et al., 1990). Based on this sequence, mammalian equivalents were identified, Mammalian Ena (Mena), Enabled/vasodilator-stimulated phosphoprotein-like protein (Evl) and Vasodilator-stimulated phosphoprotein (VASP), and shown to have roles in actin filament assembly (Gertler et al., 1996). VASP had been previously identified as a substrate of cyclic nucleotide-dependent kinase cAMP and cGMP in platelets (Haffner et al., 1995; Halbrügge and Walter, 1989). Ena/VASP proteins are highly conserved through evolution: in *C. elegans* the equivalent of Ena/VASP is UNC-34, and DdVASP in *Dictyostelium* (Han et al., 2002; Withee et al., 2004; Yu et al., 2002).

Figure 2.1 – Intracellular distribution of Ena/VASP proteins in a moving cell. VASP is mainly present in the front of the moving cell. VASP is fluorescently labelled in green, and actin in red. From (Bear and Gertler, 2009).

2.3 Role of Ena/VASP proteins in cells and *in vivo*

2.3.1 In lamellipodia and cell motility

Ena/VASP proteins are found at the leading edge of lamellipodia, at the tips of filopodia, at cell-cell contacts, in cell-substrate adhesions, and in actin stress fibers (Gertler et al., 1996; Lanier et al., 1999; Reinhard et al., 1992; Rottner et al., 1999) (Figure 2.1). In lamellipodia-based cell motility, the local level of Ena/VASP recruitment at the membrane is proportional to transient protrusion rate of that portion of membrane (Rottner et al., 1999). When Ena/VASP proteins are artificially enriched at the front of a moving cell, a network of long unbranched actin filaments form under the membrane (Figure 2.2), and although these structures protrude rapidly, they are not persistent (Bear et al., 2002; Loureiro et al., 2002), and thus increased Ena/VASP sometimes has the effect of reducing overall cell motility (Bear et al., 2000). On the other hand, when Ena/VASP is reduced at the leading edge of the cell, lamellipodia protrude more slowly than wild type, and the actin network is composed of short highly-branched filaments (Bear et al., 2002; Loureiro et al., 2002). Similarly mislocalization of Ena/VASP protein in fish keratinocytes induces altered cell shape and less efficient migration (Lacayo et al., 2007).

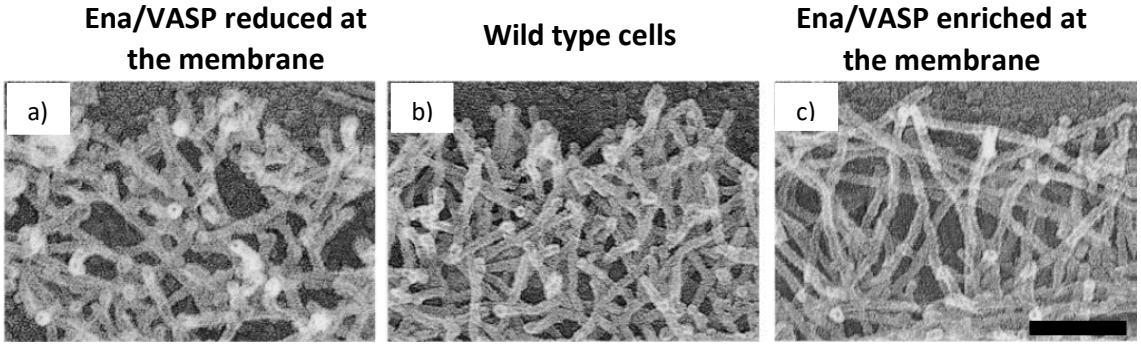

Figure 2.2 - Electron microscopy image of the actin network at the leading edge of migrating fibroblast cells. Accumulation of Ena/VASP at the leading edge using artificial targeting (c) results in an actin network with longer, less branched filaments than wild type (b). Reduction of the amount of Ena/VASP at the membrane produces a network of shorter, more highly branched filaments than wild type (a). Scale bar 100 nm. From (Bear et al., 2002).

In vivo in *Drosophila* oogenesis, border cells migrate to the posterior part of the egg chamber, and Ena mutation in these cells significantly reduces their migration speed (Gates et al., 2009). In the *Drosophila* embryo, Ena overexpression induces an increase in the rate of haemocyte migration, while Ena depletion decreases the rate of cell migration (Tucker et al., 2011). Deletion of *C. elegans* VASP, UNC-34, decreases the migration speed of leader cells during ventral enclosure, a WAVE-Arp2/3 complex dependent, lamellipodia-driven event (Havrylenko et al., 2014). T-cell movement through endothelial cell layers during extravasation in mice is also reduced by Ena/VASP protein deletion (Estin et al., 2017).

Listeria bacteria hijack Ena/VASP proteins of host cells to increase bacterial motility (Chakraborty et al., 1995; Geese et al., 2002; Skoble et al., 2001; Smith et al., 1996) . Likewise in the bead/comet system, when Ena/VASP proteins are recruited to the bead surface, they increase speed of movement (Castellano et al., 2001; Havrylenko et al., 2015; Plastino et al., 2004b; Samarin et al., 2003). Altogether, studies on cells in culture and *in vivo* suggest that Ena/VASP proteins promote cell migration, and this is confirmed in biomimetic systems.

2.3.2 In filopodia

Ena/VASP proteins also play a role in the dynamics of filopodia. Ena/VASP deficient neurons have reduced filopodia formation in their growth cones (Bear et al., 2002; Lebrand et al., 2004), and Ena/VASP knockout completely suppresses filopodia formation in capping protein-deficient mouse melanoma cells and in *Dictyostelium* (Han et al., 2002; Mejillano et al., 2004; Schirenbeck et al., 2006) (Figure 2.3).

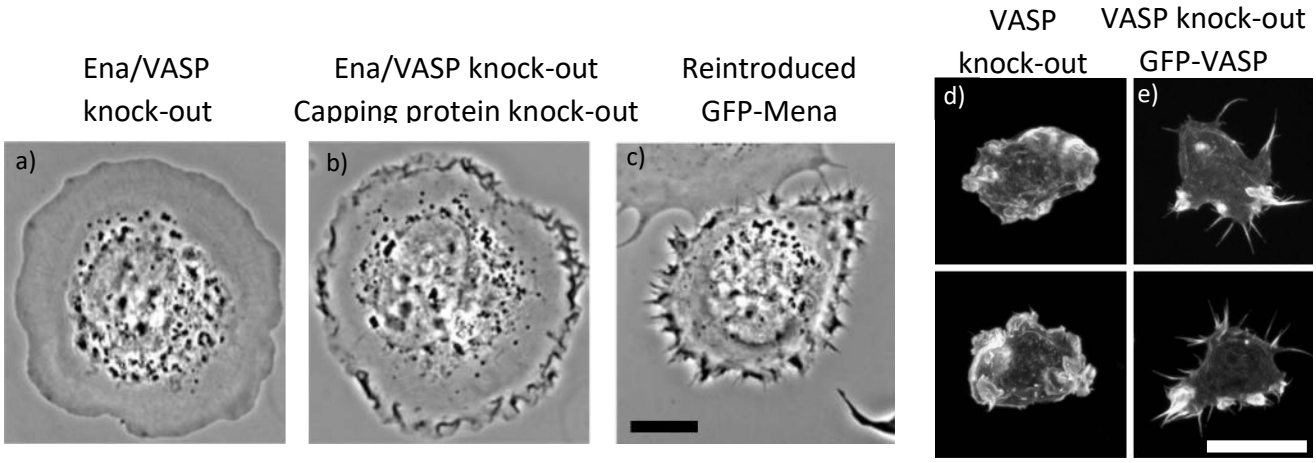

Figure 2.3- Role of Ena/VASP in filopodia dynamics. (a) Ena/VASP-deficient mouse melanoma cells, (b) the same cells lacking capping protein, and (c) with reintroduced GFP-Mena. Cells lacking Ena/VASP protein do not form filopodia in absence of capping proteins. Scale bar 10µm. From (Mejillano et al., 2004). (d) *Dictyostelium* knocked out VASP do not form filopodia. (e) Reintroducing GFP-VASP in this background induces filopodia formation. Scale bar 5µm. From (Schirenbeck et al., 2006).

2.3.3 In cell-substrate adhesions and stress fibers

Ena/VASP proteins play an important role in stress fibers and focal adhesions. Upon mechanical stress, VASP relocalizes from focal adhesions to stress fibers, and helps in their repair, thus restoring the structural integrity and the contractility of the stress fiber (Burridge and Guilluy, 2016; Smith et al., 2010; Yoshigi et al., 2005). VASP is also involved in remodeling stress fibers through cooperation with focal adhesion protein zyxin (Hoffman et al., 2006). Furthermore, Ena/VASP proteins are an integral component of focal adhesions (Kanchanawong et al., 2010).

2.3.4 In cancer

In the past two decades, several studies have emerged indicating a relation between Ena/VASP protein and cancer progression. Phosphorylation of Ena/VASP, which reduces its interaction with actin, inhibits the formation of invadopodia, essential structures for cancer cell invasion and metastasis, and thus reduces colon cancer cell circulation (Zuzga et al., 2012). Fibroblasts overexpressing Ena/VASP lose contact inhibition and are considered as potential tumorigenic cells (Liu et al., 1999), and Ena/VASP overexpression in lung adenocarcinoma cells is correlated with the progress of the tumor (Dertsiz et al., 2005). Mena is overexpressed in breast cancer cell lines, and in particular one splice form of Mena is associated with increased invasion and metastasis (Philippar et al., 2008; Roussos et al., 2010). In addition to its role in invasion, Ena/VASP plays a role in the vascularization of tumors: melanoma cancer cells transplanted into Ena/VASP deficient mice do not develop well, and tumors are smaller and significantly less vascularized (Kim et al., 2011). On a global scale, Ena/VASP proteins seem to be involved at multiple levels in the coordination of the development of metastasis.

2.2 Ena/VASP domains and their functions

All Ena/VASP family members share a conserved domain structure: an amino-terminal Ena/VASP homology 1 domain (EVH1), a central proline rich region, and a carboxy-terminal Ena/VASP homology 2 (EVH2) domain, encompassing G- and F-actin binding sites and a coiled-coil motif. Ena/VASP protein interacts with many partners and performs various functions via its different domains (Figure 2.4), as described in the following sections.

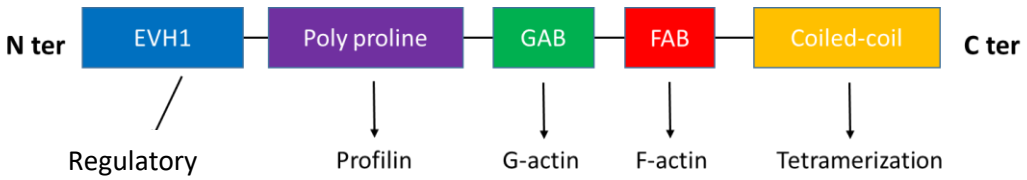

Figure 2.4 – Schematic representation of Ena/VASP, showing its domains and their interacting partners. VASP binds to both monomeric and filamentous actin. The polyproline rich domain of VASP binds profilin.

2.2.1 EVH1 domain

The N-terminal EVH1 domain of Ena/VASP proteins is part of the pleckstrin homology (PH) domain superfamily, but unlike other members of this family, it does not bind phospholipid phosphatidyl inositol-(4,5)-bisphosphate (PIP2) (Prehoda et al., 1999; Volkman et al., 2002). The EVH1 domain binds to peptide ligands containing special poly-proline sequences with FPPPP-type sequences, such as those found in the *Listeria* ActA protein and in the proline-

rich regions of WASP and WAVE molecules (Castellano et al., 2001; Havrylenko et al., 2015; Niebuhr et al., 1997). Through this interaction, Ena/VASP proteins are also recruited to cell-substrate adhesions and stress fibers by interaction with the focal adhesion components vinculin and zyxin, and to the leading edge of lamellipodia and filopodia via interaction with a membrane-bound protein lamellipodin (Krause et al., 2003; Krause et al., 2004). Studies on EVH1 domain in *C. elegans* and *Drosophila* revealed that EVH1 domain mutations interfere with the localization of Ena/VASP proteins, and reduce significantly their activity (Fleming et al., 2010; Gates et al., 2009; Shakir et al., 2006).

2.2.2 Proline rich domain

The central domain of Ena/VASP protein is a proline-rich domain that is the most diverse region in the Ena/VASP family ensuring interactions with different proteins for different regulatory mechanisms (Krause et al., 2003). The shared feature in all family members is profilin binding via this region (Reinhard et al., 1995).

2.2.3 EVH2 domain

The Ena/VASP homology 2 domain (EVH2) is located at the C-terminal of Ena/VASP, and is composed of three domains organized as follows: G-actin binding site, F-actin binding site, and a coiled-coil domain.

- **G-actin binding domain** (GAB). This domain binds G-actin, but binds profilin-complexed G-actin with an even higher affinity, unlike most GAB domains (Chereau and Dominguez, 2006). In this context, it has been proposed that profilin-bound G-actin is loaded onto the proline-rich domain and handed off to the GAB for efficient addition to the filament barbed end (Ferron et al., 2007) (Figure 2.5).

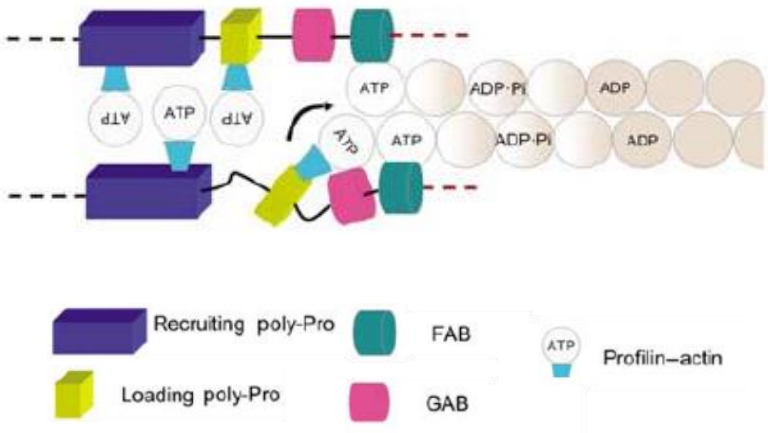

Figure 2.5 – Cartoon of how actin is handed off from the proline-rich domain of Ena/VASP to the GAB domain for efficient insertion onto the growing barbed end. Profilin does not have to dissociate from G-actin for transfer to the GAB. From (Ferron et al., 2007).

The GAB domain also has actin nucleation properties at non-physiological (low) salt conditions (Walders-Harbeck et al., 2002). *In vitro*, GAB domain seems to play an important role in Ena/VASP's anti-capping activity (Barzik et al., 2005), although it doesn't play an essential role in the capture of barbed ends (Pasic et al., 2008). In contrast, single molecule experiments show that GAB is essential for targeting Ena/VASP at the barbed end of a growing filament, and important for barbed end elongation enhancement (Hansen and Mullins, 2010). Along these same lines, a recent study shows that Ena/VASP, which is a homotetramer, uses one of its subunits to track the fast elongating barbed end, while the G-actin binding domains of the other three subunits recruit and deliver monomers to the barbed end of the filament; engineered Ena/VASP proteins with more GAB domains produce faster filament elongation (Brühmann et al., 2017). In addition to its contribution to activity, the GAB of Ena/VASP is also important for correct localization: GAB mutants localize abnormally in fibroblast filopodia (Applewhite et al., 2007; Loureiro et al., 2002).

- **F-actin binding domain** (FAB). FAB binds F-actin and bundles it so that Ena/VASP co-precipitates with actin filaments in both low and high speed sedimentation assays (Bachmann et al., 1999; Laurent et al., 1999). *In vivo,* FAB is important for localizing Ena/VASP at the leading edge of moving cells and filopodia (but not focal adhesions) (Applewhite et al., 2007; Bear et al., 2002; Loureiro et al., 2002). In *Dictyostelium*, the FAB domain shows actin bundling activity that is necessary for the formation of filopodia and for localization at the leading edge (Schirenbeck et al., 2006). *In vitro*, FAB is essential for anti-capping activity of Ena/VASP (Barzik et al., 2005), and for its localization at the barbed end and barbed end elongation enhancement (Hansen and Mullins, 2010). On the other hand, studies on DdVASP show that both FAB and GAB domains must be deleted to interfere with barbed end elongation enhancement activity, indicating a possible redundancy in functions of FAB and GAB domains (Breitsprecher et al., 2008).

- **Coiled-coil domain** (TET) is the tetramerization domain of Ena/VASP, found at the C-terminus of the protein (Bachmann et al., 1999; Zimmermann et al., 2002). This domain is essential for filopodia formation (Applewhite et al., 2007). *In vitro*, the tetramerization domain plays a role in anti-capping (Barzik et al., 2005), and in filament decoration (Hansen and Mullins, 2010). Moreover, the tetramerization domain is essential for bundle formation and barbed end elongation enhancement activity of DdVASP, although artificially clustered monomeric Ena/VASP proteins can also enhance barbed end elongation (Breitsprecher et al., 2008).

2.4 Modes of action of Ena/VASP and controversy

In keeping with its multi-domain structure, Ena/VASP has been ascribed many different modes of action as concerns actin filament dynamics, some of which are controversial.

2.4.1 Nucleation activity

Ena/VASP proteins nucleate the formation of actin filaments from monomers at low salt concentrations (Figure 2.6) (Hüttelmaier et al., 1999b; Schirenbeck et al., 2006). This activity depends on G-actin binding and tetramerization (Walders-Harbeck et al., 2002). This is mechanistically reminiscent of nucleators such as Spire that nucleate by clustering actin-binding sites together (Campellone and Welch, 2010), although other proteins probably participate *in vivo* to make this nucleation mechanism more efficient (Dominguez, 2016). In physiological salt conditions (in cells), Ena/VASP proteins do not nucleate actin polymerization (Barzik et al., 2005). The few reports of Ena/VASP nucleation at physiological salt conditions are attributable to recruitment of preformed actin filaments and barbed end elongation (Fradelizi et al., 2001; Plastino et al., 2004a; Trichet et al., 2007).

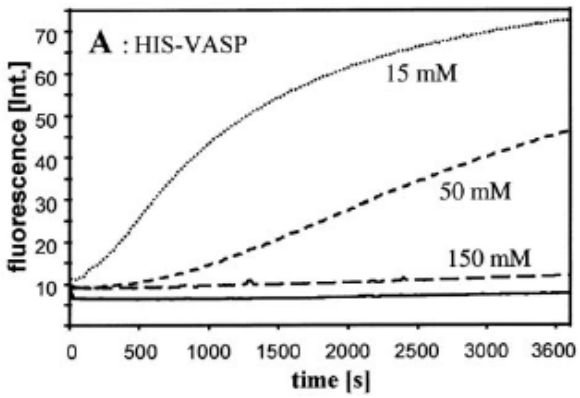

Figure 2.6 - Ena/VASP nucleation activity is dependent on salt concentration. Actin filament formation is monitored over time in the pyrene assay (see Chapter 3), in the presence of 250 nM mouse VASP and the indicated concentrations of KCl. From (Hüttelmaier et al., 1999a).

2.4.2 Anti-capping activity

As mentioned in a previous section (Figure 2.2), when Ena/VASP recruitment at the leading edge of moving fibroblasts in increased, long filaments are observed by electron microscopy, whereas when Ena/VASP is depleted from the leading edge, short filaments are observed (Bear et al., 2002). This led to the hypothesis that Ena/VASP proteins protect filaments from capping protein, allowing them to grow longer before being capped, not to be confused with uncapping activity. Indeed, purified Ena/VASP, coated on beads, could capture and elongate filaments, but not when the filaments were pre-capped (Figure 2.7) (Bear et al., 2002).

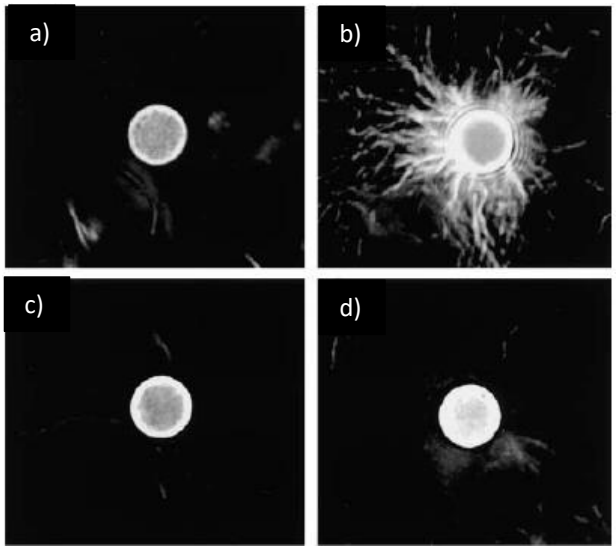

Figure 2.7 - Ena/VASP proteins can capture uncapped barbed ends and elongate them. a) Ena/VASP coated bead, b) mixed with preformed filaments or c and d) mixed with capped filaments. Fluorescence microscopy of fluorescently labeled actin. Beads 2.8 µm diameter. From (Bear et al., 2002).

In keeping with this, when cells are treated with cytochalasin D (a drug that blocks barbed ends), Ena/VASP does not localize to the leading edge of protruding lamellipodia, suggesting the need of growing barbed ends for the localization of Ena/VASP (Bear et al., 2002; Krause et al., 2004). Mathematical modeling of cell shape based on actin filament dynamics also supports the anti-capping activity of Ena/VASP (Lacayo et al., 2007). Anti-capping, but not uncapping, activity of Ena/VASP is clear in *in vitro* studies, such as the pyrene assay where Ena/VASP inhibits the activity of capping protein and promotes filament elongation in a dose-dependent manner (Figure 2.8) (Barzik et al., 2005; Bear et al., 2002). The GAB, FAB and TET domains are required for this anti-capping activity (Barzik et al., 2005). Similar results are obtained with total internal reflection fluorescence (TIRF) microscopy experiments, where individual actin filaments are followed over time (see Chapter 3). Actin filaments grow in the presence of capping protein only when Ena/VASP is added, thus supporting the anti-capping activity of Ena/VASP (Figure 2.8) (Breitsprecher et al., 2011; Hansen and Mullins, 2010; Pasic et al., 2008). Clustering of Ena/VASP enhances its anti-capping effect: when Ena/ VASP is adsorbed on a bead surface, it induces elongation of actin filaments at high concentrations of capping protein that inhibit elongation via Ena/VASP in solution (Breitsprecher et al., 2008).

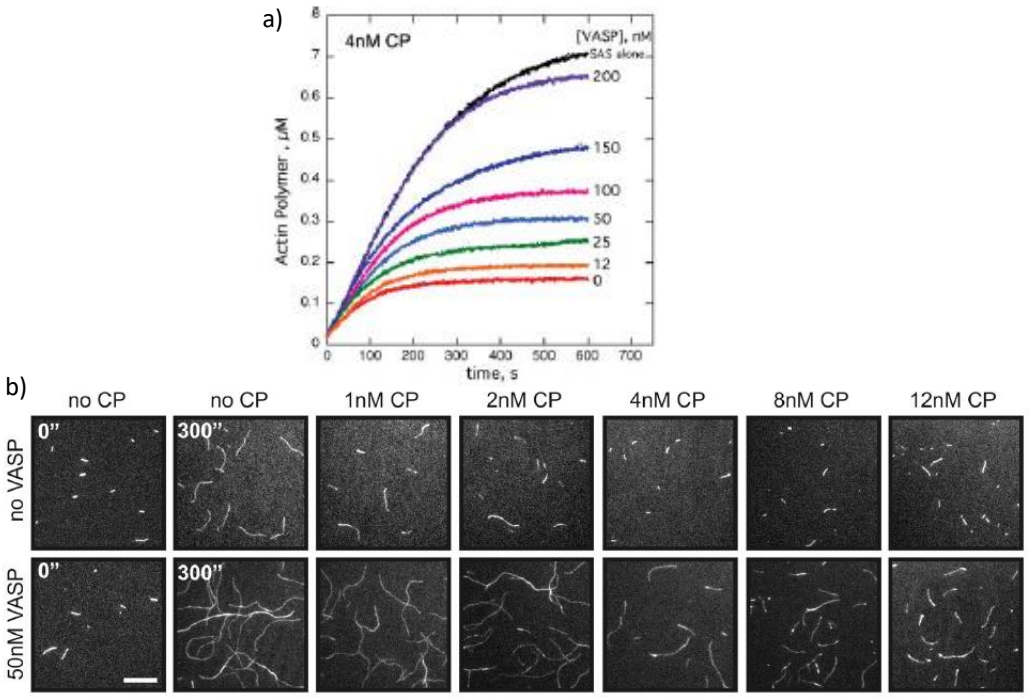

Figure 2.8 - Anti-capping activity of Ena/VASP. a) Mouse VASP at the indicated concentrations and 4 nM capping protein are added simultaneously to polymerizing actin, initiated from preformed seeds (SAS) to avoid the nucleation step. Larger doses of VASP allow the polymerization curve to approach that of SAS alone (black curve). From (Barzik et al., 2005). b) TIRF microscopy of actin filaments after five minutes of growth, in the presence of variable amounts of capping protein, without (upper panels) and with (lower panels) human Ena/VASP. Addition of Ena/VASP permits filament growth even at elevated capping protein concentrations where filament growth is suppressed. Bar 10 µm. From (Hansen and Mullins, 2010).

Interestingly, early data from *in vitro* pyrene experiments show that Ena/VASP does not rescue actin polymerization in the presence of capping activity (capping protein or gelsolin) (Boujemaa-Paterski et al., 2001a; Samarin et al., 2003). These results are difficult to reconcile with the studies mentioned in Figure 2.8, but one difference in the experimental systems in that the early pyrene assays were done in the presence of Arp2/3 complex-actin nucleation.

In conclusion on anti-capping, there is agreement that Ena/VASP proteins are not able to uncap filaments; capping proteins have a high affinity for the barbed end, and once attached, cannot be displaced by Ena/VASP (Bear et al., 2002; Schirenbeck et al., 2006). Today it is generally accepted that Ena/VASP has anti-capping activity, i.e., their interaction with the barbed end delays capping protein binding.

2.4.3 Effect on barbed end elongation

A controversy in the field centers on the effect of Ena/VASP on the elongation of filaments. Some studies report no effect of Ena/VASP on the elongation speed of actin filaments (Barzik et al., 2005; Bear et al., 2002; Samarin et al., 2003), while other studies show an increase in the polymerization speed in presence of Ena/VASP, similar to the barbed end elongation activity of formin (Breitsprecher et al., 2008; Hansen and Mullins, 2010). Again differences here are possibly attributable to different assays: barbed end elongation enhancement is observed in TIRF but not in pyrene assays. The role of the profilin in barbed end elongation enhancement by Ena/VASP proteins is not entirely clear; some studies report no effect of profilin on Ena/VASP-induced actin polymerization (Breitsprecher et al., 2008), while others observe an effect of profilin on polymerization speed and on enhancement of the anti-capping activity of Ena/VASP (Barzik et al., 2005; Hansen and Mullins, 2010). Structural studies described in Figure 2.5 indicate that Ena/VASP binds profilin-actin with both its proline-rich domain and its G-actin binding site, consistent with, but not proof of, a role for profilin-actin in barbed end elongation enhancement by Ena/VASP.

2.4.4 Effect on Arp2/3 complex branching

Ena/VASP proteins do not interact directly with Arp2/3 complex (Boujemaa-Paterski et al., 2001b), but they seem to affect Arp2/3 complex branch frequency. In general Ena/VASP protein is associated with reduced branching frequency of actin filaments by the Arp2/3 complex (Bear et al., 2002; Plastino et al., 2004b; Samarin et al., 2003; Skoble et al., 2001) although there is an exception where Ena/VASP is observed to increase branch frequency (Boujemaa-Paterski et al., 2001a) (Figure 2.9). However overall there is a consensus that Ena/VASP protein association with a network lowers the degree of branching of that network in the presence of capping protein.

In this context it is important to note that the Arp2/3 complex activators WASP and WAVE have both been observed to directly recruit Ena/VASP proteins via the interaction of WASP/WAVE proline-rich domain and the EVH1 domain of Ena/VASP (Chen et al., 2014; Havrylenko et al., 2015). This interaction could potentially place Ena/VASP proteins close to new (uncapped) barbed ends created by the Arp2/3 complex (Figure 2.10). Elongation enhancement of the barbed ends coupled with a constant on-rate for the Arp2/3 complex on the side of the growing mother filament to make a branch could explain how Ena/VASP proteins produce networks that are less highly branched.

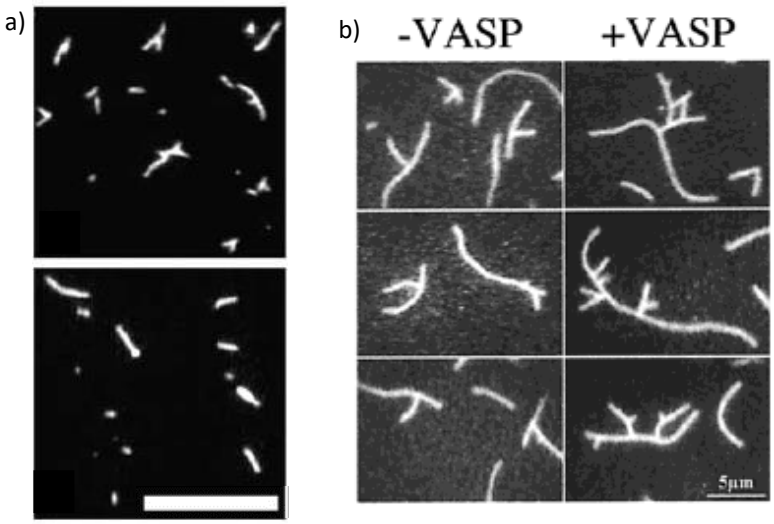

Figure 2.9 - Contradictory results concerning Ena/VASP effect on Arp2/3 complex branching. a) Arp2/3 complex activated by ActA protein without (top) and with (bottom) Ena/VASP. Branches are suppressed by Ena/VASP addition. Scale bar 10 µm. From (Skoble et al., 2001.) b) In a similar assay, adding VASP increases branch formation. From (Boujemaa-Paterski et al., 2001a).

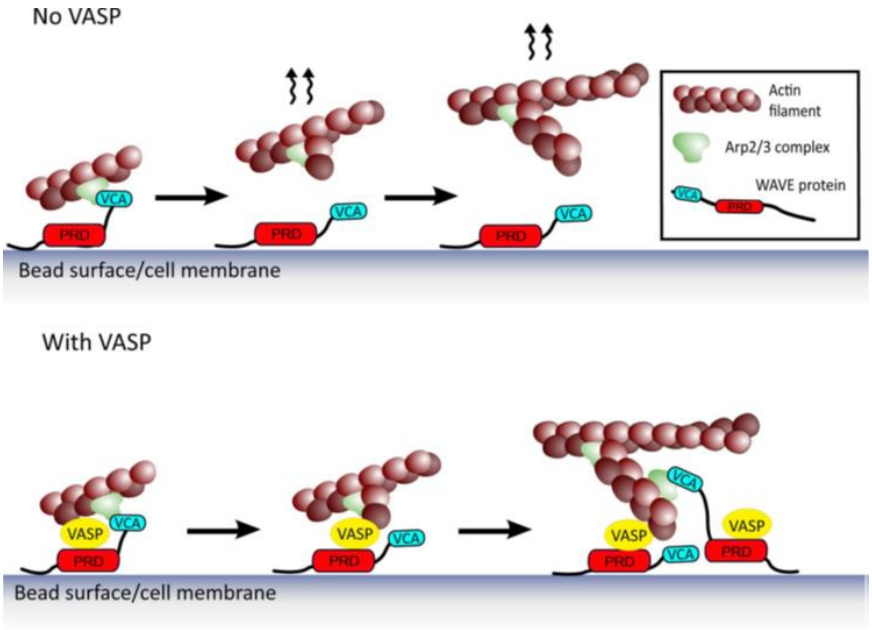

Figure 2.10 – cartoon illustrating the theory of a teamwork between the Arp2/3 complex and VASP via mutual binding to WAVE. The scenario at the top, a nascent branch could diffuse away from the surface after being formed. In presence of VASP, a hand-off of the nascent branch could happen (bottom). VASP provides the link between the surface and the network at the same time that it enhances growth of new barbed ends. From (Havrylenko et al., 2015).

Chapter 3: Experimental Methods *in vitro*

This section describes the experimental approaches employed in Chapter 4 and 5, investigating the role of Ena/VASP in actin network architecture and studying photoswitchable Arp2/3 complex inhibitors, respectively, using the *in vitro* bead system introduced in Chapter 1. The experimental part of Chapter 6, concerning nematode embryo experiments, will be presented as part of Chapter 6.

3.1. Actin network reconstitution on beads

3.1.1. DNA and proteins

Rabbit muscle actin, pyrene-labeled rabbit muscle actin and porcine Arp2/3 complex were purchased from Cytoskeleton as lyophilized powder and resuspended as per the manufacturer's instructions. Fluorescently-labeled (Alexa-488 and Alexa-594) rabbit muscle actin was purchased from Invitrogen. All other proteins were purified or labeled by John Manzi, the protein biochemist of our in-house protein purification platform BMBC168. The Arp2/3 complex was fluorescently labeled by incubation with a 10-fold molar excess of Alexa-488 C5-maleimide on ice for 3 hours. 1 mM DTT was added to quench the labeling and the protein was dialyzed overnight in 20 mM Tris, pH 7.4, 25 mM KCl, 0.25 mM DTT, 100 µM ATP, 1 mM MgCl2, 0.5 mM EDTA, centrifuged to remove precipitates and frozen. The DNA constructs for untagged human profilin and GST-pVCA-WASP-His (human WASP, residues 150-502, called GST-pVCA) were gifts of T. Pollard (Yale University) and L. Blanchoin (CEA Grenoble), respectively. Profilin was purified as in (Carvalho et al., 2013) and GST-pVCA as in (Havrylenko et al., 2015). The streptavidin tagged pVCA-WASP-His construct (S-pVCA) was made and the protein was purified as in (Carvalho et al., 2013). The DNA constructs for mouse α1β2 capping protein and wild-type and mutant forms of mouse VASP were gifts from D. Schafer (University of Virginia), and the proteins were purified as in (Palmgren et al., 2001) for capping protein and as in (Barzik et al., 2005) for VASP and VASP mutants. VASP proteins were further purified via FPLC using a Superdex 200 10/300GL column (GE Healthcare). VASP constructs were the following: ΔEVH1-VASP, lacking residues 1–114; ΔPP-VASP, lacking residues 156–207; ΔGAB-VASP double point mutation R232E, K233E; ΔFAB-VASP, lacking residues 255–273; ΔFABGAB-VASP (called ΔFG-VASP) lacking residues 255-273 and carrying the double point mutation, and ΔTET-VASP, lacking residues 331–375. All protein concentrations were measured by Bradford, and VASP concentrations are calculated with the tetramer molecular weight, even for ΔTET-VASP.

3.1.2. Bead preparation

For the bead assays, 4.5 μm diameter carboxylate beads (Polysciences) were used. 9 μL of 2.5 % bead suspension (total surface area of 3 cm^2) were coated in 40 μL of 2 μM GST-pVCA-WASP or S-pVCA-WASP in Xb (10 mM HEPES pH 7.5, 0.1 M KCl, 1 mM $MgCl_2$, and 0.1 mM $CaCl_2$). The reaction was mixed in a thermomixer for 20 minutes at 18°C and 1000 rpm. After coating, the bead surface was blocked by washing twice with 1% BSA (Bovine Serum Albumin)/Xb buffer. The coated beads were resuspended in 120 μL Xb/1% BSA and stored on ice for a day of experiments.

3.1.3. Actin polymerization on beads

Actin was thawed, diluted to 21 μM in G-buffer (2 mM Tris, 0.2 mM $CaCl_2$, 0.2 mM DTT, 0.2mM ATP pH 8.0) and allowed to depolymerize at 4°C for at least 2 days and then kept on ice and used for several weeks. (Freezing monomeric actin is known to create small oligomers, thus the necessity of the depolymerization step.) Profilin, capping protein, the Arp2/3 complex, and KCl were all diluted in MB13 buffer (10 mM HEPES, 1.5 mM ATP, 3 mM DTT, 1.5 mM $MgCl_2$, 1 mM EGTA, 50 mM KCl, 1% BSA, pH 7.5). VASP proteins were diluted in VASP buffer (20 mM Imidazole, 200 mM KCl, 1 mM EGTA, 2 mM $MgCl_2$, 1 mM DTT, pH 7.0). The *in vitro* actin polymerization reaction mix contained: 0.2 μL of coated beads (approximately 0.005 cm^2 of surface), 50 nM Arp2/3 complex, 5 or 15 μM profilin (either a 1:1 ratio or a 1:3 ratio to assure that all monomeric actin was bound to profilin) and 5 μM G-actin, with or without 25 nM capping protein and/or 37 nM VASP, except for the phase diagram experiments where the concentrations of the Arp2/3 complex and VASP were varied. The final KCl concentration was adjusted to 86 mM by addition of KCl in MB13. The final reaction volume was 8.4 μL. The entire reaction was spotted on a glass slide, covered with a coverslip (18 × 18 mm) and sealed with vaseline/lanolin/paraffin (VALAP) (1:1:1). For timed experiments, the stopwatch was started upon addition of actin, which was always added last.

3.1.4 Two-color experiments

Alexa-488 or Alexa-594-labeled actin was added to the 21 μM unlabeled actin solution in G-buffer to a final concentration of 10 % labeled actin, and allowed to depolymerize before use. For the two-color experiment, a half-batch (4.1 μL) reaction was prepared with Alexa-594-labeled actin and was allowed to polymerize in the tube at room temperature for 4 minutes. This reaction was then mixed with a second reaction mix (8.4 μL) containing Alexa-488-labeled actin, but no beads. The entire mixture was spotted on a slide and observed for about 20 minutes.

3.1.5 Bead observation and data processing

Phase contrast and epifluorescence microscopy images were obtained on an Olympus IX70 inverted microscope with a 100x oil-immersion objective and CoolSnap CCD camera (Photometrics). Spinning disc images were obtained on an inverted confocal spinning disk

microscope from Nikon using a 100x oil objective and a CoolSNAP HQ2 camera (Photometrics). Phase contrast and fluorescence quantification was done using MetaMorph software (Universal Imaging). For two-color experiments, pictures of beads were taken randomly over the whole slide over the course of 20 minutes. For each bead, 2 pictures were taken, one for green fluorescence and one for red fluorescence, and the two pictures were overlayed in MetaMorph. The linescan function of MetaMorph was used on the combined images, drawing a line from the center of the bead towards the outside. This gave the intensity of each pixel in the red and green channel with respect to its position along the line, and was plotted after subtracting the background, taken at the furthest extreme of the linescan from the bead surface. For the photoswitchable Arp2/3 inhibitor studies, unlabeled actin was used and phase contrast images were taken randomly over the whole slide over the course of about 25 minutes. Comet lengths were measured by hand in MetaMorph, and plotted against time. For evaluation of the amount of Arp2/3 complex in the actin network, spinning disc images were taken with Arp2/3 complex labeled in green and actin in red. Densities were evaluated in Metamorph by drawing a circular shape that surrounded the bead and included 1 μm of the network around the bead.

3.2 Actin polymerization assessment by pyrene assay

The pyrene assay mix (60 μL final volume) contained 50 nM Arp2/3, 15 μM profilin, 5 μM actin (~5% labeled with pyrene, diluted to 30 μM in G-buffer and allowed to depolymerize for at least 2 days before use) and 86 mM KCl in MB13 buffer. GST-pVCA and S-pVCA were diluted in MB13 and VASP was diluted in VASP buffer. As soon as the actin was added, the mix was placed in a glass cuvette and the fluorescence intensity (excitation 365 nm, emission 407 nm, excitation slit 5 nm, emission slit 5 nm) was measured every second using a fluorimeter (Cary) thermostatted at 20°C. Kaleidagraph was used to plot the data. The concentration of barbed ends was calculated with the equation: [b.e.] = (Elongation rate μM/s)/(k+ x [actin monomers]), where elongation rate at half-maximum was converted from a.u. to μM based on the curve plateau assuming all actin was in filamentous form at this point, using 2.5 μM as the actin monomer concentration at half-max and taking k+ as approximately 10 $\mu M^{-1}s^{-1}$ (Higgs et al., 1999; Pollard, 1986).

3.3 Single filament assay by TIRF microscopy

Glass coverslips were cleaned in a glass holder using 1M NaOH and sonication for 15 minutes, then washed in water, sonicated again in ethanol 96% for 15 minutes, washed in water and dried using pressure nitrogen flow. Clean coverslips were assembled into chambers where the sample was sandwiched between an 18 x 18 mm and a 24 x 50 mm coverslip separated by double-sided tape. Experiments were performed using an Eclipse Ti Inverted

Microscope with a 100x oil immersion objective and a Quantum 512SC camera (Photometrics). Actin polymerization mix contained 1.5 μM of Alexa-488 labeled actin (15% labeling), 1x profilin, 86mM KCl, 0.2% DABCO and 4% methylcellulose in MB13. VASP was added at 37nM. Samples were flowed into the chambers and sealed with VALAP. Image acquisition started 1 minute after the start of polymerization in the chamber. Images were collected at 1 second interval for 15 minutes. Actin filament lengths were measured over time, and converted to rate constants by considering that 1 μm represented 370 subunits of actin.

3.4 Photoswitchable Arp2/3 complex inhibitors

All molecules were diluted in 100% DMSO and re-diluted in MB13 buffer in order to arrive at the final concentration used in the assays. Illumination was done using 2 wavelengths:

1) 360 nm to convert the molecules from *trans* to *cis* form
2) 420 nm to convert the molecules back to *trans* form

Molecules were handled in semi-darkness to prevent unwanted conversions.

For photoconversion of LU06, in a UV-VIS spectrophotometer, the spectrum of LU06 molecule was recorded, and then the molecule was converted in a fluorimeter using 360 nm or 420 nm wavelength light for 5 minutes, then immediately transferred to the spectrophotometer to read the spectrum post-conversion. The data for both conditions (pre- and post- conversion) was extracted and plotted using Kaleidagraph.

For attempts at *in situ* conversion of LU06, the reaction mix (everything but actin) was transferred to a 24-well plate (to make sure the sample was shallow) and illuminated with LEDs of appropriate wavelength for 5-10 minutes. Actin was then added and the sample was observed. Alternatively, the reaction mix with actin was spotted on a slide, illuminated with LEDs, then the sample was covered by a coverslip, sealed and imaged.

Chapter 4: Ena/VASP Affects Polarized Actin Network Growth and Architecture

4.1 Introduction and open questions concerning the mode of action of Ena/VASP proteins

This chapter describes my main PhD work, a study I began as a Masters student and then came back to when the embryo project (Chapter 6) proved unfruitful. This chapter will be the basis of an article to be submitted after my defense; I will be the first author. As described in Chapter 1, lamellipodia formation relies principally on the Arp2/3 complex, which is activated by membrane-bound WASP/WAVE proteins to create a branched filament network beneath the plasma membrane. Added to membrane-localized nucleation is the action of capping protein that limits filament growth to the vicinity of the membrane. The end result is that networks are oriented with new growth occurring predominantly by new nucleation at the membrane surface. In this scenario the role of barbed end elongation enhancement proteins such as Ena/VASP is not entirely clear, although as described in Chapter 2, Ena/VASP proteins are invariably linked to enhanced protrusion of Arp2/3 complex-based structures. This enhancement has also been observed for certain formins, such as FMNL2, which is a better elongator than nucleator (Block et al., 2012). So enhancement of Arp2/3 complex-based protrusion seems general to elongation enhancement proteins, and not specifically associated with Ena/VASP proteins.

However, there are reports that elongation and branching are antagonistic since they compete for monomers (Akin and Mullins, 2008). Competition for monomers between the Arp2/3 complex and formins has been shown to control actin architecture in yeast and *C. elegans* embryos (Burke et al., 2017; Chan et al., 2018), and *in vitro* it has been shown that even when monomers are in large excess in the bulk, local depletion of the monomer pool occurs when polymerization is confined to a surface (Boujemaa-Paterski et al., 2017). With these questions in mind, in this chapter, I used the *in vitro* bead system (Chapter 1) to investigate the interplay between Arp2/3 complex-based nucleation and Ena/VASP for polarized (surface-directed) actin network growth.

4.2 Results

4.2.1 Mouse VASP restores polarized actin network growth in the absence of capping protein

Beads were coated with the nucleation promoting factor GST-pVCA, incubated with the actin polymerization mix containing capping protein and examined using the two-color approach (described in Chapter 3). This was performed with large beads (4.5 µm in diameter) so that comet formation was slow in order to examine homogenous network growth. I observed the formation of actin clouds with new (green) actin polymerizing at the surface while the previous (red) actin layer was pushed away from the surface (Figure 4.1a). A linescan drawn from the center of the bead towards the dark non-fluorescent area showed that the green fluorescence curve peaked close to the surface of the bead while the red fluorescence curve peaked further away. This confirmed the visual impression that the two colors were segregated. This was further verified by a correlation plot: the green and red fluorescence of each pixel was plotted, giving a wide distribution indicating low colocalization between the two colors (Figure 4.1a). Color segregation, as evaluated by peak separation in the linescan, took place in 70% of the analyzed beads and was considered as a signature of a polarized actin network (Figure 4.1d).

In contrast, when polymerization was performed in the absence of capping protein, diffuse actin halos around the beads were observed with a brighter ring at the bead surface, and when the red and green channels were superimposed, the bead surface and halo appeared yellow indicating complete colocalization of the old actin and the new actin (Figure 4.1 b). The linescan confirmed this, showing that the green and the red fluorescence curves peak together and had the same decay profile, while the correlation plot gave a straight line indicative of complete colocalization (Figure 4.1b). The percentage of beads showing color segregation in these conditions was 0% (Figure 4.1d). Total colocalization could be explained by the fact that, in the absence of capping protein, the red actin network was nucleated at the bead surface, but then grew in all directions. When green actin was added to this, new green branches were formed at the bead surface, but green actin was also incorporated into the uncapped barbed ends present throughout the actin network. The actin network looked sparse around the beads without capping protein, but this was due to the fact that the network was of low density with many long filaments growing out into the solution. This effect has been described before, and it has been shown that there is a long-range actin cloud growing several tens of microns away from the surface in the absence of capping protein, invisible by epifluorescence microscopy but visible by optical tweezer experiments (Bussonier et al., 2014).

Surprisingly, when actin was polymerized in the absence of capping protein but with added mouse VASP, color segregation occurred resulting in an effect similar to capping protein

presence both by linescan and correlation plot (Figure 4.1c). Color segregation occurred on about 75% of the beads. This suggested that VASP could restore the polarity of network growth in the absence of capping protein. When I used smaller beads, adding VASP to no capping conditions gave comet formation and motility (Figure 4.2).

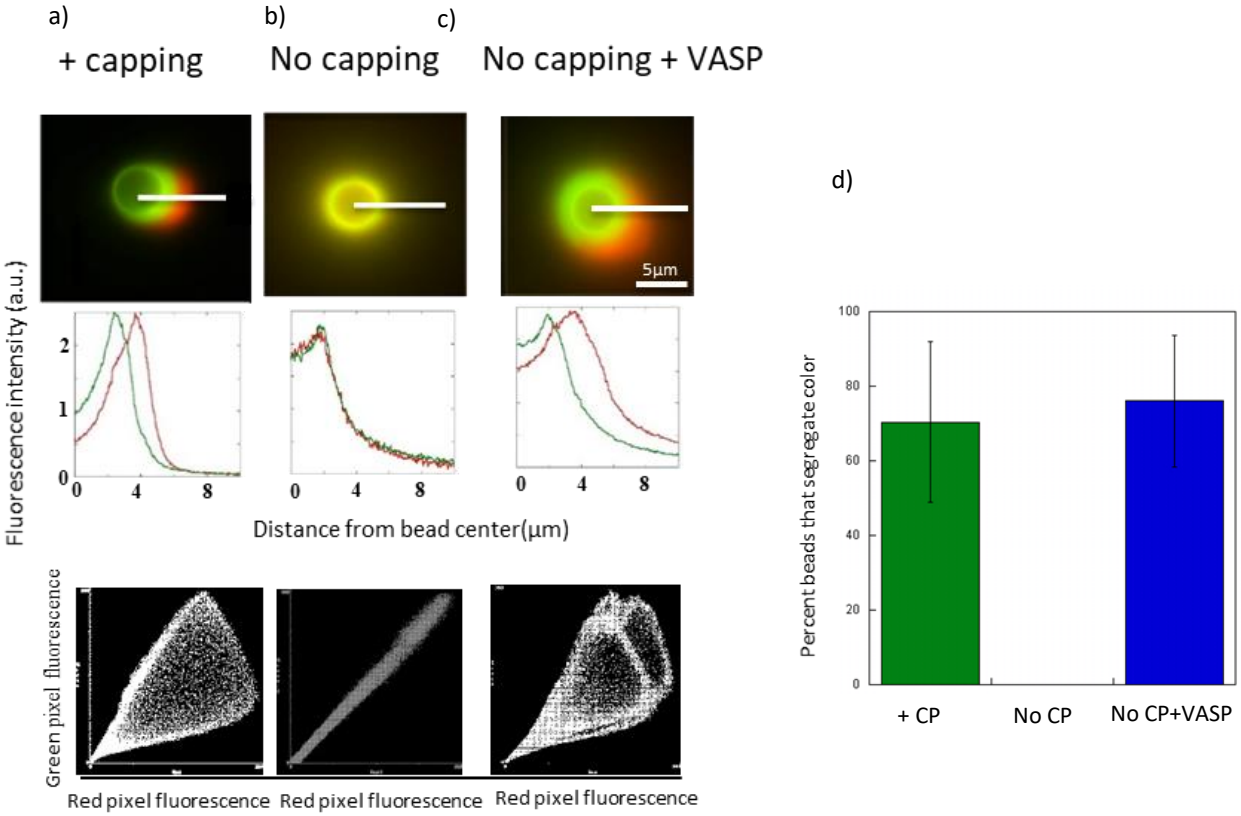

Figure 4.1 – VASP protein reestablishes surface directed polymerization in the absence of capping protein. Top panels: Fluorescent images of actin networks a) with capping protein, b) without capping protein and c) without capping protein but with added VASP. Middle panels: linescans corresponding to the white lines indicated in the top panels. Bottom panels: colocalization plots of red and green fluorescence. Epifluorescence microscopy. Scale bar 5 µm. d) Quantification of color segregation for the different conditions representing about 60 beads for each condition. Error bars represent the standard deviation from the average of 3 different days of experiments.

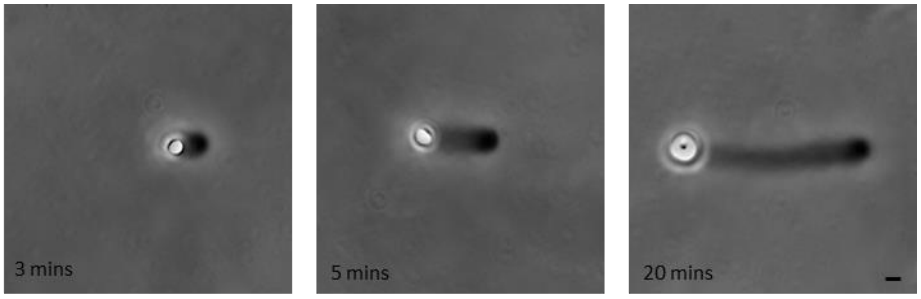

Figure 4.2 - Comet formation in the absence of capping protein but with added VASP. Actin comet tail pushes the beads forward with a certain speed. Time represents elapsed time from the start of polymerization. Scale bar 1 μm.

4.2.2 Mouse VASP is a barbed end elongation enhancement protein

It seemed likely that this activity was somehow dependent on the ability of VASP to enhance barbed end elongation. However barbed end elongation enhancement had never been actually shown for the mouse VASP that I was using. To measure the effect of VASP on barbed end elongation, I used TIRF microscopy to measure single filament growth rates in the absence and presence of mouse VASP. Time-lapse imaging was performed and all the filaments that were growing for several frames were followed over time and their length was measured. I found that addition of VASP increased filament growth rate by 60% compared to the no VASP control condition, from 1.3 μm/min to 2.3 μm/min (Figure 4.3).

Taking the conversion factor of about 370 actin subunits per μm (each subunit adds 27 Å to the filament (Huxley, 1967)), and the fact that monomeric actin is at 1.5 μM in the assay, these measurements gave a barbed end $k_+$of around 5.3 $\mu M^{-1}s^{-1}$ in the absence of VASP. This is half the value observed without profilin (about 10 $\mu M^{-1}s^{-1}$ (Pollard, 1986)), due to the inhibitory effect of excess profilin on barbed end polymerization (Pasic et al., 2008). However k_+ was increased to 9.5 $\mu M^{-1}s^{-1}$ in the presence of 37 nM VASP. So while not as active as *Dictyostelium* VASP for barbed end elongation enhancement, mouse VASP seemed to have a similar activity as human VASP (Breitsprecher et al., 2008; Hansen and Mullins, 2010).

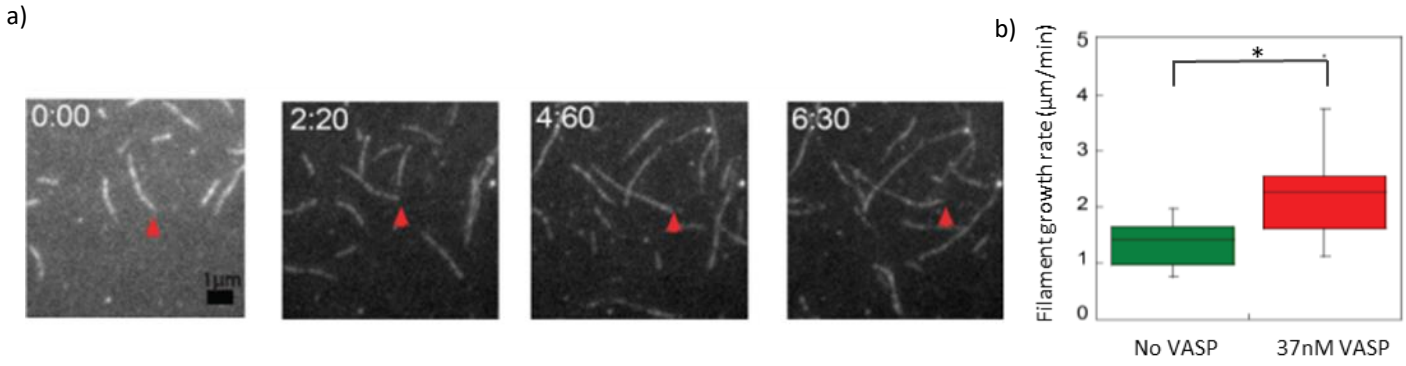

Figure 4.3 - Mouse VASP increases barbed end elongation *in vitro*. a) TIRF microscopy images of actin filament growth observed over time (noted in minutes). Red arrow indicates barbed end of a growing filament. 1.5 µM monomeric actin, 1.5 µM profilin and 37 nM VASP. Scale bar 1 µm. b) Quantification of the growth rate of barbed ends of actin filaments in the presence and absence of VASP. The difference is significant (p = 0.0004). N = 20 filaments.

4.2.3 Which VASP domains are necessary for restoring polarized growth in the absence of capping protein?

In order to get an idea as to the mechanism of VASP restoration of polarized growth in the absence of capping protein, I tested mutant VASPs lacking different functional domains. All but the double mutant of both the F-actin and the G-actin binding site were functional for at least some degree of color segregation (Figure 4.4). The FAB appeared to be the most important motif as this was the only one that on its own gave a significant reduction with respect to wild-type VASP. These results showed that recruitment to the bead surface via interaction of the EVH1 domain with the p domain of pVCA (Castellano et al., 2001; Havrylenko et al., 2015) was not essential for restoring polarized actin network growth. It also showed that the GAB domain was dispensable. This was not surprising as it had been shown for human VASP that processive barbed end elongation depended on GAB, but that the polymerase activity of a GAB mutant could be rescued by profilin-actin and an intact PP domain (Hansen and Mullins, 2010). This was consistent with barbed end elongation occurring with actin monomers coming from the GAB domain or profilin-actin monomers coming from the PP domain. In addition, the partial activity of the FAB mutant could be explained by an observation in the same paper that actin monomers bound to GAB could target VASP to the barbed end (Hansen and Mullins, 2010) (Figure 4.5). Like my mouse VASP, *Dictyostelium* VASP also preserved its barbed end elongation enhancement activity in the absence of either FAB or GAB, but was inactive in its ΔFG form (Breitsprecher et al., 2008). The TET domain has been shown not to be necessary when VASP is clustered (Breitsprecher et al., 2008), as was perhaps the case in my system with barbed ends close together at the bead surface, and the PP domain was probably expendable in my case due

to redundancy with the GAB domain, mentioned above. Taken all together, mutants that eliminated barbed end elongation enhancement of VASP appeared also to lose their ability to compensate for the absence of capping protein. This indicated that enhanced elongation, and not other activities such as F-actin bundling or pVCA binding, was the key for maintaining surface-directed polymerization without capping protein.

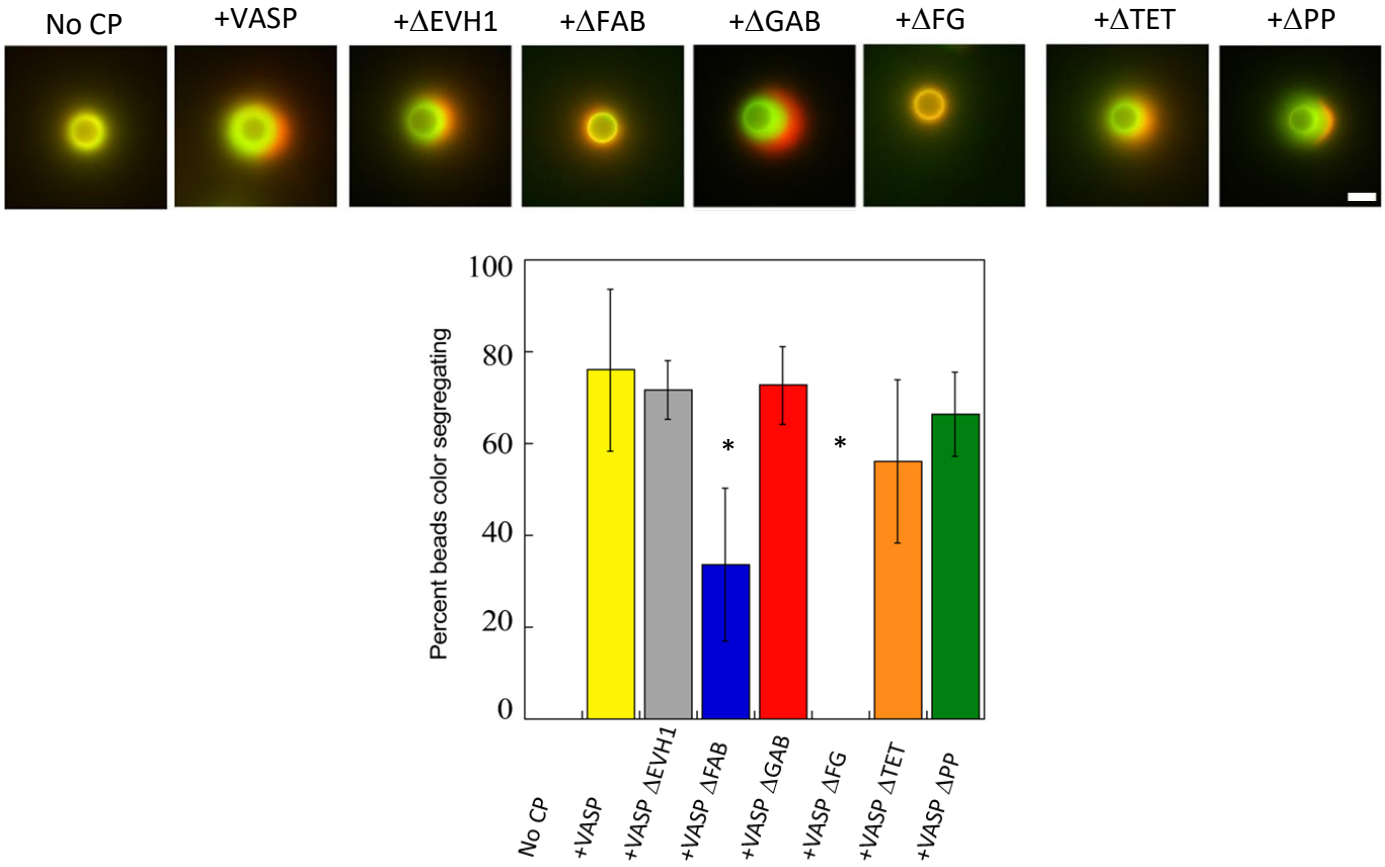

Figure 4.4 - Activity of different VASP mutants. a) Color segregation of different forms of VASP with the indicated domains deleted (FAB = F-actin binding site, GAB = G-actin binding site, FG = both F-actin and G-actin binding site, TET = coiled coil tetramerization domain, PP = polyproline domain. See also Figure 2.4, Chapter 2.) b) Quantification of % beads displaying peak separation in linescans. Only ΔFAB and ΔFG were significantly different from wild-type ($p < 0.005$) using a Chi-squared significance test. Error bars indicate the standard deviation from the mean of 3 different days of experiments. N = 90 beads.

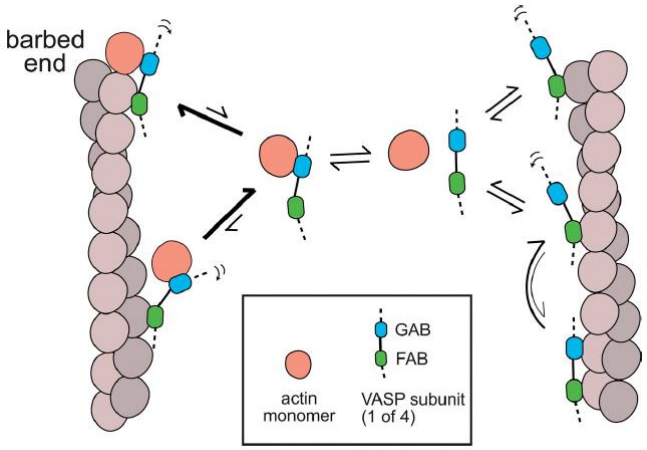

Figure 4.5 - VASP can target filaments either by side-binding via its filamentous actin binding domain (FAB domain) or by barbed end binding via its monomeric actin binding domain (GAB domain). From (Hansen and Mullins, 2010).

4.2.4 Aggressive nucleation at the surface can compensate for the absence of capping protein

Polarized (surface-directed) growth in the absence of capping protein with added VASP reminded me of other conditions I had observed where capping protein was dispensable: 1) when extra Arp2/3 complex was added to the assay or 2) when beads were coated with a form of pVCA that had enhanced ability to activate the Arp2/3 complex, called S-pVCA (Figure 4.6a). In both cases, surface–directed growth and color separation were observed in the absence of capping protein. S-pVCA was a form of pVCA WASP tagged with streptavidin, making it a homo-tetramer due to the tetramerization of streptavidin. By pyrene assay this construct was more active for Arp2/3 complex activation than GST tagged pVCA, which was a dimer due to the dimerization of the GST tag (Figure 4.6b). It was previously shown that multimeric forms of WASP were more effective for Arp2/3 complex activation than monomeric forms, as oligomerization increased WASP affinity for the Arp2/3 complex (Padrick et al., 2008). In fact, S-pVCA produced 4-5 times more barbed ends than GST-pVCA, calculated by measuring maximum polymerization speed over a range of pVCA concentrations and extrapolating to maximum activity as per (Higgs et al., 1999). (See also Chapter 3.) All together these results showed that increased surface polymerization could maintain network polarity without capping protein.

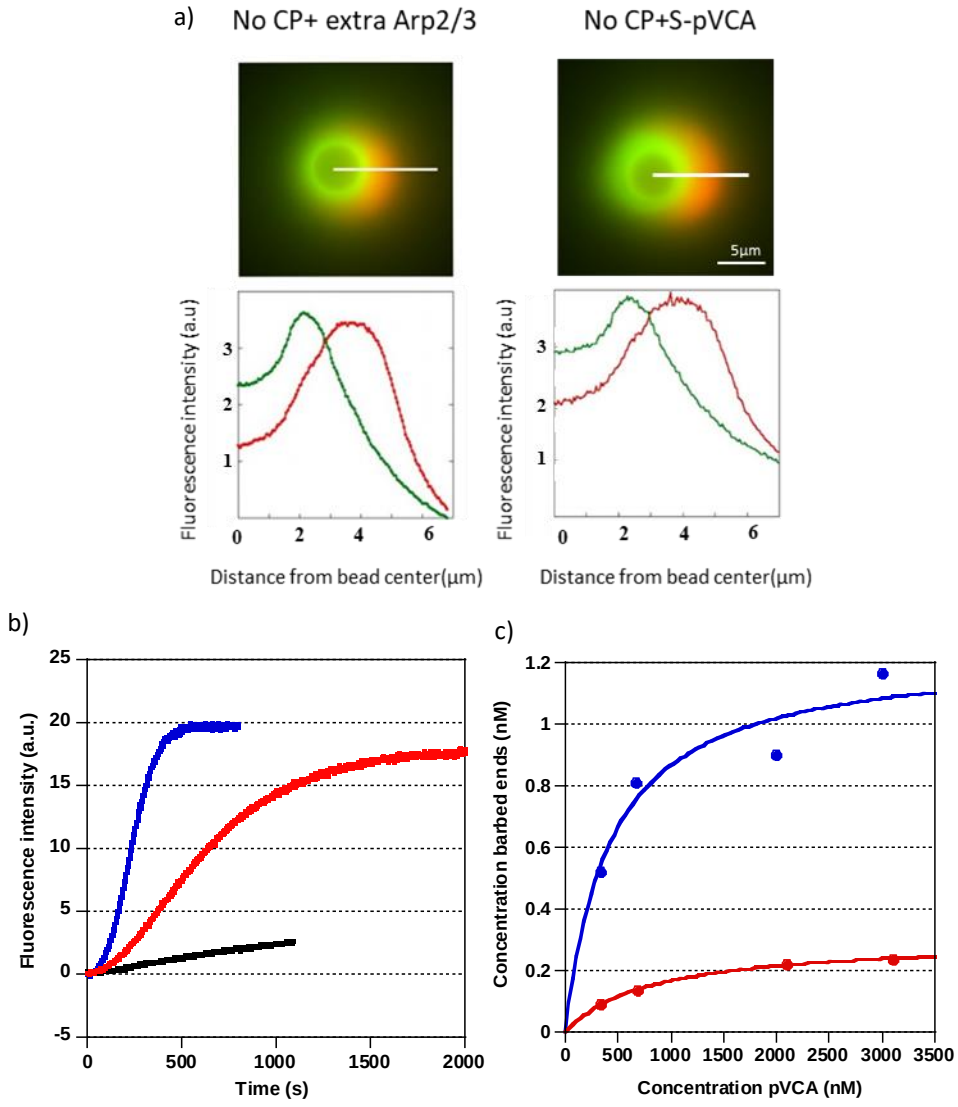

Figure 4.6 – Powerful nucleation at the surface can bypass the need for capping protein and induce the formation of a polarized actin network. a) Surface directed actin growth in absence of capping protein, using 150 nM Arp2/3 complex or using the super-active Arp2/3 complex activator S-pVCA (from left to right). Scale bar 5 µm. b) Pyrene actin assay showing the difference in activity between S-pVCA (blue curve) and GST-pVCA (red curve). Black curve is without added pVCA. c) Barbed end production evaluated for a range of S-pVCA (blue curve) and GST-pVCA (red curve).

4.2.5 VASP can compensate for reduced Arp2/3 complex in the network polarity establishment.

From the previous results, I made the hypothesis that VASP was somehow enhancing Arp2/3 complex activity since VASP addition gave a similar phenotype to increasing Arp2/3 concentration or increasing Arp2/3 complex activation. To better understand the interplay between VASP and the Arp2/3 complex, I examined a range of concentrations of the Arp2/3 complex and VASP (Figure 4.7a). At low concentrations of the Arp2/3 complex and VASP, beads displayed weak fluorescence and no color segregation. At high concentrations of the Arp2/3 complex and VASP, the phenomena of polarized growth of the actin network visualized as segregation of colors was observable. As described in the previous section, at high concentrations of the Arp2/3 complex alone, I found that actin networks around the beads were polarized with new actin assembly occurring at the surface of the bead. On the other hand, at low concentrations of the Arp2/3 complex, addition of VASP restored surface-directed polymerization. Using linescan analysis I quantified the occurrence of color segregation (Figure 4.7b). All conditions that showed color segregation more than 50% of the time were considered as color segregating beads, as indicated by the dotted box in Figure 4.7a. This polarity maintenance window showed that VASP could compensate for inadequate concentrations of Arp2/3 complex and help establish a polarized network in the absence of capping protein, suggesting that VASP was capable of somehow enhancing surface-bound Arp2/3 complex activity. It was known that VASP had no preference for ATP-actin filaments over ADP filamentous actin (Laurent et al., 1999) nor was its surface recruitment necessary (see above) for color segregation. It was not clear, therefore, how VASP could induce a surface-directed effect while enhancing barbed end elongation everywhere in the network. However, if barbed end elongation in the vicinity of the activated Arp2/3 complex on the bead surface somehow increased Arp2/3 complex branching, this could explain my results.

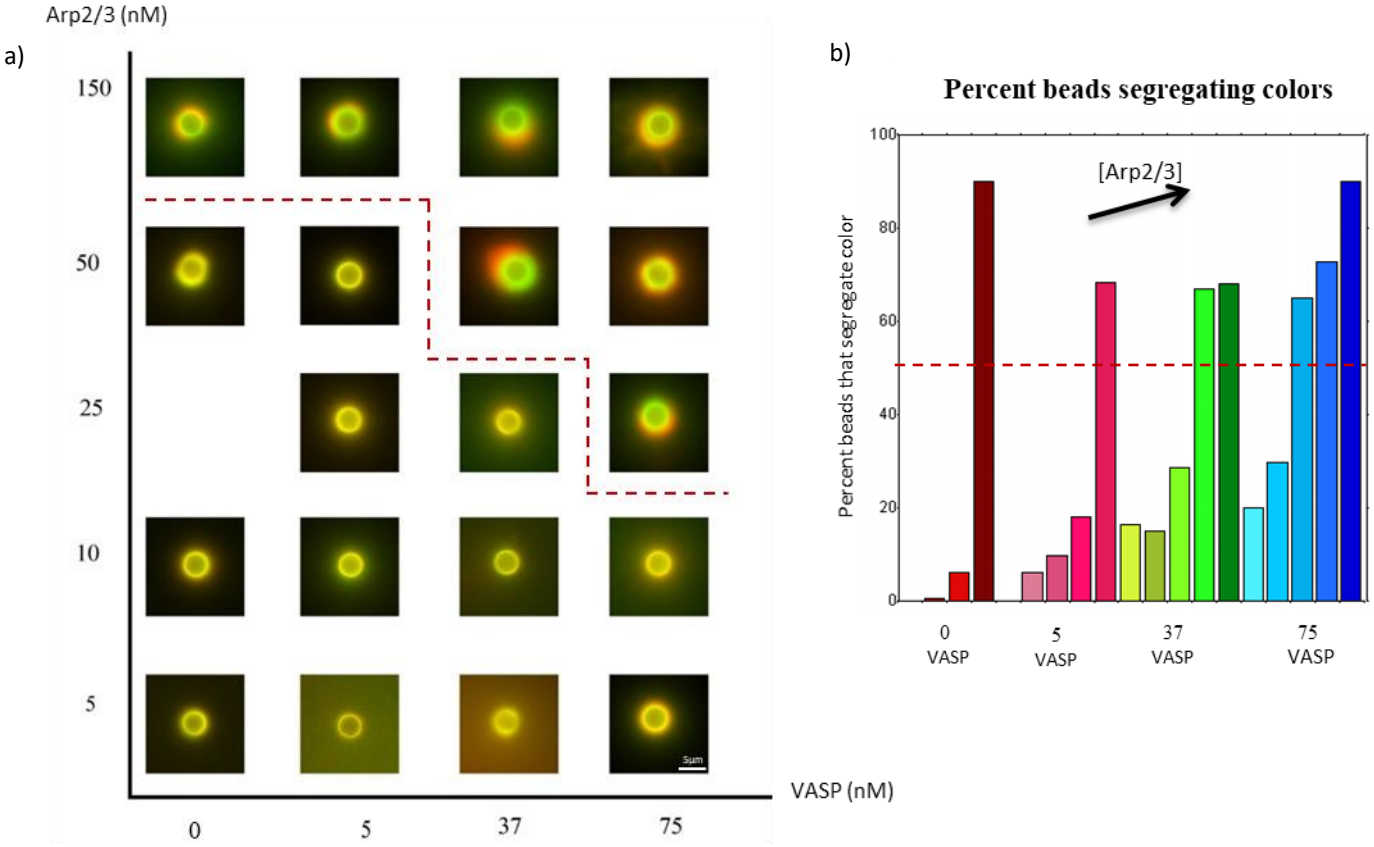

Figure 4.7 – Interplay between the Arp2/3 complex and VASP. a) Phase diagram of different concentrations of VASP and the Arp2/3 complex done using the two color experiment. Red dotted box indicates the window of conditions where color segregation occurs. The segregation or non-segregation decision was taken based on linescan analysis of the images. Scale bar 5 µm. b) Quantification of color segregation from linescans. Each color represents one concentration of VASP, and different shades of this color represent increasing concentrations of the Arp2/3 complex as shown by the arrow. The red dotted line represents the 50% color segregation limit used to draw the dashed box in a). N ≥ 30.

4.2.6 Actin network density and Arp2/3 complex levels increase at the bead surface in the presence of VASP

If this were true, I expected to see more actin and more Arp2/3 complex around beads without capping protein but with added VASP. In order to investigate this possibility, I fluorescently labelled the Arp2/3 complex and used it to produce actin clouds around GST-pVCA beads (Figure 4.8a). In conditions of absence of both capping protein and VASP, a halo of actin formed around the beads along with a thin layer of Arp2/3 complex at the bead surface. When capping protein was added, a well-defined ring of actin containing the Arp2/3 complex formed

around the beads. In the case of adding VASP without any capping protein, a thick network of actin and Arp2/3 complex formed around the beads. To quantify these impressions, a circular region was drawn around the bead, encompassing 1 μm of the actin network, and the intensity of the fluorescence signals for both actin and the Arp2/3 complex were quantified (Figure 4.8b and c).

The main result from this was that the addition of VASP in the absence of capping protein resulted in significantly higher amounts of the Arp2/3 complex in the network at the surface of the beads, as compared to all other conditions, including the normal conditions of adding capping protein. This suggested that VASP could increase the branching activity of the Arp2/3 complex. Similarly, the actin network density is affected by the action of VASP protein. In absence of VASP and capping protein, the actin rings that form have a low density at the bead surface. In the presence of VASP regardless of capping protein, the actin network around the beads was denser than the network formed in conditions of absence of VASP.

I am currently working with theoretician Remy Kusters (CRI, Paris) to develop a model that explains how barbed end elongation in proximity to activated Arp2/3 complex on the bead surface can translate to increase Arp2/3 complex branching, effectively mimicking conditions of extra Arp2/3 complex and S-pVCA bead coating. In this scenario even though VASP extends barbed ends throughout the network in the absence of capping protein, enhanced filament elongation at the surface will create more mother filaments for the Arp2/3 complex to branch from, and thus increase actin growth at the surface.

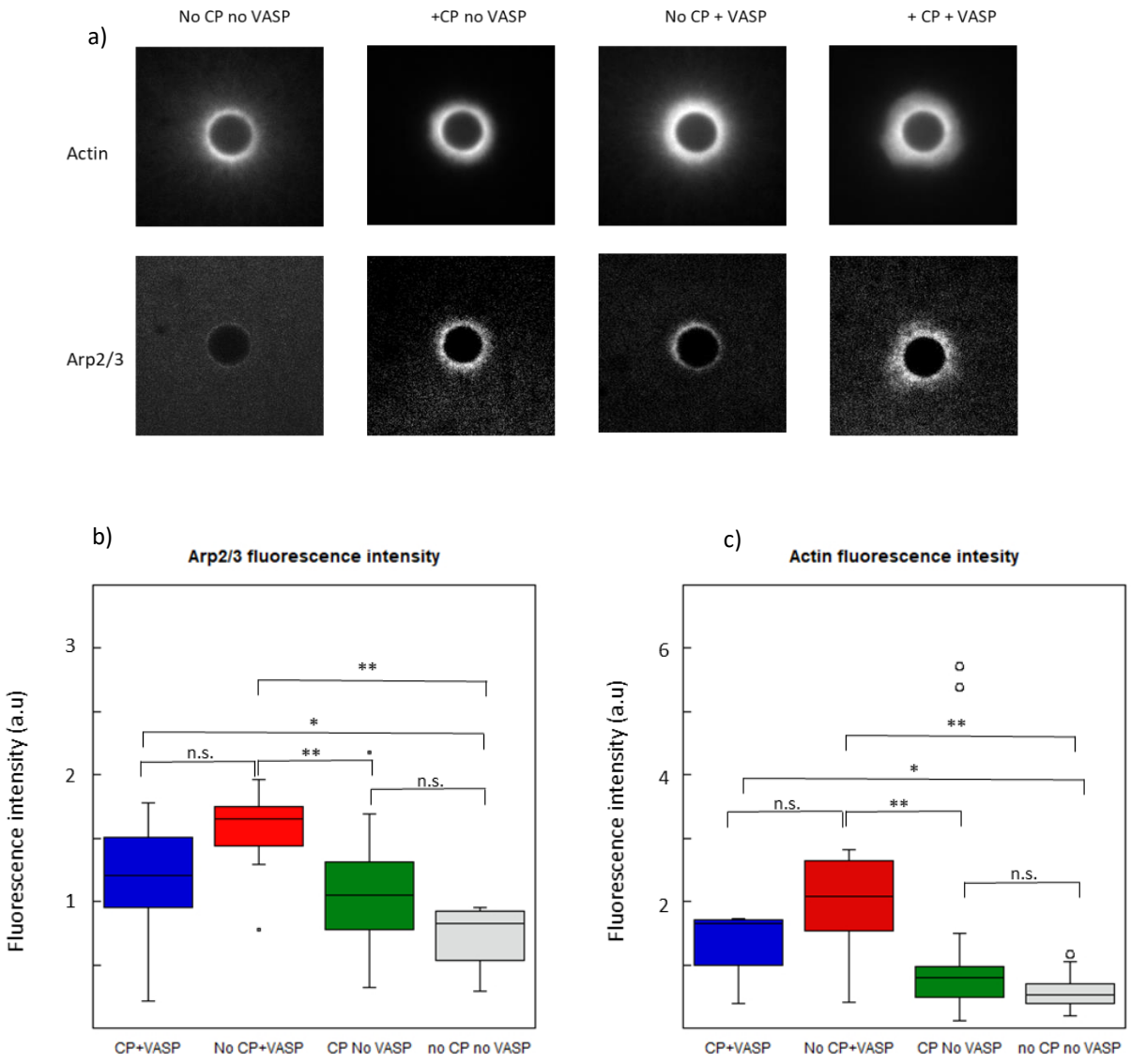

Figure 4.8 – Effect of VASP on Arp2/3 complex density and actin density at the bead surface. a) Spinning disk images of fluorescently labeled actin (first panel) and fluorescently labeled Arp2/3 complex (middle panel) in an actin network polymerized around beads with no capping protein nor VASP, in presence of either capping protein or VASP, and in presence of both of them (respectively from left to right). The bottom panel is colored representation of the Arp2/3 complex fluorescent signal where low intensity pixels are purple and high intensity pixels are orange. Scale bar 5 µm. b) Quantification of Arp2/3 fluorescence intensity and c) quantification of actin fluorescence intensity around the beads. Significant differences are marked by asterix (* $p < 0.05$, ** $p < 0.002$), n.s. indicates non-significant differences.

4.3 Conclusion and perspectives

My results on actin network polarity revealed an important role for VASP in defining network polarity. Indeed, VASP was capable of preserving surface-directed polarity in the absence of capping protein, a surprising result considering VASP's known anti-capping and polymerase activities. My hypothesis is that VASP's elongation activity provides more mother filaments that can act as substrates for Arp2/3 branching, thus increasing its activity. My experiments with the hyper-active Arp2/3 complex activator S-pVCA showed that aggressive nucleation at the bead surface can bypass the need for capping protein and maintain polarized growth toward the bead surface. By extrapolation this may be how VASP is acting as well, although by a different mechanism.

As mentioned above, future work will involve the elaboration of a physical model of actin network growth. I hope to obtain out of this quantitative information as to how the rate of branching is affected by VASP's barbed end elongation activity. Overall these results with VASP show that capping protein is not essential for surface-directed growth and actin-based motility as originally published (Loisel et al., 1999; van der Gucht et al., 2005). Aggressive actin nucleation at the surface can compensate for lack of capping protein. This activity could be important *in vivo* where capping protein levels might not be sufficient or could be locally depleted. This effect on Arp2/3 complex branching activity could also apply to other barbed end elongation enhancement proteins such as formins.

Chapter 5: Small Molecule Photoswitchable Inhibitors of the Arp2/3 Complex

As introduced in Chapter 1, the Arp2/3 complex plays a role in many actin-based cellular functions, including in cell motility and shape change events that occur during morphological and developmental processes. In the past, it was challenging to study the role of the Arp2/3 complex in specific events or at defined times during a given biological process since no small molecule inhibitors existed, as they did, for example, for myosin (blebbistatin) and actin polymerization (latrunculin, cytochalasin). Mutants of subunit complexes were made, but in some systems, this resulted in lethality (Goley and Welch, 2006). RNAi was also used, but its efficiency in mammals and worms was shown to be low (Wu et al., 2012; Zhu et al., 2016). A dominant negative approach to inhibiting Arp2/3 complex activity, consisting in the expression or injection of the VCA domain of WASP/WAVE has also been used (Cáceres et al., 2018; Koestler et al., 2013; Machesky and Insall, 1998), but again such treatments were difficult to control temporally. It was therefore a breakthrough for the field when small molecule inhibitors of the Arp2/3 complex were developed by the Pollard lab in 2009, in particular the molecule CK-666 (Nolen et al., 2009).

The goal of this chapter was to take this one step further, and to participate in the development of molecules based on CK-666 that could be switched off and on by light with the aim of achieving better control in time and space. To put this study in the context of my PhD, the original goal was to use such drugs to manipulate the actin cytoskeleton of nematode embryos from non-*Caenorhabditis* genera (Chapter 6). Since these are less amenable to genetic alteration than *C. elegans*, the use of small molecule inhibitors, especially light-controllable ones, would have been useful for perturbing actin cytoskeleton in precise ways.

5.1 Introduction to inhibition of the Arp2/3 complex

5.1.1 CK-666

CK-666 was one of a class of small molecule inhibitors of the Arp2/3 complex that were found via chemical library screening (Nolen et al., 2009). These molecules bind the Arp2/3 complex at different sites, either at the Arp2/Arp3 interface or in a pocket on the Arp3 subunit (Figure 5.1). In both cases binding interfered with the 3.1 nm shift in position of the Arp2 subunit that occurred upon activation by NPFs, thus inhibiting the activity of the Arp2/3 complex to nucleate actin filament polymerization (Hetrick et al., 2013; Nolen et al., 2009).

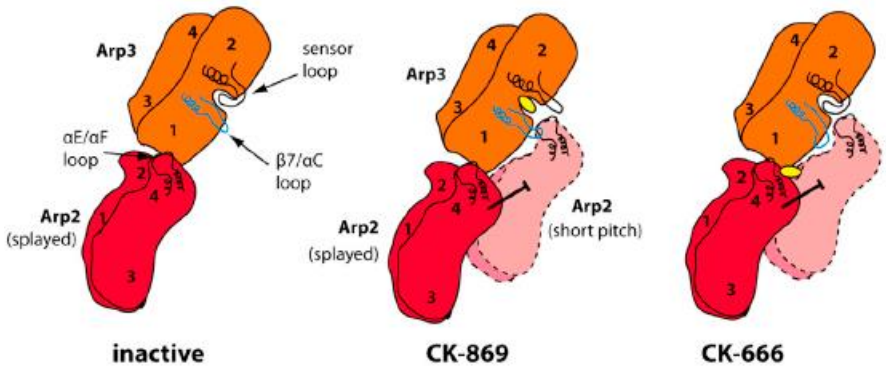

Figure 5.1- Binding sites for different Arp2/3 complex inhibitors. Light pink color represents the position of Arp2 when the complex is active. CK-869 and CK-666 binding (middle and right panel respectively) represented by yellow oval shapes, physically prevents the conformational change of the complex that brings Arp2 into the active position, represented by flat-headed arrows (middle panel). From (Hetrick et al., 2013).

The most effective and specific of these molecules was found to be CK-666 (Figure 5.2). By crystal structure analysis, it was concluded that CK-666 bound tightly at the Arp2/Arp3 interface via the interaction of the CK-666 benzene ring with the hydrophobic pocket formed by residues from both subunits (Ile 252 and Tyr 202 on Arp2 and the backbone portion of Thr 119 on Arp3), while the fluorine atom on CK-666 interacted with the back wall of the pocket via van der Waals interactions (Nolen et al., 2009) (Figure 5.2). The methyl group on the indole ring also appeared to interact with residues from Arp2. Indeed, a similar molecule, CK-636, was much less effective at inhibiting Arp2/3 complex activity, seemingly because it had a smaller thiophene ring instead of a benzene ring and thus filled the hydrophobic cavity less well (Figure 5.2). CK-689 was a completely inactive molecule (and is available commercially as a negative control for CK-666), probably due to the absence of the methyl group on the indole ring and the lack of an aromatic portion to fill the hydrophobic pocket at the Arp2/Arp3 interface (Figure 5.2).

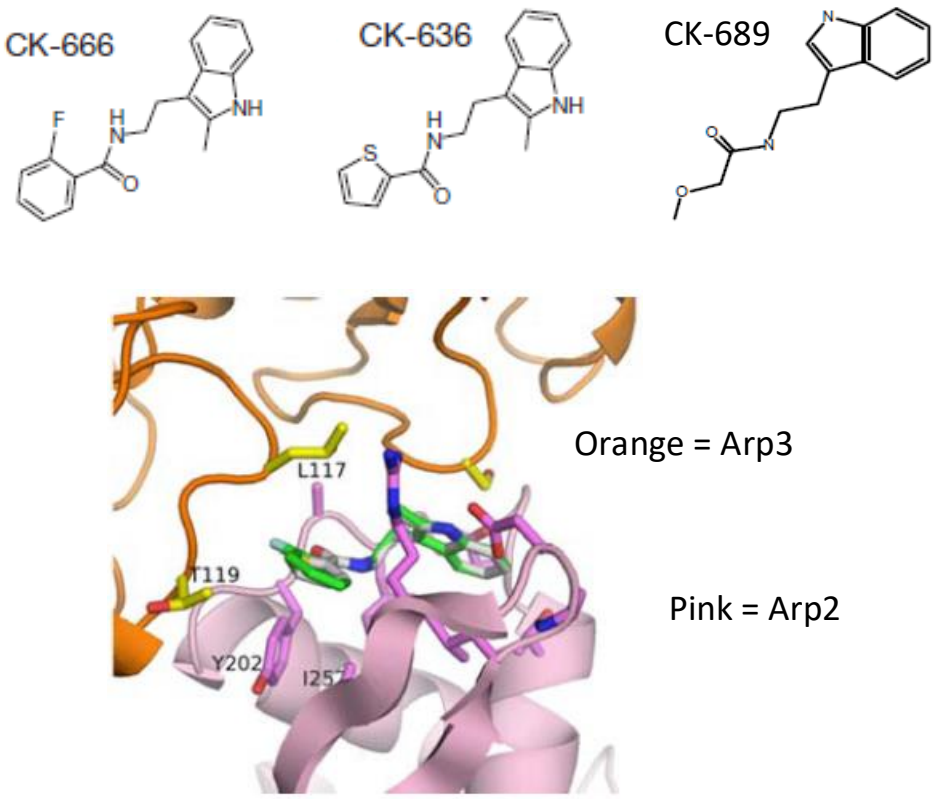

Figure 5.2 - Binding of CK-666. CK-666 (top left) binds at the Arp2/Arp3 interface as shown in the ribbon diagram (bottom). CK-636 binds less effectively and CK-689 is the inactive from of CK-666. From (Nolen et al., 2009).

CK-666 was found to inhibit Arp2/3 complex nucleation *in vitro*, but was also shown to inhibit actin comet formation on *Listeria* in cells, thus demonstrating that the molecule was cell permeable and active in cellular conditions (Figure 5.3). It was noted, however, that CK-666 potency depended on cell type and actin structure, since *Listeria* comets and monocyte podosomes (a type of adhesion structure) were completely disrupted by CK-666, but keratocyte motility and shape were only slightly affected (Nolen et al., 2009). Today CK-666 is widely used in many different contexts as it is simple to use, and has low toxicity and high efficiency. Using this drug, many actin-remodeling processes were revealed to depend on Arp2/3 complex nucleation: F-actin nucleated on chromosomes that helps their capture by microtubules (Burdyniuk et al., 2018), nuclear F-actin that drives the relocalization of heterochromatin breaks (Caridi et al., 2018), maintenance of asymmetric meiotic spindle position in mouse oocytes (Chaigne et al., 2013; Yi et al., 2011) and lamellipodial architecture and cell shape and spreading (Henson et al., 2015), just to name a few examples.

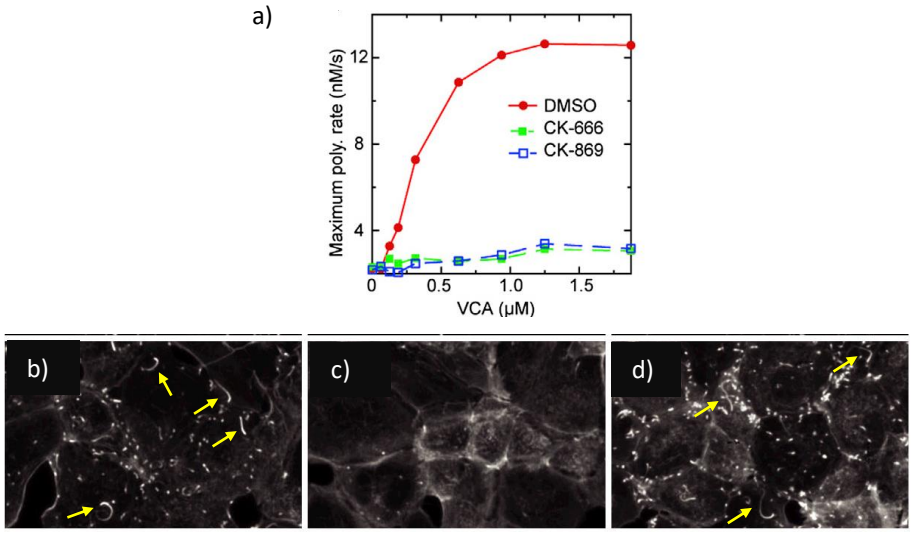

Figure 5.3 - CK-666 inhibits actin polymerization *in vitro* and *Listeria* comet formation in cells. a) Plot of polymerization rate (measured by pyrene actin assay) as a function of increasing concentrations of N-WASP-VCA, in the presence of 20 nM bovine Arp2/3 complex and 200 µM CK-666, CK-869 or DMSO. CK-666 and CK-869 inhibited actin polymerization, regardless of the concentrations of the NPF. From (Hetrick et al., 2013). Although just as functional as CK-666, CK-869 was not pursued as its mode of action was unclear (Nolen et al., 2009). b-d) Effects of CK-666 on *Listeria* comet tails in cells. b) DMSO treatment for 60 minutes where actin comets were observed on *Listeria* (yellow arrows). c) 40 µM CK-666 treatment for 60 minutes, where no actin tails were observed on *Listeria*. d) 40 µM CK-666 treatment for 60 minutes then 60 minutes washout, where actin comets appeared again (yellow arrows). Actin visualized with fluorescent phalloidin. From (Nolen et al., 2009).

5.1.2 Photoswitchable Arp2/3 complex inhibitors based on CK-666

Although CK-666 paved the way for many new studies in the field, its action was global, and there was no possibility to limit Arp2/3 complex inhibition to a specific subcellular compartment or to a specific region in more complex multicellular systems. Such spatial and temporal control of small molecule activity had been demonstrated for microtubule drugs. Chemists Oliver Thorn-Seshold and Dirk Trauner at Ludwig-Maximilians-University, Munich (Trauner current address New York University) developed microtubule inhibiting drugs based on colchicine that could be switched between active and inactive forms by illumination at different wavelengths (Borowiak et al., 2015). Amongst other tests, photostatin-1 (PST-1) had been validated on *C. elegans* embryos (Figure 5.4). We therefore contacted Thorn-Seshold in order to obtain PST-1 for treating non-*Caenorhabditis* embryos, as mentioned above and described in Chapter 6. At the time, they were in the process of developing a similar approach to inhibit Arp2/3 complex activity based on the structure of CK-666. They had developed a series of molecules, but were having trouble validating the molecules as Arp2/3 inhibitors. The

classic *in vitro* approach used to discover and characterize CK-666, the pyrene assay, was not feasible with their molecules because the emission of pyrene-actin in the fluorimeter was close to the switching wavelength of the molecules. Their tests on cells had also been inconclusive, but as mentioned previously, CK-666 itself has variable potency dependent on cell type. Since I was also interested in using photoswitchable actin drugs in my embryo project, I was happy to help characterize their molecules using the bead/comet assay described in Chapter 3.

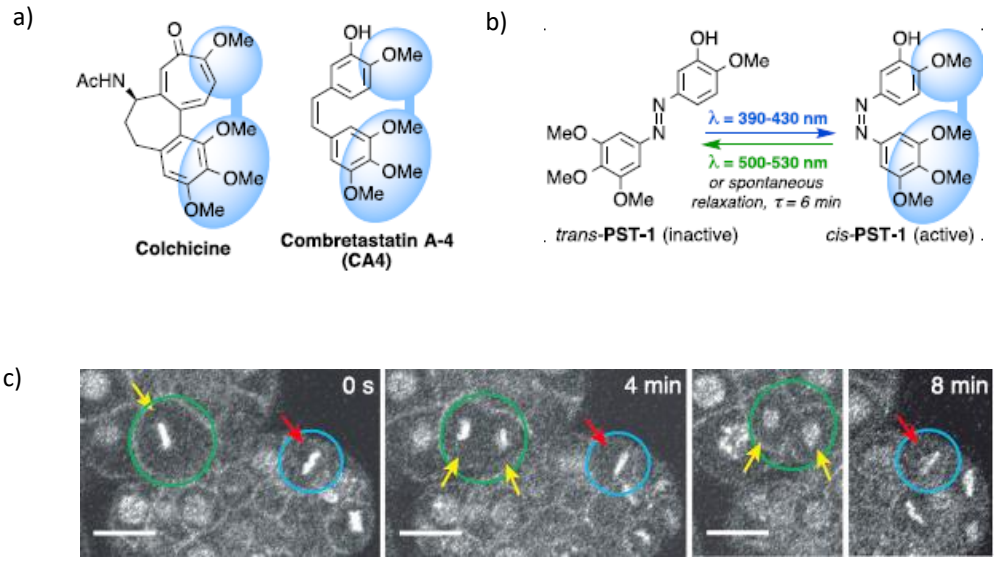

Figure 5.4 - A photoswitchable microtubule inhibitor. a) Photostatin-1 (PST-1) is based on the colchicine, combretastatin family of microtubule polymerization inhibitors. b) PST-1 can be switched from the inactive to the active form by application of blue light and reconverted to the inactive form by green light. c) Multicellular *C. elegans* embryo permeabilized and treated with 40 µM PST-1. Cells circled in blue were illuminated with blue light, while cells circled in green were illuminated with blue light followed by green light. Blue light illumination arrested cell division, while un-illuminated or blue-then-green illumination gave normal cell division. Cell membranes and histones fluorescently labeled. Scale bar 10 µm. From (Borowiak et al., 2015).

5.2 Results with photoswitchable Arp2/3 complex inhibitors

5.2.1 Effect of molecules on actin network polymerization *in vitro*

The molecules they developed were based on CK-666 with addition of motifs to the benzene ring of CK-666 to induce control by light (Table 5.1). These molecules were synthesized in a *trans* conformation and needed to be illuminated at specific wavelengths to undergo a conformational change to the *cis* conformation. Some were predicted to be active to inhibit the Arp2/3 complex in *trans* form and others in *cis* form, while switching was induced by different wavelengths, with the *cis* form sometimes switching spontaneously back to the *trans* form or requiring another wavelength illumination for the conversion (Table 5.1).

Table 5.1: Putative photoswitchable inhibitors of the Arp2/3 complex: chemical formulas, predicted active state (inhibitory) and switching parameters.

Molecule	Structure	Predicted active state	Switching properties
CK-666	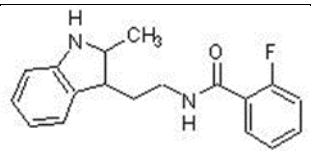		
LU06	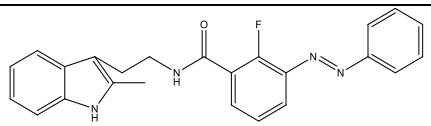	cis	350 nm trans→cis
LU16	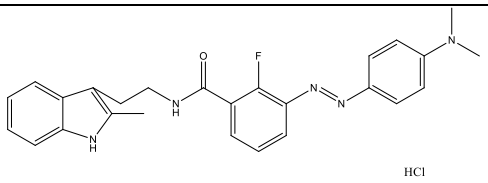	cis	450 nm trans→cis Spontaneous relaxation << 1 sec
LU09	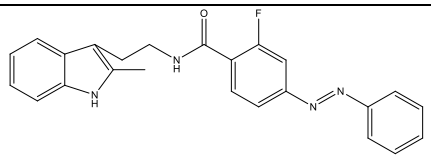	trans	350 nm trans→cis
LU14	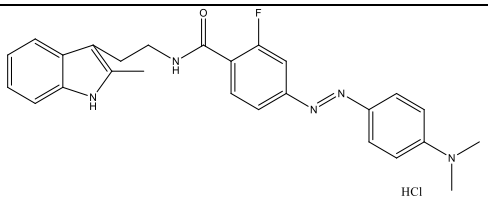	trans	Like LU16
LU50	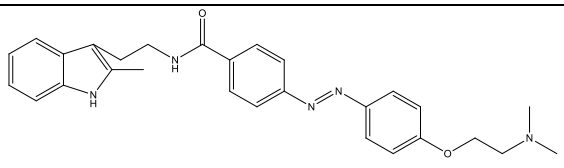	trans	380 nm trans→cis 420 nm cis→trans
LU36	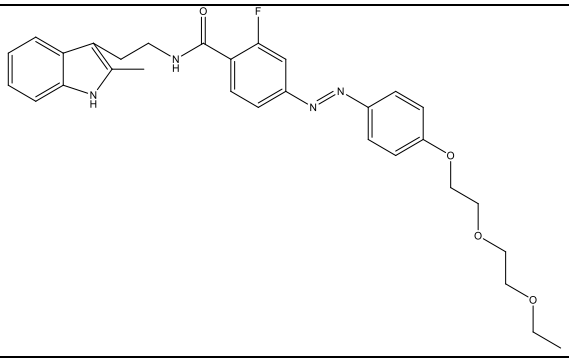	trans	380 nm trans→cis Spontaneous relaxation ~5 h 420 nm cis→trans

I first verified that CK-666 was able to inhibit comet formation in my bead assay, compared to a control with comparable amounts of DMSO. DMSO did not inhibit comet formation, but CK-666 did at 200 µM (Figure 5.5). Lower concentrations were not efficient, and even 200 µM of CK-666 could not inhibit comet formation when a more active form of pVCA was used to coat the beads (S-pVCA, see Chapter 4). This was not a problem per se, but it should be kept in mind that CK-666 inhibitory effect on Arp2/3 complex in my bead assay conditions was not as absolute as had been observed in some systems.

I then tested all the molecules in Table 5.1 in their *trans* state (without illumination), and measured comet length over time for the whole population of beads in the sample in order to calculate the speed of bead movement (Figure 5.5). Speeds ranged from 0.2 to 0.4 µm/min, which is standard for this assay with large beads, for all molecules except LU06 and LU16. Beads treated with these compounds had little actin polymerization around the beads as compared to the control, and the comets did not grow appreciably in length over time (Figure 5.5). Furthermore, detached comets were often observed with LU06 and LU16 treatment. All of these observations suggested a reduced activity of the Arp2/3 complex in the presence of LU06 and LU16. This was somewhat of a surprise as these molecules were supposed to be inactive in the *trans* state. Our chemist collaborators had no answer to this, except to say that predicting binding interactions from crystal structure data was not always accurate. Nevertheless, the inhibition activity of LU06 and LU16 was not as good as CK-666, as some actin still polymerized around the beads indicating a residual activity of the Arp2/3 complex. However, this could be due to the fact that these molecules had a major solubility problem, evidence of which I noticed as large quantities of grainy-like structures in the polymerization reaction. This was also the case of LU36 (Figure 5.5), while LU50 seemed to have the best solubility.

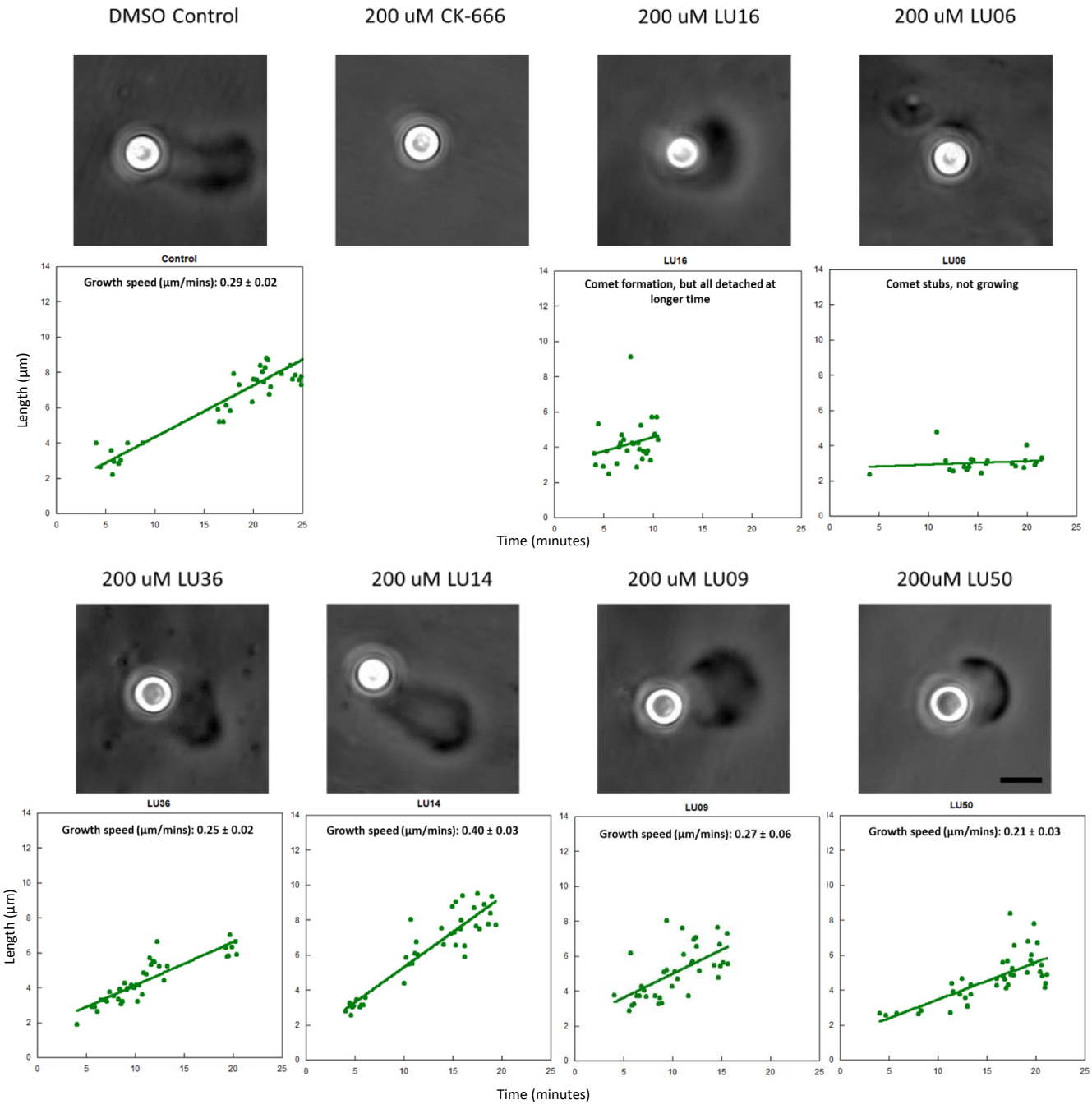

Figure 5.5 - Effect of photoswitchable molecules in their non-illuminated form on actin comet polymerization and bead speeds. Representative phase contrast microscopy images were taken 15-20 minutes after polymerization was started, except LU16 as beads detached around 12 minutes. Plots show the length of comets (measured 4-25 minutes from the beginning of the reaction) as a function of time. The slope represents the speed of comet growth. CK-666 inhibited all actin polymerization around the beads. LU06 and LU16 had little actin growth around the beads indicating they inhibit Arp2/3 complex activity. Scale bar 5 µm.

5.2.2 Photoswitching LU06

Although the discovery that LU06 and LU16 were active to inhibit the Arp2/3 complex in their *trans* conformation was a surprise, I decided to pursue photoswitching with these molecules. Since LU06 inhibited Arp2/3 complex *in vitro*, and unlike LU16, did not spontaneously convert from *cis* to *trans* state, I pursued mainly LU06. In the spectrophotometer, I succeeded in switching 20 µM LU06 from *trans* to *cis* conformation easily with light at a wavelength of 360 nm, and switching it mostly back to the *trans* state with 420 nm illumination (Figure 5.6). However, in a more concentrated solution, the *cis* to *trans* conversion was very inefficient (Figure 5.6).

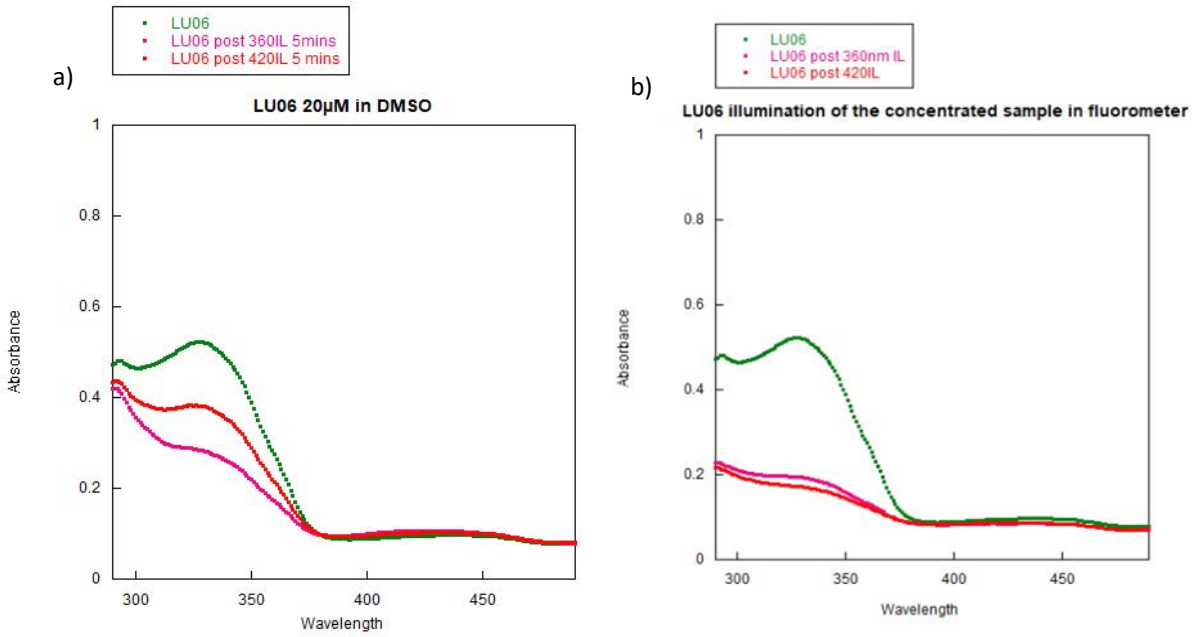

Figure 5.6 - Photoswitching of LU06. a) Absorbance curves of 20 µM LU06 diluted in DMSO using spectrophotometer. Green curve is the absorbance of LU06 in its initial *trans* state with a peak around 330 nm. The peak diminishes following 5 minutes of illumination with 360 nm light, pink curve, indicating conversion to the *cis* form. The 330 nm peak partially returns after illumination for 5 minutes with light at 420 nm, indicating partial recovery of the active *trans* state. b) The same as a) except 2 mM LU06 was used. In this concentrated solution, photoswitching back to the *trans* state did not occur.

The next step was to test the effect of photoswitching on the activity of the molecule. I converted LU06 from *trans* to *cis* with 360 nm illumination and then applied it to the bead assay. I found that this pre-treatment of LU06 induced the formation of a thick actin network around the beads that broke open and formed comets in most of the cases, just like polymerization conditions in absence of any drug (Figure 5.7). This suggested that LU06 was inactivated by illumination at a wavelength of 360nm, and its inhibitory activity of the Arp2/3 complex was significantly reduced. At the high concentrations needed to add to the bead assay,

switching the molecule back to its *trans* form proved to be complicated (Figure 5.6), so I could not test if the double illumination restored the inhibitory activity of LU06. The next step was photoswitching of LU06 *in situ* instead of pre-conversion before addition to the polymerization reaction tube. However direct illumination of samples of polymerizing actin remain to be optimized. I found that LED illumination of the polymerization reaction between slide and coverslip was toxic to actin polymerization itself even in control conditions. Probably photodamage of the actin network was caused by strong illumination for relatively long times (several minutes) at blue light wavelengths. So although I identified a molecule with photoswitchable Arp2/3 complex inhibitory properties, I could not perform live photoswitching of the molecule during the polymerization process.

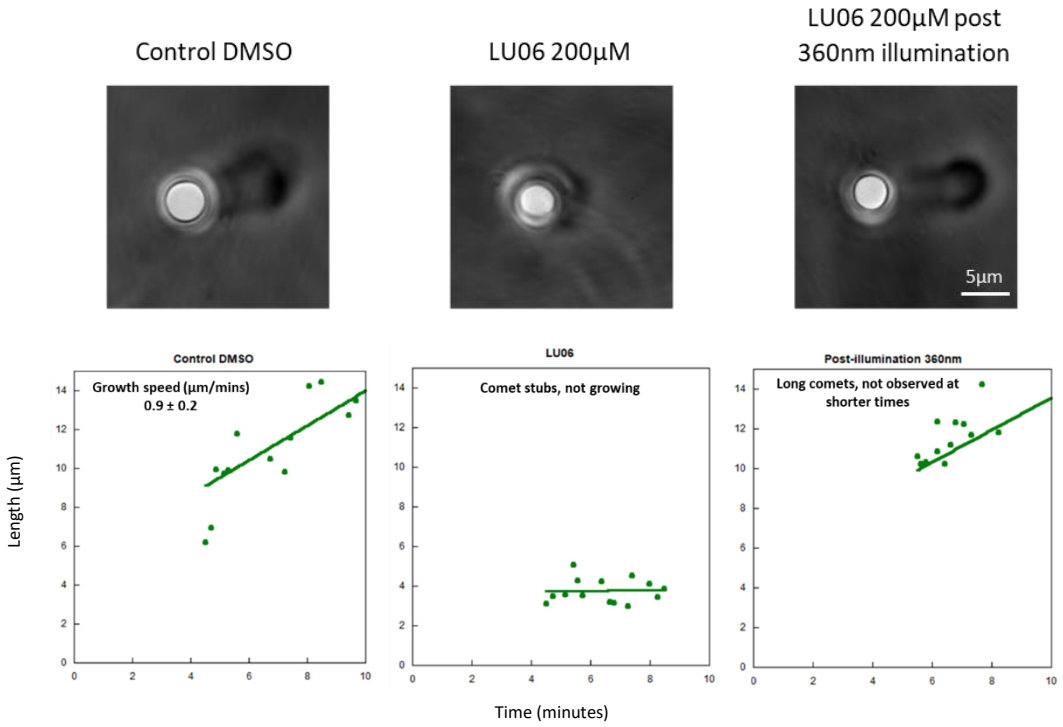

Figure 5.7 - Effect of photoswitching of LU06 on actin polymerization *in vitro.* Phase contrast microscopy images taken at 10 minutes from the start of the polymerization reaction. Dot plots represent length of comets of beads taken over timeLU06 reduced comet speed compared to control condition, as shown before. Illumination of LU06 at 360 nm before addition to the assay restored actin comet formation around the beads. Scale bar 5 µm.

5.2.3 Attempts to improve solubility of LU06-type compounds

One of the other problems with LU06 was that it was relatively insoluble in physiological conditions, and much of the sample was precipitated. It was necessary to apply large concentrations to the polymerization reactions for this reason, magnifying the photodamage problem since longer exposure times were necessary to convert more concentrated samples.

The chemists therefore synthesized two additional molecules with extensions similar to those of LU50, which as noted previously, had enhanced solubility as compared to the others (Table 5.2). I tested these molecules, and although solubility was much improved, these molecules did not inhibit comet formation in the bead assay, and could thus be considered inactive for inhibiting the Arp2/3 complex (Figure 5.8).

Table 5.2 Modifications of LU06, designed in order to increase its solubility.

NW2003	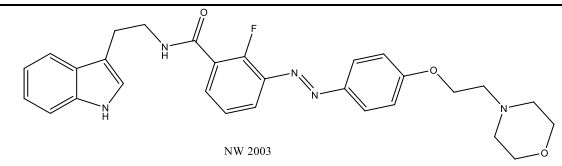	Predicted active in *trans* state by analogy to LU06
NW2069	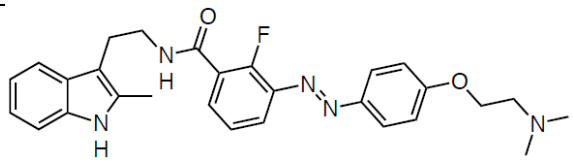	Predicted active in *trans* state by analogy to LU06

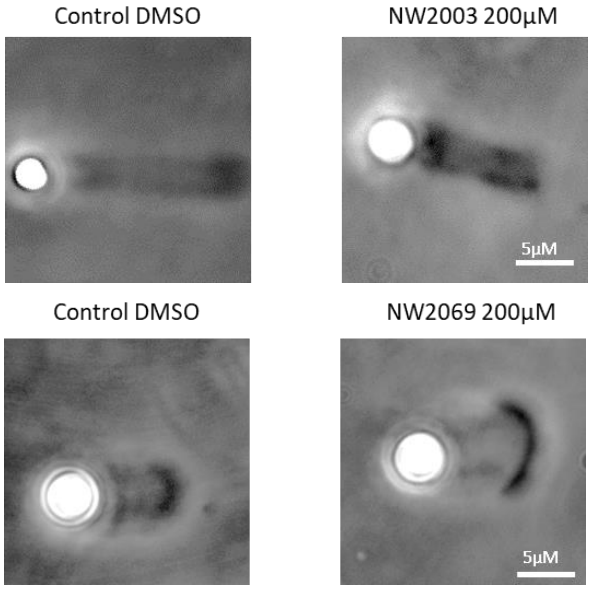

Figure 5.8 - Tests of NW2003 and NW2069 molecules and their effect on actin polymerization around beads (2 µm beads for NW2003 and 4.5 µm beads for NW2069). Phase contrast microscopy images taken at 10 minutes from the start of the polymerization reaction. Both molecules had good solubility but had no inhibitory effect on actin polymerization *in vitro*, suggesting that they are incapable of inhibiting Arp2/3 complex. Scale bar 5 µm.

5.3 Conclusions and perspectives.

In this study, I identified through a collaboration with chemists a new molecule that inhibits the Arp2/3 complex, LU06, based on CK-666 as a structural backbone. I showed that LU06 activity could be controlled by light: being active in its *trans* state, it can be inactivated to the *cis* state after a few minutes of illumination with blue light. This molecule is very promising, yet it still needs optimization to increase its solubility in physiological conditions. Increased solubility will enhance the inhibitory effect it has on the Arp2/3 complex, so lower doses can be used, thus boosting its photoswitching capacity (more dilute solutions photoswitch more rapidly) and thus solving the phototoxicity issue by allowing for a reduction in illumination times. With future versions of LU06, local control of Arp2/3 complex activity will become possible. Cells, tissues or organisms can be soaked in the inactive form of the drug, and then localized illumination to activate the molecule will produce a local zone of Arp2/3 complex inhibition. Adjacent zones can be flashed with the deactivating wavelength to assure that diffusing active molecule is converted back to the inactive form. When the experiment is over, the original region of interest can be illuminated with the deactivating wavelength as well, so that subsequent processes are not interfered with. Photoswitchable derivatives of LU06 will give us added control over the inhibition of the Arp2/3 complex that current drug treatments and genetic modifications do not provide.

Chapter 6: Exploring Actin Architecture *in vivo* in Nematode Embryos

6.1 Introduction

At the outset Chapter 4 and 5 were side-projects, and the subject of this chapter was my main PhD project. At the two-year mark, I had made lots of progress in determining what didn't work, as detailed in this chapter. However, projecting ahead, it seemed unlikely that I would obtain enough results with the nematode embryos to author a publication. This was due to several factors, not least the slow growth and tricky manipulation of embryos from non-*Caenorhabditis elegans* embryos that were the subject of this chapter, but also due to technical advances by other labs, which rendered some of my preliminary results less interesting to pursue because better methods had become available since I had started the project. So overall this is an exploratory chapter in which I tested different tools to investigate the role of the acto-myosin cytoskeleton in the first asymmetric cell division in different nematode species. Since these are essentially trouble-shooting results, some of the materials and methods are detailed along with the preliminary results, except for standard protocols and buffer recipes, which are described in section 6.5 of this chapter.

6.1.1 Goal of the study

Cell division, including asymmetric cell division, is known to rely in part on the acto-myosin cortex, introduced in Chapter 1. In this chapter I aimed to understand how drastically different acto-myosin cortical dynamics could invariantly give rise to asymmetric cell divisions, both in fate and in size. This project came out of discussions with Marie Delattre (ENS, Lyon) who had observed that although nematode embryos outside the *Caenorhabditis* genus all undergo a first asymmetric cell division like *C. elegans*, with differential daughter cell sizes and fates (Valfort et al., 2018), the steps leading up to division appeared very different in non-*Caenorhabditis* genera. In particular, nematodes from other genera often had embryos with drastically enhanced cortical shape changes right up to the moment of cytokinesis. It was not clear, in these cases, how asymmetric division was assured with the same fidelity as in *C. elegans*. The goal of this project was to understand how the acto-myosin cortical cytoskeleton contributed to the first asymmetric cell division across nematode species, with the broader goal of understanding asymmetric cell division beyond what was known from current model systems.

6.1.2 Asymmetric cell division

Asymmetric cell divisions are characterized by differential inheritance of cell fate determinants and also often involve precise size differences between daughter cells (Cabernard, 2017). Such divisions are often a key step in cell differentiation programs, including those that maintain pools of stem and progenitor cells. Indeed, misregulation of asymmetric cell divisions in flies, mice and humans has been linked to lack of differentiation, inappropriate proliferation and tumorigenesis (Gomez-Lopez et al., 2014; Knoblich, 2010). To date, much of our knowledge on the mechanisms of asymmetric mitotic cell division has been based on a relatively limited number of model systems, most notably *Drosophila melanogaster* neuroblasts and the *Caenorhabditis elegans* embryo. It is currently not known if all asymmetric mitotic events occur like this or if alternative strategies exist. The first cell division in *C. elegans* results in two daughter cells that are asymmetric both in size and fate determinants, which is essential for subsequent tissue specification during the development of the embryo. In the following, I will explain briefly the major steps of the first asymmetric cell division in *C. elegans*, consisting of symmetry breaking, polarity establishment and finally spindle positioning for asymmetric division.

6.1.3 Symmetry breaking

The first step in the sequence of events leading to asymmetric cell division is oocyte fertilization. In *C. elegans*, fertilization takes place as non-polarized oocytes pass through the spermatheca of the worm (Figure 6.1). Consequently, the embryo moves through the uterus as it continues embryogenesis until egg-laying via the vulva. The sperm usually enters the oocyte at the end opposite from the female pronucleus or readjusts to the opposite pole upon a more lateral entry (Goldstein and Hird, 1996). The sperm cell contributes DNA to the egg, in addition to a pair of centrioles that form the centrosome. Contact of the centrosome to the cortex is the cue to break the symmetry of the zygote (Cowan and Hyman, 2004). This triggers the polarization of the embryo and defines the anterior – posterior axis: the sperm entry site becomes the posterior pole and the opposite one is the anterior (Figure 6.2a, b).

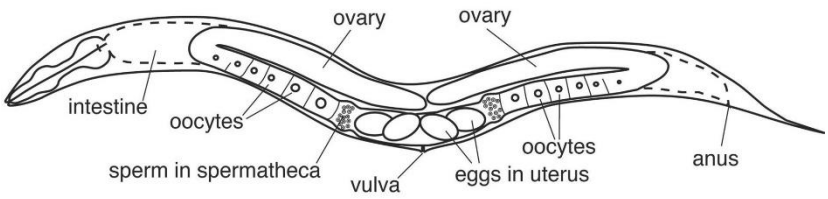

Figure 6.1 - Schematic representation of an adult *C. elegans* worm. The two-armed gonad is shown. Oocytes pass through the spermatheca, and then the embryo continues developing in the uterus until being laid via the vulva. From (Zarkower, 2006).

Polarization involves cortical flow in the anterior direction and posterior-directed cytoplasmic flow, which compensates for the anterior-directed cortical movement (Hird and White, 1993). Cortical flows coincide with the flow of acto-myosin foci at the cortex induced by the contraction of the entire acto-myosin network toward the anterior pole (Munro et al., 2004). This contractility is damped out after pronuclear meeting as the pronuclei migrate to the center of the embryo (Figure 6.2c).

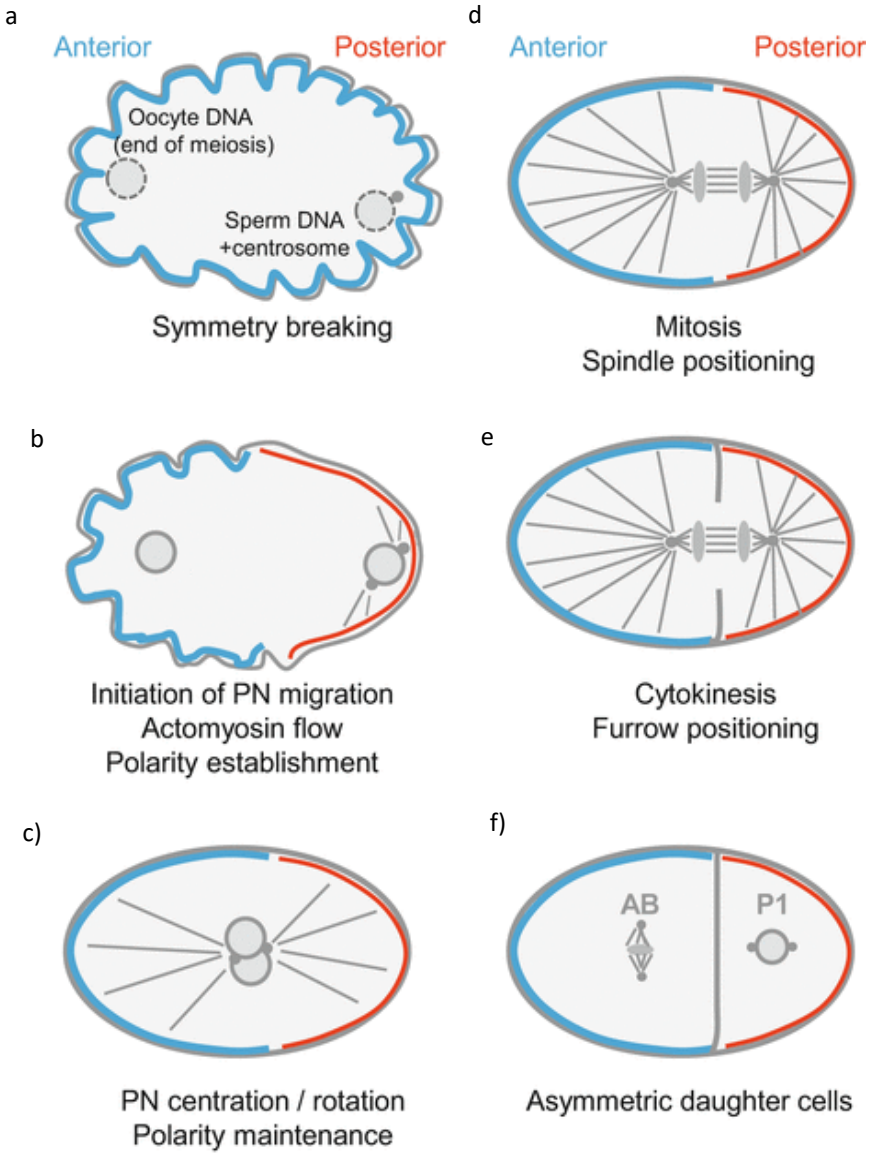

Figure 6.2 - Schematic representation of the steps leading to the first asymmetric cell division in the *C. elegans* embryo. The process is triggered by the sperm entry that leads to a symmetry breaking event, following by a phase of polarity establishment, spindle positioning and finally division. The asymmetric daughter cells will have different fates subsequently. From (Pacquelet, 2017).

6.1.4 Polarity establishment

Acto-myosin network contraction in the one cell embryo induces the asymmetric distribution of partitioning defective (PAR) proteins (Cowan and Hyman, 2007). In *C. elegans* there are six PAR genes that are essential for establishing anterior-posterior polarity (Kemphues et al., 1988). PAR-3 and PAR-6 proteins form a complex with protein kinase C (PKC-3). Shortly after fertilization, the complex diminishes from the posterior pole and evenly distributes at the cortex of the anterior pole (Cuenca et al., 2003). Contrary to the PAR-6/PAR-3/PKC complex, PAR-2 and PAR-1 localize to the posterior cortex only (Cuenca et al., 2003; Guo and Kemphues, 1995). Cortical flow of PAR-6 protein is coupled with movement of cortical myosin NMY-2, and consequently both of them are reduced when acto-myosin network contraction is diminished (Munro et al., 2004). FRAP experiments showed that PAR-6 and PAR-2 associate with the cortex dynamically during the cortical flow (Cheeks et al., 2004; Robin et al., 2014), while PAR-4 and PAR-5 proteins are uniformly distributed throughout the cortex and the cytoplasm (Watts et al., 2000). Interestingly, PAR proteins along with CDC-42 regulate acto-myosin flow in a positive feedback loop (Motegi and Sugimoto, 2006; Munro et al., 2004).

Following polarity establishment, a distinct maintenance phase takes place after pronuclei meeting. Since no physical boundaries exist between the two domains to prevent the flow of anterior and posterior PAR proteins, the mechanisms leading to mutual exclusion between PARs are essential in this phase (Cuenca et al., 2003; Goehring et al., 2011). PAR-2 is phosphorylated and thus excluded from the anterior cortex (Hao et al., 2006), while in the posterior cortex, it induces the phosphorylation and thus the exclusion of PAR-3 (Motegi et al., 2011). Furthermore, PAR-2 contributes to polarity maintenance through regulation of myosin but the mechanism is unknown (Munro et al., 2004).

6.1.5 Spindle positioning

During prometaphase, the spindle is assembled at the center of the embryo, but during anaphase it gets displaced toward the posterior part of the embryo (Figure 6.2d). Pulling forces exerted by astral microtubules emanating from the spindle poles and contacting the cortex contribute to this displacement (Grill et al., 2001; Grill et al., 2003). A cortical complex composed of Gα/GPR/LIN-5 proteins is required (Gotta et al., 2003; Park and Rose, 2008). When these proteins are depleted, the mitotic spindle stays in the center of the embryo which consequently divides symmetrically (Gotta et al., 2003). The microtubule motor dynein is also required for force generation, and is anchored to the cortex by the Gα /GPR/LIN-5 complex (Pecreaux et al., 2006). Pulling forces are stronger on the posterior side of the embryo because the Gα /GPR/LIN-5 complex is enriched there, and this enrichment is regulated by the PAR proteins (Gotta et al., 2003; Park and Rose, 2008). Actin as well contributes to the regulation of pulling forces exerted on the spindle: actin depolymerization increases pulling forces at the

anterior pole, suggesting that actin enrichment at the anterior cortex could negatively regulate anterior pulling forces by increasing cortex rigidity (Berends et al., 2013; Kozlowski et al., 2007). Since the spindle midzone is what dictates the division plane in most systems (McNally, 2013), the final result of the complex positioning machinery described above is the formation of the cytokinesis furrow off-centered from the middle of the embryo, resulting in a big anterior cell and a small posterior cell (Figure 6.2e, f).

Although the first asymmetric cell division in *C. elegans* is dictated by microtubules with actin playing a more minor role, other asymmetric divisions are driven by acto-myosin cytoskeleton dynamics. For example in mouse oocyte meiosis, the pronounced size asymmetry between the tiny polar body and the large oocyte is due to spindle positioning entirely dependent on cytoplasmic actin networks and the acto-myosin cortex as there are no centrosomes and no astral microtubules in these cells (Almonacid et al., 2015; Chaigne et al., 2015). Similarly, in *C. elegans* neuroblast mitosis, enhanced acto-myosin contractility at the cortex of one of the daughter cells results in an asymmetric cleavage (Ou et al., 2010).

6.2 Preliminary results actin visualization

In order to examine the diversity of behaviors leading up to the asymmetric cell division of the nematode one-cell embryo, I chose to work with two nematode species evolutionarily distant from *C. elegans*: *Oscheius tipulae* (CEW1) and *Pristionchus pacificus* (PS312). We chose these species because they could be maintained and manipulated in the lab following procedures for *C. elegans*, and their genomes had been sequenced. One cell embryos of *C. elegans*, *O. tipulae* and *P. pacificus* were filmed for the whole period of the first cell division. By DIC microscopy *O. tipulae* and *P. pacificus* embryos displayed enhanced shape changes in the anterior cortex, accompanied by pronounced cytoplasmic flows (Figure 6.3), as also previously observed by our collaborator Marie Delattre (ENS Lyon, personal communication). Cortical deformations continued after pronuclear meeting and well into the spindle centering phase, while similar cortical deformations (called the pseudo cleavage furrow) in *C. elegans* disappeared at pronuclear meeting and the cortex remained smooth until cytokinesis. Cortical shape changes indicated high acto-myosin contractility at the anterior pole of these embryos, suggesting an upregulation of acto-myosin dynamics over a longer time window during mitosis compared to *C. elegans.* This suggested that *O. tipulae* and *P. pacificus* embryos might have enhanced actin signal at the anterior pole compared to *C. elegans*. To test this hypothesis, I set out to visualize the actin cytoskeleton in *O. tipulae* and *P. pacificus* embryos. At the time neither one of these species was genetically modifiable so expressing fluorescent reporter proteins, as had so fruitfully done with *C. elegans*, was not an option. I therefore searched for alternative methods to visualize the actin cytoskeleton.

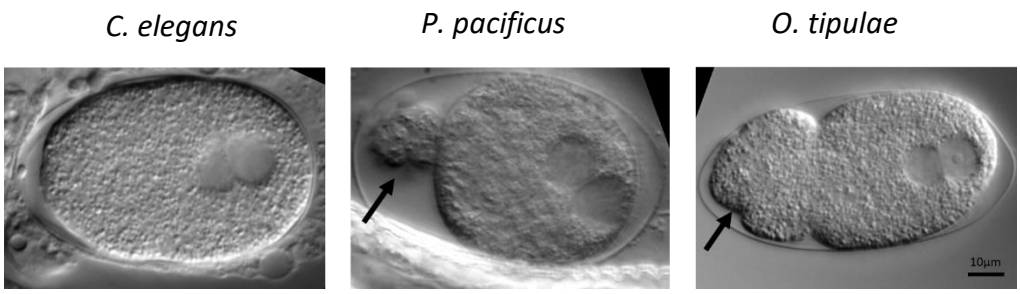

Figure 6.3 - Cortical shape variability across nematode species at the stage of pronuclear meeting. The anterior pole is to the left. Cortical ruffling is apparent in the anterior pole in *P. pacificus* and *O. tipulae,* while such deformations are not present in *C. elegans* embryos. Arrows point to cortical ruffling. DIC microscopy. Scale bar 10 µm.

6.2.1 Actin labeling of live embryos

SiR-actin tests

One method I tested was the injection of fluorescent labels into the syncytial gonad of *P. pacificus* for subsequent uptake into the nascent embryos upon cellularization. First I tried the newly developed actin live imaging probe SiR-Actin (Lukinavičius et al., 2014) (Figure 6.4). SiR-actin is a cell-permeable fluorescent label of filamentous actin based on the actin drug jasplakinolide modified with a silicon rhodamine far red fluorophore for live imaging of actin cytoskeleton in cells (D'Este et al., 2015; Romarowski et al., 2018).

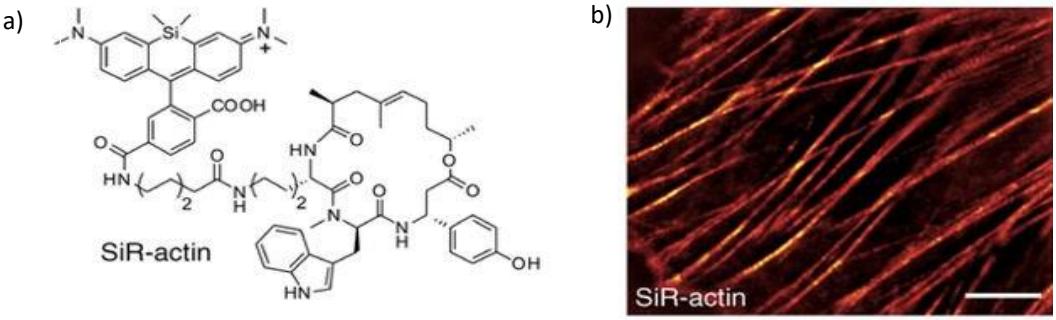

Figure 6.4 - Sir-actin probe to mark actin filaments. a) Structure of SiR-actin probe. b) Structured illumination microscopy (SIM) images of human fibroblasts stained with SiR-actin. Scale bar 5 µm. From (Lukinavičius et al., 2014).

After injection of 500 µM SiR-actin label, worms were incubated for four to six hours to allow for uptake, and then embryos were dissected out and mounted to be imaged. Using a spinning disk microscope, I noticed that the newly formed embryos did not have any SiR-actin fluorescence signal. In fact, imaging whole worms, I consistently observed that SiR-actin was not incorporated into the newly formed embryos at all, but was instead stuck in the membrane at the injection site (Figure 6.5). One explanation for such an effect could be the greasy nature of the molecule that rendered it hydrophobic and led to its aggregation in the gonadal membrane.

Figure 6.5 - SiR-Actin aggregates in the worm gonad at the injection site and is not incorporated into the newly formed embryos. Transmitted light image overlayed with spinning disk far red fluorescence channel.

Lifeact-FITC tests

As an alternative to SiR-actin I turned to Lifeact a 17-amino-acid peptide from yeast (Riedl et al., 2008) used successfully in many cells and organisms to visualize actin cytoskeleton dynamics (Riedl et al., 2008; Riedl et al., 2010; Suarez et al., 2015). I used a custom-made FITC-labeled Lifeact peptide that was delivered by injecting 250 µM into the gonad similarly to SiR-actin. Unlike SiR-actin, Lifeact-FITC got taken up into the embryos, but did not appear to label actin filaments, instead displaying fluorescent puncta (Figure 6.6a). On the other hand, I demonstrated by TIRF microscopy that the Lifeact-FITC label was able to decorate preformed actin filaments *in vitro* (Figure 6.6b). Since the custom-made peptide was active *in vitro*, its lack of activity *in vivo* was probably a consequence of proteases *in vivo* that degraded the peptide due to its unfolded structure. Much later I learned that Kinneret Keren (The Technion, Israel) had had a similar experience with Lifeact peptide injection in hydra, and she had found that

injection of the GFP labeled peptide got around this degradation problem (K. Keren, personal communication).

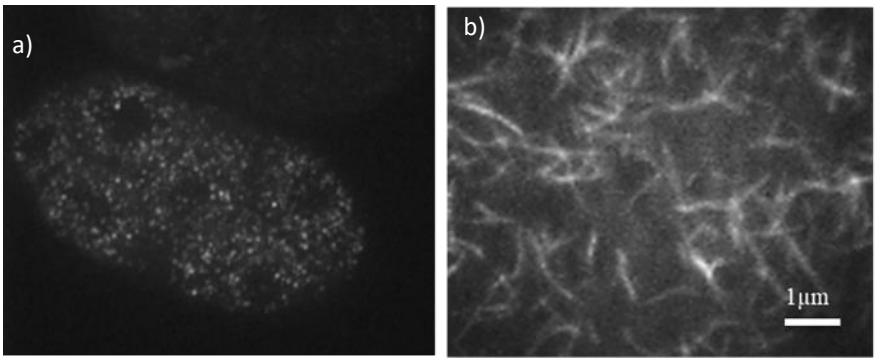

Figure 6.6 - Lifeact-FITC peptide *in vivo* and *in vitro*. a) Multistage embryo showing spotty fluorescence after 8 hours of Lifeact-FITC injection into the gonad of the worm. No actin filaments are labelled. b) TIRF image of labeling of preformed non-fluorescent actin filaments using Lifeact-FITC.

6.2.2 Phalloidin labeling of fixed samples

Since live-embryo imaging was not possible due to difficulty with actin labeling, I turned to fixation and phalloidin staining to observe the actin network in *O. tipulae* and *P. pacificus* embryos, as compared to *C. elegans*. I used a protocol for permeabilizing, fixing and staining embryos inspired by the protocol for *C. elegans* embryos that I adapted for my species (Costa et al., 1997). Briefly embryos were extracted from worms and transferred to polylysine coated slides and incubated in chitinase solution (300 µL, 2U/mL final solution) for 10 minutes in order to permeabilize the eggshell. Embryos where then fixed in Fix Solution (see section 6.5) supplemented with unlabeled phalloidin to stabilize the actin cytoskeleton for 30-40 minutes. After washes with PBST (section 6.5), the embryos were incubated with 0.2 µg/mL phalloidin Alexa-488 for 1 hour in the dark. Slides were mounted in Vectashield solution containing 5 µg/mL DAPI, sealed and imaged using a spinning disk microscope.

Some of the nicest images obtained with this treatment are shown in Figure 6.7. Looking at the medial plane, the asymmetry in actin appeared similar in *C. elegans*, *P. pacificus* and *O. tipulae*, but this was less obvious in the cortical plane for *P. pacificus* and *O. tipulae*. Qualitative differences in the cortical plane were also observed, with *P. pacificus* and *O. tipulae* displaying more bundles and long-range structures, seemingly extending into the cytoplasm of *O. tipulae*. This data should be taken with a grain of salt however, as the results were not very reproducible. As an example, Figure 6.8 shows 6 other images of *O. tipulae*, all more or less at the moment of pronuclear meeting (DAPI staining was not always effective and stage was determined roughly from DIC images). Both in the medial and cortical planes, phalloidin staining was highly variable as some embryos showed abundant cytoplasmic actin structures

(top middle), other showed little cytoplasmic actin (bottom middle). Some showed a high density of actin at the cortex (top left) while others did not show actin signal at the cortex (top middle) or showed inhomogeneity in the actin signal at the cortex between the posterior and anterior poles (bottom right). *P. pacificus* was of similar variability. It was not clear why the data was so inconsistent. Possibly protocols designed for *C. elegans* were not suitable for *P. pacificus* and *O. tipulae* due to differences in the eggshell or the underlying vitelline membrane. Also the low number of embryos obtained at the correct stage for *P. pacificus* and *O. tipulae* made it difficult to obtain adequate statistics. Due to differences in egg-laying, *C.* elegans routinely held several embryos of which one or two were the right stage, while *P. pacificus* and *O. tipulae* held only one or two embryos total and at least 30 worms had to be dissected to get a handful of appropriately-staged embryos. Even with that, very few one cell embryos were at the exact same stage.

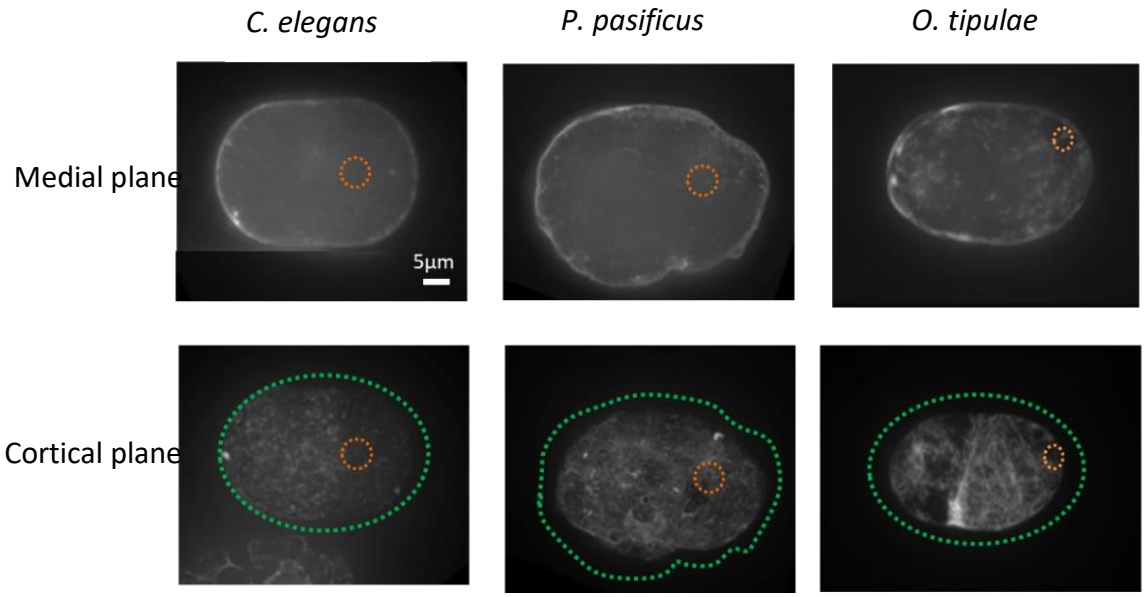

Figure 6.7 - Actin cortex in different nematode species. Phalloidin staining of the actin cytoskeleton of fixed embryos of *P. pacificus* and *O. tipulae*, compared to *C. elegans*, at similar stages during the first cell division. Posterior poles are towards the right; top panels are the medial plane (the cross-section), and bottom panels the cortical plane (the embryo surface). Pronuclei position was determined using transmitted light images and is represented by orange circles. Spinning disk confocal microscopy. Scale bar 5 µm.

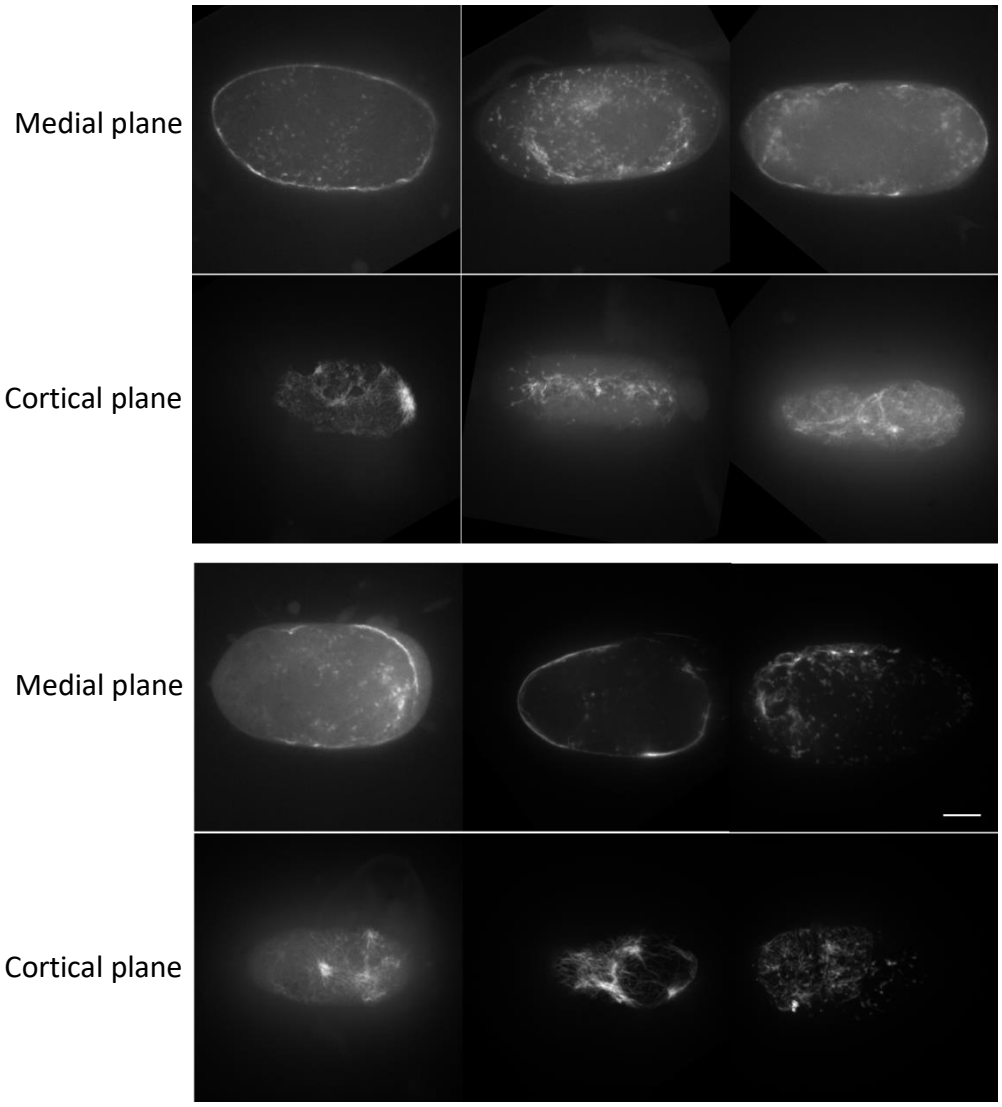

Figure 6.8 – Example of variability in phalloidin staining of permeabilized embryos. Embryos of *O. tipulae* that are around the same stage (pronuclear meeting/early after pronuclear meeting). The cortical and medial planes for each embryo look different from the others. Stage was determined using DIC. Posterior poles are towards the right. Spinning disk confocal microscopy. Scale bar 5 µm.

6.2.3 Conclusions actin visualization

The overall conclusion from these attempts was that actin visualization, both in live embryos and in fixed samples, would have to wait for the development of genetic methods of label expression in these species, since both injection of fluorescent labels and permeabilization/staining proved to be inefficient and irreproducible. Two studies have now been published that confirm that genetic modification is possible. *P. pacificus* was shown to be amenable to transgenesis by bombardment with antibiotic selection (Namai and Sugimoto, 2018). Furthermore, this group has successfully produced *P. pacificus* expressing Lifeact-GFP in the one-cell embryo (personal communication, Asako Sugimoto, Tohoku University). *O. tipulae* has been shown to be responsive to CRISPR/Cas9 treatment (Vargas-Velazquez et al., 2019), opening up the possibility of introducing Lifeact-GFP into the genome. In the face of these technological advances and given the difficulty of using non-genetic methods for visualizing actin, I did not continue this project.

6.3 First tests rheology of nematode embryos

Although in the previous sections I focused on the acto-myosin cortex, it was possible that some of the differences observed between *C. elegans*, *P. pacificus* and *O. tipulae* were due to differences in cytoplasmic properties. Indeed, work of our collaborator, Marie Delattre, showed that stereotypical transverse oscillations of the spindle, characteristic of astral microtubule pulling forces in *C. elegans* embryos, were missing in *O. tipulae* and *P. pacificus* (Valfort et al., 2018). It was possible that the lack of classical spindle movements was due to increased cytoplasmic viscosity, perhaps because of increased cytoplasmic actin or differences in myosin activity. In our lab, rheological measurements based on optical trapping of endogenous vesicles in mouse oocytes has been used to demonstrate that cytoplasmic molecular motors fluidize the cytoplasm of mouse oocytes, important for nuclear centering (Figure 6.9) (Almonacid et al., 2015). With that in mind, I sought to measure local mechanical properties within embryos of different species and in *C. elegans*.

6.3.1 Optical trapping of endogenous granules

The first idea was to optically trap endogenous vesicles present in the cytoplasm of embryos. Applying a sinusoidal force and measuring the resulting displacement could then be used to calculate the elastic and viscous moduli of the surrounding cytoplasm. This approach had the advantage of being completely non-invasive and not requiring fluorescent labels.

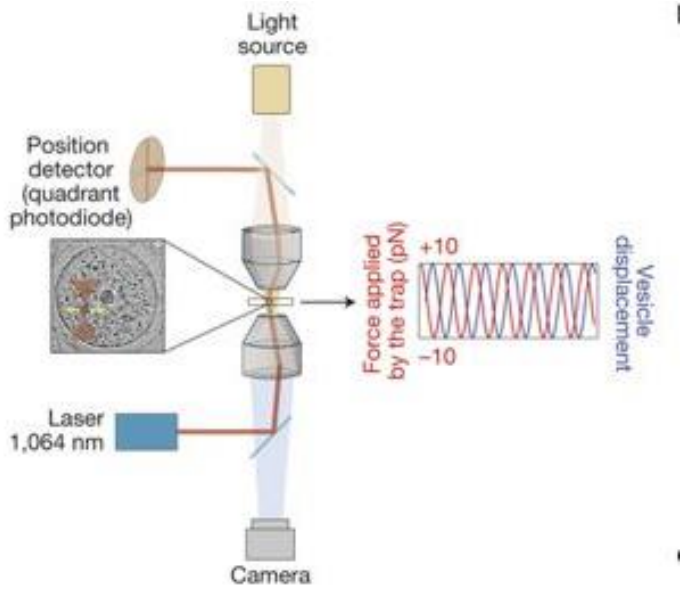

Figure 6.9 - Optical tweezer system to measure mechanical properties of the oocyte cytoplasm. A sinusoidal force was applied to trapped vesicles and the displacement was measured to calculate elastic and viscous moduli. From (Almonacid et al., 2015).

The experiments were done in collaboration with Wylie Ahmed, a post-doc in the team at the time. *C. elegans* worms were tested first to see if the method was feasible. Worms were incubated in levamisole/azide solution for around 25 minutes until the worms stopped moving. Anesthetized worms were transferred to an agar pad, covered with a coverslip and sealed with VALAP. The embryos inside the worms continued to develop normally. Endogenous granules present in the cytoplasm of *C. elegans* embryo were trapped and active microrheology (AMR) readings were performed. From these readings it became clear that the trapped particles were increasing in size over time, and this could be observed by transmitted light microscopy as large black patches where the trap had been applied (Figure 6.10). The optical trap appeared to be attracting granules into the trap and inducing coalescence thus falsifying the measurements. This was an unsurmountable problem since rheology could not be performed with a probe particle that was constantly changing size in an unpredictable way. Coalescence under the laser was probably due to the fact that many of the granules in the embryo were membrane-less organelles called P granules (Strome, 2005). Unlike real vesicles, like those that Wylie had successfully trapped in the mouse oocyte, the granules of the *C. elegans* embryo were not surrounded by a lipid bilayer, and therefore could fuse once the laser trap brought them close together. This fusion has been shown in other contexts (Brangwynne et al., 2009).

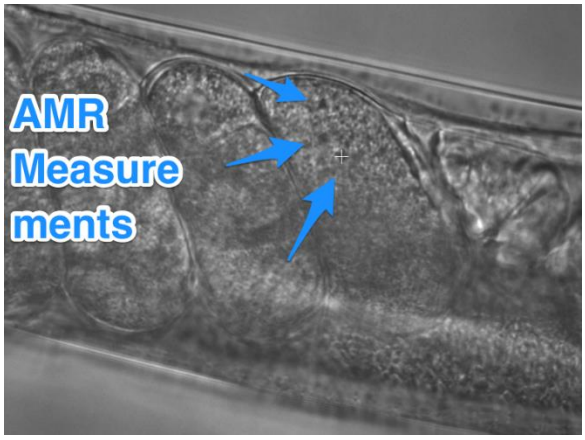

Figure 6.10 – Active microrheology (AMR) attempt with *C. elegans*. Three embryos are visible in the anesthetized adult. Trapping was performed where indicated by blue arrows. In two of the three trapping locations, a dark spot accumulated in the trap. Transmitted light microscopy.

6.3.2 Tests with bead injection

In order to overcome the issue of coalescence of granules, I decided to introduce exogenous particles as rheology probes. The idea was to inject beads into the syncytial gonad so that they would be taken up into the embryos during the process of cellularization as has been reported (Daniels et al., 2006; Garzon-Coral et al., 2016). After incorporation of beads into the embryo, the beads would be trapped using an optical trap and rheology would be performed.

Fluorescent beads (1 µm diameter) were microinjected into *C. elegans* worms. Injection proved to be difficult as commercial microinjection needles were too small and became quickly clogged, while custom-made needles with wider openings tended to kill the animal. I corresponded with the Carlos Garzon-Coral (formerly Howard Lab, MPI, Dresden) who had successfully injected paramagnetic beads of 1 µm into the *C. elegans* gonad in order to perform spindle displacements by magnetic tweezers (Garzon-Coral et al., 2016). It had taken him a year to perfect injection to a point where by injecting 20 worms, he could get 1-3 embryos with beads in them, more or less a day's work. He encouraged me to try smaller beads, but for my experiments, there was no point in doing this. For rheology the trapped particle must be as big as the mesh-size of the cytoplasmic actin network. I had no idea what this was, but 1 µm was a good start although 2 µm would have been better. This was probably why another paper on micro-rheology of *C. elegans* determined that the cytoplasm displayed no measurable elasticity, but was viscous (Daniels et al., 2006). In that study the authors used 100 nm beads, which are so small as compared to the probable mesh-size of a cytoplasmic actin network that they would diffuse through the network as if nothing were there.

6.3.3 Conclusions rheology

The discouraging time-line to success outlined by Carlos Garzon-Coral and the departure of Wylie Ahmed, the post-doc who performed the optical trapping experiments and analysis, put an end to this project. Carlos Garzon-Coral had also pointed out that even with beads, I would still face possible coalescence and heating problems with optical tweezing, which is why they had used the magnetic approach.

6.4 Overall conclusion and perspectives

As concerns the rheology project, the lab will not continue for the moment, the lack of a local collaborator being the main reason. For the actin visualization part, based on my trouble-shooting and technical advances in the field, another PhD student in the lab has taken over this project. On one hand the approach will be to reproduce the Sugimoto lab's transgenesis results with *P. pacificus* in order to apply this to labeling other molecules potentially important for actin polymerization in the *P. pacificus* embryo. So far, this has been problematic. On the other hand, another species will be examined such as *Diploscapter pachys*, one of the few non *C. elegans* nematode species that has been shown recently to be amenable to RNAi (Fradin et al., 2017). *D. pachys* is particularly interesting because it is a parthenogenetic species, and eggs develop without fertilization. It will be interesting to see how symmetry is broken in this case. RNAi opens up the possibility for easy permeabilization of embryos via *perm-1* RNAi, a treatment for fragilizing the eggshell in *C. elegans* (Carvalho et al., 2011). This will allow for labeling of the actin cytoskeleton as well as drug application to inhibit different actin-binding proteins (formins, the Arp2/3 complex, myosin) in order to examine their role in embryogenesis.

6.5 Procedures and solution recipes

6.5.1 Worm manipulation and embryo isolation

Worms were grown at 20-25°C on NGM media (Nematode Growth Media) plates with a spot of *E. coli* strain OP50 to provide food. The worms were maintained and passaged regularly in order to keep a population of healthy adults. In order to observe the first cell division in the embryos, gravid adult worms were selected and transferred into a watch glass containing M9 media. Embryos were liberated using a scalpel by dissecting the adult worm around the uterus. The embryos were then transferred using a glass capillary to a flat 2% agarose pad on a glass slide, then covered with a glass coverslip and sealed using VALAP. Embryos were filmed using either an upright Olympus BX51 microscope, equipped with DIC and epifluorescence optics, or an inverted confocal spinning disk microscope from Nikon using a 100x oil objective and a CoolSNAP HQ2 camera (Photometrics).

For optical trapping rheology experiments, worms were mounted on 4.5% agar pads. The optical tweezer system utilizes a near-infrared fiber laser (λ = 1064 nm, YLM-1-1064-LP; IPG Photonics, Oxford, MA) that passes through a pair of acoustooptical modulators (AA-Optoelectronics, Orsay, France) to control the intensity and deflection of the trapping beam. The laser is coupled into the beam path via dichroic mirrors (ThorLabs, Newton, NJ) and focused into the object plane by a water immersion objective (60×, 1.2 NA; Olympus, Tokyo, Japan). The condenser is replaced by a long-distance water immersion objective (40×, 0.9 NA; Olympus) to collect the light and imaged by a 1:4 telescope on a InGaAs quadrant photodiode (G6849 QPD; Hamamatsu, Hamamatsu City, Japan). The resulting signal is amplified by a custom-built amplifier system (Oeffner Electronics, Heidelberg, Germany) and digitized at a 500-kHz sampling rate, 16 bits, using an analog input card (PCIe-6353; National Instruments, Austin, TX). For bead injection a Nikon Eclipse Ti-S injector was used.

6.5.2 Solutions

M9 media: 3 g KH_2PO_4, 6 g Na_2HPO_4, 5 g NaCl, 1 ml 1 M $MgSO_4$, H_2O to 1 liter

4x Egg Salts: 472 mM NaCl, 160 mM KCl, 13.6 mM $CaCl_2$, 13.6 mM $MgCl_2$

Fix Solution 5 ml total volume (freshly prepared each experiment):

1. 1.4 mL dH20
2. 2.5 mL 2x Eggs Salts diluted from 4X stock with 10 mM Hepes
3. 0.1 mL 0.5 M EGTA
4. 1.0 mL 16% paraformaldehyde (high grade)

Chitinase Sigma # C-6137 diluted to 4 U/ml in sterile 1x egg salts

Phalloidin Alexa-488 from Molecular Probes

Levamisole/azide solution: 0.02% levamisole 20mM azide

PBST: PBS with 0.05% Tween-20, pH 8.0

6.5.3 Polylysine slides

1. Wipe 'pre-cleaned' frosted edge slides very clean with kim-wipes.
2. Place slides back-to-back (frosted sides exposed) in slide holder.
3. Shake 30 minutes in dilute ionic detergent (e.g., squirt of dishwashing soap in water).
4. Rinse in running water for about 1 minute.
5. Rinse in running distilled water for about 1 minute.
6. Shake in 70% ethanol + 1% HCl for 5 minutes.
7. Rinse in distilled water 5 minutes.
8. Dry using compressed air
9. Shake in the poly-L-lysine solution for 5 minutes.
10. Take the slides apart by sliding a scalpel between the slides
11. Air dry in the hood.

General Conclusion

The overall aim of this thesis was to deepen our understanding of the actin cytoskeleton by investigating network architecture both *in vivo* and *in vitro,* with the long term goal of revealing the contribution of actin to specific cell shape change events.

In **Chapter 4**, I used a minimal reconstituted system to understand the polarity of an actin network and the contribution of several actin binding proteins in the establishment of this polarity. I revealed the contribution of VASP in polarizing the growth of an actin network towards a surface in the absence of capping protein, and showed evidence that VASP promotes Arp2/3 complex activity at the surface that initiates actin network growth. I suggest a mode of action where VASP enhances Arp2/3 complex-based growth by providing mother filaments for Arp2/3 complex branch initiation. In **Chapter 5** through a collaboration with chemists from the group of Oliver Thorn-Seshold and Dirk Trauner, I participated in the identification of a new molecule based on CK-666, LU06, that inhibits Arp2/3 complex activity and that can be controlled using light. In **Chapter 6** I started exploring actin architecture and the rheological properties of the cytoplasm during the first cell division of nematode species that are genetically distant from the well-characterized system *C. elegans*. I narrowed the window of tools that can be used to visualize the actin network in such nematodes by showing the inefficiency of some strategies widely used in other model organisms.

Overall the main contribution of this PhD was to show that capping protein was not necessary for polarized actin growth and motility when VASP was present. VASP induced the formation of a polarized actin network *in vitro* by enhancing the activity of the Arp2/3 complex. My other main contribution was the identification of a photoswitchable Arp2/3 complex inhibitor, subsequent derivatives of which could be used to study the role of the Arp2/3 complex in cellular processes in a controlled manner.

References

Abella, J.V.G., C. Galloni, J. Pernier, D.J. Barry, S. Kjaer, M.-F. Carlier, and M. Way. 2016. Isoform diversity in the Arp2/3 complex determines actin filament dynamics. *Nat. Cell Biol.* 18:76-86.

Abu Shah, E., and K. Keren. 2014. Symmetry breaking in reconstituted actin cortices. *Elife*. 3:e01433.

Achard, V., J.-L. Martiel, A. Michelot, C. Guérin, A.-C. Reymann, L. Blanchoin, and R. Boujemaa-Paterski. 2010. A "Primer"-Based Mechanism Underlies Branched Actin Filament Network Formation and Motility. *Curr. Biol.* 20:423-428.

Aguilar-Cuenca, R., A. Janes-Garcia, and M. Vicente-Manzanares. 2014. Myosin II in mechanotransduction: master and commander of cell migration, morphogenesis, and cancer. *Cell. Mol. Life Sci.* 71:479-492.

Akin, O., and R.D. Mullins. 2008. Capping protein increases the rate of actin-based motility by promoting filament nucleation by the Arp2/3 complex. *Cell*. 133:841-851.

Alberts, B., A. Johnson, J. Lewis, M. Raff, K. Roberts, and P. Walter. 2002. Molecular Biology of the Cell.

Almonacid, M., W.W. Ahmed, M. Bussonnier, P. Mailly, T. Betz, R. Voituriez, N.S. Gov, and M.-H. Verlhac. 2015. Active diffusion positions the nucleus in mouse oocytes. *Nat. Cell Biol.* 17:470-479.

Applewhite, D.A., M. Barzik, S.-i. Kojima, T.M. Svitkina, F.B. Gertler, and G.G. Borisy. 2007. Ena/VASP Proteins Have an Anti-Capping Independent Function in Filopodia Formation. *Mol. Biol. Cell*. 18:2579–2591.

Bachmann, C., L. Fischer, U. Walter, and M. Reinhard. 1999. The EVH2 domain of the vasodilator-stimulated phosphoprotein mediates tetramerization, F-actin binding and actin bundle formation. *J. Biol. Chem.* 274:23549-23557.

Barzik, M., T.I. Kotova, H.N. Higgs, L. Hazelwood, D. Hanein, F.B. Gertler, and D.A. Schafer. 2005. Ena/VASP Proteins Enhance Actin Polymerization in the Presence of Barbed End Capping Proteins. *J. Biol. Chem.* 280:28653-28662.

Bear, J.E., and F.B. Gertler. 2009. Ena/VASP: towards resolving a pointed controversy at the barbed end. *J. Cell Sci.* 122:1947-1953.

Bear, J.E., J.J. Loureiro, I. Libova, R. Fässler, J. Wehland, and F.B. Gertler. 2000. Negative regulation of fibroblast motility by Ena/VASP proteins. *Cell*. 101:717-728.

Bear, J.E., J.F. Rawls, and C.L. Saxe. 1998. SCAR, a WASP-related protein, isolated as a suppressor of receptor defects in late Dictyostelium development. *J. Cell Biol.* 142:1325-1335.

Bear, J.E., T.M. Svitkina, M. Krause, D.A. Schafer, J.J. Loureiro, G.A. Strasser, I.V. Maly, O.Y. Chaga, J.A. Cooper, G.G. Borisy, and F.B. Gertler. 2002. Antagonism between Ena/VASP proteins and actin filament capping regulates fibroblast motility. *Cell*. 109:509-521.

Berends, C.W., J. Muñoz, V. Portegijs, R. Schmidt, I. Grigoriev, M. Boxem, A. Akhmanova, A.J. Heck, and S. van den Heuvel. 2013. F-actin asymmetry and the endoplasmic reticulum-associated TCC-1 protein contribute to stereotypic spindle movements in the Caenorhabditis elegans embryo. *Mol Biol Cell*. 24:2201-2215.

Bernheim-Groswasser, A., S. Wiesner, R.M. Golsteyn, M.-F. Carlier, and C. Sykes. 2002. The dynamics of actin-based motility depend on surface parameters. *Nature*. 417:308-311.

Bieling, P., S.D. Hansen, O. Akin, T.D. Li, C.C. Haysen, D.A. Fletcher, and R.D. Mullins. 2018. WH2 and proline-rich domains of WASP-family proteins collaborate to accelerate actin filament elongation. *EMBO J.* 37:102-121.

Bieling, P., T.-D. Li, J. Weichsel, R. McGorty, P. Jreij, B. Huang, D.A. Fletcher, and R.D. Mullins. 2016. Force feedback controls motor activity and mechanical properties of self-assembling branched actin networks. *Cell*. 164:115-127.

Blanchoin, L., K.J. Amann, H.N. Higgs, J.-B. Marchand, D.A. Kaiser, and T.D. Pollard. 2000. Direct observation of dendretic actin filament networks nucleated by Arp2/3 complex and WASP/Scar proteins. *Nature*. 404:1007-1111.

Blanchoin, L., R. Boujemaa-Paterski, C. Sykes, and J. Plastino. 2014. Actin dynamics, architecture and mechanics in cell motility. *Physiol. Rev.* 94:235-263.

Blanchoin, L., and T.D. Pollard. 1998. Interaction of actin monomers with Acanthamoeba actophorin (ADF/cofilin) and profilin. *J. Biol Chem*. 273:23106-25111.

Blanchoin, L., and T.D. Pollard. 1999. Mechanism of interaction of Acanthamoeba actophorin (ADF/Cofilin) with actin filaments. *J. Biol Chem*. 247:15538-15546.

Blanchoin, L., and T.D. Pollard. 2002. Hydrolysis of ATP by Polymerized Actin Depends on the Bound Divalent Cation but Not Profilin. *Biochemistry*. 41:597-602.

Block, J., D. Breitsprecher, S. Kühn, M. Winterhoff, F. Kage, R. Geffers, P. Duwe, J.L. Rohn, B. Baum, C. Brakebusch, M. Geyer, T.E.B. Stradal, J. Faix, and K. Rottner. 2012. FMNL2 drives actin-based protrusion and migration downstream of Cdc42. *Curr. Biol.* 22:1005-1012.

Borowiak, M., W. Nahaboo, M. Reynders, K. Nekolla, P. Jalinot, J. Hasserodt, M. Rehberg, M. Delattre, S. Zahler, A. Vollmar, D. Trauner, and O. Thorn-Seshold. 2015. Photoswitchable inhibitors of microtubule dynamics optically control mitosis and cell death. *Cell*. 162:403-411.

Boujemaa-Paterski, R., E. Gouin, G. Hansen, S. Samarin, C. Le Clainche, D. Didry, P. Dehoux, P. Cossart, C. Kocks, M.-F. Carlier, and D. Pantaloni. 2001a. *Listeria* protein ActA mimics WASP family proteins: it activates filament barbed end branching by Arp2/3 complex. *Biochemistry*. 40:11390-11404.

Boujemaa-Paterski, R., E. Gouin, G. Hansen, S. Samarin, C. Le Clainche, D. Didry, P. Dehoux, P. Cossart, C. Kocks, M.F. Carlier, and D. Pantaloni. 2001b. Listeria Protein ActA Mimics WASP Family Proteins: It Activates Filament Barbed End Branching by Arp2/3 Complex. *Biochemistry*. 40:11390-11404.

Boujemaa-Paterski, R., C. Suarez, T. Klar, J. Zhu, C. Guérin, A. Mogilner, M. Théry, and L. Blanchoin. 2017. Network heterogeneity regulates steering in actin-based motility. *Nat. Commun.* 8:655.

Boukellal, H., O. Campas, J.-F. Joanny, J. Prost, and C. Sykes. 2004. Soft *Listeria*: actin-based propulsion of liquid drops. *Phys. Rev. E*. 69:061906/061901-061906/061904.

Brangwynne, C.P., C.R. Eckmann, D.S. Courson, A. Rybarska, C. Hoege, J. Gharakhani, F. Jülicher, and A.A. Hyman. 2009. Germline P granules are liquid droplets that localize by controlled dissolution/condensation. *Science*. 324:1729-1732.

Breitsprecher, D., A.K. Kiesewetter, J. Linkner, C. Urbanke, G.P. Resch, J.V. Small, and J. Faix. 2008. Clustering of VASP actively drives processive, WH2 domain-mediated actin filament elongation. *EMBO J.* 27:2943-2954.

Breitsprecher, D., A.K. Kiesewetter, J. Linkner, M. Vinzenz, T. Stradal, J.V. Small, U. Curth, R.B. Dickinson, and J. Faix. 2011. Molecular mechanism of Ena/VASP-mediated actin-filament elongation. *EMBO J.* 30:456-467.

Brühmann, S., D.S. Ushakov, M. Winterhoff, R.B. Dickinson, U. Curth, and J. Faix. 2017. Distinct VASP tetramers synergize in the processive elongation of individual actin filaments from clustered arrays. *Proc. Natl. Acad. Sci.* 114:E5815-E5824.

Burdyniuk, M., A. Callegari, M. Mori, F. Nedelec, and P. Lenart. 2018. F-Actin nucleated on chromosomes coordinates their capture by microtubules in oocyte meiosis. *J. Cell Biol.* 217:2661-2674.

Burke, T.A., A.J. Harker, R. Dominguez, and D.R. Kovar. 2017. The bacterial virulence factors VopL and VopF nucleate actin from the pointed end. *J. Cell Biol.* 216:1267-1276.

Burridge, K., and C. Guilluy. 2016. Focal adhesions, stress fibers and mechanical tension. *Exp. Cell Res.* 343:14-20.

Bussonier, M., K. Carvalho, J. Lemière, J.-F. Joanny, C. Sykes, and T. Betz. 2014. Mechanical detection of a long-range actin network emanating from a biomimetic cortex. *Biophys. J.* 107:854-862.

Cabernard, C. 2017. Sibling cell size matters. *Elife*. 6:e24038.

Cáceres, R., N. Bojanala, L.C. Kelley, J. Dreier, J. Manzi, F. Di Federico, Q. Chi, T. Risler, I. Testa, D.R. Sherwood, and J. Plastino. 2018. Forces drive basement membrane invasion in Caenorhabditis elegans. *Proc. Natl. Acad. Sci.* 115:11537-11542.

Cameron, L.A., M.J. Footer, A. Van Oudenaarden, and J.A. Theriot. 1999. Motility of ActA protein-coated microspheres driven by actin polymerization. *Proc. Natl. Acad. Sci.* 96:4908-4913.

Cameron, L.A., T.M. Svitkina, D. Vignjevic, J.A. Theriot, and G.G. Borisy. 2001. Dendritic organization of actin comet tails. *Curr. Biol.* 11:130-135.

Campellone, K.G., and M.D. Welch. 2010. A nucleator arms race: cellular control of actin assembly. *Nat. Rev. Mol. Cell Biol.* 11:237-251.

Cao, W., J.P. Goodarzi, and E.M. De La Cruz. 2006. Energetics and kinetics of cooperative cofilin-actin filament interactions. *J. Mol. Biol.* 361:257-267.

Caorsi, V., J. Lemière, C. Campillo, M. Bussonier, J. Manzi, T. Betz, J. Plastino, K. Carvalho, and C. Sykes. 2016. Cell-sized liposome doublets reveal active tension build-up driven by acto-myosin dynamics. *Soft Matter*. 12:6223-6231.

Caridi, C.P., C. D'Agostino, T. Ryu, G. Zapotoczny, L. Delabaere, X. Li, V.Y. Khodaverdian, N. Amaral, E. Lin, A.R. Rau, and I. Chiolo. 2018. Nuclear F-actin and myosins drive relocalization of heterochromatic breaks. *Nat. Cell Biol.* 559:54-60.

Carlier, M.F. 1991. Actin: protein structure and filament dynamics. *J Biol Chem*. 226:1-4.

Carlier, M.F., C. Jean, K.J. Rieger, M. Lenfant, and D. Pantaloni. 1993. Modulation of the interaction between G-actin and thymosin beta 4 by the ATP/ADP ratio: possible implication in the regulation of actin dynamics. *Proc. Natl. Acad. Sci.* 90:5034-5038.

Carlier, M.F., C. Le Clainche, S. Wiesner, and D. Pantaloni. 2003. Actin-based motility : from molecules to movement. *BioEssays*. 25:336-345.

Carlier, M.F., and D. Pantaloni. 1986. Direct evidence for ADP-Pi-F-actin as the major intermediate in ATP-actin polymerization. Rate of dissociation of Pi from actin filaments. *Biochemistry*. 25:7789-7792.

Carlier, M.F., D. Pantaloni, J.A. Evans, P.K. Lambooy, E.D. Korn, and M.R. Webb. 1988. The hydrolysis of ATP that accompanies actin polymerization is essentially irreversible. *FEBS Lett.* 235:211-214.

Carvalho, A., S.K. Olson, E. Gutierrez, K. Zhang, L.B. Noble, E. Zanin, A. Desai, A. Groisman, and K. Oegema. 2011. Acute drug treatment in the early *C. elegans* embryo. *PLOS One*. 6:e24656.

Carvalho, K., J. Lemière, F. Faqir, J. Manzi, L. Blanchoin, J. Plastino, T. Betz, and C. Sykes. 2013. Actin polymerization or myosin contraction: two ways to build up cortical tension for symmetry breaking. *Phil. Trans. R. Soc. B*. 368:20130005.

Castellano, F., C. Le Clainche, D. Patin, M.-F. Carlier, and P. Chavrier. 2001. A WASP-VASP complex regulates actin polymerization at the plasma membrane. *EMBO J.* 20:5603-5614.

Caswell, P.T., and T. Zech. 2018. Actin-Based Cell Protrusion in a 3D Matrix. *Trends Cell Biol.* 28:823-834.

Chaigne, A., C. Campillo, N.S. Gov, R. Voituriez, J. Azoury, C. Umaña-Diaz, M. Almonacid, I. Queguiner, P. Nassoy, C. Sykes, M.-H. Verlhac, and M.-E. Terret. 2013. A soft cortex is essential for asymmetric spindle positioning in mouse oocytes. *Nat. Cell Biol.* 15:958-966.

Chaigne, A., C. Campillo, N.S. Gov, R. Voituriez, C. Sykes, M.-H. Verlhac, and M.-E. Terret. 2015. A narrow window of cortical tension guides asymmetric spindle positioning in the mouse oocyte. *Nat. Commun.* 6:6027.

Chakraborty, T., F. Ebel, E. Domann, K. Niebuhr, B. Gerstel, S. Pistor, C.J. Temm-Grove, B.M. Jockusch, M. Reinhard, U. Walter, and J. Wehland. 1995. A focal adhesion factor directly linking intracellularly motile Listeria monocytogenes and Listeria ivanovii to the actin-based cytoskeleton of mammalian cells. *EMBO J.* 14:1314-1321.

Chan, F.Y., A.M. Silva, J. Saramago, J. Pereira-Sousa, H.E. Brighton, M. Pereira, K. Oegema, R. Gassmann, and A.X. Carvalho. 2018. The ARP2/3 complex prevents excessive formin activity during cytokinesis. *Mol. Biol. Cell*. 30:96-107.

Cheeks, R.J., J.C. Canman, W.N. Gabriel, N. Meyer, S. Strome, and B. Goldstein. 2004. C. elegans PAR proteins function by mobilizing and stabilizing asymmetrically localized protein complexes. *Curr. Biol.* 14:851–862.

Chen, B., H.T. Chou, C.A. Brautigma, W. Xing, S. Yang, L. Henry, L.K. Doolittle, T. Walz, and M.K. Rosen. 2017. Rac1 GTPase activates the WAVE regulatory complex through two distinct binding sites. *Elife*. 6.

Chen, X.J., A.J. Squarr, R. Stephan, B. Chen, T.E. Higgins, D.J. Barry, M.C. Martin, M.K. Rosen, S. Bogdan, and M. Way. 2014. Ena/VASP proteins cooperate with the WAVE complex to regulate the actin cytoskeleton. *Dev. Cell*. 30:569–584.

Chen, Z., D. Borek, S.B. Padrick, T.S. Gomez, Z. Metlagel, A.M. Ismail, J. Umetani, D.D. Billadeau, Z. Otwinowski, and M.K. Rosen. 2010. Structure and control of the actin regulatory WAVE complex. *Nature*. 468:533-538.

Chereau, D., and R. Dominguez. 2006. Understanding the role of the G-actin-binding domain of Ena/VASP in actin assembly. *J. Struct. Biol.* 155:195.

Chugh, P., and E.K. Paluch. 2018. The actin cortex at a glance. *J. Cell Sci.* 131.

Ciobanasu, C., B. Faivre, and C. Le Clainche. 2013. Integrating actin dynamics, mechanotransduction and integrin activation: the multiple functions of actin binding proteins in focal adhesions. *Eur. J. Cell Biol.* 92:339-348.

Costa, M., B.W. Draper, and J.R. Priess. 1997. The Role of Actin Filaments in Patterning the Caenorhabditis elegans Cuticle. *Dev. Biol.* 184:373-384.

Cowan, C.R., and A.A. Hyman. 2004. Centrosomes direct cell polarity independently of microtubule assembly in C. elegans embryos. *Nature* 431:92–99.

Cowan, C.R., and A.A. Hyman. 2007. Acto-myosin reorganization and PAR polarity in C. elegans. *Development*. 134:1035-1043.

Cuenca, A.A., A. Schetter, D. Aceto, K. Kemphues, and G. Seydoux. 2003. Polarization of the C. elegans zygote proceeds via distinct establishment and maintenance phases. . *Development*. 130:1255–1265.

D'Este, E., D. Kamin, F. Göttfert, A. El-Hady, and S.W. Hell. 2015. STED Nanoscopy Reveals the Ubiquity of Subcortical Cytoskeleton Periodicity in Living Neurons. *Cell Rep*. 10:1246-1251.

Daniels, B.R., B.C. Masi, and D. Wirtz. 2006. Probing single-cell micromechanics *in vivo*: the microrheology of *C. elegans* developing embryos. *Biophys. J.* 90:4712-4719.

De La Cruz, E.M., A. Mandinova, M.O. Steinmetz, D. Stoffler, U. Aebi, and T.D. Pollard. 2000. Polymerization and Structure of Nucleotide-free Actin Filaments. *J. Mol. Biol.* 295:517-526.

Derivery, E., B. Lombard, D. Loew, and A. Gautreau. 2009. The Wave complex is intrinsically inactive. *Cell Motil. Cytoskel.* 66:777-790.

Dertsiz, L., G. Ozbilim, Y. Kayisli, G.A. Gokhan, A. Demircan, and U.A. Kayisli. 2005. Differential expression of VASP in normal lung tissue and lung adenocarcinomas. *Thorax*. 60:576-581.

Dominguez, R. 2016. The WH2 Domain and Actin Nucleation: Necessary but Insufficient. *Trends Biochem Sci*. 41:478-490.

Dürre, K., F.C. Keber, P. Bleicher, F. Brauns, C.J. Cyron, J. Faix, and A.R. Bausch. 2018. Capping protein-controlled actin polymerization shapes lipid membranes. *Nat Commun.* 9:1630.

Espinoza-Sanchez, S., L.A. Metskas, S.Z. Chou, E. Rhoades, and T.D. Pollard. 2018. Conformational changes in Arp2/3 complex induced by ATP, WASp-VCA, and actin filaments. *Proc. Natl. Acad. Sci.* 115:8642-8651.

Estin, M.L., S.B. Thompson, B. Taxinger, M.H. Fisher, R.S. Friedman, and J. Jacobelli. 2017. Ena/VASP family of cytoskeletal proteins regulate activated T cell trafficking by promoting diapedesis during transendothelial migration. *Proc. Natl. Acad. Sci.* 114:E2901-E2910.

Ferron, F., G. Rebowski, S.H. Lee, and R. Dominguez. 2007. Structural basis for the recruitment of profilin-actin complexes during filament elongation by Ena/VASP. *EMBO J.* 26:4597-4606.

Fleming, T., S.-C. Chien, P.J. Vanderzalm, M. Dell, M.K. Gavin, W.C. Forrester, and G. Garriga. 2010. The role of C. elegans Ena/VASP homolog UNC-34 in neuronal polarity and motility. *Dev. Biol.* 344:94-106.

Fradelizi, J., V. Noireaux, J. Plastino, B. Menichi, D. Louvard, C. Sykes, R.M. Golsteyn, and E. Friederich. 2001. ActA and human zyxin harbour Arp2/3-independent actin-polymerization activity. *Nat. Cell Biol.* 3:699-707.

Fradin, H., K. Kiontke, C. Zegar, M. Gutwein, J. Lucas, M. Kovtun, D.L. Corcoran, L.R. Baugh, D.H.A. Fitch, F. Piano, and s.K.C. Gunsalu. 2017. Genome Architecture and Evolution of a Unichromosomal Asexual Nematode. *Curr. Biol.* 27:2928-2939.

Fujiwara, I., S. Takakashi, H. Tadakuma, T. Funatsu, and S. Ishiwata. 2002. Microscopic analysis of polymerization dynamics with individual actin filaments. *Nat. Cell Biol.* 4:666-673.

Garzon-Coral, C., H.A. Fantana, and J. Howard. 2016. A force-generating machinery maintains the spindle at the cell center during mitosis. *Science*. 352:1124-1127.

Gates, J., S.H. Nowotarski, H. Yin, J.P. Mahaffey, T. Bridges, C. Herrera, C.C.F. Homem, F. Janody, D.J. Montell, and M. Peifer. 2009. Enabled and Capping protein play important roles in shaping cell behavior during Drosophila oogenesis. *Dev. Biol.* 333:90-107.

Gautreau, A., H.Y. Ho, J. Li, H. Steen, S.P. Gygi, and M.W. Kirschner. 2004. Purification and architecture of the ubiquitous Wave complex. *Proc. Natl. Acad. Sci.* 101:4379-4383.

Geese, M., J.J. Loureiro, J.E. Bear, J. Wehland, F.B. Gertler, and A.S. Sechi. 2002. Contribution of Ena/VASP proteins to intracellular motility of *Listeria* requires phosphorylation and proline-rich core but not F-actin binding or multimerization. *Mol. Biol. Cell*. 13:2383-2396.

Gertler, F.B., J.S. Doctor, and F.M. Hoffmann. 1990. Genetic suppression of mutations in the Drosophila abl proto-oncogene homolog. *Science*. 248:857-860.

Gertler, F.B., K. Niebuhr, M. Reinhard, J. Wehland, and P. Soriano. 1996. Mena, a relative of VASP and Drosophila enabled, is implicated in the control of microfilament dynamics. *Cell*. 87:227-239.

Goehring, N.W., C. Hoege, S.W. Grill, and A.A. Hyman. 2011. PAR proteins diffuse freely across the anterior-posterior boundary in polarized C. elegans embryos. *J. Cell Biol.* 193:583–594.

Goldschmidt-Clermont, P.J., M.I. Furman, D. Wachsstock, D. Safer, V.T. Nachmias, and T.D. Pollard. 1992. The control of actin nucleotide exchange by thymosin beta 4 and profilin. A potential regulatory mechanism for actin polymerization in cells. *Mol. Biol. Cell*. 3:1015-1024.

Goldschmidt-Clermont, P.J., L.M. Machesky, S.K. Doberstein, and T.D. Pollard. 1991. Mechanism of the interaction of human platelet profilin with actin. *J. Cell Biol.*:1081-1089.

Goldstein, B., and S.N. Hird. 1996. Specification of the anteroposterior axis in Caenorhabditis elegans. *Development*. 122:1467-1474.

Goley, E.D., and M.D. Welch. 2006. The ARP2/3 complex: an actin nucleator comes of age. *Nat. Rev. Mol. Cell Biol.* 7:317-326.

Gomez-Lopez, S., R.G. Lerner, and C. Petritsch. 2014. Asymmetric cell division of stem and progenitor cells during homeostasis and cancer. *Cell. Mol. Life Sci.* 71:575-597.

Goode, B.L., and M.J. Eck. 2007. Mechanism and function of formins in the control of actin assembly. *Annu. Rev. Biochem.* 76:593-627.

Gotta, M., Y. Dong, Y.K. Peterson, S.M. Lanier, and J. Ahringer. 2003. Asymmetrically distributed C. elegans homologs of AGS3/PINS control spindle position in the early embryo. . *Curr Biol* 13:1029–1037.

Gouin, E., H. Gantelet, C. Egile, I. Lasa, H. Ohayon, V. Villiers, P. Gounon, P.J. Sansonetti, and P. Cossart. 1999. A comparative study of the actin-based motilities of the pathogenic bacteria Listeria monocytogenes, Shigella flexneri and Rickettsia conorii. *J. Cell Sci.* 112:1697-1708.

Grill, S.W., P. Gönczy, E.H.K. Stelzer, and A.A. Hyman. 2001. Polarity controls forces governing asymmetric spindle positioning in the *Caenorhabditis elegans* embryo. *Nature*. 409:630-633.

Grill, S.W., J. Howard, E. Schäffer, E.H.K. Stelzer, and A.A. Hyman. 2003. The distribution of active force generators controls mitotic spindle position. *Science*. 301.

Gunning, P.W., U. Ghoshdastider, S. Whitaker, D. Popp, and R.C. Robinson. 2015. The evolution of compositionally and functionally distinct actin filaments. *J. Cell Sci.* 128.

Guo, S., and K.J. Kemphues. 1995. par-1, a gene required for establishing polarity in C. elegans embryos, encodes a putative Ser/Thr kinase that is asymmetrically distributed. *Cell*. 81:611–620.

Haffner, C., T. Jarchau, M. Reinhard, J. Hoppe, S.M. Lohmann, and U. Walter. 1995. Molecular cloning, structural analysis and functional expression of the proline-rich focal adhesion and microfilament-associated protein VASP. *EMBO J.* 14:19-27.

Halbrügge, M., and U. Walter. 1989. Purification of a vasodilator-regulated phosphoprotein from human platelets. *Eur. J. Biochem.* 185:41-51.

Han, Y.-H., C.Y. Chung, D. Wessels, S. Stephens, M.A. Titus, D.R. Soll, and R.A. Firtel. 2002. Requirement of a Vasodilator-stimulated phosphoprotein family member for cell adhesion, the formation of filopodia and chemotaxis in Dictyostelium. *J. Biol. Chem.* 277:49877-49887.

Hansen, S.D., and R.D. Mullins. 2010. VASP is a processive actin polymerase that requires monomeric actin for barbed end association. *J. Cell Biol.* 191:571-584.

Hanukoglu, I., N. Tanese, and E. Fuchs. 1983. Complementary DNA sequence of a human cytoplasmic actin. Interspecies divergence of 3' non-coding regions. *J. Mol. Biol.* 163:673-678.

Hao, Y., L. Boyd, and G. Seydoux. 2006. Stabilization of cell polarity by the C. elegans RING protein PAR-2. *Dev. Cell*. 10:199–208.

Harris, E.S., F. Li, and H.N. Higgs. 2004. The mouse formin, FRLalpha, slows actin filament barbed end elongation, competes with capping protein, accelerates polymerization from monomers, and severs filaments. *J. Biol. Chem.* 279:20076-20087.

Havrylenko, S., X. Mezanges, E.L. Batchelder, and J. Plastino. 2014. Extending the molecular clutch beyond actin-based cell motility *New J. Phys.* 16:105012.

Havrylenko, S., P. Noguera, M. Abou-Ghali, J. Manzi, F. Faqir, A. Lamora, C. Guérin, L. Blanchoin, and J. Plastino. 2015. WAVE binds Ena/VASP for enhanced Arp2/3 complex-based actin assembly. *Mol. Biol. Cell*. 26:55-65.

Henson, J.H., M. Yeterian, R.M. Weeks, A.E. Medrano, B.L. Brown, H.L. Geist, M.D. Pais, R. Oldenbourg, and C.B. Shuster. 2015. Arp2/3 complex inhibition radically alters

lamellipodial actin architecture, suspended cell shape, and the cell spreading process. *Mol. Biol. Cell*. 26:887-900.

Hetrick, B., M.S. Han, L.A. Helgeson, and B.J. Nolen. 2013. Small Molecules CK-666 and CK-869 Inhibit Actin-Related Protein 2/3 Complex by Blocking an Activating Conformational Change. *Chem. Biol.*:701-712.

Higgs, H.N., L. Blanchoin, and T.D. Pollard. 1999. Influence of the C terminus of Wiskott-Aldrich syndrome protein (WASp) and the Arp2/3 complex on actin polymerization. *Biochemistry*. 38:15212-15222.

Higgs, H.N., and T.D. Pollard. 1999. Regulation of actin polymerization by Arp2/3 complex and WASp/Scar proteins. *J. Biol. Chem.* 274:32531-32534.

Hird, S.N., and J.G. White. 1993. Cortical and cytoplasmic flow polarity in early embryonic cells of Caenorhabditis elegans. *J. Cell Biol.*:1343–1355.

Hoffman, L.M., C.C. Jensen, S. Kloeker, C.-L.A. Wang, M. Yoshigi, and M.C. Beckerle. 2006. Genetic ablation of zyxin causes Mena/VASP mislocalization, increased motility, and deficits in actin remodeling. *J. Cell Biol.* 172:771-782.

Hotulainen, P., and P. Lappalainen. 2006. Stress fibers are generated by two distinct actin assembly mechanisms in motile cells. *J. Cell Biol.* 173:383-394.

Hüttelmaier, S., B. Harbeck, O. Steffens, T. Messerschmidt, S. Illenberger, and B.M. Jockusch. 1999a. Characterization of the actin binding properties of the vasodilator-stimulated phosphoprotein VASP. *FEBS Lett.* 451:68-74.

Hüttelmaier, S., B. Harbeck, O. Steffens, T. Messerschmidt, S. Illenberger, and B.M. Jockusch. 1999b. Characterization of the actin binding properties of the vasodilator-stimulated phosphoprotein VASP. *FEBS Lett*. 451:68-74.

Huxley, H.E. 1967. Recent x-ray diffraction and electron microscope studies of striated muscle. *J. Gen. Physiol.* 50:71-83.

Ismail, A.M., S.B. Padrick, B. Chen, J. Umetani, and M.K. Rosen. 2009. The WAVE regulatory complex is inhibited. *Nat. Struct. Mol. Biol.* 16:561-563.

Iwasa, J.H., and R.D. Mullins. 2007. Spatial and temporal relationships between actin-filament nucleation, capping, and disassembly. *Curr. Biol.* 17:395-406.

Jacquemet, G., H. Hamidi, and J. Ivaska. 2015. Filopodia in cell adhesion, 3D migration and cancer cell invasion. *Curr. Opin. Cell Biol.* 36:23-31.

Jean, C., K. Rieger, L. Blanchoin, M.F. Carlier, M. Lenfant, and D. Pantaloni. 1994. Interaction of G-actin with thymosin beta 4 and its variants thymosin beta 9 and thymosin beta met9. *J. Muscle Res. Cell Motil.* 15:278-286.

Kabsch, W., H.G. Mannherz, and D. Suck. 1985. Three-dimensional structure of actin and DNase I at 4.5 A resolution. *EMBO J.* 4:2113-2118.

Kaiser, D.A., V.K. Vinson, D.B. Murphy, and T.D. Pollard. 1999. Profilin is predominantly associated with monomeric actin in Acanthamoeba. *J. Cell Sci*. 112:3779-3790.

Kanchanawong, P., G. Shtengel, A.M. Pasapera, E.B. Ramko, M.W. Davidson, H.F. Hess, and C.M. Waterman. 2010. Nanoscale architecture of integrin-based cell adhesions. *Nature*. 468:580-584.

Kawska, A., K. Carvalho, J. Manzi, R. Boujemaa-Paterski, L. Blanchoin, J.-L. Martiel, and C. Sykes. 2012. How actin network dynamics control the onset of actin-based motility. *Proc. Natl. Acad. Sci.* 109:14440–14445.

Kemphues, K.J., J.R. Priess, D.G. Morton, and N. Cheng. 1988. Identification of genes required for cytoplasmic localization in early C. elegans embryos. *Cell* 52:311–320.

Kim, A.S., L.T. Kakalis, N. Abdul-Manan, G.A. Liu, and M.K. Rosen. 2000. Autoinhibition and activation mechanisms of the Wiskott–Aldrich syndrome protein. *Nat. Cell Biol.* 404:151-158.

Kim, Y.M., C. Renné, S. Seifert, K. Schuh, and T. Renné. 2011. Impaired melanoma growth in VASP deficient mice. *FEBS Lett.* 585:2533-2536.

Knoblich, J.A. 2010. Asymmetric cell division: recent developments and their implications for tumour biology. *Nat. Rev. Mol. Cell Biol.* 11:849-860.

Kocks, C., R. Hellio, P. Gounon, H. Ohayon, and P. Cossart. 1993. Polarized distribution of Listeria monocytogenes surface protein ActA at the site of directional actin assemby. *J. Cell Sci.* 105:699-710.

Kocks, C., J.B. Marchand, G. Gouin, H. d'Hauteville, P.J. Sansonetti, M.F. Carlier, and P. Cossart. 1995. The unrelated surface proteins ActA of Listeria monocytogenes and IcsA of Shigella flexneri are sufficient to confer actin-based motility on Listeria innocula and Escherichia coli respectively. *Mol. Microbiol.* 18:413-423.

Koestler, S.A., A. Steffen, M. Nemethova, M. Winterhoff, N. Luo, J.M. Holleboom, J. Krupp, S. Jacob, M. Vinzenz, F. Schur, K. Schlüter, P.W. Gunning, C. Winkler, C. Schmeiser, J. Faix, T.E.B. Stradal, J.V. Small, and K. Rottner. 2013. Arp2/3 complex is essential for actin network treadmilling as well as for targeting of capping protein and cofilin. *Mol. Biol. Cell*. 24:2861-2875.

Kozlowski, C., M. Srayko, and F. Nedelec. 2007. Cortical microtubule contacts position the spindle in *C. elegans* embryos. *Cell*. 129:499-510.

Krause, M., E.W. Dent, J.E. Bear, J.J. Loureiro, and F.B. Gertler. 2003. Ena/VASP proteins: regulators of the actin cytoskeleton and cell migration. *Annu. Rev. Cell Dev. Biol.* 19:541-564.

Krause, M., and A. Gautreau. 2014. Steering cell migration: lamellipodium dynamics and the regulation of directional persistence. *Nat. Rev. Mol. Cell Biol.* 15:577_590.

Krause, M., J.D. Leslie, M. Stewart, E.M. Lafuente, F. Valderrama, R. Jagannathan, G.A. Strasser, D.A. Rubinson, H. Liu, M. Way, M.B. Yaffe, V.A. Boussiotis, and F.B. Gertler. 2004. Lamellipodin, an Ena/VASP ligand, is implicated in the regulation of lamellipodial dynamics. *Dev. Cell*. 7:571-583.

Kuhn, J.R., and T.D. Pollard. 2005. Real-Time Measurements of Actin Filament Polymerization by Total Internal Reflection Fluorescence Microscopy. *Biophys. J.* 88:1387–1402.

Lacayo, C.I., Z. Pincus, M.M. VanDuijn, C.A. Wilson, D.A. Fletcher, F.B. Gertler, A. Mogilner, and J.A. Theriot. 2007. Emergence of large-scale cell morphology and movement from local actin filament growth dynamics. *PLOS Biol.* 5:2035-2052.

Lanier, L.M., M.A. Gates, W. Witke, A.S. Menzies, A.M. Wehman, J.D. Macklis, D. Kwiatkowski, P. Soriano, and F.B. Gertler. 1999. Mena is required for neurulation and commissure formation. *Neuron*. 22:313-325.

Laurent, V., T.P. Loisel, B. Harbeck, A. Wehman, L. Gröbe, B.M. Jockusch, J. Wehland, F.B. Gertler, and M.-F. Carlier. 1999. Role of proteins of the Ena-VASP family in actin-based motility of Listeria monocytogenes. *J. Cell Biol.* 144:1245-1258.

Lebrand, C., E.W. Dent, G.A. Strasser, L.M. Lanier, M. Krause, T.M. Svitkina, G.G. Borisy, and F.B. Gertler. 2004. Critical role of Ena/VASP proteins for filopodia formation in neurons and in function downstream of netrin-1. *Neuron*. 42:37-49.

Levayer, R., and T. Lecuit. 2012. Biomechanical regulation of contractility: spatial control and dynamics. *Trends Cell Biol.* 22:61-81.

Liu, K., L. Li, P.E. Nisson, C. Gruber, J. Jessee, and S.N. Cohen. 1999. Reversible tumorigenesis induced by deficiency of vasodilator-stimulated phosphoprotein. *Mol. Cell Biol.* 19:3696-3703.

Lodish, H., A. Berk, S.L. Zipursky, P. Matsudaira, D. Baltimore, and J. Darnell. 2000. Molecular Cell Biology. *W. H. Freeman*. 4th edition.

Loisel, T.P., R. Boujemaa, D. Pantaloni, and M.F. Carlier. 1999. Reconstitution of actin-based motility of Listeria and Shigella using pure proteins. *Nature*. 401:613-616.

Loureiro, J.J., D.A. Rubinson, J.E. Bear, G.A. Baltus, A.V. Kwiatkowski, and F.B. Gertler. 2002. Critical roles of phosphorylation and actin binding motifs, but not the central proline-rich region, for Ena/Vasodilator-stimulated Phosphoprotein (VASP) function during cell migration. *Mol. Biol. Cell*. 13:2533-2546.

Lukinavičius, G., L. Reymond, E. D'Este, A. Masharina, F. Göttfert, H. Ta, A. Güther, M. Fournier, S. Rizzo, H. Waldmann, C. Blaukopf, C. Sommer, D.W. Gerlich, H.D. Arndt, S.W. Hell, and K. Johnsson. 2014 Fluorogenic probes for live-cell imaging of the cytoskeleton. *Nat. Methods*. 11:731-733.

Machesky, L.M., S.J. Atkinson, C. Ampe, J. Vandekerckhove, and T.D. Pollard. 1994. Purification of a cortical complex containing two unconventional actins from Acanthamoeba by affinity chromatography on profilin agarose. *J. Cell Biol.* 127:107-115.

Machesky, L.M., and R.H. Insall. 1998. Scar1 and the related Wiskott-Aldrich syndrome protein, WASP, regulate the actin cytoskeleton through the Arp2/3 complex. *Curr. Biol.* 8:1347-1356.

Machesky, L.M., R.D. Mullins, H.N. Higgs, D.A. Kaiser, L. Blanchoin, R.C. May, M.E. Hall, and T.D. Pollard. 1999. Scar, a WASp-related protein, activates nucleation of actin filaments by the Arp2/3 complex. *Proc. Natl. Acad. Sci.* 96:3739-3744.

Mallavarapu, A., and T. Mitchison. 1999. Regulated actin cytoskeleton assembly at filopodium tips controls their extension and retraction. *J Cell Biol.* 146:1097-1106.

Marchand, J.-B., D.A. Kaiser, T.D. Pollard, and H.N. Higgs. 2001. Interaction of WASP/Scar proteins with actin and vertebrate Arp2/3 complex. *Nat. Cell Biol.* 3:76-82.

McCullough, B.R., E.E. Grintsevich, C.K. Chen, H. Kang, A.L. Hutchison, A. Henn, W. Cao, C. Suarez, J.L. Martiel, L. Blanchoin, E. Reisler, and E.M. De La Cruz. 2011. Cofilin-linked changes in actin filament flexibility promote severing. *Biophys J.* 101:151-159.

McGough, A., B. Pope, W. Chiu, and A. Weeds. 1997. Cofilin changes the twist of F-actin: implications for actin filament dynamics and cellular function. *J. Cell Biology*. 138:771-781.

McNally, F.J. 2013. Mechanisms of spindle positioning. *J. Cell Biol.* 200:131-140.

Mejillano, M.R., S. Kojima, D.A. Applewhite, F.B. Gertler, T.M. Svitkina, and G.G. Borisy. 2004. Lamellipodial versus filopodial mode of the actin nanomachinery: pivotal role of the filament barbed end. *Cell*. 118:363-373.

Miki, H., K. Miura, and T. Takenawa. 1996. N-WASP, a novel actin-depolymerizing protein, regulates the cortical cytoskeletal rearrangement in a PIP2-dependent manner downstream of tyrosine kinases. *EMBO J.* 15:5326-5335.

Miki, H., S. Suetsugu, and T. Takenawa. 1998. WAVE, a novel WASP-family protein involved in actin reorganization induced by Rac. *EMBO J.* 17:6932-6941.

Mogilner, A., and B. Rubinstein. 2005. The physics of filopodial protrusion. *Biophys. J.* 89:782-795.

Motegi, F., and A. Sugimoto. 2006. Sequential functioning of the ECT-2 RhoGEF, RHO-1 and CDC-42 establishes cell polarity in Caenorhabditis elegans embryos. *Nat. Cell Biol.* 8:978–985.

Motegi, F., S. Zonies, Y. Hao, A.A. Cuenca, E. Griffin, and G. Seydoux. 2011. Microtubules induce self-organization of polarized PAR domains in Caenorhabditis elegans zygotes. *Nat Cell Biol*. 13:1361–1367.

Mueller, J., G. Szep, M. Nemethova, I. De Vries, A.D. Lieber, C. Winkler, K. Kruse, J.V. Small, C. Schmeiser, K. Keren, R. Hauschild, and M. Sixt. 2017. Load Adaptation of Lamellipodial Actin Networks. *Cell*. 171:188-200.

Mullins, R.D., J.A. Heuser, and T.D. Pollard. 1998. The interaction of Arp2/3 complex with actin: nucleation, high affinity pointed end capping, and formation of branching networks of filaments. *Proc. Natl. Acad. Sci.* 95:6181-6186.

Munro, E., J. Nance, and J.R. Priess. 2004. Cortical flows powered by asymmetrical contraction transport PAR proteins to establish and maintain anterior-posterior polarity in the early *C. elegans* embryo. *Dev. Cell*. 7:413-424.

Nadkarni, A.V., and W.M. Brieher. 2014. Aip1 destabilizes cofilin-saturated actin filaments by severing and accelerating monomer dissociation from ends. *Curr. Biol.* 24:2749-2757.

Namai, S., and A. Sugimoto. 2018. Transgenesis by microparticle bombardment for live imaging of fluorescent proteins in Pristionchus pacificus germline and early embryos. *Dev. Genes Evol.* 228:75-82.

Naumanen, P., P. Lappalainen, and P. Hotulainen. 2008. Mechanisms of actin stress fibre assembly. *J. Microsc.* 231:446-454.

Niebuhr, K., F. Ebel, R. Frank, M. Reinhard, E. Domann, U.D. Carl, U. Walter, F.B. Gertler, J. Wehland, and T. Chakraborty. 1997. A novel proline-rich motif present in ActA of Listeria monocytogenes and cytoskeletal proteins is the ligand for the EVH1 domain, a protein module present in the Ena/VASP family. *EMBO J.* 16:5433-5444.

Nishida, E. 1985. Opposite effects of cofilin and profilin from porcine brain on rate of exchange of actin-bound adenosine 5'-triphosphate. *Biochemistry*. 24:1160-1164.

Noireaux, V., R.M. Golsteyn, E. Friederich, J. Prost, C. Antony, D. Louvard, and C. Sykes. 2000. Growing an actin gel on spherical surfaces. *Biophys. J.* 278:1643-1654.

Nolen, B.J., N. Tomasevic, A. Russel, D.W. Pierce, Z. Jia, C.D. McCormick, J. Hartman, R. Sakowicz, and T.D. Pollard. 2009. Characterization of two classes of small molecule inhibitors of Arp2/3 complex. *Nature*. 460:1031-1034.

Otterbein, L.R., P. Graceffa, and R. Dominguez. 2001. The crystal structure of uncomplexed actin in the ADP state. *Science*. 293:708-711.

Ou, G., N. Stuurman, M. D'Ambrosio, and R.D. Vale. 2010. Polarized myosin produces unequal-size daughters during asymmetric cell division. *Science*. 330:677-680.

Pacquelet, A. 2017. Asymmetric Cell Division in the One-Cell C. elegans Embryo: Multiple Steps to Generate Cell Size Asymmetry. *Results Probl. Cell Differ.* 61:115-140.

Padrick, S.B., H.-C. Cheng, A.M. Ismail, S.C. Panchal, L.K. Doolittle, S. Kim, B.M. Skehan, J. Umetani, C.A. Brautigam, J.M. Leong, and M.K. Rosen. 2008. Hierarchical regulation of WASP/WAVE proteins. *Mol. Cell*. 32:426-438.

Palmgren, S., P.J. Ojala, M.A. Wear, J.A. Cooper, and P. Lappalainen. 2001. Interactions with PIP_2, ADP-actin monomers, and capping protein regulate the activity and localization of yeast twinfilin. *J. Cell Biol.* 155:251-260.

Park, D.H., and L.S. Rose. 2008. Dynamic localization of LIN-5 and GPR-1/2 to cortical force generation domains during spindle positioning. *Dev Biol*. 315:42–54.

Pasic, L., T. Kotova, and D.A. Schafer. 2008. Ena/VASP Proteins Capture Actin Filament Barbed Ends. *J. Biol. Chem.* 283:9814-9819.

Pecreaux, J., J.C. Röper, K. Kruse, F. Jülicher, A.A. Hyman, S.W. Grill, and J. Howard. 2006. Spindle oscillations during asymmetric cell division require a threshold number of active cortical force generators. *Curr. Biol.* 16:2111-2122.

Pellegrin, S., and H. Mellor. 2007. Actin stress fibers. *J. Cell Sci.* 120:3491-3499.

Petrie, R.J., N. Gavara, R.S. Chadwick, and K.M. Yamada. 2012. Nonpolarized signaling reveals two disctinct modes of 3D cell migration. *J. Cell Biol.* 197:439-455.

Philippar, U., E.T. Roussos, M. Oser, H. Yamaguchi, H.-D. Kim, S. Giampieri, Y. Wang, S. Goswami, J.B. Wyckoff, D.A. Lauffenburger, E. Sahai, J.S. Condeelis, and F.B. Gertler. 2008. A Mena invasion isoform potentiates EGF-induced carcinoma cell invasion and metastasis. *Dev. Cell*. 15:813-828.

Plastino, J., and L. Blanchoin. 2018. Dynamic stability of the actin ecosystem. *J. Cell Sci.* 132.

Plastino, J., I. Lelidis, J. Prost, and C. Sykes. 2004a. The effect of diffusion, depolymerization and nucleation promoting factors on actin gel growth. *Eur. Biophys. J.* 33:310-320.

Plastino, J., S. Olivier, and C. Sykes. 2004b. Actin filaments align into hollow comets for rapid VASP-mediated propulsion. *Curr. Biol.* 14:1766-1771.

Plastino, J., and C. Sykes. 2005. The actin slingshot. *Curr. Opin. Cell Biol.* 17:62-66.

Pollard, T.D. 1986. Rate constants for the reactions of ATP- and ADP-actin with the ends of actin filaments. *J. Cell Biol.* 103:2747-2754.

Pollard, T.D. 2016. Actin and Actin-Binding Proteins. *Cold Spring Harb. Perspect. Biol.* 8:a01822.

Pollard, T.D., L. Blanchoin, and R.D. Mullins. 2000. Molecular mechanisms controlling actin filament dynamics in nonmuscle cells. *Annu. Rev. Biophys. Biomol. Struct.* 29:545-576.

Pollard, T.D., and G.G. Borisy. 2003. Cellular motility driven by assembly and disassembly of actin filaments. *Cell*. 112:453-465.

Pontani, L.-L., J. Van der Gucht, G. Salbreaux, J. Heuvingh, J.-F. Joanny, and C. Sykes. 2009. Reconstitution of an actin cortex inside a liposome. *Biophys. J.* 96:192-198.

Prehoda, K.E., D.L. Lee, and W.A. Lim. 1999. Structure of the enabled/VASP homology 1 domain-peptide complex: a key component in the spatial control of actin assembly. *Cell*. 97:471-480.

Prehoda, K.E., J.A. Scott, R.D. Mullins, and W.A. Lim. 2000. Integration of multiple signals through cooperative regulation of the N-WASP-Arp2/3 complex. *Science*. 290:801-806.

Pring, M., M. Evangelista, C. Boone, C. Yang, and S.H. Zigmond. 2003. Mechanism of Formin-Induced Nucleation of Actin Filaments. *Biochemistry*. 42:486-496.

Pruyne, D., M. Evangelista, C. Yang, E. Bi, S. Zigmond, A. Bretscher, and C. Boone. 2002. Role of formins in actin assembly: nucleation and barbed-end association. *Science*. 297:612-615.

Reinhard, M., C. Giehl, K. Abel, C. Haffner, T. Jarchau, V. Hoppe, B.M. Jockusch, and U. Walter. 1995. The proline-rich focal adhesion and microfilament protein VASP is a ligand for profilins. *EMBO J.* 14:1583-1589.

Reinhard, M., M. Halbrügge, U. Scheer, C. Wiegand, B.M. Jockusch, and U. Walter. 1992. The 46/50 kDa phosphoprotein VASP purified from human platelets is a novel protein associated with actin filaments and focal contacts. *EMBO J.* 11:2063-2070.

Revenu, C., R. Athman, S. Robine, and D. Louvard. 2004. The co-workers of actin filaments: from cell structures to signals. *Nat. Rev. Mol. Cell Biol.* 5:635-646.

Reymann, A.-C., R. Boujemaa-Paterski, J.-L. Martiel, C. Guérin, W. Cao, H.F. Chin, E.M. De La Cruz, M. Théry, and L. Blanchoin. 2012. Actin network architecture can determine myosin motor activity. *Science*. 336:1310-1314.

Reymann, A.-C., J.-L. Martiel, T. Cambier, L. Blanchoin, R. Boujemaa-Paterski, and M. Théry. 2010. Nucleation geometry governs ordered actin networks structures. *Nat. Mater.* 9:827-832.

Ridley, A.J., and A. Hall. 1992. The small GTP-binding protein rho regulates the assembly of focal adhesions and actin stress fibers in response to growth factors. *Cell*. 70:389-399.

Ridley, A.J., M.A. Schwartz, K. Burridge, R.A. Firtel, M.H. Ginsberg, G. Borisy, J.T. Parsons, and A.R. Horwitz. 2003. Cell migration: integrating signals from front to back. *Science*. 320:1704-1709.

Riedl, J., A.H. Crevenna, K. Kessenbrock, J.H. Yu, D. Neukirchen, M. Bista, F. Bradke, D. Jenne, T.A. Holak, Z. Werb, M. Sixt, and R. Wedlich-Soldner. 2008. Lifeact: a versatile marker to visualize F-actin. *Nat. Methods*. 5:605-607.

Riedl, J., K.C. Flynn, A. Raducanu, F. Gärtner, G. Beck, M. Bösl, F. Bradke, S. Massberg, A. Aszodi, M. Sixt, and R. Wedlich-Söldner. 2010. Lifeact mice for studying F-actin dynamics. *Nat. Methods*. 7:168-169.

Robin, F.B., W.M. McFadden, B. Yao, and E.M. Munro. 2014. Single-molecule analysis of cell surface dynamics in Caenorhabditis elegans embryos. *Nat. Methods*. 11:677-682.

Rohatgi, R., H.Y. Ho, and M.W. Kirschner. 2000. Mechanism of N-WASP activation by CDC42 and phosphatidylinositol 4, 5-bisphosphate. *J. Cell Biol.* 150:1299-1310.

Romarowski, A., Á.G. Velasco Félix, P. Torres Rodríguez, M.G. Gervasi, X. Xu, G.M. Luque, G. Contreras-Jiménez, C. Sánchez-Cárdenas, H.V. Ramírez-Gómez, D. Krapf, P.E. Visconti, D. Krapf, A. Guerrero, A. Darszon, and M.G. Buffone. 2018. Super-resolution imaging of live sperm reveals dynamic changes of the actin cytoskeleton during acrosomal exocytosis. *J Cell Sci.* 131.

Romero, S., C. Le Clainche, D. Didry, C. Egile, D. Pantaloni, and M.-F. Carlier. 2004. Formin is a processive motor that requires profilin to accelerate actin assembly and associated ATP hydrolysis. *Cell*. 119:419-429.

Rottner, K., B. Behrendt, J.V. Small, and J. Wehland. 1999. VASP dynamics during lamellipodia protrusion. *Nat. Cell Biol.* 1:321-322.

Rouiller, I., X.P. Xu, K.J. Amann, C. Egile, S. Nickell, D. Nicastro, R. Li, T.D. Pollard, N. Volkmann, and D. Hanein. 2008. The structural basis of actin filament branching by the Arp2/3 complex. *J. Cell Biology*. 180:887-895.

Roussos, E.T., Y. Wang, J.B. Wyckoff, R.S. Sellers, W. Wang, J. Li, J.W. Pollard, F.B. Gertler, and J.S. Condeelis. 2010. Mena deficiency delays tumor progression and decreases metastasis in polyoma middle-T transgenic mouse mammary tumors. *Breast Cancer Res*. 12.

Salbreux, G., G. Charras, and E. Paluch. 2012. Actin cortex mechanics and cellular morphogenesis. *Trends Cell Biol.* 22:536-545.

Samarin, S., S. Romero, C. Kocks, D. Didry, D. Pantaloni, and M.-F. Carlier. 2003. How VASP enhances actin-based motility. *J. Cell Biol.* 163:131-142.

Schafer, D.A., P.B. Jennings, and J.A. Cooper. 1996. Dynamics of capping protein and actin assembly in vitro: Uncapping barbed ends by polyphosphoinositides. *J. Cell Biol.* 135:169-179.

Schirenbeck, A., R. Arasada, T. Bretschneider, T. Stradal, M. Schleicher, and J. Faix. 2006. The bundling activity of vasodilator-stimulated phosphoprotein is required for filopodium formation. *Proc. Natl. Acad. Sci.* 103:7694-7699.

Schirenbeck, A., T. Bretschneider, R. Arasada, M. Schleicher, and J. Faix. 2005. The Diaphanous-related formin dDia2 is required for the formation and maintenance of filopodia. *Nat. Cell Biol.* 7:619-625.

Shakir, M.A., J.S. Gill, and E.A. Lundquist. 2006. Interactions of UNC-34 Enabled with Rac GTPases and the NIK Kinase MIG-15 in Caenorhabditis elegans axon pathfinding and neuronal migration. *Genetics*. 172:893-913.

Simon, C., V. Caorsi, C. Campillo, and C. Sykes. 2018. Interplay between membrane tension and the actin cytoskeleton determines shape changes. *Phys. Biol.* 15:065004.

Skoble, J., V. Auerbuch, E.D. Goley, M.D. Welch, and D.A. Portnoy. 2001. Pivotal role of VASP in Arp2/3 complex-mediated actin nucleation, actin branch-formation, and *Listeria monocytogenes* motility. *J. Cell Biol.* 155:89-100.

Skoble, J., D.A. Portnoy, and M.D. Welch. 2000. Three regions within ActA promote Arp2/3 complex-mediated actin nucleation and *Listeria monocytogenes* motility. *J. Cell Biol.* 150:527-537.

Skruber, K., T.A. Read, and E.A. Vitriol. 2018. Reconsidering an active role for G-actin in cytoskeletal regulation. *J Cell Sci.* 131.

Small, J.V., and G.P. Resch. 2005. The comings and goings of actin: coupling protrusions and retraction in cell motility. *Curr. Opin. Cell Biol.* 17:517-523.

Smith, G.A., J.A. Theriot, and D.A. Portnoy. 1996. The tandem repeat domain in the Listeria monocytogenes ActA protein controls the rate of actin-based motility, the percentage of moving bacteria, and the localization of vasodilator-stimulated phosphoprotein and profilin. *J. Cell Biol.* 135:647-660.

Smith, M.A., E. Blankman, M.L. Gardel, L. Luettjohann, C.M. Waterman, and M.C. Beckerle. 2010. A zyxin-mediated mechanism for actin stress fiber maintenance and repair. *Dev Cell*. 19:365-376.

Stevenson, R.P., D.M. Veltman, and L.M. Machesky. 2012. Actin-bundling proteins in cancer progression at a glance. *J. Cell Sci.* 125:1073-1079.

Strome, S. 2005. Specification of the germ line. *WormBook*.

Suarez, C., R.T. Carroll, T.A. Burke, J.R. Christensen, A.J. Bestul, J.A. Sees, M.L. James, V. Sirotkin, and D.R. Kovar. 2015. Profilin regulates F-actin network homeostasis by favoring formin over Arp2/3 complex. *Dev. Cell*. 32:43-53.

Suarez, C., J. Roland, R. Boujemaa-Paterski, H. Kang, B.R. McCullough, A.C. Reymann, C. Guérin, J.L. Martiel, E.M. De La Cruz, and L. Blanchoin. 2011. Cofilin tunes the nucleotide state of actin filaments and severs at bare and decorated segment boundaries. *Curr. Biol.* 21:862-868.

Svitkina, T.M., and G.C. Borisy. 1999. Arp2/3 complex and actin depolymerizing factor/cofilin in dendritic organization and treadmilling of actin filament array in lamellipodia. *J. Cell Biol.* 145:1009-1026.

Svitkina, T.M., E.A. Bulanova, O.Y. Chaga, D.M. Vignjevic, S. Kojima, J.M. Vasiliev, and G.G. Borisy. 2003. Mechanism of filopodia intitiation by reorganization of a dendritic network. *J. Cell Biol.* 160:409-421.

Svitkina, T.M., A.B. Verkhovsky, K.M. McQuade, and G.G. Borisy. 1997. Analysis of the Actin-Myosin II System in Fish Epidermal Keratocytes: Mechanism of Cell Body Translocation. *J. Cell Biol.* 139:397-415.

Sykes, C., and J. Plastino. 2010. Actin filaments up against a wall. *Nature*. 464:365-366.

Symons, M., J.M.J. Derry, B. Karlak, S. Jiang, V. Lemahieu, F. McCormick, U. Franke, and A. Abo. 1996. Wiskott-Aldrich Syndrome Protein, a novel effector for the GTPase CDC42Hs, is implicated in actin polymerization. *Cell*. 84:723-734.

Tanaka, K., S. Takeda, K. Mitsuoka, T. Oda, C. Kimura-Sakiyama, Y. Maéda, and A. Narita. 2018. Structural basis for cofilin binding and actin filament disassembly. *Nat. Commun.* 9.

Tang, H., A. Li, J. Bi, D.M. Veltman, T. Zech, H.J. Spence, X. Yu, P. Timpson, R.H. Insall, M.C. Frame, and L.M. Machesky. 2013. Loss of Scar/WAVE complex promotes N-WASP and FAK-dependent invasion. *Curr. Biol.* 23:107-117.

Tilney, L.G., D.J. DeRosier, and M.S. Tilney. 1992. How Listeria exploits host cell actin to form its own cytoskeleton. I. Formation of a tail and how that tail might be involved in movement. *J. Cell Biol.* 118:71-81.

Tilney, L.G., and D.A. Portnoy. 1989. Actin filaments and the growth, movement, and spread of the intracellular bacterial parasite, Listeria monocytogenes. *J. Cell Biol.* 109:1597-1608.

Tojkander, S., G. Gateva, and P. Lappalainen. 2012. Actin stress fibers--assembly, dynamics and biological roles. *J. Cell Sci.* 125:1855-1864.

Tojkander, S., G. Gateva, G. Schevzov, P. Hotulainen, P. Naumanen, C. Martin, P.W. Gunning, and P. Lappalainen. 2011. A molecular pathway for myosin II recruitment to stress fibers. *Curr. Biol.* 21:539-550.

Trichet, L., O. Campas, C. Sykes, and J. Plastino. 2007. VASP governs actin dynamics by modulating filament anchoring. *Biophys. J.* 92:1081-1089.

Trichet, L., C. Sykes, and J. Plastino. 2008. Relaxing the actin cytoskeleton for adhesion and movement with Ena/VASP. *J. Cell Biol.* 181:19-25.

Tucker, P.K., I.R. Evans, and W. Wood. 2011. Ena drives invasive macrophage migration in Drosophila embryos. *Dis. Model Mech.* 4:126-134.

Urban, E., S. Jacob, M. Nemethova, G.P. Resch, and J.V. Small. 2010. Electron tomography reveals unbranched networks of actin filaments in lamellipodia. *Nat. Cell Biol.* 12:429-435.

Valfort, A.C., C. Launay, M. Sémon, and M. Delattre. 2018. Evolution of mitotic spindle behavior during the first asymmetric embryonic division of nematodes. *PLoS Biol.* 16:e2005099.

van der Gucht, J., E. Paluch, J. Plastino, and C. Sykes. 2005. Stress release drives symmetry breaking for actin-based movement. *Proc. Natl. Acad. Sci.* 102:7847-7852.

Vargas-Velazquez, A.M., F. Besnard, and M.A. Félix. 2019. Necessity and contingency in developmental genetic screens: EGF, Wnt and Semaphorin pathways in vulval induction of the nematode Oscheius tipulae. *Genetics*. in press.

Vedula, P., and A. Kashina. 2018. The makings of the 'actin code': regulation of actin's biological function at the amino acid and nucleotide level. *J. Cell Sci.* 131.

Vicente-Manzanares, M., X. Ma, R.S. Adelstein, and A.R. Horwitz. 2009. Non-muscle myosin II takes centre stage in cell adhesion and migration. *Nat. Rev. Mol. Cell Biol.* 10:778-790.

Vignjevic, D., S.-i. Kojima, Y. Aratyn, O. Danciu, T. Svitkina, and G.G. Borisy. 2006. Role of fascin in filopodial protrusion. *J. Cell Biol.* 174:863-875.

Volkman, B.F., K.E. Prehoda, J.A. Scott, F.C. Peterson, and W.A. Lim. 2002. Structure of the N-WASP EVH1 Domain-WIP Complex: Insight into the Molecular Basis of Wiskott-Aldrich Syndrome. *Cell*. 111:565–576.

Walders-Harbeck, B., S.Y. Khaitlina, H. Hinssen, B.M. Jockusch, and S. Illenberger. 2002. The vasodilator-stimulated phosphoprotein promotes actin polymerisation through direct binding to monomeric actin. *FEBS Lett.* 529:275-280.

Watanabe, N., P. Madaule, T. Reid, T. Ishizaki, G. Watanabe, A. Kakizuka, Y. Saito, K. Nakao, B.M. Jockusch, and S. Narumiya. 1997. p140mDia, a mammalian homolog of Drosophila diaphanous,is a target protein for Rho small GTPase and is a ligand for profilin. *EMBO J.* 16:3044-3056.

Watts, J.L., D.G. Morton, J. Bestman, and K.J. Kemphues. 2000. The C. elegans par-4 gene encodes a putative serine-threonine kinase required for establishing embryonic asymmetry. . *Development*. 127:1467–1475.

Wegner, A. 1976. Head to Tail Polymerization of Actin *J. Mol. Biol.* 108:139-150.

Welch, M.D., A. Iwamatsu, and T.J. Mitchison. 1997. Actin polymerization is induced by Arp2/3 protein complex at the surface of Listeria monocytogenes. *Nature*. 385:265-269.

Welch, M.D., J. Rosenblatt, J. Skoble, D.A. Portnoy, and T.J. Mitchison. 1998. Interaction of human Arp2/3 complex and the Listeria monocytogenes ActA protein in actin filament nucleation. *Science*. 281:105-108.

Wioland, H., B. Guichard, Y. Senju, S. Myram, P. Lappalainen, A. Jégou, and G. Romet-Lemonne. 2017. ADF/Cofilin Accelerates Actin Dynamics by Severing Filaments and Promoting Their Depolymerization at Both Ends. *Curr. Biol.* 27:1956-1967.

Withee, J., B. Galligan, N. Hawkins, and G. Garriga. 2004. *Caenorhabditis elegans* WASP and Ena/VASP protiens play compensatory roles in morphogenesis and neuronal cell migration. *Genetics*. 167:1165-1176.

Wu, C., S.B. Asokan, M.E. Berginski, E.M. Haynes, N.E. Sharpless, J.D. Griffith, S.M. Gomez, and J.E. Bear. 2012. Arp2/3 is critical for lamellipodia and response to extracellular matrix cues but is dispensable for chemotaxis. *Cell*. 148:973-987.

Xue, B., C. Leyrat, J.M. Grimes, and R.C. Robinson. 2014. Structural basis of thymosin-β4/profilin exchange leading to actin filament polymerization. *Proc. Natl. Acad. Sci.* 111:E4596-4605.

Yamaguchi, H., H. Miki, S. Suetsugu, L. Ma, M.W. Kirschner, and T. Takenawa. 2000. Two tandem verprolin homology domains are necessary for a strong activation of Arp2/3 complex-induced actin polymerization and induction ofmicrospike formation by N-WASP. *Proc. Natl. Acad. Sci.* 97:12631-12636.

Yang, C., and T. Svitkina. 2011. Visualizing branched actin filaments in lamellipodia by electron tomography *Nat. Cell Biol.* 13:1012-1013.

Yi, K., J.R. Unruh, M. Deng, B.D. Slaughter, B. Rubinstein, and R. Li. 2011. Dynamic maintenance of asymmetric meiotic spindle position through Arp2/3-complex-driven cytoplasmic streaming in mouse oocytes. *Nat. Cell Biol.* 13:1252-1258.

Yoshigi, M., L.M. Hoffman, C.C. Jensen, H.J. Yost, and M.C. Beckerle. 2005. Mechanical force mobilizes zyxin from focal adhesions to actin filaments and regulates cytoskeletal reinforcement. *J. Cell Biol.* 171:209-215.

Yu, T.W., J.C. Hao, W. Lim, M. Tessier-Lavigne, and C.I. Bargmann. 2002. Shared receptors in axon guidance: SAX-3/Robo signals via UNC-34/Enabled and a Netrin-independent UNC-40/DCC function. *Nat. Neurosci.* 5:1147-1154.

Zalevsky, J., L. Lempert, H. Kranitz, and R.D. Mullins. 2001. Different WASP family proteins stimulate different Arp2/3 complex-dependent actin-nucleating activities. *Curr. Biol.* 11:1903-1913.

Zarkower, D. 2006. Somatic sex determination. *WormBook*.

Zhu, Z., Y. Chai, Y. Jiang, W. Li, H. Hu, W. Li, J.-W. Wu, Z.-Z. Wang, S. Huang, and G. Ou. 2016. Functional coordination of WAVE and WASP in *C. elegans* neuroblast migration. *Dev. Cell*. 39:224-238.

Zimmermann, J., D. Labudde, T. Jarchau, U. Wlater, H. Oschkinat, and L.J. Ball. 2002. Relaxation, equilibrium oligomerization, and molecular symmetry of the VASP (336-380) EVH2 tetramer. *Biochemistry*. 41:11143-11151.

Zuzga, D.S., J. Pelta-Heller, P. Li, A. Bombonati, S.A. Waldman, and G.M. Pitari. 2012. Phosphorylation of vasodilator-stimulated phosphoprotein Ser239 suppresses filopodia and invadopodia in colon cancer. *Int. J. Cancer*. 130:2539-2548.

Annex 1: Review article *Biochimica et Biophysica Acta* 2015

"Reconstituting the actin cytoskeleton at or near surfaces *in vitro*"

Authors: Rodrigo Cáceres, **Majdouline Abou-Ghali**, Julie Plastino

My contribution: I provided images (original data) for one of the figures of this review, and I re-read and commented on the manuscript.

Biochimica et Biophysica Acta 1853 (2015) 3006–3014

Contents lists available at ScienceDirect

Biochimica et Biophysica Acta

journal homepage: www.elsevier.com/locate/bbamcr

Review

Reconstituting the actin cytoskeleton at or near surfaces *in vitro*☆

Rodrigo Cáceres [a,b,c,d], Majdouline Abou-Ghali [a,b,c], Julie Plastino [a,b,c,*]

[a] Institut Curie, Centre de Recherche, Paris F-75248 France
[b] Centre National de la Recherche Scientifique, Unité Mixte de Recherche 168, Paris F-75248 France
[c] Université Pierre et Marie Curie, Paris F-75248, France
[d] Université Paris Descartes, Paris F-75248, France

ARTICLE INFO

Article history:
Received 9 March 2015
Received in revised form 15 July 2015
Accepted 16 July 2015
Available online 31 July 2015

Keywords:
Actin polymerization
Biomimetic systems
Actin-based motility
Contractility
Actin cortex
Lamellipodium

ABSTRACT

Actin filament dynamics have been studied for decades in pure protein solutions or in cell extracts, but a breakthrough in the field occurred at the turn of the century when it became possible to reconstitute networks of actin filaments, growing in a controlled but physiological manner on surfaces, mimicking the actin assembly that occurs at the plasma membrane during cell protrusion and cell shape changes. The story begins with the bacteria *Listeria monocytogenes*, the study of which led to the reconstitution of cellular actin polymerization on a variety of supports including plastic beads. These studies made possible the development of liposome-type substrates for filament assembly and micropatterning of actin polymerization nucleation. Based on the accumulated expertise of the last 15 years, many exciting approaches are being developed, including the addition of myosin to biomimetic actin networks to study the interplay between actin structure and contractility. The field is now poised to make artificial cells with a physiological and dynamic actin cytoskeleton, and subsequently to put these cells together to make *in vitro* tissues. This article is part of a Special Issue entitled: Mechanobiology.

1. Introduction

Actin is a protein that exists in a globular soluble form and in an assembled filamentous form, echoing a common theme observed in other types of cytoskeleton like microtubules and intermediate filaments. Cell shape changes in general, including cell motility, cell division and cancer cell invasion, are due in part to the controlled assembly of actin into filamentous networks that can push membranes or contract in the presence of the molecular motor myosin thus leading to cell shape changes. The fact that actin filaments are polar, with a dynamic barbed end that grows and shrinks more quickly than the pointed end, is important for the directionality of network growth and for myosin motor activity.

Actin has been studied since the 1940s when it was first isolated from muscle. By the time the last century was drawing to a close, the dynamics of individual actin filaments had been well characterized *in vitro* [1] and much had been discovered about other factors that interacted with both the globular and filamentous forms of actin [2]. The great step forward at the turn of the century was the successful recreation of dynamic actin networks growing at surfaces in a controlled fashion using cellular components, a departure from previous single filament studies where polymerization was generally occurring in the bulk solution. This review will be about the progress over the last 15 years in the field of reconstitution of dynamic actin and acto-myosin networks at surfaces or under confinement, and how technological advances have been used to further our understanding of cellular actin dynamics. Other excellent reviews on reconstitution have been published over the last 5 years concentrating on actin and adhesion, membrane-bound actin and single filament dynamics [3–7]. The focus here is actin and acto-myosin networks at or near surfaces *in vitro*, to mimic cellular confinement and geometry.

2. The beginnings of actin network reconstitution

2.1. Listeria in cells

Somewhat surprisingly, most modern approaches to studying actin networks *in vitro* can trace their inspiration back to the food-borne pathogen *Listeria monocytogenes* (Fig. 1). This bacterium propels itself in the host cell cytosol not by swimming with a flagellum, but by building a network of filamentous actin behind itself, dubbed an actin tail or actin comet due to its appearance by electron and light microscopy (reviewed in [8]). What made this motility mode interesting to the general cell biology community was the discovery that the bacteria produced a single factor necessary for its motility, the ActA protein, which was displayed on its surface and was responsible for forming the actin comet from host cell components (reviewed in [9]). In addition landmarking experiments in the actin network of moving cells and in *Listeria* tails showed that both processes involved insertion of newly polymerized actin at the cell membrane or bacterial surface, and this was

☆ This article is part of a Special Issue entitled: Mechanobiology.
* Corresponding author at: Institut Curie, Centre de Recherche, Paris F-75248 France.
E-mail address: julie.plastino@curie.fr (J. Plastino).

http://dx.doi.org/10.1016/j.bbamcr.2015.07.021
0167-4889/

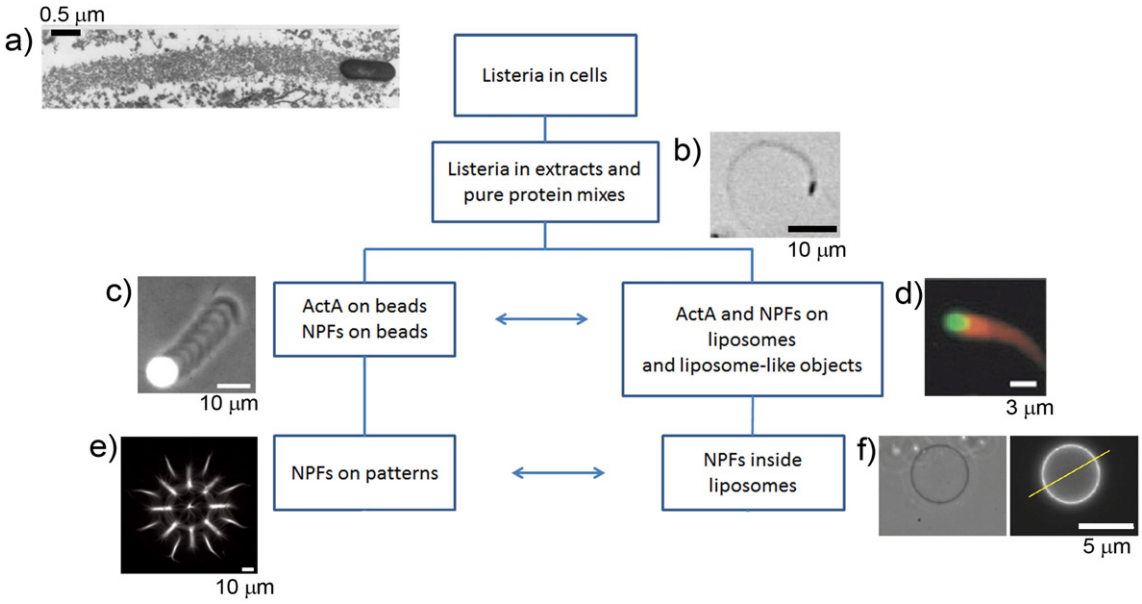

Fig. 1. The family tree of biomimetic systems of actin motility and dynamics. The original inspiration came from *Listeria* motility in cells a), which led to studies of *Listeria* in cell extracts and pure protein mixes b). The next generation of *in vitro* systems can be split into two groups, one involving reconstitution on solid supports such as beads c) and the other involving the use of fluid, deformable substrates such as liposomes d). ActA from *Listeria* was used to coat the beads and liposomes, but also mammalian nucleation promoting factors (NPFs) of the WASP/WAVE/Scar family. The recent innovations in each branch of the family consist of reconstitution of actin dynamics on micropatterns on one hand e), and reconstitution of actin cortices inside liposomes on the other hand f). The lateral double-headed arrows indicate cross-talk between the different systems. a) Reprinted from [114]: *Cell*, vol. 68, C. Kocks, E. Gouin, M. Tabouret, P. Berche, H. Ohayon, P. Cossart, *L. monocytogenes*-induced actin assembly requires the *actA* gene product, a surface protein, 521–531 (1992), with permission from Elsevier. b) Adapted by permission from Macmillan Publishers Ltd: *Nature* [28], 1999. c) Adapted by permission from Macmillan Publishers Ltd: *Nature* [68], 2002. d) Adapted by permission from the National Academy of Sciences: *PNAS* [74], 2003. e) Adapted by permission from Macmillan Publishers Ltd: *Nature Materials* [101], 2010. f) Reprinted from [95]: *Biophysical Journal*, vol. 96, L.-L. Pontani, J. Van der Gucht, G. Salbreaux, J. Heuvingh, J.-F. Joanny, C. Sykes, Reconstitution of an actin cortex inside a liposome, 192–198 (2009), with permission from Elsevier.

hypothesized to be the driving force for propulsion in both cases [10,11]. It was quickly realized by pioneers in the field that the *Listeria* actin network could be a powerful tool to study the biochemical basis of mammalian actin assembly, in isolation from cell signaling and adhesion. This discovery also opened up new avenues for studying how actin assembly created movement from a physical perspective since bacterial movement was a more tractable object to manipulate and model than an entire cell [12,13]. We will discuss here *Listeria* motility, but other pathogens with similar motility mechanisms have also been useful in the study of actin-based motility [14].

Initial experiments involved observation of *Listeria* movement in living cells. Such studies revealed that many host cell actin-binding proteins were present in the *Listeria* comet tail ([15] and references therein). Further this type of experiment led to more unexpected results, such as the fact that the actin tail composition changed depending on the intracellular location: in the cell body, comets contained α-actinin, while in cell protrusions, comets shed α-actinin concomitant with an evolution of the comet structure toward an aligned unbranched array of long filaments [16]. Information about how the actin network was constructed was also gleaned from altering the ActA protein itself and observing how this changed *Listeria* motility in cells, notably identifying the Arp2/3 complex and Ena/VASP binding domains as important motility motifs [17,18]. However the limitations of this approach quickly became apparent. For example, a back-to-back study of *Listeria* motility in cells expressing different forms of Ena/VASP proteins as compared to the movement of the cells themselves showed that cell movement and *Listeria* movement required different domains of Ena/VASP [19,20]. This perplexing result could have resulted from off-target effects, including mislocalization of the mutant proteins in the host cells, and changes in the internal structure of the host cell that could have decreased or enhanced *Listeria* motility. Indeed other studies showed that the mechanical inhomogeneity of the cell interior altered the motile behavior of *Listeria* [21].

2.2. Listeria in cell extracts and pure protein mixes

The cell interior was too complex of a place to conduct controlled biochemical motility assays, and physical manipulations were rendered difficult. The solution to the confounding effects of the biochemical and mechanical heterogeneity of the cell interior was the use of cell extracts, homogenous cytosolic preparations lacking organelles and cell membrane. Although not without its own challenges, mostly associated with obtaining cell extracts sufficiently concentrated in cytoskeleton factors that were not even entirely known at the time, cell extracts were successfully used to perform some first quantitative physical and biochemical characterizations. For example *Listeria* actin tail elasticity was measured using optical tweezers, and the roles of profilin and Ena/VASP proteins in *Listeria* movement were examined [22–24]. At about the same time, great advances were being made in the understanding of how actin assembly was catalyzed in cells. A major step was the discovery of the Arp2/3 complex as a weak catalyzer or "nucleator" of actin assembly that made branches from the sides of existing filaments, and the subsequent finding that the *Listeria* ActA protein and the mammalian nucleation promoting factors (NPFs) WASp and Scar activated the activity of the Arp2/3 complex [25–27]. All together these findings paved the way for the next great advance: the reconstitution of *Listeria* motility in a mix of pure proteins [28]. The purified protein mix provided tight control of biochemical parameters, and is still today the method of choice for studying actin-based motility, especially for attaining the reproducibility needed for quantitative measurements.

However cell extracts should not be neglected. The study of a pure protein can reveal its mechanism in isolation, but not necessarily its mode of action *in vivo* in association with other proteins. A case in point is ADF/cofilin, an actin filament fragmenting protein. When pure ADF/cofilin was mixed with pure actin filaments in conditions where ADF/cofilin fully decorated the filaments, ADF/cofilin lost its ability to

sever [29]. This was perplexing since high ratios of ADF/cofilin to actin are in fact physiological in some cell types. Recent results using cell extracts showed that an additional factor, Aip1, was present in cytosol that permitted ADF/cofilin to efficiently sever and disassemble actin at high ratios [30], although the exact mode of action of Aip1 is the subject of some controversy [31–33]. The use of cell extracts also permitted other exciting developments such as the reconstruction of complex actin structures like the cleavage furrow in cytokinesis [34]. Recent advances make possible the production of mutant extracts to study individual proteins while retaining the complexity of the cell cytosol and the preparation of staged extracts to examine how actin assembly varies with the cell cycle [35,36].

3. The next generation

3.1. Replacing Listeria with beads

The first reconstituted motility systems using *Listeria* set the stage for the next generation of *in vitro* systems where the pathogen was replaced by a bead or other particle coated with the ActA protein (Fig. 1). This allowed for control of the size and properties of the cargo and the density and nature of the activating protein on the surface, including, importantly, the use of mammalian factors (next section).

The first successful bead systems were performed with ActA-coated particles in cell extracts [37]. This study brought to light one of the stumbling blocks of working with particles in the place of *Listeria*: homogenous distribution of the ActA protein on the bead surface led to homogenous actin growth, which had to undergo "symmetry breaking" to form a polarized actin network and directional motility. Symmetry breaking was shown to depend on particle size, coating density and the concentration of the cell extract, and could be circumvented by preparing artificially asymmetric beads *via* silicon monoxide shadowing [37,38]. Studies of such comets allowed for the important demonstration that actin comet tails observed by electron microscopy had a similar dendritic organization to that found in the lamellipodia of moving cells, thus further validating the use of the bead system as a mini-lamellipodium mimic [39].

Although an impediment to forming actin comets, symmetry breaking was an interesting topic in and of itself, and much was learned about actin network mechanics by observing the growth and rupture of actin networks on spherical beads. In particular it was demonstrated that the network had elastic properties, due to its entangled nature, and stresses could develop in the network and affect growth dynamics [40,41]. Later with the purified protein mix, symmetry breaking on beads was thoroughly characterized and it was shown that stress build-up drove the polarization of the actin network and that stress development depended in predictable ways on the biochemical components of the protein mixture and the balance between nucleation of new filaments, capping and crosslinking [42–44].

3.2. What to coat the beads with?

ActA-coated beads are less employed today, but these original studies opened the door to grafting beads with the mammalian equivalent of ActA, the WASP/WAVE/Scar proteins. Reconstitution of actin comet tails and motility of beads coated with the NPF WASP in bovine brain extracts was the first entirely mammalian reconstitution of actin-based motility [45]. Subsequently the WASP proteins and the related Scar/WAVE molecules were picked apart by absorbing different protein fragments to bead surfaces and observing which domains gave optimal actin network growth and optimal motility in cell extracts and pure protein mixes [46–48]. Different domains from different actin-binding proteins were also absorbed simultaneously and in different proportions to bead surfaces, for example to recruit and activate the Arp2/3 complex in varying proportions with Ena/VASP proteins [49]. When formin proteins were identified as actin polymerization nucleators that produced unbranched networks, in contrast to the Arp2/3 complex-based branched networks, formin-based actin assembly and movement were also reproduced on bead surfaces [50,51]. Given this history, it is remarkable that no one has yet recreated Arp2/3 complex-based and formin-based nucleation together on a bead surface, despite the biological relevance to the lamellipodium where both nucleation systems co-exist and actin networks are generally mixes of branched and unbranched filaments [52,53]. This is particularly pertinent given a recent study that showed that the Arp2/3 complex and formin worked together in a mechanism where the new filament ends created by the Arp2/3 complex were captured and elongated by the formin FMNL2 [54]. However other studies showed that formin and the Arp2/3 complex compete for actin monomers in cells [55], and are not favored by the same conditions in profilin *in vitro* [56], so reconstitution of the two activities together may be a challenge.

In general exotic surface coatings remain rare in the biomimetic field, and the predominant activating proteins used today in *in vitro* systems are human WASP protein fragments, in particular the VCA domain that binds and activates the Arp2/3 complex or its variant pVCA that additionally encompasses the proline-rich portion of WASP that binds profilin actin. VCA is also called WA, due to vocabulary created simultaneously by different labs [57–59]. The pVCA construct is more effective for Arp2/3 complex activation than VCA when monomeric actin is bound with profilin [27]. Indeed most modern reconstitution studies use high concentrations of globular actin bound with profilin to prevent spontaneous nucleation, a closer mimic of actual conditions in cell cytosol and a departure from the original pure protein reconstitution system which used a reservoir of prepolymerized filamentous actin to maintain a low but stable concentration of actin monomers *via* depolymerization [28,60].

The choice of pVCA from WASP as the most-used NPF is more motivated by history than by physiology. WASP is in fact a protein that is only found in hematopoietic cells, while the closely-related N-WASP protein is ubiquitous, but was discovered later (reviewed in [61]). N-WASP-coated beads were used in some studies [62,63], and it is the VCA domain of human N-WASP that is currently commercially available. N-WASP is a more effective Arp2/3 complex activator than either WASP or WAVE/Scar due to the enhanced acidity of the A domain in the case of N-WASP, not as originally believed due to the extra V domain that N-WASP proteins contain [64]. WAVE/Scar-derived bead coatings have been used for some studies, but less extensively than the other NPFs [46,65]. WAVE proteins exist in regulatory complexes, which are impossible to mimic in pure protein mixtures although the WAVE regulatory complex has been successfully recruited to membrane-coated glass beads to form actin comets in cell extracts [66]. In the cell, NPFs have very different roles downstream of signaling cascades: WAVE/Scar proteins are involved in lamellopodial protrusion, while WASP proteins are implicated in filopodia formation and endocytosis (for review [67]). However, as far as biomimetics are concerned, where the regulatory portions of the NPFs are removed, the different NPFs can be used interchangeably since the VCA portion of the different NPFs give the same end product: an Arp2/3 complex-branched network.

3.3. The power of the bead system in the pure protein mix

The combination of the bead system with the pure protein mix changed the face of how actin polymerization was studied. Most importantly it made possible a type of biophysical experiment that had been impossible before, namely varying biochemical and physical parameters and observing how that changed actin assembly and motility. For example it was observed that simply changing particle size or bead-coating density could completely change how the actin comet created movement, switching between continuous and periodic, even though biochemical conditions were identical [68]. Controlled force measurements also became possible in a variety of different experimental set-ups [62,69]. Bead/pure protein mixes were also used to

study the role of the important actin factor, capping protein, showing that capping protein restricted polymerization to the surface *via* promotion of Arp2/3 complex activity [70,71].

Bead speeds were a particularly easy parameter to measure while changing the biochemistry of the mix. As one example, this approach was used to resolve the confusion concerning Ena/VASP proteins and *Listeria* motility mentioned previously. When recruited to the bead surface, Ena/VASP proteins were shown to indeed increase bead speed and different mutants of Ena/VASP showed concordant effects on beads and on an *in vivo* cell motility event [49,65,72]. However the relation between actin polymerization and particle speed is a complex one. It has been observed since the conception of the pure protein mix that movement velocity has a bell-curve dependence on the concentration of polymerization factors: both too much and too little of a given component can reduce speed [28]. In the case of Ena/VASP for example, under different conditions than the study cited above, it was observed that a bead that was already moving very efficiently displayed drastically reduced motility when treated with Ena/VASP, concomitant with the production of a much denser comet tail (Fig. 2). So it seems that when motility is optimal, adding factors that increase polymerization (like Ena/VASP or even the Arp2/3 complex) can slow bead motility and this is something to keep in mind when using bead velocity as a readout of protein function.

4. Polymerization from soft, fluid and deformable substrates

The work on beads spawned a whole other branch of the reconstitution family (Fig. 1) involving polymerization on an assortment of fluid and sometimes deformable substrates like oil droplets, liposomes, lipid-coated beads or supported bilayers, moving one step closer to the real conditions for actin polymerization at a cell membrane bilayer.

The first of such studies involved the absorption of a His-tagged form of ActA to liposomes containing nickel lipids and incubation in cell extracts or cell extracts supplemented in the Arp2/3 complex to form actin comets [73,74]. Several interesting observations came out of these studies, observations that were corroborated subsequently

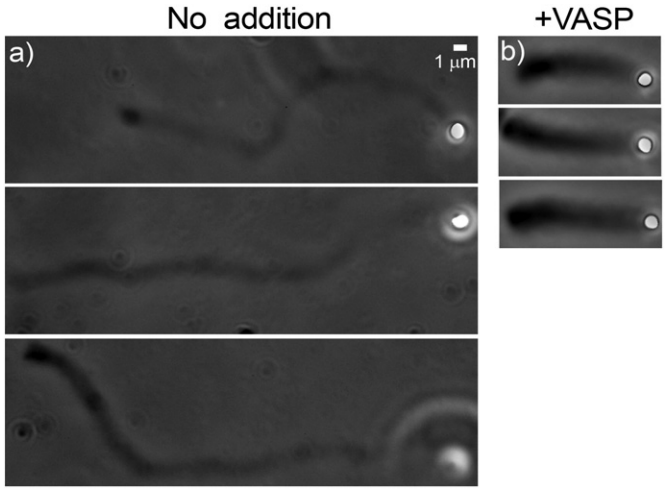

Fig. 2. Enhancing polymerization does not always increase bead motility. a) When motility is very fast (2–3 μm/min), the addition of VASP b) slows the beads down (below 1 μm/min) even though the comet is denser. So the effect of VASP on motility seems to depend on the initial state of the system, and when speed is already optimal, adding an enhancing molecule like VASP does not have the expected effect. Images taken at about 10–15 min reaction time of PRD-VCA-WAVE-coated beads in reconstituted motility mix as described in [65], but with commercial Arp2/3 complex. Phase contrast microscopy. Comet appears as a dark streak behind the white bead. Since there is no depolymerization in this system, comet length is proportional to bead velocity. Images M. Abou-Ghali, 2014.

under different conditions: using the mammalian NPFs VCA-WASP and N-WASP absorbed to liposomes or non-specifically to oil droplets and incubated in either cell extracts or purified protein mixes [75–77]. Although liposomes were more physiological, the advantage of oil droplets was that the surface tension was known so the curvature of the droplet surface could be used to calculate stresses exerted by the growing actin cytoskeleton. One of the main findings from such studies was, first of all, a direct visual proof of the elastic squeezing effect evoked to explain symmetry breaking, mentioned previously. The growth of an actin gel on a convex surface created compressive or squeezing stresses, and this could be clearly seen with both liposomes and oil droplets as a deformation from spherical shape (Fig. 3a, b). Furthermore it was shown that the actin comet exerted retarding or pulling forces on its substrate, presumably due to transient attachments between the actin network and the surface-bound NPFs mediated by the Arp2/3 complex. As a result, the NPFs on the fluid surface were convected under the comet (Fig. 3c). In line with this, another study using the bead system showed that cortactin enhanced motility by releasing NPF molecules from new branches [78]. Another proposed mechanism for transient network-surface attachment was the binding of the WH2 (or V) domain of NPFs to filament barbed ends, an interaction that was mediated by monomeric actin, giving convection of NPFs on lipid-coated glass beads [79]. WASP/WAVE WH2 domains do not bind profilin–actin [80], the predominant form of actin *in vivo* so, in the cell, a combination of attachment *via* the Arp2/3 complex and WH2 domains may be occurring. From all this, it is clear that actin growth exerts both protrusive and braking forces on the objects it acts upon.

However much was also gleaned from biomimetic membrane systems in conjunction with actin polymerization in the absence of motility (for review [7]). For example actin polymerization was shown to induce phase separation of lipids in giant vesicles grafted with N-WASP, incubated in actin and the Arp2/3 complex [81]. In a similar experiment, the branched actin network produced by Arp2/3 complex-based polymerization was observed to be reorganized into bundled filopodia-type structures by the deformable lipid bilayer [82]. Even simpler, and in a continuum with approaches using lipid-coated glass beads, actin polymerization was reproduced on supported lipid bilayers. In particular filopodia formation was recreated on such bilayers, showing that recruitment of biochemical factors from the cell extract gave spontaneous self-assembly of the bundled structure in the absence of membrane deformation [83].

Overall the actin network-on-liposome/droplet systems were a great advance in the field because they brought information as to the interplay between actin assembly and lipid bilayer properties and also opened the door to looking at actin-based deformations. Supported bilayers as a subset of this family have the advantage that they are easier to manipulate physically and image by techniques such as Total Internal Reflection Microscopy (TIRF), but give up the deformability of the liposome system and reduce the mobility of factors in the membrane *via* friction with the support [7].

5. Expanding the biomimetic repertoire

5.1. Confining physiologically nucleated dynamic actin networks

There is nothing new about encapsulating actin polymerization. For decades people have been incorporating monomeric actin into liposomes, triggering polymerization and then observing shape changes. A non-exhaustive list of such studies includes [84–88]. Some studies included non-physiological bonds between the encapsulated actin network and the liposome inner leaflet, such as the linking of biotin actin to biotin lipids *via* streptavidin [89]. Similar experiments have been performed with pure actin and actin-binding proteins or with cell extracts confined in stabilized aqueous-in-oil emulsions, two examples of which are [90,91]. More recently actin polymerization has been confined in

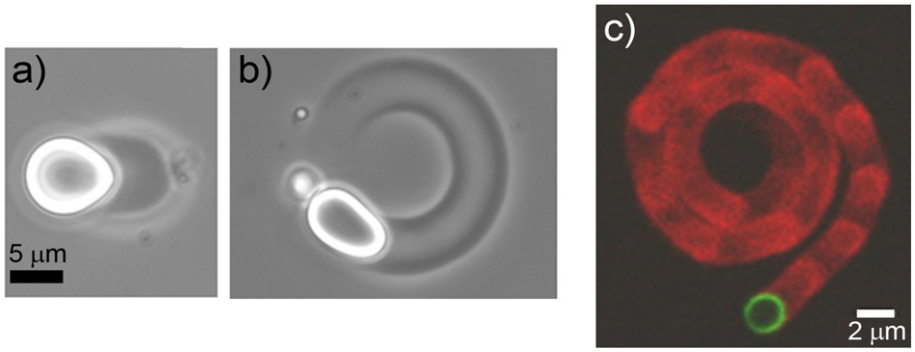

Fig. 3. Actin polymerization on deformable, fluid supports. a) and b) Oil droplets are deformed by the actin comet, depending on how the comet is organized. When the oil droplet is grafted with VCA a), motility is slow, comets are uniform and dense and the droplet is deformed in a pear shape. When the droplet is coated with a mix of VCA and PRO b), a fragment of the ActA protein that recruits VASP, movement is rapid, the comet is partially hollow and the droplet is therefore deformed differently than in a) into a kiwi shape. See also [77]. Phase contrast microscopy. c) On the fluid surface of the oil droplet, VCA (green) is enriched under the comet (actin in red), as observed by the dimmer intensity of VCA at the front of the droplet. The droplet is undergoing jumping movement. For more details see [77]. Confocal fluorescence microscopy. All images Léa Trichet, 2004–2005.

microchambers [92]. In all cases restricting actin polymerization led to interesting phenomena including self-organization, which were not seen in unconfined solutions. This can be understood in the larger framework of how confinement changes biological processes, including cytoskeleton dynamics [93].

A new development concerning confined actin polymerization builds on these experiments, but with several additional characteristics that were previously absent. Namely, to truly reproduce cellular dynamics, the actin network should be growing from the surface *via* localized actin polymerization nucleation. This means that there are transient attachments between the network and the surface, and the barbed ends are growing mostly toward or near the surface. The actin network should also be depolymerizing, and monomers continually recharging with ATP and repolymerizing to make a dynamic network. These aspects are important for mimicking not only lamellipodia-type protrusions, but also for reconstituting other cytoskeletal organelles as we will see in the next section.

Advances have been made in this direction over the last few years. Liposomes were made from native membranes and swelled in the presence of actin, with or without the membrane-actin crosslinking proteins ankyrin/spectrin. In the presence of ankyrin/spectrin, polymerized actin was anchored and bundled at the membrane [94]. This was a physiological link, however the filaments were not dynamic. At about the same time, liposomes were made by a different technique, the inverted emulsion technique, whereby the reconstituted motility mix of pure proteins described earlier was encapsulated in low salt conditions that prevented polymerization and then polymerization was triggered by inserting pores in the membrane to allow passage of salts [95]. Importantly polymerization occurred preferentially at the membrane because a VCA protein was specifically bound there by interaction of its histidine tag with nickel lipids in the membrane, and additionally this actin layer was shown to be actively turning over due to the presence of actin depolymerizing and recycling factors in the liposome interior. This study produced for the first time a dynamic membrane-associated actin structure in a liposome, polymerized in a physiological manner. Subsequently the inverted emulsion technique was used for actin/actin-binding protein encapsulation and micropipette aspiration experiments to show that the membrane-associated actin layer was determinant for the mechanical properties of the liposome [96,97]. Additionally membrane-bound actin layers have since been formed in aqueous-in-oil emulsions, using interface-targeted ActA protein and cell extracts [98]. These actin networks were shown to not only be actively turning over, but also were capable of auto-organization to break symmetry. An added motivation to use liposome-type biomimetic systems is to study proteins that recognize or impose membrane curvature and also interface with the actin cytoskeleton, such as BAR domain proteins [99].

5.2. Patterning actin assembly

Another innovation in the actin biomimetics field is that of making defined actin structures *via* micropatterning of nucleation sites [100]. In some ways this is similar to the previous challenge, but the confinement is imposed by the filament source instead of being created by the envelope. A pioneering study showed that the angle and distance between nucleation sites for actin assembly determined the proportion of parallel bundles *versus* anti-parallel structures within a given actin network although the biochemistry of the networks was identical [101]. This showed that the geometry of filament growth could determine macroscopic structure formation, something that had previously been ascribed to actin-binding proteins. However in cells there is surely a mixture of both geometrical and biochemical control, for when the anti-parallel actin bundler α-actinin was added in high concentrations into the actin polymerization mix, antiparallel filament structures were favored even though the geometry dictated predominant parallel bundle formation [101].

6. Reconstituting acto-myosin contractility *in vitro* in cell-like systems

The stage is now set for one of the next big challenges in actin biomimetics: reproducing the acto-myosin contractile structure found in non-muscle cells juxtaposed to the plasma membrane, an organelle commonly called the cell cortex. This mixed network of actin filaments and myosin motors dynamically polymerizes, depolymerizes and contracts, while at the same time being transiently linked to the plasma membrane that it deforms to produce cell shape changes. In the well-studied contractile system of the muscle sarcomere, unbranched actin filaments are arranged in an anti-parallel manner so as to enable myosin-based contraction. In non-muscle cells, the actin network in the cell cortex is a random array of branched and unbranched actin filaments, not organized like in a muscle sarcomere [52,53]. The question then is: how does the cortex contract efficiently? To answer this, the previously-described techniques are being used to produce cell-like dynamic actin networks, but now containing myosin.

6.1. Interplay between actin organization and myosin contractility

As would be predicted from consideration of how myosin functions, it has been shown experimentally that the overall actin architecture can modify where and how effectively myosin contracts the actin network. The micropatterning approach described above was used to create different network geometries, mixed parallel bundles and anti-parallel structures. When myosin was added to this network, it preferentially contracted anti-parallel structures although it decorated parallel

bundles as well [102]. Myosin was capable of contracting entangled branched networks, albeit much more slowly. However this appeared to be due to the spontaneous occurrence of anti-parallel structures within such networks that were the real substrate for myosin function [102]. A very different experimental approach involving acto-myosin layers near but not attached to supported lipid bilayers also showed that a disordered actin network was efficiently contracted by myosin, but only above a critical myosin concentration [103].

When a static disordered acto-myosin network was attached to the outside or the inside of a lipsome, the outcome of contraction was modulated by the attachment to the bilayer [104]. In the "outside geometry", the balance between contraction and membrane attachment determined whether the acto-myosin network compacted and peeled off the exterior of the lipsome or whether the network contracted and crushed the liposome. In the "inside geometry", contraction either occurred on the bilayer or pulled off the bilayer depending on attachment strength. Taking this experiment one step further, actin was polymerized in the outside geometry with a physiological attachment to the bilayer *via* a membrane-bound VCA molecules, with the Arp2/3 complex, capping protein and profilin to mimic cellular actin polymerization [105]. It was observed that both myosin contraction and actin polymerization contributed to stress build-up in this system, and importantly, that the cocktail of actin-binding proteins determined the window where myosin produced contraction. All together, these results emphasize the importance of the geometry of the network, its attachment to the bilayer and the biochemistry of network formation for determining myosin contractility. This is why there is much to be learned by performing biomimetic experiments, which could give very different behavior from pure acto-myosin networks in the absence of constraints, attachments and physiological polymerization.

Another aspect of actin architecture that could affect myosin contractility efficiency is the presence of crosslinkers. The contraction of the anti-parallel regions of the actin network grown from micropatterns was slower in the presence of the anti-parallel cross-linking protein α-actinin, presumably due to resistance to filament sliding imposed by the cross-links [102]. However a macroscopic contraction assay using suspended actin layers showed that the connectivity conferred by actin cross-linking proteins was necessary for a global contraction [106]. These biomimetic studies show that cross-linking may play a role in controlling how the network contracts. Indeed cross-linking proteins are abundant in the acto-myosin cell cortex [107], and myosin-regulatory roles for the actin-binding proteins fascin and ADF/cofilin, sometimes contradictory in the latter case, have been recently reported in cells [31,108–110]. These issues will be one of the many questions to address in the future with biomimetics.

6.2. Myosin contractility as a disassembly agent

Contraction was expected to change the organization of the actin network by compacting it. What was somewhat unexpected was the observation that motor activity also severed and dismantled the network. This had been observed with actin bundles in bulk assays [111]. However as concerns biomimetic networks, this depolymerization effect was most clearly demonstrated with the micropatterning experiments where contraction of the anti-parallel portions of the network led to their disappearance, and seemingly liberated monomeric actin,

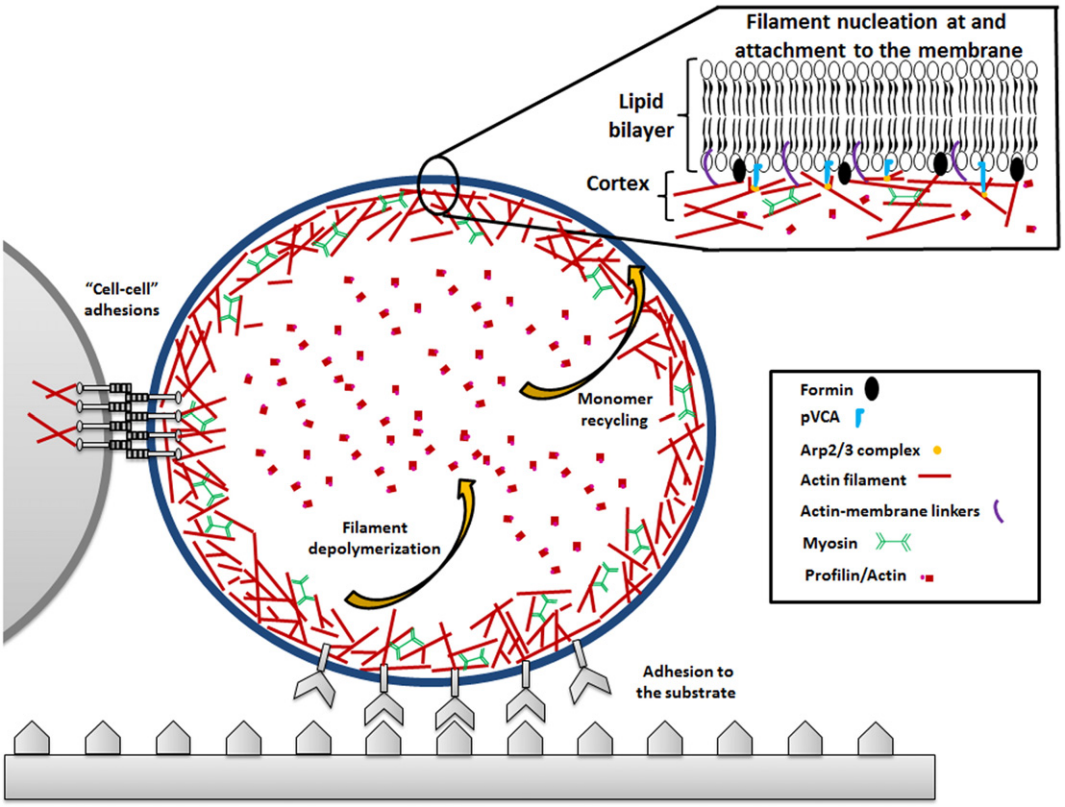

Fig. 4. The ideal artificial acto-myosin *in vitro* system. The main characteristics include: 1) the system has a cell-like geometry confined by a lipid bilayer to mimic the cell membrane, 2) actin filament nucleation occurs at the membrane by physiological factors such as the Arp2/3 complex or another nucleator such as formin, 3) attachment to the membrane is ensured by transient links *via* the Arp2/3 complex and physiological actin filament-membrane linkers such as ezrin, 4) non-muscle myosins are included in the artificial cell interior, 5) actin filaments disassemble either due to the activity of proteins such as ADF/cofilin or to the buckling/severing action that results from myosin contraction and 6) the actin monomers thus liberated are recycled to the cell membrane for subsequent rounds of nucleation. Like in cells, spontaneous formation of filaments in the "cell" interior is inhibited by maintaining free actin in its profilin-bound form. In gray are depicted the future of such systems where, in addition to all the characteristics listed above, the artificial cell is also capable of adhering to its substrate and to its neighboring "cells" *via* its cytoskeleton and transmembrane proteins, thus mimicking epithelial tissues.

as evidenced by an enhanced growth of the parallel bundles in the assay [102]. This macroscopic effect reflected what was happening on the single filament level, where myosin activity was observed to buckle and fragment filaments that were attached to a lipid bilayer [112,113].

7. Conclusion

One of the next challenges for biomimetics is to put together all that we have learned over the last 15 years in order to produce the ideal artificial acto-myosin *in vitro* system (Fig. 4). The goal is to reconstitute inside a cell-like confinement the acto-myosin network, while preserving the architecture of the network as found in living cells, its attachment to the bilayer and the biochemistry of network formation, all of which appear to be important for determining myosin contractility. Such systems should allow for the *in vitro* study of shape changes and spontaneous oscillations. Down the road, the next step will be to include adhesion to the substrate to make motile biomimetic cells, and adhesion to adjacent "cells" to build up artificial tissues in order to mimic and study collective shape changes.

Transparency document

The Transparency document associated with this article can be found, in the online version.

Acknowledgments

We thank Cécile Sykes for discussions and reading of the manuscript. This work was funded by the Fondation pour la Recherche Médicale (Grant DEQ20120323737). R.C. was funded by a PhD fellowship from ITMO Cancer.

References

[1] T.D. Pollard, Rate constants for the reactions of ATP- and ADP-actin with the ends of actin filaments, J. Cell Biol. 103 (1986) 2747–2754.
[2] T.D. Pollard, L. Blanchoin, R.D. Mullins, Molecular mechanisms controlling actin filament dynamics in nonmuscle cells, Annu. Rev. Biophys. Biomol. Struct. 29 (2000) 545–576.
[3] D. Brüggemann, J.P. Frohnmayer, J.P. Spatz, Model systems for studying cell adhesion and biomimetic actin networks, Beilstein J. Nanotechnol. 5 (2014) 1193–1202.
[4] S.K. Vogel, P. Schwille, Minimal systems to study membrane–cytoskeleton interactions, Curr. Opin. Biotechnol. 23 (2012) 758–765.
[5] R.D. Mullins, S.D. Hansen, In vitro studies of actin filament and network dynamics, Curr. Opin. Cell Biol. 25 (2013) 6–13.
[6] A.P. Liu, D.A. Fletcher, Biology under construction: in vitro reconstitution of cellular function, Nat. Rev. Mol. Cell Biol. 10 (2009) 644–650.
[7] M. Loose, P. Schwille, Biomimetic membrane systems to study cellular organization, J. Struct. Biol. 168 (2009) 143–151.
[8] L.G. Tilney, M.S. Tilney, The wily ways of a parasite: induction of actin assembly by *Listeria*, Trends Microbiol. 1 (1993) 25–31.
[9] P. Cossart, Actin-based bacterial motility, Curr. Opin. Cell Biol. 7 (1995) 94–101.
[10] J.A. Theriot, T.J. Mitchison, Actin microfilament dynamics in locomoting cells, Nature 352 (1991) 126–131.
[11] J.A. Theriot, T.J. Mitchison, L.G. Tilney, D.A. Portnoy, The rate of actin-based motility of intracellular *Listeria monocytogenes* equals the rate of actin polymerization, Nature 357 (1992) 257–260.
[12] C.S. Peskin, G.M. Odell, G.F. Oster, Cellular motions and thermal fluctuations: the Brownian ratchet, Biophys. J. 65 (1993) 316–324.
[13] A. Mogilner, G. Oster, Cell motility driven by actin polymerization, Biophys. J. 71 (1996) 3030–3045.
[14] E. Gouin, H. Gantelet, C. Egile, I. Lasa, H. Ohayon, V. Villiers, P. Gounon, P.J. Sansonetti, P. Cossart, A comparative study of the actin-based motilities of the pathogenic bacteria Listeria monocytogenes, *Shigella flexneri* and *Rickettsia conorii*, J. Cell Sci. 112 (1999) 1697–1708.
[15] S. Pistor, T. Chakraborty, U. Walter, J. Wehland, The bacterial actin nucleator protein ActA of Listeria monocytogenes contains multiple binding sites for host microfilament proteins, Curr. Biol. 5 (1995) 517–525.
[16] A. Sechi, J. Wehland, J.V. Small, The isolated comet tail pseudopodium of Listeria monocytogenes: a tail of two actin filament populations, long and axial and short and random, J. Cell Biol. 137 (1997) 155–167.
[17] J. Skoble, D.A. Portnoy, M.D. Welch, Three regions within ActA promote Arp2/3 complex-mediated actin nucleation and *Listeria monocytogenes* motility, J. Cell Biol. 150 (2000) 527–537.
[18] J. Skoble, V. Auerbuch, E.D. Goley, M.D. Welch, D.A. Portnoy, Pivotal role of VASP in Arp2/3 complex-mediated actin nucleation, actin branch-formation, and *Listeria monocytogenes* motility, J. Cell Biol. 155 (2001) 89–100.
[19] J.J. Loureiro, D.A. Rubinson, J.E. Bear, G.A. Baltus, A.V. Kwiatkowski, F.B. Gertler, Critical roles of phosphorylation and actin binding motifs, but not the central proline-rich region, for Ena/Vasodilator-stimulated Phosphoprotein (VASP) function during cell migration, Mol. Biol. Cell 13 (2002) 2533–2546.
[20] M. Geese, J.J. Loureiro, J.E. Bear, J. Wehland, F.B. Gertler, A.S. Sechi, Contribution of Ena/VASP proteins to intracellular motility of *Listeria* requires phosphorylation and proline-rich core but not F-actin binding or multimerization, Mol. Biol. Cell 13 (2002) 2383–2396.
[21] P.A. Giardini, J.A. Theriot, Effects of intermediate filaments on actin-based motility of *Listeria monocytogenes*, Biophys. J. 81 (2001) 3193–3203.
[22] F. Gerbal, V. Laurent, A. Ott, M.-F. Carlier, P. Chaikin, J. Prost, Measurement of the elasticity of the actin tail of *Listeria monocytogenes*, Eur. Biophys. J. 29 (2000) 134–140.
[23] J.A. Theriot, J. Rosenblatt, D.A. Portnoy, P.J. Goldschimdt-Clermont, T.J. Mitchison, Involvement of profilin in the actin-based motility of *L. monocytogenes* in cells and cell-free extracts, Cell 76 (1994) 505–517.
[24] V. Laurent, T.P. Loisel, B. Harbeck, A. Wehman, L. Gröbe, B.M. Jockusch, J. Wehland, F.B. Gertler, M.-F. Carlier, Role of proteins of the Ena-VASP family in actin-based motility of *Listeria monocytogenes*, J. Cell Biol. 144 (1999) 1245–1258.
[25] R.D. Mullins, J.A. Heuser, T.D. Pollard, The interaction of Arp2/3 complex with actin: nucleation, high affinity pointed end capping, and formation of branching networks of filaments, Proc. Natl. Acad. Sci. 95 (1998) 6181–6186.
[26] M.D. Welch, J. Rosenblatt, J. Skoble, D.A. Portnoy, T.J. Mitchison, Interaction of human Arp2/3 complex and the Listeria monocytogenes ActA protein in actin filament nucleation, Science 281 (1998) 105–108.
[27] L.M. Machesky, R.D. Mullins, H.N. Higgs, D.A. Kaiser, L. Blanchoin, R.C. May, M.E. Hall, T.D. Pollard, Scar, a WASp-related protein, activates nucleation of actin filaments by the Arp2/3 complex, Proc. Natl. Acad. Sci. 96 (1999) 3739–3744.
[28] T.P. Loisel, R. Boujemaa, D. Pantaloni, M.F. Carlier, Reconstitution of actin-based motility of *Listeria* and *Shigella* using pure proteins, Nature 401 (1999) 613–616.
[29] E. Andrianantoandro, T.D. Pollard, Mechanism of actin filament turnover by severing and nucleation at different concentrations of ADF/Cofilin, Mol. Cell 24 (2006) 13–23.
[30] A.V. Nadkarni, W.M. Brieher, Aip1 destabilizes cofilin-saturated actin filaments by severing and accelerating monomer dissociation from ends, Curr. Biol. 24 (2014) 2749–2757.
[31] Q. Chen, N. Courtemanche, T.D. Pollard, Aip1 promotes actin filament severing by cofilin and regulates constriction of the cytokinetic contractile ring, J. Biol. Chem. 290 (2015) 2289–2300.
[32] L. Gressin, A. Guillotin, C. Guérin, L. Blanchoin, A. Michelot, Architecture dependence of actin filament network disassembly, Curr. Biol. 25 (2015) 1437–1447.
[33] S. Jansen, A. Collins, S.M. Chin, C.A. Ydenberg, J. Gelles, B.L. Goode, Single-molecule imaging of a three-component ordered actin disassembly mechanism, Nat. Commun. 6 (2015) 7202.
[34] P.A. Nguyen, A.C. Groen, M. Loose, K. Ishihara, M. Wühr, C.M. Field, T.J. Mitchison, Spatial organization of cytokinesis signaling reconstituted in a cell-free system, Science 346 (2014) 244–247.
[35] Y. Miao, C.C.L. Wong, V. Mennella, A. Michelot, D.A. Agard, L.J. Holt, J.R.I. Yates, D.G. Drubin, Cell-cycle regulation of formin-mediated actin cable assembly, Proc. Natl. Acad. Sci. U. S. A. 110 (2013) E4446–E4455.
[36] A. Michelot, A. Grassart, V. Okreglak, M. Costanzo, C. Boone, D.G. Drubin, Actin filament elongation in Arp2/3-derived networks is controlled by three distinct mechanisms, Dev. Cell 24 (2013) 182–195.
[37] L.A. Cameron, M.J. Footer, A. Van Oudenaarden, J.A. Theriot, Motility of ActA protein-coated microspheres driven by actin polymerization, Proc. Natl. Acad. Sci. 96 (1999) 4908–4913.
[38] L.A. Cameron, T.M. Svitkina, D. Vignjevic, J.A. Theriot, G.G. Borisy, Dendritic organization of actin comet tails, Curr. Biol. 11 (2001) 130–135.
[39] T.M. Svitkina, G.C. Borisy, Arp2/3 complex and actin depolymerizing factor/cofilin in dendritic organization and treadmilling of actin filament array in lamellipodia, J. Cell Biol. 145 (1999) 1009–1026.
[40] V. Noireaux, R.M. Golsteyn, E. Friederich, J. Prost, C. Antony, D. Louvard, C. Sykes, Growing an actin gel on spherical surfaces, Biophys. J. 278 (2000) 1643–1654.
[41] J. Plastino, I. Lelidis, J. Prost, C. Sykes, The effect of diffusion, depolymerization and nucleation promoting factors on actin gel growth, Eur. Biophys. J. 33 (2004) 310–320.
[42] J. van der Gucht, E. Paluch, J. Plastino, C. Sykes, Stress release drives symmetry breaking for actin-based movement, Proc. Natl. Acad. Sci. U. S. A. 102 (2005) 7847–7852.
[43] M.J. Dayel, O. Akin, M. Landeryou, V. Risca, A. Mogilner, R.D. Mullins, In silico reconstitution of actin-based symmetry breaking and motility, PLoS Biol. 7 (2009) 1000201.
[44] A. Kawska, K. Carvalho, J. Manzi, R. Boujemaa-Paterski, L. Blanchoin, J.-L. Martiel, C. Sykes, How actin network dynamics control the onset of actin-based motility, Proc. Natl. Acad. Sci. U. S. A. 109 (2012) 14440–14445.
[45] D. Yarar, W. To, A. Abo, M.D. Welch, The Wiskott–Aldrich syndrome protein directs actin-based motility by stimulating actin nucleation with the Arp2/3 complex, Curr. Biol. 9 (1999) 555–558.
[46] D. Yarar, J.A. D'Alessio, R.L. Jeng, M.D. Welch, Motility determinants in WASP family proteins, Mol. Biol. Cell 13 (2002) 4045–4059.
[47] F. Castellano, C. Le Clainche, D. Patin, M.-F. Carlier, P. Chavrier, A WASP–VASP complex regulates actin polymerization at the plasma membrane, EMBO J. 20 (2001) 5603–5614.

[48] J. Fradelizi, V. Noireaux, J. Plastino, B. Menichi, D. Louvard, C. Sykes, R.M. Golsteyn, E. Friederich, ActA and human zyxin harbour Arp2/3-independent actin-polymerization activity, Nat. Cell Biol. 3 (2001) 699–707.
[49] J. Plastino, S. Olivier, C. Sykes, Actin filaments align into hollow comets for rapid VASP-mediated propulsion, Curr. Biol. 14 (2004) 1766–1771.
[50] S. Romero, C. Le Clainche, D. Didry, C. Egile, D. Pantaloni, M.-F. Carlier, Formin is a processive motor that requires profilin to accelerate actin assembly and associated ATP hydrolysis, Cell 119 (2004) 419–429.
[51] A. Michelot, J. Berro, C. Guérin, R. Boujemaa-Paterski, C.J. Staiger, J.-L. Martiel, L. Blanchoin, Actin-filament stochastic dynamics mediated by ADF/Cofilin, Curr. Biol. 17 (2007) 825–833.
[52] M. Bovellan, Y. Romeo, M. Biro, A. Boden, P. Chugh, A. Yonis, M. Vaghela, M. Fritzsche, D. Moulding, R. Thorogate, A. Jégou, A.J. Thrasher, G. Romet-Lemonne, P.P. Roux, E. Paluch, G. Charras, Cellular control of cortical actin nucleation, Curr. Biol. 24 (2014) 1628–1635.
[53] N. Morone, T. Fujiwara, K. Murase, R.S. Kasai, H. Ike, S. Yuasa, J. Usukura, A. Kusumi, Three-dimensional reconstruction of the membrane skeleton at the plasma membrane interface by electron tomography, J. Cell Biol. 174 (2006) 851–862.
[54] J. Block, D. Breitsprecher, S. Kühn, M. Winterhoff, F. Kage, R. Geffers, P. Duwe, J.L. Rohn, B. Baum, C. Brakebusch, M. Geyer, T.E.B. Stradal, J. Faix, K. Rottner, FMNL2 drives actin-based protrusion and migration downstream of Cdc42, Curr. Biol. 22 (2012) 1005–1012.
[55] T.A. Burke, J.R. Christensen, E. Barone, C. Suarez, V. Sirotkin, D.R. Kovar, Homeostatic actin cytoskeleton networks are regulated by assembly factor competition for monomers, Curr. Biol. 24 (2014) 579–585.
[56] C. Suarez, R.T. Carroll, T.A. Burke, J.R. Christensen, A.J. Bestul, J.A. Sees, M.L. James, V. Sirotkin, D.R. Kovar, Profilin regulates F-actin network homeostasis by favoring formin over Arp2/3 complex, Dev. Cell 32 (2015) 43–53.
[57] R. Rohatgi, L. Ma, H. Miki, M. Lopez, H. Kirchausen, T. Takenawa, M. Kirschner, The interaction between N-Wasp and the Arp2/3 complex links Cdc42-dependent signals to actin assembly, Cell 97 (1999) 221–231.
[58] L.M. Machesky, R.H. Insall, Scar1 and the related Wiskott–Aldrich syndrome protein, WASP, regulate the actin cytoskeleton through the Arp2/3 complex, Curr. Biol. 8 (1998) 1347–1356.
[59] H. Miki, S. Suetsugu, T. Takenawa, WAVE, a novel WASP-family protein involved in actin reorganization induced by Rac, EMBO J. 17 (1998) 6932–6941.
[60] L. Blanchoin, R. Boujemaa-Paterski, C. Sykes, J. Plastino, Actin dynamics, architecture and mechanics in cell motility, Physiol. Rev. 94 (2014) 235–263.
[61] H. Miki, T. Takenawa, Regulation of actin dynamics by WASP family proteins, J. Biochem. 134 (2003) 309–313.
[62] Y. Marcy, J. Prost, M.-F. Carlier, C. Sykes, Forces generated during actin-based propulsion: a direct measurement by micromanipulation, Proc. Natl. Acad. Sci. U. S. A. (2004) 5992–5997.
[63] S. Wiesner, E. Helfer, D. Didry, G. Ducouret, F. Lafuma, M.-F. Carlier, D. Pantaloni, A biomimetic motility assay provides insight into the mechanism of actin-based motility, J. Cell Biol. 160 (2003) 387–398.
[64] J. Zalevsky, L. Lempert, H. Kranitz, R.D. Mullins, Different WASP family proteins stimulate different Arp2/3 complex-dependent actin-nucleating activities, Curr. Biol. 11 (2001) 1903–1913.
[65] S. Havrylenko, P. Noguera, M. Abou-Ghali, J. Manzi, F. Faqir, A. Lamora, C. Guérin, L. Blanchoin, J. Plastino, WAVE binds Ena/VASP for enhanced Arp2/3 complex-based actin assembly, Mol. Biol. Cell 26 (2015) 55–65.
[66] V. Koronakis, P.J. Hume, D. Humphreys, T. Liu, O. Horning, O.N. Jensen, E.J. McGhie, WAVE regulatory complex activation by cooperating GTPases Arf and Rac1, Proc. Natl. Acad. Sci. U. S. A. 108 (2011) 14449–14454.
[67] K.G. Campellone, M.D. Welch, A nucleator arms race: cellular control of actin assembly, Nat. Rev. Mol. Cell Biol. 11 (2010) 237–251.
[68] A. Bernheim-Groswasser, S. Wiesner, R.M. Golsteyn, M.-F. Carlier, C. Sykes, The dynamics of actin-based motility depend on surface parameters, Nature 417 (2002) 308–311.
[69] T. Pujol, O. du Roure, M. Fermigier, J. Heuvingh, Impact of branching on the elasticity of actin networks, Proc. Natl. Acad. Sci. U. S. A. 109 (2012) 10364–10369.
[70] O. Akin, R.D. Mullins, Capping protein increases the rate of actin-based motility by promoting filament nucleation by the Arp2/3 complex, Cell 133 (2008) 841–851.
[71] V. Achard, J.-L. Martiel, A. Michelot, C. Guérin, A.-C. Reymann, L. Blanchoin, R. Boujemaa-Paterski, A "primer"-based mechanism underlies branched actin filament network formation and motility, Curr. Biol. 20 (2010) 423–428.
[72] S. Samarin, S. Romero, C. Kocks, D. Didry, D. Pantaloni, M.-F. Carlier, How VASP enhances actin-based motility, J. Cell Biol. 163 (2003) 131–142.
[73] A. Upadhyaya, J.R. Chabot, A. Andreeva, A. Samadani, A. van Oudenaarden, Probing polymerization forces by using actin-propelled lipid vesicles, Proc. Natl. Acad. Sci. 100 (2003) 4521–4526.
[74] P.A. Giardini, D.A. Fletcher, J.A. Theriot, Compression forces generated by actin comet tails on lipid vesicles, Proc. Natl. Acad. Sci. 100 (2003) 6493–6498.
[75] H. Boukellal, O. Campas, J.-F. Joanny, J. Prost, C. Sykes, Soft *Listeria*: actin-based propulsion of liquid drops, Phys. Rev. E 69 (2004) (061906/061901-061906/061904).
[76] V. Delatour, E. Helfer, D. Didry, K.H.D. Lê, J.-F. Gaucher, M.-F. Carlier, G. Romet-Lemonne, Arp2/3 controls the motile behavior of N-WASP-functionalized GUVs and modulates N-WASP surface distribution by mediating transient links with actin filaments, Biophys. J. 94 (2008) 4890–4905.
[77] L. Trichet, O. Campas, C. Sykes, J. Plastino, VASP governs actin dynamics by modulating filament anchoring, Biophys. J. 92 (2007) 1081–1089.
[78] O. Siton, Y. Ideses, S. Albeck, T. Unger, A.D. Bershadsky, N.S. Gov, A. Bernheim-Groswasser, Cortactin releases the brakes in actin-based motility by enhancing WASP-VCA detachment from Arp2/3 branches, Curr. Biol. 21 (2011) 2092–2097.
[79] C. Co, D.T. Wong, S. Gierke, V. Change, J. Taunton, Mechanism of actin network attachment to moving membranes: barbed end capture by N-WASP WH2 domains, Cell 128 (2007) 901–913.
[80] F. Ferron, G. Rebowski, S.H. Lee, R. Dominguez, Structural basis for the recruitment of profilin–actin complexes during filament elongation by Ena/VASP, EMBO J. 26 (2007) 4597–4606.
[81] A.P. Liu, D.A. Fletcher, Actin polymerization serves as a membrane domain switch in model lipid bilayers, Biophys. J. 91 (2006) 4064–4070.
[82] A.P. Liu, D.L. Richmond, L. Maibaum, S. Pronk, P.L. Geissler, D.A. Fletcher, Membrane-induced bundling of actin filaments, Nat. Phys. 4 (2008) 789–793.
[83] K. Lee, J.L. Gallop, K. Rambani, M.W. Kirschner, Self-assembly of filopodia-like structures on supported lipid bilayers, Science 329 (2010) 1341–1345.
[84] J.D. Cortese, B. Schwab III, C. Frieden, E.L. Elson, Actin polymerization induces a shape change in actin-containing vesicles, Proc. Natl. Acad. Sci. U. S. A. 86 (1989) 5773–5777.
[85] L. Limozin, M. Bärmann, E. Sackmann, On the organization of self-assembled actin networks in giant vesicles, Eur. Phys. J. E 10 (2003) 319–330.
[86] L. Limozin, E. Sackmann, Polymorphism of cross-linked actin networks in giant vesicles, Phys. Rev. Lett. 89 (2002) 168103.
[87] H. Miyata, H. Hotani, Morphological changes in liposomes caused by polymerization of encapsulated actin and spontaneous formation of actin bundles, Proc. Natl. Acad. Sci. U. S. A. 89 (1992) 11547–11551.
[88] H. Miyata, S. Nishiyama, K.-I. Akashi, K. Kinosita Jr., Protrusive growth from giant liposomes driven by actin polymerization, Proc. Natl. Acad. Sci. U. S. A. 96 (1999) 2048–2053.
[89] F.-C. Tsai, B. Stuhrmann, G. Koenderink, Encapsulation of active cytoskeletal protein networks in cell-sized liposomes, Langmuir 27 (2011) 10061–10071.
[90] M. Pinot, V. Steiner, B. Dehapiot, B.-K. Yoo, F. Chesnel, L. Blanchoin, C. Kervrann, Z. Gueroui, Confinement induces actin flow in a meiotic cytoplasm, Proc. Natl. Acad. Sci. U. S. A. 109 (2012) 11705–11710.
[91] M.M.A.E. Claessens, M. Bathe, E. Frey, A.R. Bausch, Actin-binding proteins sensitively mediate F-actin bundle stiffness, Nat. Mater. 5 (2006) 748–753.
[92] J. Alvarado, B.M. Mulder, G.H. Koenderink, Alignment of nematic and bundled semiflexible polymers in cell-sized confinement, Soft Matter 10 (2014) 2354–2364.
[93] M.D. Vahey, D.A. Fletcher, The biology of boundary conditions: cellular reconstitution in one, two, and three dimensions, Curr. Opin. Cell Biol. 26 (2014) 60–68.
[94] D. Merkle, N. Kahya, P. Schwille, Reconstitution and anchoring of cytoskeleton inside giant unilamellar vesicles, ChemBioChem 9 (2008) 2673–2681.
[95] L.-L. Pontani, J. Van der Gucht, G. Salbreaux, J. Heuvingh, J.-F. Joanny, C. Sykes, Reconstitution of an actin cortex inside a liposome, Biophys. J. 96 (2009) 192–198.
[96] T. Luo, V. Srivastava, Y. Ren, D.N. Robinson, Mimicking the mechanical properties of the cell cortex by the self-assembly of an actin cortex in vesicles, Appl. Phys. Lett. 104 (2014) 153701.
[97] C. Campillo, P. Sens, D. Köster, L.-L. Pontani, D. Lévy, P. Bassereau, P. Nassoy, C. Sykes, Unexpected membrane dynamics unveiled by membrane nanotube extrusion, Biophys. J. 104 (2013) 1248–1256.
[98] E.A. Shah, K. Keren, Symmetry breaking in reconstituted actin cortices, eLife 3 (2014) e01433.
[99] S. Suetsugu, S. Kurisu, T. Takenawa, Dynamic shaping of cellular membranes by phospholipids and membrane-deforming proteins, Physiol. Rev. 94 (2014) 1219–1248.
[100] A.-C. Reymann, C. Guérin, M. Théry, L. Blanchoin, R. Boujemaa-Paterski, Geometrical control of actin assembly and contractility, Methods Cell Biol. 120 (2014) 19–38.
[101] A.-C. Reymann, J.-L. Martiel, T. Cambier, L. Blanchoin, R. Boujemaa-Paterski, M. Théry, Nucleation geometry governs ordered actin networks structures, Nat. Mater. 9 (2010) 827–832.
[102] A.-C. Reymann, R. Boujemaa-Paterski, J.-L. Martiel, C. Guérin, W. Cao, H.F. Chin, E.M. De La Cruz, M. Théry, L. Blanchoin, Actin network architecture can determine myosin motor activity, Science 336 (2012) 1310–1314.
[103] M. Murrell, M.L. Gardel, Actomyosin sliding is attenuated in contractile biomimetic cortices, Mol. Biol. Cell 25 (2014) 1845–1853.
[104] K. Carvalho, F.-C. Tsai, E. Lees, R. Voituriez, G. Koenderink, C. Sykes, Cell-sized liposomes reveal how actomyosin cortical tension drives shape change, Proc. Natl. Acad. Sci. U. S. A. 110 (2013) 16456–16461.
[105] K. Carvalho, J. Lemière, F. Faqir, J. Manzi, L. Blanchoin, J. Plastino, T. Betz, C. Sykes, Actin polymerization or myosin contraction: two ways to build up cortical tension for symmetry breaking, Philos. Trans. R. Soc. B 368 (2013) 20130005.
[106] J. Alvarado, M. Sheinman, A. Sharma, F.C. MacKintosh, G.H. Koenderink, Molecular motors robustly drive active gels to a critically connected state, Nat. Phys. 9 (2013) 591–597.
[107] G.T. Charras, C.-K. Hu, M. Coughlin, T.J. Mitchison, Reassembly of contractile actin cortex in cell blebs, J. Cell Biol. 175 (2006) 477–490.
[108] N. Elkhatib, M.B. Neu, C. Zensen, K.M. Schmoller, D. Louvard, A.R. Bausch, T. Betz, D.M. Vignjevic, Fascin plays a role in stress fiber organization and focal adhesion disassembly, Curr. Biol. 24 (2014) 1492–1499.
[109] O. Wiggan, A.E. Shaw, J.G. DeLuca, J.R. Bamburg, ADF/Cofilin regulates actomyosin assembly through competitive inhibition of Myosin II binding to F-actin, Dev. Cell 22 (2012) 530–543.
[110] I. Mendes Pinto, B. Rubinstein, A. Kucharavy, J.R. Unruh, R. Li, Actin depolymerization drives actomyosin ring contraction during budding yeast cytokinesis, Dev. Cell 22 (2012) 1247–1260.

[111] L. Haviv, D. Gillo, F. Backouche, A. Bernheim-Groswasser, A cytoskeletal demolition worker: myosin II acts as an actin depolymerization agent, J. Mol. Biol. 375 (2008) 325–330.
[112] M.P. Murrell, M.L. Gardel, F-actin buckling coordinates contractility and severing in a biomimetic actomyosin cortex, Proc. Natl. Acad. Sci. 109 (2012) 20820–20825.
[113] S.K. Vogel, Z. Petrasek, F. Heinemann, P. Schwille, Myosin motors fragment and compact membrane-bound actin filaments, eLife 2 (2013) e00116.
[114] C. Kocks, E. Gouin, M. Tabouret, P. Berche, H. Ohayon, P. Cossart, *L. monocytogenes*-induced actin assembly requires the *actA* gene product, a surface protein, Cell 68 (1992) 521–531.

Annex 2: Research article *Molecular Biology of the Cell* 2015

"WAVE binds Ena/VASP for enhanced Arp2/3 complex–based actin assembly"

Authors: Svitlana Havrylenko*, Philippe Noguera*, **Majdouline Abou-Ghali**, John Manzi, Fahima Faqir, Audrey Lamora, Christophe Guérin, Laurent Blanchoin, and Julie Plastino

My contribution: I performed control experiments concerning VASP's effect on the speed of comet-based motility.

WAVE binds Ena/VASP for enhanced Arp2/3 complex–based actin assembly

Svitlana Havrylenko[a,b,c,*], Philippe Noguera[a,b,c,*], Majdouline Abou-Ghali[a,b,c], John Manzi[a,b,c], Fahima Faqir[a,b,c], Audrey Lamora[a,b,c], Christophe Guérin[d], Laurent Blanchoin[d], and Julie Plastino[a,b,c]

[a]Institut Curie, Centre de Recherche, [b]Centre National de la Recherche Scientifique, Unité Mixte de Recherche 168, and [c]Université Pierre et Marie Curie, Paris F-75248, France; [d]Laboratoire de Physiologie Cellulaire et Végétale, Institut de Recherches en Technologies et Sciences pour le Vivant, CNRS/CEA/INRA/UJF, Grenoble 38054, France

ABSTRACT **The WAVE complex is the main activator of the Arp2/3 complex for actin filament nucleation and assembly in the lamellipodia of moving cells. Other important players in lamellipodial protrusion are Ena/VASP proteins, which enhance actin filament elongation. Here we examine the molecular coordination between the nucleating activity of the Arp2/3 complex and the elongating activity of Ena/VASP proteins for the formation of actin networks. Using an in vitro bead motility assay, we show that WAVE directly binds VASP, resulting in an increase in Arp2/3 complex–based actin assembly. We show that this interaction is important in vivo as well, for the formation of lamellipodia during the ventral enclosure event of *Caenorhabditis elegans* embryogenesis. Ena/VASP's ability to bind F-actin and profilin-complexed G-actin are important for its effect, whereas Ena/VASP tetramerization is not necessary. Our data are consistent with the idea that binding of Ena/VASP to WAVE potentiates Arp2/3 complex activity and lamellipodial actin assembly.**

Monitoring Editor
Thomas D. Pollard
Yale University

Received: Jul 10, 2014
Revised: Sep 22, 2014
Accepted: Oct 21, 2014

INTRODUCTION

The assembly of branched actin networks, nucleated by the Arp2/3 complex, is the driving force behind the protrusion of lamellipodia structures at the leading edge of many types of moving cells (Blanchoin *et al.*, 2014). In lamellipodia, the Arp2/3 complex is activated by the WAVE regulatory complex (WRC) downstream of activation by Rac GTPase and acidic phospholipids, whereas the WASP family of Arp2/3 complex activators is implicated in the formation of filopodia and invadopodia downstream of activation by Cdc42 (Yamaguchi *et al.*, 2005; Sarmiento *et al.*, 2008; Derivery *et al.*, 2009; Lebensohn and Kirschner, 2009; Campellone and Welch, 2010). Another important player in actin dynamics and cell migration is Ena/VASP (Krause *et al.*, 2003). Ena/VASP proteins are correlated with increased actin assembly and lamellipodia-based motility in vivo (Grevengoed *et al.*, 2001, 2003; Gates *et al.*, 2007; Kwiatkowski *et al.*, 2007; Tucker *et al.*, 2011) and increased leading edge protrusion of cells in culture (Rottner *et al.*, 1999; Bear *et al.*, 2002; Lacayo *et al.*, 2007). In keeping with this, the various members of the family (Mena, VASP, and EVL) are part of the invasive signature of human cancers, including those of breast and lung, as well as being associated with other pathologies (Dertsiz *et al.*, 2005; Hu *et al.*, 2008; Philippar *et al.*, 2008; Pula and Krause, 2008). However, these proteins are not actin polymerization nucleators/activators at physiological salt concentrations but instead have anticapping and barbed-end elongation enhancement activity (Barzik *et al.*, 2005; Breitsprecher *et al.*, 2008, 2011; Hansen and Mullins, 2010; Winkleman *et al.*, 2014).

It is not entirely clear how Ena/VASP exercises its effect on actin assembly. In addition to an N-terminal EVH1 domain that binds proline-rich repeats, Ena/VASP proteins possess a central polyproline domain that binds profilin and a C-terminal EVH2 domain that harbors G- and F-actin binding sites and a tetramerization domain (Krause *et al.*, 2003). Several studies of various developmental processes in *Drosophila* and *Caenorhabditis elegans* indicated that removal of the tetramerization domain reduced but did not eliminate activity, whereas mutations in the EVH1 domain interfered with localization and gave reduced activity (Shakir *et al.*, 2006; Gates *et al.*, 2007, 2009; Homem and Peifer, 2009; Fleming *et al.*, 2010). On the

This article was published online ahead of print in MBoC in Press (http://www.molbiolcell.org/cgi/doi/10.1091/mbc.E14-07-1200) on October 29, 2014.

*These authors contributed equally to this work and are listed in alphabetical order.

Address correspondence to: Julie Plastino (julie.plastino@curie.fr).

Abbreviations used: FAB, F-actin binding domain; GAB, G-actin binding domain; GFP, green fluorescent protein; LC, leader cell; LCT, leader cell touch; PC, pocket cell; PP, profilin binding domain; PRD, proline-rich domain; RNAi, RNA interference; TET, tetramerization domain; WRC, WAVE regulatory complex.

Supplemental Material can be found at:
http://www.molbiolcell.org/content/suppl/2014/10/28/mbc.E14-07-1200v1.DC1

other hand, removal of the entire EVH2 domain was equivalent to complete lack of protein. However, the EVH2 domain has not been dissected in vivo in model organisms to evaluate the relative contributions of the F- and G-actin binding domains and the importance of the profilin-binding site to Ena/VASP activity. In cells in culture, a study of cell protrusion and *Listeria* motility in the presence of different VASP deletion mutants gave conflicting results. For example, the form of VASP lacking its F-actin binding site impeded cell protrusion, whereas it enhanced *Listeria* motility (Geese *et al.*, 2002; Loureiro *et al.*, 2002).

It is also not known how Ena/VASP activity is coordinated with that of the bona fide actin polymerization nucleator, the Arp2/3 complex, at the leading edge of moving cells. Speaking to this point, two Arp2/3 complex activators, ActA protein from the *Listeria* bacteria and human WASP, bind Ena/VASP's EVH1 domain, leading to enhanced motility (Niebuhr *et al.*, 1997; Castellano *et al.*, 2001; Lin *et al.*, 2010). Regarding WAVE, several studies point to possible interactions between the WAVE complex and Ena/VASP proteins (Tani *et al.*, 2003; Hirao *et al.*, 2006; Dittrich *et al.*, 2010; Maruoka *et al.*, 2012; Okada *et al.*, 2012). Most of these studies identify the Abi subunit of the complex as the site of interaction between Ena/VASP and the WAVE complex, including one recent work that defines the exact amino acids involved in the Abi-Ena/VASP interaction (Chen *et al.*, 2014). However, another study shows that a proline-rich domain (PRD) from the WAVE polypeptide itself pulls down Ena/VASP from cell extracts (Okada *et al.*, 2012). A WAVE-Ena/VASP interaction might explain how Ena/VASP is targeted to the leading edge of moving cells. Lamellipodin was previously believed to fill this role, but in a recent study, removing lamellipodin's Ena/VASP- binding sites did not affect lamellipodia formation (Law *et al.*, 2013).

Here we investigate the idea that there is a conserved mechanism by which Arp2/3 complex activators additionally bind Ena/VASP to maximize actin assembly. We show that this is true for WAVE and test the functional significance of the Ena/VASP-WAVE polypeptide interaction. We further define what functional domains of Ena/VASP proteins are necessary for its effect on WAVE-based actin polymerization. For this study, we use a dual in vitro bead system/in vivo embryogenesis approach. In the in vitro system, cellular actin polymerization is reproduced on the surface of a bead in the form of an actin comet tail capable of propelling the bead forward, similar to the pushing out of the plasma membrane at the front of a moving cell (Wiesner *et al.*, 2002; Plastino and Sykes, 2005). By changing what form of WAVE we absorb to the bead surface and what form of VASP we add to the motility mix, we address the functional consequences of the putative WAVE-VASP interaction and, in addition, which domains of VASP are required for its activity. In parallel, we ask the same questions in the ventral enclosure event of the developing *C. elegans* embryo. Enclosure involves the formation of actin-filled protrusions by the ventral epidermal cells and their migration to the ventral midline of the embryo to seal the epithelial monolayer (Williams-Masson *et al.*, 1997). As for lamellipodium formation in mammalian cells, WAVE and VASP (WVE-1 and UNC-34, respectively, in *C. elegans* vocabulary) are major players in ventral enclosure, with WAVE being the essential factor: when WAVE is removed, enclosure fails due to lack of migration of the epidermal cells (Patel *et al.*, 2008).

In both the *C. elegans* embryo and using the comet assay, we show evidence for a direct interaction between WAVE and VASP, observe that VASP reinforces Arp2/3 complex–based actin assembly when recruited by WAVE, and determine that the G- and F-actin and profilin-binding domains are critical for VASP function but not its tetramerization domain. We propose that WAVE brings the Arp2/3 complex and VASP together for cooperative enhancement of actin assembly.

RESULTS

Ena/VASP interacts with the proline-rich domain of WAVE to enhance actin-based motility in vitro

We first looked for a direct WAVE-VASP interaction using pure proteins, since the previous studies mentioned in the *Introduction* were done with cell extracts. We coated polystyrene beads with PRD-VCA-WAVE, a form of WAVE comprising both the proline-rich domain and the VCA domain, which is the part that activates the Arp2/3 complex (Figure 1a). When these beads were incubated in purified VASP (Supplemental Figure S1) and then immunostained for VASP, they showed bright staining (Figure 1b). As a positive control for VASP binding, we coated beads with the PRD-VCA construct of human WASP, previously shown to bind VASP (Castellano *et al.*, 2001). These beads showed bright staining, comparable to PRD-VCA-WAVE beads. On the other hand, VCA-coated beads showed dim VASP staining, comparable to that observed when all three types of beads were incubated in ΔEVH1-VASP, a form of VASP lacking the capacity to bind proline-rich domains (Figure 1b). Overall this experiment showed that there was a direct interaction between the EVH1 domain of VASP and the PRD of WAVE.

We next sought to determine whether and how this interaction affected WAVE-based motility. To evaluate this, we turned to the actin comet assay. Beads were coated with PRD-VCA-WAVE and incubated in a reconstituted motility mix containing the Arp2/3 complex, capping protein, and profilin/G-actin (Achard *et al.*, 2010). This mix mimicked the high concentration of monomeric actin complexed with profilin in cellular cytosol and also minimized F-actin formation in the bulk solution, targeting actin assembly to the bead surface.

Addition of VASP to the motility mix containing PRD-VCA-WAVE–coated beads gave bead displacement that was 1.7-fold that produced in the presence of ΔEVH1-VASP or with no addition, indicating that surface recruitment of VASP by WAVE had an enhancing effect on motility (Figure 1c). In fact, adding ΔEVH1-VASP gave identical speeds to the control, no-addition case, meaning that VASP in the bulk had no effect on PRD-VCA-WAVE bead motility. As an additional negative control, we prepared VCA-WAVE–coated beads, but they did not form comets, probably due to low Arp2/3 complex activation in the profilin–actin motility mix without the PRD to recruit profilin–actin. Overall these results suggested that VASP was exercising its enhancing effect on motility via direct binding to the PRD domain of WAVE.

Assessing WAVE and Ena/VASP interaction in vivo

Our tests on beads were done with the recombinant WAVE polypeptide in isolation, not taking into account the fact that this polypeptide is part of the WRC in vivo, regulated by Rac GTPase, phospholipids, and phosphorylation. Indeed, although the native WRC has been successfully recruited to membrane-coated glass beads to form actin comets in cell extract, this approach is not adaptable to our pure-protein mix conditions (Koronakis *et al.*, 2011). However, the PRD of WAVE is a disordered domain that is exposed on the surface of the WAVE complex, so access of VASP to this site should not be hampered in vivo (Chen *et al.*, 2010). Given this, we turned to a cell motility event that was known to depend on the WAVE complex—ventral enclosure during *C. elegans* embryogenesis—and tested whether the PRD of WAVE in the WRC interacted with VASP and increased actin dynamics in vivo as we saw on beads.

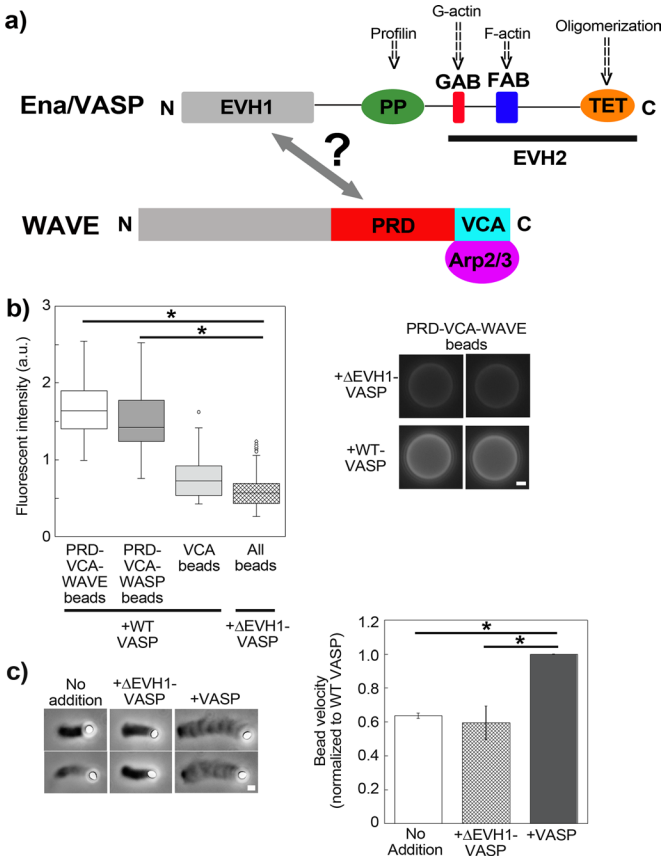

FIGURE 1: WAVE binds Ena/VASP for increased motility in vitro. (a) Scheme of general Ena/VASP and WAVE domain organization, with the putative interaction between the two marked by a double arrow. (b) Immunolabeling of beads coated with different PRD-VCA and VCA constructs incubated in either full-length VASP or ΔEVH1-VASP (lacking the putative site for interaction with WAVE). Only beads carrying the PRD domain light up and only when incubated in VASP possessing its EVH1 domain; $p < 0.0001$. PRD-VCA-WAVE and PRD-VCA-WASP beads in VASP are also significantly higher than VCA in VASP, $p < 0.0001$, not marked on the graph for clarity. Left, fluorescence intensity measurements; right, representative images. From 20 to 50 beads were analyzed per condition. Epifluorescence microscopy. (c) Comets on PRD-VCA-WAVE beads in the presence of wild-type VASP and ΔEVH1-VASP and with no addition. Actin comets appear as darker streaks behind the beads, which appear white. All pictures were taken at ~10- to 15-min reaction time. In the graph, speeds for PRD-VCA-WAVE beads are represented normalized to wild-type VASP addition to account for day-to-day variations. No addition and addition of ΔEVH1-VASP give speeds that are 60% that of wild type, $p = 0.004$ and 0.003, respectively. PRD-VCA-WAVE beads moved at speeds of 0.3–1.4 μm/min, depending on the day and the additive. Phase contrast microscopy. All data are represented as averages ± SD. *p* values calculated with the Student's *t* test. Bars, 1 μm.

To evaluate actin dynamics during ventral closure, we expressed Lifeact–green fluorescent protein (GFP) under an epidermal-specific promoter. We observed the presence of dynamic F-actin structures at the protruding edge of the epidermal cells, especially in the anteriormost "leader cells" (Figure 2, a and b, and Supplemental Video S1), as previously reported using a fluorescently tagged actin-binding domain from VAB-10 (Patel *et al.*, 2008; Gally *et al.*, 2009; Bernadskaya *et al.*, 2012). Also as previously observed, in a VASP-null strain, ventral enclosure still occurred, but the lamellipodia of the leader cells were blunted and less dynamic (Figure 2a and Supplemental Video S2; Sheffield *et al.*, 2007). Somewhat counterintuitively, we observed that the pocket area at the moment of contact of the leader cells in the VASP-null worms was half that of wild type, largely due to the fact that the VASP-null pocket was smaller along its vertical axis, as evidenced by a larger aspect ratio (Figure 2, a and b).

To understand this difference in pocket area, we quantified the speeds of leader cells as compared with pocket cells for wild-type and VASP-null embryos using kymograph analysis. The leader cells in the wild-type embryos migrated almost 1.7-fold faster than those of the VASP-null embryo, whereas the speeds of pocket cell movement were identical (Figure 2c). The difference in pocket area upon leader cell contact in the VASP-null mutant versus the wild type therefore seemed to result from the fact that leader cells and pocket cells moved with similar slow speeds in the VASP-null case, whereas in the wild-type case, leader cells were more dynamic and ran ahead of the sheet. Pocket area at the moment of leader cell touch provided a robust visual readout of the dynamics of the leader cells, and we therefore use this measurement, along with cell migration speeds, to quantify the effects of our different mutants.

Mimicking what we had done on beads, we removed the putative Ena/VASP binding site, the PRD of WAVE. This deletion form of WAVE had been studied in vitro and shown to be correctly incorporated into the mammalian and *Drosophila* WAVE complex (Ismail *et al.*, 2009). We introduced ΔPRD-WAVE and wild-type WAVE as a positive control into a WAVE-null, Lifeact-GFP–positive background, and filmed ventral enclosure events. We observed that reintroduced wild-type WAVE restored leader cell speeds and pocket areas to normal levels, whereas ΔPRD-WAVE gave results that were identical to the VASP-null case shown in Figure 2, even though wild-type VASP was still present in these embryos (Figure 3, a–c, and Supplemental Videos S3 and S4). Other ligands for the PRD domain of WAVE in *C. elegans* are not known. In vertebrates, the PRD of WAVE2 strongly binds IRSp53, a protein implicated in enhancing WAVE activity (Miki *et al.*, 2000). However *C. elegans* WAVE is a WAVE1-type protein, and vertebrate WAVE1 proteins have been shown to have a very weak interaction with IRSp53 (Miki *et al.*, 2000; Kurisu and Takenawa, 2009).

We also performed the converse experiment, removing the putative WAVE binding site, the EVH1 domain, of *C. elegans* VASP. This ΔEVH1-VASP construct was introduced as a GFP fusion into a VASP-null background, and a wild-type, GFP-tagged VASP transgenic was also prepared as a control. Wild-type VASP-GFP and ΔEVH1-VASP-GFP were localized at cell borders, although cytoplasmic diffuse staining was present for ΔEVH1-VASP-GFP (Supplemental Figure S2a). The bright puncta throughout the cells may have resulted from GFP labeling, since these were not apparent for native VASP observed by immunostaining (Sheffield *et al.*, 2007). Puncta had also been observed upon GFP-Ena expression during dorsal closure in *Drosophila*, so this seemed to be a general observation for Ena/VASP-GFP overexpression in vivo and did not appear to disrupt cell function (Gates *et al.*, 2007).

The GFP-tagged strains were additionally crossed with a Lifeact-mCherry strain in order to visualize leader cell dynamics and pocket morphology. The double labeling made it clear that VASP was very faint at the leading edge of leader cells, although bright at cell–cell borders, as also observed in *Drosophila* dorsal closure (Gates *et al.*, 2007; Supplemental Video S5). It seemed probable that the lamellipodia were too thin and dynamic to reliably observe VASP at the leading edge of leader cells. However, observation of F-actin dynamics in the red channel for reintroduced WT-VASP-GFP and ΔEVH1-VASP-GFP embryos revealed blunted leader cells with

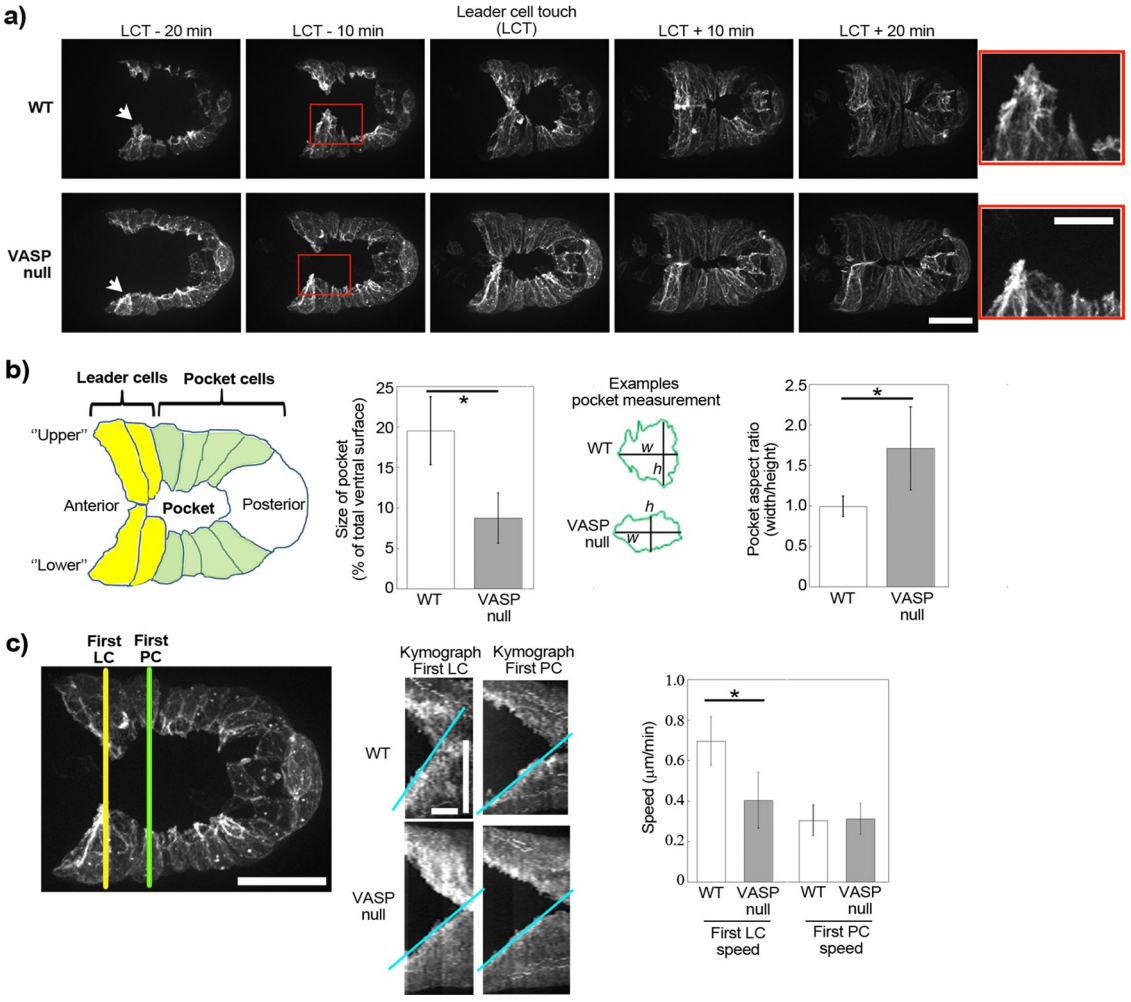

FIGURE 2: VASP affects lamellipodial actin dynamics during ventral enclosure. (a) Imaging of Lifeact-GFP expressed exclusively in epidermal cells during ventral enclosure for wild-type embryos and for embryos lacking VASP. Times are indicated in minutes in relation to leader cell touch (LCT). The lamellipodia of the lower leader cells are indicated by arrows, and zooms of the boxed red area are shown on the right. In the absence of VASP, leader cell protrusions are blunted and only slightly in advance of adjacent pocket cells. *z*-stack projections over several micrometers. Spinning disk fluorescence microscopy; ventral view, anterior is to the left. See also Supplemental Videos S1 and S2. (b) Cartoon of the embryo and measurement of the size of the ventral pocket at the moment of leader cell touching. Pocket sizes are represented as percentages: area of pocket/total area of embryo visible by fluorescence. The pocket in the VASP null case is significantly smaller than in the wild-type case (left, $p < 0.0001$). This is largely due to the fact that the height (*h*) of the VASP-null pocket is smaller, whereas pocket widths (*w*) are identical for wild-type and VASP-null embryos, giving a higher pocket aspect ratio for VASP-null embryos (right, $p < 0.001$). Between 5 and 10 embryos/condition. (c) Migration speeds of leader cells and pocket cells during ventral enclosure. Kymographs are taken as indicated (left) to measure the speed of the first leader cell (LC) and the first pocket cell (PC). Middle, representative kymographs of wild-type and VASP-null embryos (slopes of kymograph in blue; lower cells only for clarity; for PC speeds, only the first, fast phase of enclosure was quantified). Right, LC and PC speeds from several kymographs (6–14). VASP-null leader cells move significantly more slowly than wild type ($p = 0.0006$). The first LCs in VASP-null embryos move essentially at the same speed as pocket cells in both wild-type and VASP-null conditions. All data are represented as averages ± SD. *p* values calculated with the Student's *t* test. Bars, (a) 15 μm, zoom 7.5 μm; (c) 15 μm; kymographs: horizontal bars, 10 min; vertical bar, 15 μm.

reduced protrusion speeds and reduced pocket areas in the latter case, meaning that this form of VASP was unable to rescue leader cell dynamics (Figure 3, a–c, and Supplemental Videos S5 and S6).

Taken together these results showed that interfering with domains that ensure the WAVE-VASP interaction gave ventral enclosure events that resembled the VASP-null case. To confirm this result for a whole population of worms, we turned to a synthetic lethal assay consisting of RNA interference (RNAi) against WASP (WSP-1). WASP knockdown is known to sensitize the embryo, making the absence of VASP embryonic lethal due to ventral enclosure failure (Withee *et al.*, 2004; Sheffield *et al.*, 2007), even though WASP removal on its own has no effect on ventral enclosure (Supplemental Figure S3 and Supplemental Video S7). In the following, we use WASP RNAi as a tool to expose deficiencies in VASP activity. The advantage of using this assay is the ability to evaluate hundreds of embryos by a high-throughput visual assessment of embryonic survival.

We first reproduced previous results showing ~0% survival upon RNAi against WASP in a VASP-null scenario (Figure 3d).

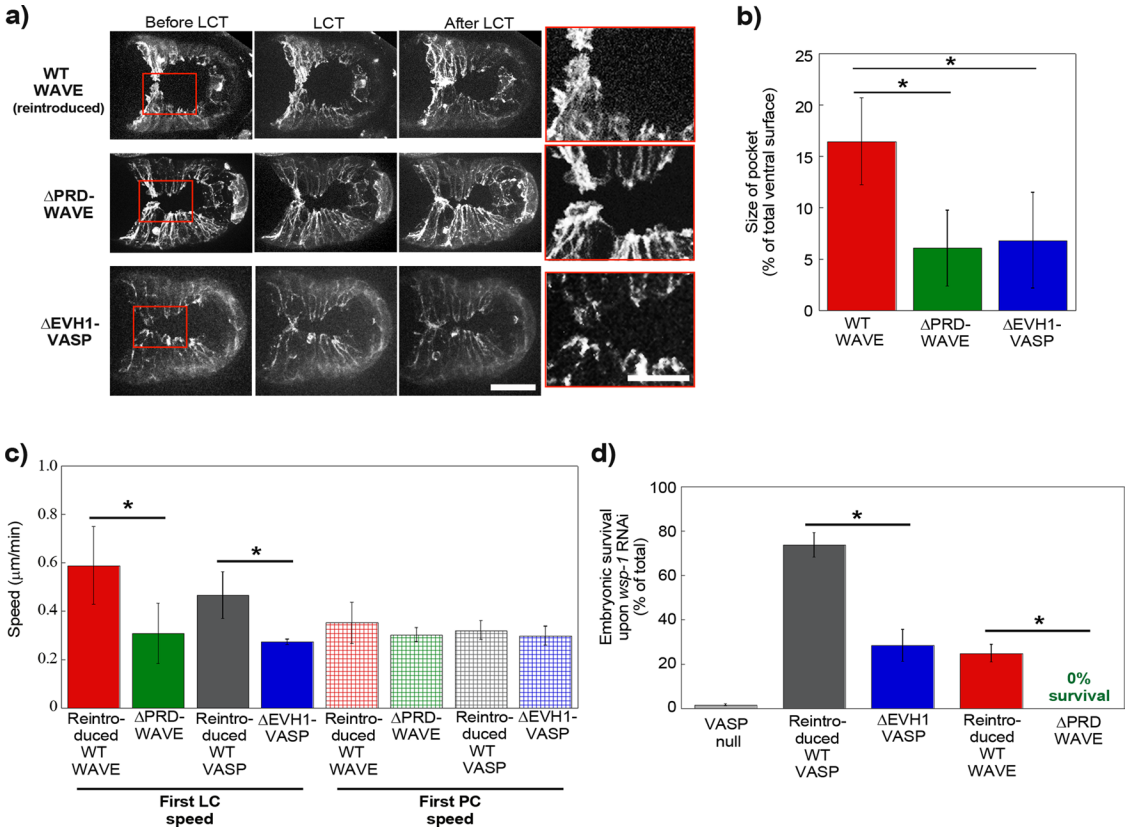

FIGURE 3: WAVE recruits VASP for enhanced actin-based motility in vivo. (a) Lifeact-GFP imaging (WT WAVE and ΔPRD-WAVE) or Lifeact-mCherry imaging (ΔEVH1-VASP) of ventral enclosure in embryos with reintroduced wild-type WAVE or with mutant WAVE and VASP lacking putative interaction sites. Going from left to right, images are shown just before, at the moment of, and just after leader cell touch. Right, zooms of the boxed red areas. Reintroduced wild-type WAVE looks normal (see Figure 2), but introduction of either of the mutants gives leader cell protrusions that are blunted and only slightly in advance of adjacent pocket cells, as if VASP is not present (Figure 2). *z*-stack projections over several micrometers. Spinning disk fluorescence microscopy; ventral view, anterior is to the left. See also Supplemental Videos S3, S4, and S6. These differences are confirmed by pocket area measurements (b) and leader cell speed measurements (c). ΔPRD-WAVE and ΔEVH1-VASP have significantly smaller pocket sizes than reintroduced wild-type ($p < 0.0001$ and $p = 0.049$, respectively) and slower leader cell motility ($p = 0.0015$ and 0.01, respectively), although pocket cell speeds are unchanged with respect to wild type. (d) Synthetic lethal assay with embryonic survival represented as percentage of total eggs laid. On RNAi against WASP, most VASP-null embryos do not survive. ΔEVH1-VASP and ΔPRD-WAVE have much reduced survival compared with reintroduced wild-type proteins ($p < 0.0001$ for both), although both mutants are about as viable as reintroduced wild-type in absence of RNAi treatment (unpublished data). All data are represented as averages ± SD. *p* values calculated with the Student's *t* test. Bar, 15 μm; zoom, 7.5 μm.

Reintroduced wild-type VASP increased survival to 74%, <100%, perhaps due to less efficient expression from extrachromosomal arrays (Stinchcomb *et al.*, 1985). On the other hand, reintroduced ΔEVH1-VASP rescued embryo survival to only 29%, confirming what we had observed concerning leader cell dynamics, that this mutant was much attenuated in its ability to play the role of VASP in ventral enclosure. Its residual activity (not 0% survival like VASP null) indicated that ΔEVH1-VASP was still performing some of its functions. Similarly, we subjected ΔPRD-WAVE transgenic worms to WASP RNAi. As a positive control, we did the same experiment with worms carrying reintroduced wild-type WAVE. Embryonic survival was 25% in the positive control, again perhaps due to inefficient expression from extrachromosomal arrays. However, when ΔPRD-WAVE worms were treated with RNAi against WASP, survival was a solid 0%, phenocopying a Ena/VASP-null phenotype and confirming what we had observed concerning leader cell dynamics and pocket morphology.

Overall these results taken together indicated that when Ena/VASP was present in the cells but not recruited by WAVE, it was inactive to enhance motility, which is what we had also observed with pure proteins in vitro.

Ena/VASP's binding to F-actin and profilin/G-actin are important for its function in vivo

We next wanted to define which domain(s) of VASP, in addition to its WAVE-binding site, were essential to its function of increasing WAVE-based actin dynamics. Into the VASP-null background, we introduced GFP-tagged *C. elegans* VASP constructs lacking individually the F-actin binding site, the G-actin binding site, the tetramerization site, and the profilin-binding region, ΔFAB-VASP, ΔGAB-VASP, ΔTET-VASP, and ΔPP-VASP, respectively (Figure 1a). We also introduced a mutant composed of just the EVH1 domain and thus lacking both the PP and EVH2 regions, called EVH1-VASP. The GAB site is ill defined in *C. elegans* VASP, but by sequence

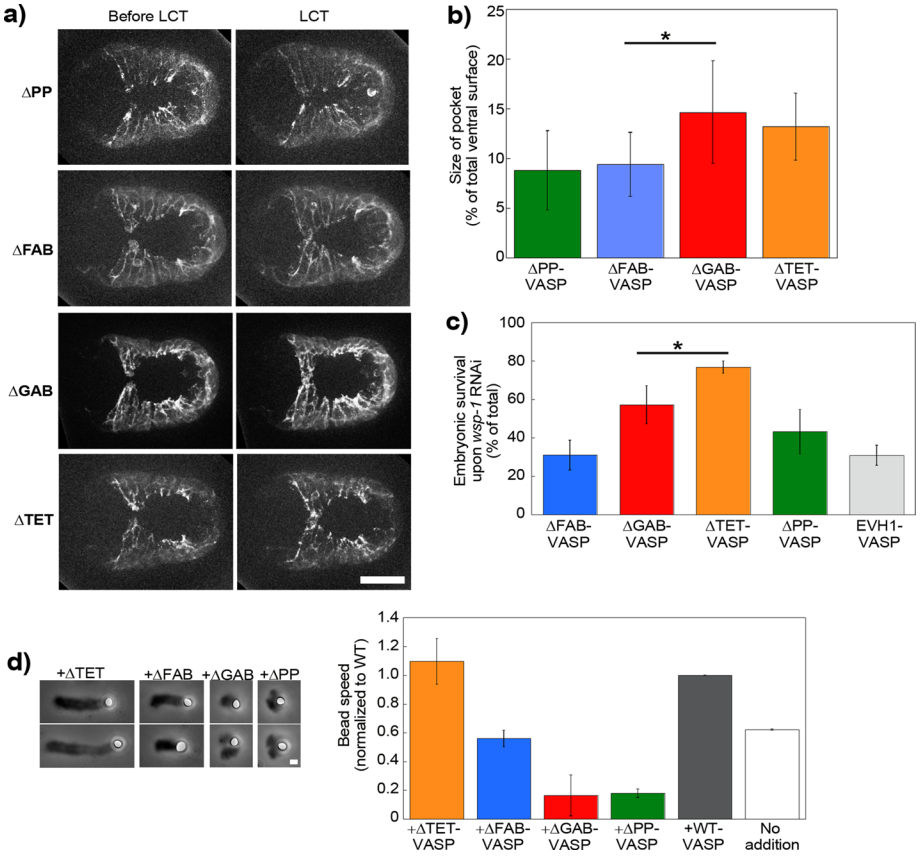

FIGURE 4: VASP's F-actin and profilin/G-actin binding activities are important for its effect on WAVE-based motility. (a) Lifeact-mCherry imaging of ventral enclosure in embryos carrying GFP-tagged VASP proteins mutant for profilin binding, F- and G-actin binding, and tetramerization (ΔPP, ΔFAB, ΔGAB, and ΔTET, respectively). Left image is just before leader cell touch, and right image is at the moment of contact. The leader cell protrusion is rounded and less in advance of the adjacent pocket cells in the ΔPP and ΔFAB cases as compared with the two others. (b) This gives correspondingly smaller pocket areas for ΔPP and ΔFAB ($p = 0.016$), whereas ΔGAB and ΔTET are identical to reintroduced wild-type protein (unpublished data; $p = 0.79$ and 0.87, respectively). See also Supplemental Videos S8 and S9. (c) Embryonic survival of mutant VASP embryos subjected to the synthetic lethal RNAi treatment. ΔTET had a level of survival like wild-type (Figure 3d), whereas ΔGAB was reduced ($p = 0.04$ as compared with reintroduced wild type), although not as much as ΔFAB and ΔPP, which were identical to the negative control EVH1 ($p = 0.97$ and 0.12, respectively). (d) PRD-VCA-WAVE–coated beads incubated in the motility mix with different forms of VASP. Left, representative comets at 10- to 15-min reaction time. See Figure 1 for pictures of wild-type, ΔEVH1-VASP, and no-addition comets. Phase contrast microscopy. Right, bead speeds normalized to the wild-type speed for each day, which was on average ~0.8 μm/min. Two to four independent experiments were averaged for each condition. Wild type and no addition are replotted from Figure 1c for comparison. ΔTET-VASP addition is the same as wild type ($p = 0.3$), whereas ΔFAB-VASP gives identical speeds to no addition ($p = 0.12$). ΔGAB-VASP and ΔPP-VASP inhibit motility. All data are represented as averages ± SD. p values calculated with the Student's t test. Bars, 15 μm (a), 1 μm (d).

alignments, we identified a site that contained a Leu residue adjacent to basic amino acids, which we mutated to acidic amino acids to make our ΔGAB-VASP construct as per Walders-Harbeck *et al.* (2002) and Barzik *et al.* (2005). All constructs localized to cell borders as observed for wild type, whereas ΔTET-VASP displayed additional cytoplasmic staining, and EVH1-VASP was also present in the cytoplasm and the nucleus as previously observed in fibroblasts for EVH1-EGFP of Mena (Bear *et al.*, 2000; Supplemental Figure S2b).

ΔPP-VASP, ΔFAB-VASP, ΔGAB-VASP, and ΔTET-VASP GFP-tagged mutant strains were crossed with a Lifeact-mCherry strain, and we observed that leader cell dynamics and the pocket area at the moment of leader cell touch were reduced for ΔPP-VASP and ΔFAB-VASP, identical to that of VASP-null embryos shown earlier, indicating that VASP required its F-actin and profilin-binding sites to exert its function in vivo (Figure 4, a and b, and Supplemental Video S8). On the other hand, ΔTET-VASP and ΔGAB-VASP embryos had dynamic leader cell lamellipodia and resembled the wild-type situation, with pocket areas similar to wild type, indicating that these domains were not essential for VASP function in vivo (Figure 4, a and b, and Supplemental Video S9). In all mutants, pocket cell speeds were identical to each other, so differences in pocket area resulted from differences in leader cell dynamics only (Supplemental Figure S4).

However, the synthetic lethality assay of these mutants revealed a slight difference between ΔTET-VASP and ΔGAB-VASP. Indeed, when the ΔTET-VASP worms were subjected to WASP RNAi, the lethality was low, identical to wild type shown in Figure 3d, whereas ΔGAB-VASP was mid way between wild type and ΔFAB-VASP (Figure 4c). We performed the synthetic lethality assay on two additional constructs—EVH1-VASP as a negative control, lacking all VASP functional domains for interaction with actin, and ΔPP-VASP. Embryonic lethality of 50–70% was observed in worms carrying ΔPP-VASP, statistically identical to ΔFAB-VASP and to the negative control EVH1-VASP (Figure 4c). We concluded from this that the necessary domains for VASP function in vivo were the F-actin and profilin-binding domains, whereas the tetramerization domain was dispensable. In addition, it appeared that we had correctly identified the G-actin binding domain, and although its removal was not blatantly deleterious to leader cell dynamics, it did appear to play a minor role, as evidenced by the enhanced mortality observed in the RNAi assay.

Ena/VASP's binding to F-actin and profilin/G-actin is important for its function in vitro

In parallel with the ventral enclosure study of the VASP mutants, we used the bead assay to determine which VASP domains were essential for its enhancement of WAVE-based movement in vitro. We applied the different mutants to PRD-VCA-WAVE–coated beads. Addition of VASP lacking the F-actin binding site (ΔFAB-VASP) gave speeds that were 60% that of wild-type protein addition and identical to no addition (Figure 4d). The addition of monomeric VASP (ΔTET-VASP), on the other hand, gave speeds identical to wild type (Figure 4d). Addition of VASP mutants lacking the capacity to interact with G-actin and G-actin/profilin complexes (ΔGAB-VASP and ΔPP-VASP) decreased bead motility, giving split and deformed comets that propelled beads at reduced speeds as compared with no addition (Figure 4d).

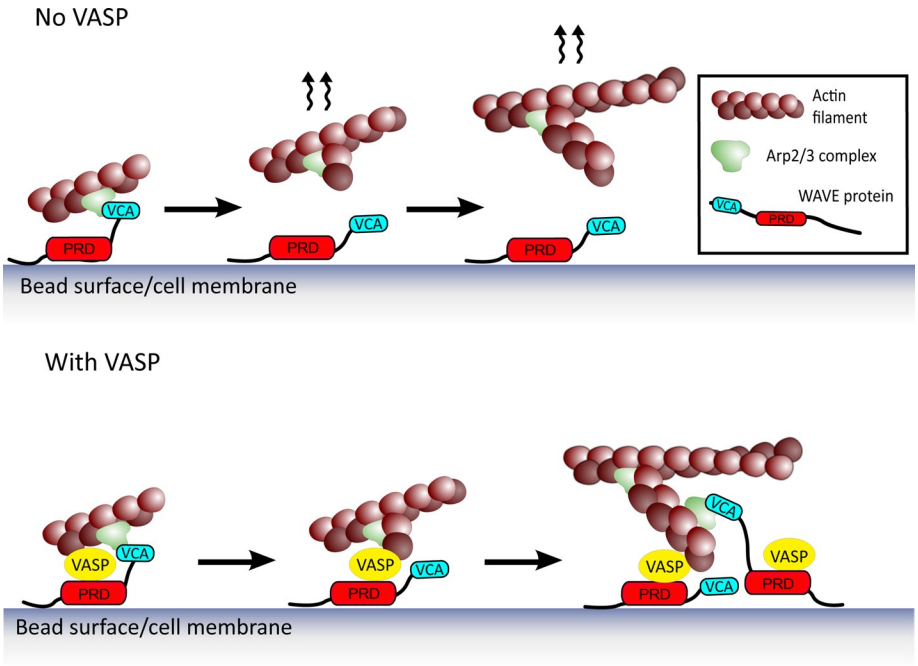

FIGURE 5: Teamwork between the Arp2/3 complex and VASP via mutual binding to WAVE. Membrane/bead-bound WAVE activates the Arp2/3 complex with its VCA domain, which then dissociates from the activated Arp2/3 complex to allow the new branch to grow, giving the scenario at the top, where the nascent branch could diffuse away from the surface. When WAVE recruits VASP in addition to binding and activating the Arp2/3 complex, a hand-off of the nascent branch could happen (bottom). VASP provides the link between the surface and the network at the same time that it enhances growth of new barbed ends. This could not only increase surface-directed polymerization on its own, but it could also contribute to providing new filament primers for subsequent rounds of Arp2/3 complex–based branching (bottom, right vignette).

These results confirmed our in vivo results showing that monomeric VASP was active for motility enhancement and the importance of F-actin and profilin–actin binding. The bead assay further confirmed that the G-actin binding site was important, although it was less essential in vivo.

DISCUSSION

Taken together, our in vivo and in vitro results indicate that the proline-rich domain of WAVE in both *C. elegans* and human protein interacts with VASP and that this association leads to enhanced actin assembly dynamics and increased motility. When VASP is present in the cytosol/in solution but not recruited to the leading edge/bead surface because WAVE is lacking the proline-rich domain or because VASP lacks its EVH1 domain, actin dynamics resembles that of the no-VASP case. Motility enhancement is only observed when VASP is recruited by WAVE to the membrane or bead surface where Arp2/3 complex branches are being formed.

In both embryo and bead systems, monomeric VASP is just as effective in increasing motility as tetrameric (wild-type) protein, so tetramerization appears to be dispensable for lamellipodial-type actin-based protrusion. Tetramerization may be important for other situations, such as in filopodia formation, where bundling is required (Applewhite *et al.*, 2007). On the other hand, interfering with VASP's F-actin or profilin/G-actin binding abolishes the enhancing effect on actin assembly. This result extends to actin networks in vivo and on beads what has already been observed in single filament in vitro assays: Ena/VASP protein binds filaments via its F-actin binding site and delivers monomers from the G-actin and/or profilin-actin binding site to the barbed end (Chereau and Dominguez, 2006; Ferron *et al.*, 2007; Breitsprecher *et al.*, 2008, 2011; Hansen and Mullins, 2010). The lesser effect observed in vivo for the G-actin binding site deletion may reflect the fact that at in vivo salt concentrations, the main polymerization entity is profilin–actin. This has been shown by in vitro measurements of single filament elongation, where it was hypothesized that the mainly electrostatic interaction of the G-actin binding site with G-actin is not favorable under physiological conditions, whereas the hydrophobic interaction of profilin–actin to proline-rich domains is favored (Hansen and Mullins, 2010).

Our results are consistent with a teamwork mechanism between two different actin polymerization machineries, the Arp2/3 complex and VASP, facilitated by mutual binding to WAVE (Figure 5). The WAVE-activated Arp2/3 complex creates a new branch on the side of an existing filament, and this branch is handed off directly to a molecule of VASP, localized at the bead or membrane surface by its association with the proline-rich domain of WAVE. This point is particularly important in light of recent results showing that Arp2/3 complex activators must dissociate from the Arp2/3 complex in order to allow the new branch to grow (Smith *et al.*, 2013). Another candidate for barbed-end capturing at the surface is the WH2 domain of WASP/WAVE, which binds barbed ends (Co *et al.*, 2007). However, this interaction depends on an intervening molecule of monomeric actin, and WH2 domains are not able to bind profilin–actin (Ferron *et al.*, 2007), so the relevance of this barbed-end capture mechanism is not clear in the high-profilin conditions of in vivo polymerization. We propose therefore that WAVE-bound VASP may act as the link between the surface and the actin network at the same time that it enhances barbed-end growth via the profilin–actin loading mechanism. Together this would enhance polymerization at the surface, which not only would increase protrusion on its own, but also provide more filament primers for further Arp2/3 branching events (Figure 5; Achard *et al.*, 2010).

In the bead system, eliminating VASP's ability to interact with either G-actin or profilin/G-actin inhibits bead motility: movement is slower than with no addition. This implies that when VASP is localized at the barbed end via its FAB domain but unable to add actin monomers via its G-actin or profilin-actin binding sites, it slows barbed-end elongation. This result is surprising because for single filaments, interfering with VASP's G-actin binding or with the VASP-profilin/G-actin interaction does not reduce polymerization below that observed for virgin filaments, although it does decrease VASP's capacity to enhance barbed-end elongation (Breitsprecher *et al.*, 2008; Hansen and Mullins, 2010). However, in single-filament assays, VASP does not continue to localize to the barbed end when G-actin binding is abrogated (Hansen and Mullins, 2010). Our observation of motility inhibition may be a reflection of the more complex dynamics of actin network growth confined at a surface where components do not diffuse away as they do from a single filament.

Overall our in vivo and in vitro results allow us to propose a teamwork-type mechanism between the Arp2/3 complex and VASP that leads to enhanced protrusion and motility probably as a result of localized barbed-end elongation enhancement and/or anticapping activity via VASP's capacity to bind profilin, G-actin, and F-actin. Our results ride the wave of similar studies that have brought to light the collaboration of other actin machineries that were previously considered as distinct and independent—for example, the Arp2/3 complex and the formin FMNL2, and the nucleator APC and the formin mDia1 (Block *et al.*, 2012; Breitsprecher *et al.*, 2012). In the light of recent results concerning the direct interaction of the WAVE complex subunit Abi and Ena/VASP proteins (Chen *et al.*, 2014), it seems probable that WAVE coordinates this molecular collaboration between the Arp2/3 complex and Ena/VASP via multiple, perhaps complementary interactions. This mechanism explains why VASP is present in dynamic WAVE-based protrusions in moving cells and gives a first characterization of how VASP activity synergizes with Arp2/3 complex nucleation.

MATERIALS AND METHODS

Worm strains and handling

Worms were maintained and handled using standard techniques (Brenner, 1974). The VASP-null strain *unc-34*(*gm104*) was isolated from PE159 strain [*unc-34*(*gm104*) *hmp-1* (fe4)/mIs10 V] (a gift of Jonathon Pettitt, University of Aberdeen, Aberdeen, United Kingdom). OX308 strain carrying *wve-1*(ne350) I/hT2[bli-4(e937) let-?(q782) qIs48](I;III) was a gift of Martha Soto (Rutgers University, Piscataway, NJ). NG324 *wsp-1(gm324)* and DP38 *unc119(ed3)* were from the *Caenorhabditis* Genetics Center (University of Minnesota, Minneapolis, MN). The following strains were generated in the present study: JUP30 *unc119(ed3)*; Is[Plin-26::Lifeact::GFP::unc54 3′UTR; Cb-unc119], JUP38 unc119(ed3); Is[Plin-26::Lifeact::mCherry::unc54 3′UTR; Cb-unc119], JUP22 unc34(gm104); Ex[Plin-26::unc-34(WT(full-length cDNA))::GFP::unc54 3′UTR; pRF4; pCFJ90], JUP24 unc34(gm104); Ex[Plin-26::unc-34(ΔTET(Δ415-468aa))::GFP::unc54 3′UTR; pRF4; pCFJ90], JUP26 unc34(gm104); Ex[Plin-26::unc-34(ΔFAB(Δ301-318aa))::GFP::unc54 3′UTR; pRF4; pCFJ90], JUP29 unc34(gm104); Ex[Plin-26::unc-34(ΔPP(Δ196-256aa))::GFP::unc54 3′UTR; pRF4; pCFJ90], JUP32 unc34(gm104); Ex[Plin-26::unc-34(ΔEVH1(Δ3-195aa))::GFP::unc54 3′UTR; pRF4; pCFJ90], JUP34 unc34(gm104); Ex[Plin-26::unc-34(ΔGAB($LK_{273}MR_{275}$->LEME))::GFP::unc54 3′UTR; pRF4; pCFJ90], JUP36 unc34(gm104); Ex[Plin-26::unc-34(EVH1(1-195aa))::GFP::unc54 3′UTR; pRF4; pCFJ90], JUP40 wve-1(ne350); Ex[wve-1; pRF4; pCFJ90], JUP44 wve-1(ne350); Ex[wve-1(ΔPRD(Δ200-390aa)); pRF4; pCFJ90]. pRF4 encodes the dominant rol-6(su1006) cotransformation marker. pCFJ90 encodes Pmyo-2::mCherry cotransformation marker. Crossing of JUP30 with unc34(gm104) and NG324 gave JUP46 and JUP47, respectively. JUP48–JUP53 were issued from crossing of JUP38 with JUP22, JUP24, JUP26, JUP29, JUP32, and JUP34, respectively. JUP54 and JUP55 were issued from crossing of JUP30 with JUP40 and JUP44, respectively.

Constructions

C. elegans expression vectors generated in this study and primers used for their construction are summarized in Supplemental Tables S1 and S2. The pAW5 plasmid, carrying nucleotide sequences for *C. elegans lin-26* promoter, *unc-34* cDNA (VASP), and *unc-54* 3′UTR, was a gift of J. Pettitt (Sheffield *et al.*, 2007). Domain boundaries for *C. elegans* VASP (UNC-34) were predicted by alignment with human and mouse VASP. Constructs coding for ΔPP-VASP (lacking residues 196–256, inclusive numbering), ΔEVH1-VASP (lacking residues 3–195), ΔFAB-VASP (lacking residues 301–318), ΔTET-VASP (lacking residues 415–468) mutants of VASP, or its EVH1 domain (first 195 residues only) were prepared by Splicing by Overlapping Extension PCR (SOEing) using oligonucleotides 1–15 (see Supplemental Tables S2 and S3 for details), followed by digestion/ligation into *Kas*I-*Bst*Z17I fragment of pAW5. Constructs coding for ΔEVH1-VASP and ΔGAB-VASP (K273E, R275E; primers 16–19) were prepared similarly, except that *Sgr*AI–*Not*I or *Kas*I–*Not*I sites were used for religation, respectively.

The *wve-1* rescuing fragment was prepared as described previously (Patel *et al.*, 2008). Briefly, the *wve-1* gene was amplified from genomic DNA using attB-tailed oligonucleotides 20 and 21 and recombined with pDONR201 via Gateway BP reaction (Invitrogen), giving pENTR201/wve-1. The ΔPRD mutant (lacking amino acids 201–390) was prepared by SOEing mutagenesis using primers 20–25 and religation after *Bgl*II/*Eco*RI double digestion into pENTR201/wve-1. As for previous studies (Ismail *et al.*, 2009; Chen *et al.*, 2010), a $(Gly\text{-}Gly\text{-}Ser)_6$ linker was inserted in place of the PRD to link the N- and C-terminal parts of the molecule.

Sequence for Lifeact and linker was taken as in Riedl *et al.* (2008) but with *C. elegans* codon usage and used to amplify GFP from the vector pID3.01B (gift of Geraldine Seydoux, Johns Hopkins University, Baltimore, MD) with attB-tailed oligonucleotides 26 and 27. The product was recombined into pDONR221 and then fused with *lin-26* promoter sequence (from pAW5) and the *unc-54* 3′UTR (gift of G. Seydoux; Addgene plasmid 17253: pCM5.37) in the destination vector pCFJ210 (gift of Erik Jorgensen; Addgene plasmid 30538) using the Multisite Gateway System (Invitrogen). pCFJ210/Plin-26::Lifeact::mCherry::*unc543*′UTR was prepared in the same way, except that Lifeact::mCherry was prepared by amplifying mCherry from pGH8 (gift of Erik Jorgensen; Addgene plasmid 19359) and fusing it by PCR to the Lifeact sequence of pENTR[1,2]Lifeact-GFP to avoid integrating the long Lifeact sequence on a single oligo (primers 28–33).

Human WAVE-2 cDNA was a gift of Alexis Gautreau (Laboratoire d'Enzymologie et Biochimie Structurales, Gif-sur-Yvette, France). The PRD-VCA domain of WAVE-2, Lys195– Asp498 (full-length protein numbering), was equipped with an N-terminal glutathione *S*-transferase tag by inserting it between the *Bam*HI and *Not*I sites of pGEX-4T1 (GE Healthcare). A C-terminal Gly linker and octahistidine tag were added before the stop codon. The VCA domain was prepared in the same way and consisted of Thr424–Asp498. All mouse VASP constructs were from Dorothy Schafer (University of Virginia, Charlottesville, VA) and carried an N-terminal hexahistidine tag (Barzik *et al.*, 2005).

Protein purification

The Arp2/3 complex was purified from bovine thymus using the method described for human leukocytes (Higgs *et al.*, 1999). Bovine brain Arp2/3 complex purchased from Cytoskeleton was not used, as it was found to give very fast PRD-VCA-WAVE bead motility (2–3 μm/min) as compared with home-made Arp2/3 complex, and VASP addition in this situation gave motility inhibition (speeds <1 μm/min). VCA protein (from human N-WASP) and rabbit muscle actin were purchased from Cytoskeleton. The mouse α1β2 capping protein construct was a gift of D. Schafer and was purified as in Palmgren *et al.* (2001). Untagged human profilin was expressed in *Escherichia coli* strain Rosetta 2(DE3) pLysS (Novagen) and purified as in Carvalho *et al.* (2013). Mouse VASP protein and mutants were purified as previously described (Barzik *et al.*, 2005). VASP proteins were further purified via fast protein liquid chromatography using a Superdex 200 10/300GL column (GE Healthcare). Mouse VASP

constructs were the following: ΔEVH1-VASP, lacking residues 1–114; ΔPP-VASP, lacking residues 156–207; ΔGAB-VASP double point mutation R232E, K233E; ΔFAB-VASP, lacking residues 255–273; and ΔTET-VASP, lacking residues 331–375.

PRD-VCA-WAVE was expressed in BL21-CodonPlus(DE3)-RIPL (Stratagene) overnight at 30°C with 1 mM isopropyl-β-D-thiogalactoside (IPTG) in 2YT medium containing 50 µg/µl ampicillin and 17 µg/µl chloramphenicol. Cells were lysed in 20 mM Tris, pH 8.0, 200 mM NaCl, 1 mM ETDA, 0.1% Triton X-100, and 1 mM dithiothreitol (DTT) supplemented with complete EDTA-free protease inhibitor cocktail (Roche) then purified using glutathione Sepharose (GE Healthcare). Proteins were eluted with 20 mM Tris, pH 8.0, 200 mM NaCl, 1 mM ETDA, 1 mM DTT, and 25 mM reduced glutathione and then supplemented to 20 mM imidazole. Proteins were then bound to Ni Sepharose High Performance column (GE Healthcare) and eluted in 20 mM Tris, pH 8.0, 200 mM NaCl, 1 mM DTT, and 300 mM imidazole. Proteins were further purified over the Superdex 200 10/300GL column (GE Healthcare) in 20 mM Tris, pH 8.0, 200 mM NaCl, 0.5 mM ETDA, and 1 mM DTT. Protein was dialyzed into 20 mM Tris, pH 8.0, 200 mM NaCl, 0.5 mM ETDA, 1 mM DTT, and 5% glycerol and stored at –80°C. VCA-WAVE was purified essentially in the same way, except that Rosetta 2(DE3) pLysS (Novagen) were used and the Superdex step was omitted. The PRD-VCA-WASP protein was likewise expressed in Rosetta 2(DE3) pLysS but with an overnight expression at 20°C instead of 30°C with 1 mM IPTG. In addition, eluate from the glutathione Sepharose was supplemented to 40 mM imidazole instead of 20 mM before application to the Ni column.

C. elegans transgenesis and imaging

To create *wve-1* transgenics, wve-1(ne350) I/hT2[bli-4(e937) let-?(q782) qIs48](I;III) heterozygous animals were injected with DNA coding for either wild-type or ΔPRD mutant versions of *wve-1* and the injection markers pRF4 (Mello *et al.*, 1991) and pCFJ90 (Pmyo-2::mCherry; Frokjaer-Jensen *et al.*, 2008). Noninjected homozygous *wve-1* animals show Egl (egg-laying defective) and Mel (maternal embryonic lethal) phenotypes. Homozygous *wve-1* animals from established transgenic lines, identified as GFP(-) mCherry (+) rollers, were assayed for rescue of these phenotypes. Wild-type (WT) and ΔPRD mutants of *wve-1* effectively restored laying of eggs (brood size 278 ± 19 for WT vs. 210 ± 26 for ΔPRD) and abated embryonic lethality of their progeny (72 and 82% eggs dead for WT vs. ΔPRD). The assay was done in triplicate, and 12 animals/strain were assayed.

Lifeact-GFP and Lifeact-mCherry animals were generated by microparticle bombardment (Bio-Rad) as described previously (Praitis *et al.*, 2001). To create VASP transgenic animals, VASP-null hermaphrodites were injected with pAW5 (coding for WT-VASP-GFP) or derived plasmids (coding for GFP-tagged forms of ΔEVH1-VASP, ΔFAB-VASP, ΔGAB-VASP, ΔTET-VASP, ΔPP-VASP, or EVH1 domain) along with pCFJ90 (Pmyo-2::mCherry) and pRF4 injection markers. For ventral enclosure imaging, embryos were extruded from transgenic adults by cutting them in a drop of M9 solution and mounted on a 2% agarose pad. Image acquisition was performed at 22°C. Spinning disk confocal fluorescence images were acquired at a Nikon Eclipse TE2000-E microscope equipped with an oil immersion objective, 100×/1.40 numerical aperture, a piezo stage (Nanoscan Prior), a Yokogawa CSU22 confocal head, a HQ2 charge-coupled device camera (Roper Scientific), and a 491-nm diode laser controlled by MetaMorph software 7.5 (Molecular Devices). The 10- to 20-µm *z*-stacks were acquired with 0.5-µm distance between planes. For time-lapse imaging of Lifeact-GFP and Lifeact-mCherry during ventral enclosure, *z*-stacks were acquired at 60- to 90-s intervals on the spinning disk. Owing to low signal, Lifeact-mCherry single-channel images were denoised with the program Safir (Boulanger *et al.*, 2010).

C. elegans RNAi and analysis

Standard RNAi feeding techniques were used (Kamath and Ahringer, 2003). To create *wsp-1* RNAi feeding vector, a full-length *wsp-1a* cDNA was PCR amplified from yk184g1 cDNA clone (gift of Yuji Kohara, National Institute of Genetics, Mishima, Japan) using 5′-GGGCCATGGATGTCGGTATATCCTCCCACGCCGAC and 5′-GGGCTCGAGCTAATCTGACCATTCATTTTTGTCA oligonucleotides and cloned into *Xho*I–*Nco*I sites of L4440 plasmid. *C. elegans* animals were synchronized by hypochlorite treatment. Feeding was carried out at 20°C. A triplicate of Pmyo-2::mCherry(+) embryos issued from 10–20 Pmyo-2::mCherry(+) adult hermaphrodites/condition was assayed for ability to complete embryonic development. Embryos unable to hatch 24 h postlaying were scored as dead. In case of transgenic lines, only mCherry(+) progeny were taken into account. Data are the average of two experiments.

Bead preparation

Carboxylated polystyrene beads of both 1- and 4.5-µm diameter (Polysciences) were coated in Xb (10 mM 4-(2-hydroxyethyl)-1-piperazineethanesulfonic acid [HEPES], pH 7.5, 0.1 M KCl, 1 mM $MgCl_2$, and 0.1 mM $CaCl_2$) with 4.5 µM coating protein at 20 min in a thermomixer (Eppendorf) at 18°C, 1000 rpm. The amount of beads in 40 µl of protein solution was adjusted to a total surface area of 3 cm^2. After coating, the beads were washed twice in 1% bovine serum albumin (BSA)/Xb, resuspended in 120 µl 1% BSA/Xb, and stored on ice for 1 d for bead motility assays.

Immunolabeling of beads

A 0.2-µl amount of coated beads was mixed with 4 µl of 500 nM VASP or ΔEVH1-VASP in Xb/1% BSA, and the reaction was sandwiched between two 12-mm-round coverslips separated by a Parafilm spacer. The reactions were incubated 1 h in a moist chamber at room temperature, and then the sandwiches were floated apart and simultaneously fixed by submersion in a 2% glutaraldehyde/phosphate-buffered saline (PBS) solution. Fixation was continued for 1 h at room temperature, and then the coverslips were neutralized for 10 min in 2 mg/ml $NaBH_4$ in PBS. Coverslips were labeled with a VASP antibody that recognized the C-terminus to detect both wild-type and ΔEVH1-VASP protein (Thermo Scientific) and counterstained with a secondary antibody (goat anti-rabbit) coupled to Alexa 488 (Invitrogen).

Motility assay

The motility medium contained 95 nM Arp2/3 complex, 50 nM capping protein, 5.5 µM profilin, and 5.5 µM G-actin. Actin was diluted to 23 µM in G-buffer (2 mM Tris, 0.2 mM $CaCl_2$, 0.2 mM DTT, pH 8.0) and allowed to depolymerize at 4°C for at least 2 d and used for several weeks. Proteins were diluted in MB13 (10 mM HEPES, 1.5 mM ATP, 3 mM DTT, 1.5 mM $MgCl_2$, 1 mM ethylene glycol tetraacetic acid [EGTA], 1% BSA, and 50 mM KCl, pH 7.5, with 0.1–0.2% methylcellulose [M0512, 4000 cP; Sigma-Aldrich]). We added 150 nM VASP proteins (calculated using the tetramer molecular weight, even for the ΔTET mutant) or the equivalent in VASP buffer (20 mM imidazole, 200 mM KCl, 1 mM EGTA, 2 mM $MgCl_2$, and 1 mM DTT, pH 7.0). The final KCl concentration was brought up to 86 mM by addition of KCl in MB13. Owing to dilution by VASP buffer and G-actin solution, final reaction conditions were ~1 mM ATP, 2 mM DTT, 0.7 mM EGTA, 0.6% BSA, and 0.6–1.2% methylcellulose.

For a final reaction volume of 8.4 µl, 0.2 µl of coated beads was added, and the entire volume was placed between a glass slide and coverslip (18 × 18 mm) and sealed with Vaseline/lanolin/paraffin (1:1:1).

Bead observation and data processing

Phase contrast (for motility assay) and epifluorescence (for immunolabeling) microscopy were performed on an Olympus BX51 upright microscope or an Olympus IX70 inverted microscope with a 100× oil-immersion objective and CoolSnap charge-coupled device camera (Photometrics). Phase contrast and fluorescence quantification was done using MetaMorph software (Universal Imaging). Bead velocities were calculated by measuring lengths of the whole population of comets (pictures taken at random over the entire sample) over time. The slope of comet length versus time gave the average velocity of the entire population. This approach meant that at least 50 comets went into each measurement. The measurement was repeated on different days, and reported speeds are the average 2–4 different days, representing the measurement of hundreds of comets.

ACKNOWLEDGMENTS

We thank Jean-Louis Bessereau for use of his worm injection setup for initial experiments and Vincent Galy and Marie-Anne Felix for use of their microparticle bombardment equipment. For microscope use and support, we acknowledge the imaging facility PICT-IBiSA, Institut Curie, Paris, France, a member of the France BioImaging national research infrastructure. We thank Dorothy Schafer and Kevin Carvalho for discussions and Cécile Sykes and Renaud Legouis for discussions and reading of the manuscript. This work was funded by a Fondation Pierre-Gilles de Gennes grant to S.H., a Human Frontiers Science Program Organization Young Investigator's Grant to J.P., and the Fondation pour la Recherche Médicale (Grant DEQ20120323737) to J.P., Cécile Sykes, and Timo Betz. Some strains were provided by the CGC, which is funded by the National Institutes of Health Office of Research Infrastructure Programs (P40 OD010440).

REFERENCES

Achard V, Martiel J-L, Michelot A, Guérin C, Reymann A-C, Blanchoin L, Boujemaa-Paterski R (2010). A "primer"-based mechanism underlies branched actin filament network formation and motility. Curr Biol 20, 423–428.

Applewhite DA, Barzik M, Kojima S-i, Svitkina TM, Gertler FB, Borisy GG (2007). Ena/VASP proteins have an anti-capping independent function in filopodia formation. Mol Biol Cell 18, 2579–2591.

Barzik M, Kotova TI, Higgs HN, Hazelwood L, Hanein D, Gertler FB, Schafer DA (2005). Ena/VASP proteins enhance actin polymerization in the presence of barbed end capping proteins. J Biol Chem 280, 28653–28662.

Bear JE, Loureiro JJ, Libova I, Fässler R, Wehland J, Gertler FB (2000). Negative regulation of fibroblast motility by Ena/VASP proteins. Cell 101, 717–728.

Bear JE, Svitkina TM, Krause M, Schafer DA, Loureiro JJ, Strasser GA, Maly IV, Chaga OY, Cooper JA, Borisy GG, Gertler FB (2002). Antagonism between Ena/VASP proteins and actin filament capping regulates fibroblast motility. Cell 109, 509–521.

Bernadskaya YY, Wallace A, Nguyen J, Mohler WA, Soto MC (2012). UNC-40/DCC, SAX-3/Robo, and VAB-1/Eph polarize F-actin during embryonic morphogenesis by regulating the WAVE/SCAR actin nucleation complex. PLoS Genet 8, e1002863.

Blanchoin L, Boujemaa-Paterski R, Sykes C, Plastino J (2014). Actin dynamics, architecture and mechanics in cell motility. Physiol Rev 94, 235–263.

Block J, Breitsprecher D, Kühn S, Winterhoff M, Kage F, Geffers R, Duwe P, Rohn JL, Baum B, Brakebusch C, *et al*. (2012). FMNL2 drives actin-based protrusion and migration downstream of Cdc42. Curr Biol 22, 1005–1012.

Boulanger J, Kervrann C, Bouthemy P, Elbau P, Sibarita JB, Salamero J (2010). Patch-based nonlocal functional for denoising fluorescence microscopy image sequences. IEEE Trans Med Imaging 29, 442–454.

Breitsprecher D, Jaiswal R, Bombardier JP, Gould CJ, Gelles J, Goode BL (2012). Rocket launcher mechanism of collaborative actin assembly defined by single-molecule imaging. Science 336, 1164–1168.

Breitsprecher D, Kiesewetter AK, Linkner J, Urbanke C, Resch GP, Small JV, Faix J (2008). Clustering of VASP actively drives processive, WH2 domain-mediated actin filament elongation. EMBO J 27, 2943–2954.

Breitsprecher D, Kiesewetter AK, Linkner J, Vinzenz M, Stradal T, Small JV, Curth U, Dickinson RB, Faix J (2011). Molecular mechanism of Ena/VASP-mediated actin-filament elongation. EMBO J 30, 456–467.

Brenner S (1974). The genetics of *Caenorhabditis elegans*. Genetics 77, 71–94.

Campellone KG, Welch MD (2010). A nucleator arms race: cellular control of actin assembly. Nat Rev Mol Cell Biol 11, 237–251.

Carvalho K, Lemière J, Faqir F, Manzi J, Blanchoin L, Plastino J, Betz T, Sykes C (2013). Actin polymerization or myosin contraction: two ways to build up cortical tension for symmetry breaking. Philos Trans R Soc B 368, 20130005.

Castellano F, Le Clainche C, Patin D, Carlier M-F, Chavrier P (2001). A WASP-VASP complex regulates actin polymerization at the plasma membrane. EMBO J 20, 5603–5614.

Chen XJ, Squarr AJ, Stephan R, Chen B, Higgins TE, Barry DJ, Martin MC, Rosen MK, Bogdan S, Way M (2014). Ena/VASP proteins cooperate with the WAVE complex to regulate the actin cytoskeleton. Dev Cell 30, 569–584.

Chen Z, Borek D, Padrick SB, Gomez TS, Metlagel Z, Ismail AM, Umetani J, Billadeau DD, Otwinowski Z, Rosen MK (2010). Structure and control of the actin regulatory WAVE complex. Nature 468, 533–538.

Chereau D, Dominguez R (2006). Understanding the role of the G-actin-binding domain of Ena/VASP in actin assembly. J Struct Biol 155, 195.

Co C, Wong DT, Gierke S, Change V, Taunton J (2007). Mechanism of actin network attachment to moving membranes: barbed end capture by N-WASP WH2 domains. Cell 128, 901–913.

Derivery E, Lombard B, Loew D, Gautreau A (2009). The Wave complex is intrinsically inactive. Cell Motil Cytoskel 66, 777–790.

Dertsiz L, Ozbilim G, Kayisli Y, Gokhan GA, Demircan A, Kayisli UA (2005). Differential expression of VASP in normal lung tissue and lung adenocarcinomas. Thorax 60, 576–581.

Dittrich M, Strassberger V, Fackler M, Tas P, Lewandrowski U, Sickmann A, Walter U, Dandekar T, Birschmann I (2010). Characterization of a novel interaction between vasodilator-stimulated phosphoprotein and Abelson Interactor 1 in human platelets: a concerted computational and experimental approach. Arterioscler Thromb Vasc Biol 30, 843–850.

Ferron F, Rebowski G, Lee SH, Dominguez R (2007). Structural basis for the recruitment of profilin-actin complexes during filament elongation by Ena/VASP. EMBO J 26, 4597–4606.

Fleming T, Chien S-C, Vanderzalm PJ, Dell M, Gavin MK, Forrester WC, Garriga G (2010). The role of C. elegans Ena/VASP homolog UNC-34 in neuronal polarity and motility. Dev Biol 344, 94–106.

Frokjaer-Jensen C, Davis MW, Hopkins CE, Newman BJ, Thummel JM, Olesen S-P, Grunnet M, Jorgensen EM (2008). Single-copy insertion of transgenes in *Caenorhabditis elegans*. Nat Genet 40, 1375–1383.

Gally C, Wissler F, Zahreddine H, Quintin S, Landmann F, Labouesse M (2009). Myosin II regulation during C. elegans embryonic elongation: LET-502/ROCK, MRCK-1 and PAK-1, three kinases with different roles. Development 136, 3109–3119.

Gates J, Mahaffey JP, Rogers SL, Emerson M, Rogers EM, Sottile SL, Van Vactor D, Gertler FB, Peifer M (2007). Enabled plays key roles in embryonic epithelial morphogenesis in Drosophila. Development 134, 2027–2039.

Gates J, Nowotarski SH, Yin H, Mahaffey JP, Bridges T, Herrera C, Homem CCF, Janody F, Montell DJ, Peifer M (2009). Enabled and Capping protein play important roles in shaping cell behavior during Drosophila oogenesis. Dev Biol 333, 90–107.

Geese M, Loureiro JJ, Bear JE, Wehland J, Gertler FB, Sechi AS (2002). Contribution of Ena/VASP proteins to intracellular motility of *Listeria* requires phosphorylation and proline-rich core but not F-actin binding or multimerization. Mol Biol Cell 13, 2383–2396.

Grevengoed EE, Fox DT, Gates J, Peifer M (2003). Balancing different types of actin polymerization at distinct sites: roles for Abelson kinase and Enabled. J Cell Biol 163, 1267–1279.

Grevengoed EE, Loureiro JJ, Jesse TL, Peifer M (2001). Abelson kinase regulates epithelial morphogenesis in Drosophila. J Cell Biol 155, 1185–1197.

Hansen SD, Mullins RD (2010). VASP is a processive actin polymerase that requires monomeric actin for barbed end association. J Cell Biol 191, 571–584.

Higgs HN, Blanchoin L, Pollard TD (1999). Influence of the C terminus of Wiskott-Aldrich syndrome protein (WASp) and the Arp2/3 complex on actin polymerization. Biochemistry 38, 15212–15222.
Hirao N, Sato S, Gotoh T, Maruoka M, Suzuki J, Matsuda S, Shishido T, Tani K (2006). NESH (Abi-3) is present in the Abi/WAVE complex but does not promote c-Abl-mediated phosphorylation. FEBS Lett 580, 6464–6470.
Homem CCF, Peifer M (2009). Exploring the roles of Diaphanous and Enabled activity in shaping the balance between filopodia and lamellipodia. Mol Biol Cell 20, 5138–5155.
Hu L-D, Zou H-F, Zhan S-X, Cao K-M (2008). EVL (Ena/VASP-like) expression is up-regulated in human breast cancer and its relative expression level is correlated with clinical stages. Oncol Rep 19, 1015–1020.
Ismail AM, Padrick SB, Chen B, Umetani J, Rosen MK (2009). The WAVE regulatory complex is inhibited. Nat Struct Mol Biol 16, 561–563.
Kamath RS, Ahringer J (2003). Genome-wide RNAi screening in Caenorhabditis elegans. Methods 30, 313–321.
Koronakis V, Hume PJ, Humphreys D, Liu T, Horning O, Jensen ON, McGhie EJ (2011). WAVE regulatory complex activation by cooperating GTPases Arf and Rac1. Proc Natl Acad Sci USA 108, 14449–14454.
Krause M, Dent EW, Bear JE, Loureiro JJ, Gertler FB (2003). Ena/VASP proteins: regulators of the actin cytoskeleton and cell migration. Annu Rev Cell Dev Biol 19, 541–564.
Kurisu S, Takenawa T (2009). The WASP and WAVE family proteins. Genome Biol 10, 226.
Kwiatkowski AV, Rubinson DA, Dent EW, van Veen JE, Leslie JD, Zhang J, Mebane LM, Philippar U, Pinheiro EM, Burds AA, *et al*. (2007). Ena/VASP is required for neuritogenesis in the developing cortex. Neuron 56, 441–455.
Lacayo CI, Pincus Z, VanDuijn MM, Wilson CA, Fletcher DA, Gertler FB, Mogilner A, Theriot JA (2007). Emergence of large-scale cell morphology and movement from local actin filament growth dynamics. PLoS Biol 5, 2035–2052.
Law A-L, Vehlow A, Kotini M, Dodgson L, Soong D, Theveneau E, Bodo C, Taylor E, Navarro C, Perera U, *et al*. (2013). Lamellipodin and the Scar/WAVE complex cooperate to promote cell migration in vivo. J Cell Biol 203, 673–689.
Lebensohn AM, Kirschner MW (2009). Activation of the WAVE complex by coincident signals controls actin assembly. Mol Cell 36, 512–524.
Lin W-H, Nelson SE, Hollingsworth RJ, Chung CY (2010). Functional roles of VASP phosphorylation in the regulation of chemotaxis and osmotic stress response. Cytoskeleton 67, 259–271.
Loureiro JJ, Rubinson DA, Bear JE, Baltus GA, Kwiatkowski AV, Gertler FB (2002). Critical roles of phosphorylation and actin binding motifs, but not the central proline-rich region, for Ena/Vasodilator-stimulated Phosphoprotein (VASP) function during cell migration. Mol Biol Cell 13, 2533–2546.
Maruoka M, Sato M, Yuan Y, Ichiba M, Fuji R, Ogawa T, Ishida-Kitagawa N, Takeya T, Watanabe N (2012). Abi-1-bridged tyrosine phosphorylation of VASP by Abelson kinase impairs association of VASP to focal adhesions and regulates leukaemic cell adhesion. Biochem J 441, 889–899.
Mello CC, Kramer JM, Stinchcomb D, Ambros V (1991). Efficient gene transfer in C. elegans: extrachromosomal maintenance and integration of transforming sequences. EMBO J 10, 3959–3970.
Miki H, Yamaguchi H, Suetsugu S, Takenawa T (2000). IRSp53 is an essential intermediate between Rac and WAVE in the regulation of membrane ruffling. Nature 408, 732–735.
Niebuhr K, Ebel F, Frank R, Reinhard M, Domann E, Carl UD, Walter U, Gertler FB, Wehland J, Chakraborty T (1997). A novel proline-rich motif present in ActA of Listeria monocytogenes and cytoskeletal proteins is the ligand for the EVH1 domain, a protein module present in the Ena/VASP family. EMBO J 16, 5433–5444.
Okada H, Uezu A, Soderblom EJ, Moseley III MA, Gertler FB, Soderling SH (2012). Peptide Array X-linking (PAX): a new peptide-protein identification approach. PLoS One 7, e37035.
Palmgren S, Ojala PJ, Wear MA, Cooper JA, Lappalainen P (2001). Interactions with PIP_2, ADP-actin monomers, and capping protein regulate the activity and localization of yeast twinfilin. J Cell Biol 155, 251–260.
Patel FB, Bernadskaya YY, Chen E, Jobanputra A, Pooladi Z, Freeman KL, Gally C, Mohler WA, Soto MC (2008). The WAVE/SCAR complex promotes polarized cell movements and actin enrichment in epithelia during C. elegans embryogenesis. Dev Biol 324, 297–309.
Philippar U, Roussos ET, Oser M, Yamaguchi H, Kim H-D, Giampieri S, Wang Y, Goswami S, Wyckoff JB, Lauffenburger DA, *et al*. (2008). A Mena invasion isoform potentiates EGF-induced carcinoma cell invasion and metastasis. Dev Cell 15, 813–828.
Plastino J, Sykes C (2005). The actin slingshot. Curr Opin Cell Biol 17, 62–66.
Praitis V, Casey E, Collar D, Austin J (2001). Creation of low-copy integrated transgenic lines in *Caenorhabditis elegans*. Genetics 157, 1217–1226.
Pula G, Krause M (2008). Role of Ena/VASP proteins in homeostasis and disease. Handb Exp Pharmacol 186, 39–65.
Riedl J, Crevenna AH, Kessenbrock K, Yu JH, Neukirchen D, Bista M, Bradke F, Jenne D, Holak TA, Werb Z, *et al*. (2008). Lifeact: a versatile marker to visualize F-actin. Nat Methods 5, 605.
Rottner K, Behrendt B, Small JV, Wehland J (1999). VASP dynamics during lamellipodia protrusion. Nat Cell Biol 1, 321–322.
Sarmiento C, Wang W, Dovas A, Yamaguchi H, Sidani M, El-Sibai M, DesMarais V, Holman HA, Kitchen S, Backer JM, *et al*. (2008). WASP family members and formin proteins coordinate regulation of cell protrusions in carcinoma cells. J Cell Biol 180, 1245–1260.
Shakir MA, Gill JS, Lundquist EA (2006). Interactions of UNC-34 Enabled with Rac GTPases and the NIK Kinase MIG-15 in Caenorhabditis elegans axon pathfinding and neuronal migration. Genetics 172, 893–913.
Sheffield M, Loveless T, Hardin J, Pettitt J (2007). *C. elegans* enabled exhibits novel interactions with N-WASP, Abl and cell-cell junctions. Curr Biol 17, 1791–1796.
Smith BA, Padrick SB, Doolittle LK, Daugherty-Clarke K, Correa IR, Xu M-Q, Goode BL, Rosen MK, Gelles J (2013). Three-color single molecule imaging shows WASP detachment from Arp2/3 complex triggers actin filament branch formation. eLife 2, e01008.
Stinchcomb DT, Shaw JE, Carr SH, Hirsh D (1985). Extrachromosomal DNA transformation of Caenorhabditis elegans. Mol Cell Biol 5, 3484–3496.
Tani K, Sato S, Sukezane T, Kojima H, Hirose H, Hanafusa H, Shishido T (2003). Abl Interactor 1 promotes tyrosine 296 phosphorylation of mammalian Enabled (Mena) by c-Abl kinase. J Biol Chem 278, 21685–21692.
Tucker PK, Evans IR, Wood W (2011). Ena drives invasive macrophage migration in Drosophila embryos. Dis Model Mech 4, 126–134.
Walders-Harbeck B, Khaitlina SY, Hinssen H, Jockusch BM, Illenberger S (2002). The vasodilator-stimulated phosphoprotein promotes actin polymerisation through direct binding to monomeric actin. FEBS Lett 529, 275–280.
Wiesner S, Boujemaa-Paterski R, Carlier M-F (2002). Actin-based motility of *Listeria monocytogenes* and *Shigella flexneri*. Methods Microbiol 31, 245–262.
Williams-Masson EM, Malik AN, Hardin J (1997). An actin-mediated two-step mechanism is required for ventral enclosure of the *C. elegans* hypodermis. Development 124, 2889–2901.
Winkleman JD, Bilancia CG, Peifer M, Kovar DR (2014). Ena/VASP Enabled is a highly processive actin polymerase tailored to self-assemble parallel-bundled F-actin networks with Fascin. Proc Natl Acad Sci USA 111, 4121–4126.
Withee J, Galligan B, Hawkins N, Garriga G (2004). *Caenorhabditis elegans* WASP and Ena/VASP proteins play compensatory roles in morphogenesis and neuronal cell migration. Genetics 167, 1165–1176.
Yamaguchi H, Lorenz M, Kempiak S, Sarmiento C, Coniglio S, Symons M, Segall J, Eddy R, Miki H, Takenawa T, Condeelis J (2005). Molecular mechanisms of invadopodium formation: the role of the N-WASP–Arp2/3 complex pathway and cofilin. J Cell Biol 168, 441–452.

Annex 3: Research article *Nature Physics* accepted

"Actin dynamics drive cell-like membrane deformation"

Authors: Camille Simon, Remy Kusters, Valentina Caorsi, Antoine Allard, **Majdouline Abou-Ghali**, John Manzi, Aurélie Di Cicco, Danile Lévy, Martin Lenz, Jean-François Joanny, Clément Campillo, Julie Plastino, Pierre Sens, Cécile Sykes

My contribution: I performed pyrene assays to assess actin-binding protein activity, and performed trouble-shooting experiments to optimize polymerization on surfaces.

Title: Actin dynamics drive cell-like membrane deformation.

Camille Simon[†1,2], Rémy Kusters[†1,2], Valentina Caorsi[†1,2], Antoine Allard[1,2,3], Majdouline Abou-Ghali[1,2], John Manzi[1,2], Aurélie Di Cicco[1,2], Daniel Lévy[1,2], Martin Lenz[4], Jean-François Joanny[1,2,5], Clément Campillo[3], Julie Plastino[1,2], Pierre Sens[1,2&], Cécile Sykes[1,2&]

[†]These authors contributed equally to this work.

[&]These authors contributed equally to this work.

Abstract: Cell membrane deformations are crucial for proper cell function. Specialized protein assemblies initiate inward or outward membrane deformations that the cell uses respectively to uptake external substances or probe the environment. The assembly and dynamics of the actin cytoskeleton are involved in this process, although their detailed role remains controversial. We show here that a dynamic, branched actin network is sufficient to initiate both inward and outward membrane deformation. The polymerization of a dense actin network at the membrane of liposomes produces inward membrane bending at low tension, while outward deformations are robustly generated regardless of tension. Our results shed light on the mechanism cells use to internalize material, both in mammalian cells, where actin polymerization forces are required when membrane tension is increased, and in yeast, where those forces are necessary to overcome the opposing turgor pressure. By combining experimental observations with physical modeling, we propose a mechanism that explains how membrane tension and the architecture of the actin network regulate cell-like membrane deformations.

[1] Laboratoire Physico Chimie Curie, Institut Curie, PSL Research University, CNRS UMR168, 75005, Paris, France. [2] Sorbonne Universités, UPMC Univ Paris 06, 75005, Paris, France. [3] LAMBE, Université Evry, CNRS, CEA, Université Paris-Saclay, Evry F-91025, France. [4] LPTMS, CNRS, Univ. Paris-Sud, Université Paris-Saclay, 91405 Orsay, France. [5] ESPCI-Paris, 10 rue Vauquelin, 75005, Paris, France.

Many cell functions rely on the ability of cells to change their shape. The deformation of the cell membrane is produced by the activity of various proteins that curve the membrane inwards or outwards, by exerting pulling and pushing forces or by imposing membrane curvature via structural effects. When cells take up external material, it is often associated with membrane invaginations followed by vesicle transport. This process is called endocytosis. Such inward deformation of the cell membrane can be initiated by specific proteins, such as clathrin, which coat the membrane and impose geometrical constraints that bend the membrane inwards. In this view, the action of the actin cytoskeleton, a filamentous network that forms at the membrane, is crucial only at a later stage for membrane elongation. Nevertheless, impressive correlation methods revealed unambiguously that, in yeast, membrane bending is not triggered by the presence of coat proteins, but by a dynamic actin network formed at the membrane through the Arp2/3 complex branching agent [1, 2, 3]. In mammalian cells, clathrin-mediated endocytosis requires the involvement of actin if the plasma membrane is tense, *e.g.* following osmotic swelling or mechanical stretching [4]. However, the exact mechanism of membrane deformation in this process is still poorly understood. Strikingly, the same type of branched actin network is able to bend the membrane the other way in, outward-pointing membrane deformations, called dendritic filopodia. These structures are precursors of dendritic spines in neurons, and essential for signal transmission [5]. Dendritic filopodia differ from conventional filopodia, localized at the leading edge of the cell, where actin filaments are parallel. Whereas the pioneering work of Liu et al[6] already established how thin filopodia form by bundling actin filaments, the production of a dendritic filopodia-like membrane protrusion containing a branched actin network has never been investigated.

How the same branched actin structure can be responsible for the initiation of filopodia, which are outward-pointing membrane deformations, as well as endocytic invaginations that deform the membrane inward, is what we want to address in this paper. Such a question is difficult to investigate in cells that contain redundant mechanisms for cell deformation. Actin dynamics triggered at a liposome membrane provide a control on experimental parameters such as membrane composition, curvature and tension, and allow the specific role of actin dynamics to be addressed. We unambiguously show that the same branched actin network is able to produce both endocytosis-like and dendritic filopodia-like deformations. With a theoretical model, we predict under which conditions the stress exerted on the membrane will lead to inward and/or outward pointing membrane deformations. Combining experiments and theory allows us to decipher how the interplay between membrane tension, actin dynamics, and actin network structure produces inward or outward membrane deformations.

Membrane deformations: tubes and spikes

Liposomes are covered with an activator of the Arp2/3 complex, pVCA, the proline rich domain-verprolin homology-central-acidic sequence from human WASP, which is purified with a streptavidin tag, and that we call hereafter S-pVCA. A branched actin network grows at their surface when placed in a mixture containing monomeric actin, profilin, the Arp2/3 complex and capping protein (CP) ("reference condition", Methods and Fig. 1a). Strikingly, the membrane of liposomes is not smooth, but instead displays a rugged profile: membrane tubes, hereafter called "tubes", radiate from the liposome surface and extend into the actin network (Fig. 1b), even when comet formation has occurred [7, 8] (Supplementary Fig. 1a). The initiation of these tubes is reminiscent of early stage of endocytosis. Interestingly, some liposomes display another type of membrane deformation, characterized by a conical shape, hereafter referred to as "spikes" that points towards the liposome interior (Fig. 1b), and are

reminiscent of dendritic filopodia structures in cells. Some of the liposomes carry both tubes and spikes, while others are "undetermined", as no membrane deformation is visually detectable (Fig. 1b). Spikes have a wide base of a few microns and a length that spans at least half of the liposome diameter. In contrast, tubes are thin, with a diameter under the resolution limit of optical microscopy (< a few 100 nm). When membrane tension is unaffected, 63.0% of liposomes display tubes only, 2.3% spikes only, while 6.1% of liposomes carry a mix of both, and 28.6% are undetermined (Fig. 1c, non-deflated liposomes). To examine how membrane tension affects the occurrence of tubes and spikes, liposomes are deflated by a hyper-osmotic shock (Methods) before actin polymerization is triggered. This treatment leads to a huge increase in the number of liposomes displaying spikes: 65.0% of deflated liposomes display spikes (with or without tubes), compared to 8.4% in non-deflated conditions (Fig. 1c, $p < 0.0001$). Yet, the frequency with which tubes (with or without spikes) are observed is essentially unaffected: 69.1% for non-deflated liposomes compared to 74.8% for deflated liposomes (not significant, $p = 0.24 > 0.05$, Supplementary Fig. 1b). An increase in membrane tension by a hypo-osmotic treatment (Methods) does not change the occurrence of tubes and spikes significantly (Supplementary Fig. 1c).

Membrane tubes and spikes exclusively rely on the presence of the actin network, as they disappear when the network is destructed[7] (Fig. 1, d and e and Methods). A possible effect of membrane pre-curvature induced by pVCA attachment to the membrane is ruled out (Supplementary Information and Supplementary Fig. 2).

Characterization of tubes

To assess where new actin monomers are incorporated during tube growth, we incorporate differently labeled monomers (green) after 20 minutes (Methods). As previously observed for actin networks growing around polystyrene beads [9, 10], new monomers insert at

98 the liposome surface (Fig. 2a). Strikingly, new (green) monomers are also observed within
99 the already grown (red) actin network (Fig. 2a), indicating new actin incorporation on the
100 sides of membrane tubes (tubes are evidenced by phase contrast imaging, Fig. 2a, top), This
101 observation is confirmed by the localization, along tubes and at the liposome surface, of S-
102 pVCA (Fig. 2b), the Arp2/3 complex (Fig. 2c), and free barbed ends (Supplementary Fig. 3).
103 Moreover, the presence of the Arp2/3 complex everywhere in the whole volume of the actin
104 network demonstrates its dentritic nature (Fig. 2c).
105 We find that the average length of the longest tubes increases linearly with network thickness
106 (Fig. 3, a and b). In fact, maximal tube length roughly equals the thickness of the actin
107 network, independently of membrane tension (Fig. 3b, slope 0.89 ± 0.04), albeit deflated
108 liposomes produce a smaller actin cortex. Moreover, we find that tubes grow simultaneously
109 with the actin network (Fig. 3, c and d and Supplementary Fig. 4). Tubes shorter than the
110 network thickness are also present, as evidenced by confocal microscopy (Supplementary
111 Fig. 5a).
112 The origin of the accumulation in membrane fluorescence detected at the tip of some of the
113 longer tubes is unclear. We observe that S-pVCA forms aggregates on membranes and sticks
114 membranes together, even in the absence of actin (Supplementary Fig. 6). It is possible that
115 small vesicles are attached via S-pVCA to the membrane before polymerization starts and are
116 pushed outward by actin growth. However, the presence of different tube lengths
117 (Supplementary Fig. 5) rules out that tubes could be only formed by pre-existing attached
118 vesicles.
119
120 **Characterization of spikes**
121 We find that new actin is incorporated at the tips of the spikes as well as at the sides (Fig. 4a),
122 consistent with the localization of S-pVCA (Fig. 4b). Spikes are filled in with the Arp2/3

123 complex and CP (Fig. 4c and Supplementary Fig. S7), characteristic of a branched network.
124 A clump of actin is observable at the base of the spikes (Fig. 4d). The thickness of the clump
125 bears no clear correlation with the length of the spikes (Supplementary Fig. 8a), but slightly
126 correlates with their width (Supplementary Fig. 8b). Spikes initially elongate with time until
127 polymerization slows down, the basal width of spikes, however, remains roughly constant
128 over time (Fig. 4e and Supplementary Fig. 8c).
129
130 **Effect of network meshsize and membrane tension**
131 Lowering the Arp2/3 complex or CP concentrations, could, in principle, result in loosening
132 the network, but fails to form a cohesive thick enough (> 500 nm), network[11]. Using the
133 property of profilin to inhibit branching and therefore loosen the actin network[12], we obtain a
134 visible, thick, network comparable to reference conditions (Supplementary Fig. 9a and
135 Methods). We find that the occurrence of tubes is reduced in these conditions (74.8% of
136 liposomes display tubes when profilin is in excess compared to 91.4% in reference
137 conditions, Supplementary Fig. 9b, $p < 0.0001$). Strikingly, decreasing membrane tension in
138 loosened network conditions significantly increases the presence of tubes and spikes
139 (Supplementary Fig. 9b, $p < 0.0001$).
140
141 **Theoretical models for spikes and tubes**
142 The appearance of large-scale membrane deformations (spikes) driven by a uniformly
143 polymerizing actin network is rationalized using analytical modeling and numerical Finite
144 Element calculations (Methods). The actin network behaves as a viscoelastic material with an
145 elastic behavior at short time and a viscous behavior at long time due to network
146 rearrangement, the cross-over time being on the order of 1-10 s [13, 14, 15]. We focus on the
147 viscous behavior as the growth of the network occurs on timescales of tens of minutes.

We model the growth of the actin network with a uniform actin polymerization velocity v_g normal to the liposome membrane (motivated by Fig. 4a) and solve the hydrodynamic force balance equation at low Reynolds number (the "Stokes equation") (Methods). Actin polymerization on a flat membrane results in a uniform actin flow which does not generate any mechanical stress. Small perturbations of membrane shape modulate the actin velocity field and generate viscous stress on the membrane. For a periodic deformation (Fig. 5a, left), the actin stress varies as the square of the deformation amplitude (Methods) in agreement with actin growth on a curved surface[13, 16]. For a localized (Gaussian) membrane perturbation $u(x) = Ae^{-(x/b)^2}$ with amplitude A and width b (Fig. 5a, right), we calculate the pressure and velocity fields in the actin layer numerically (Fig. 5b). Velocity gradients in the growing actin layer, generated by the deformed surface, induce a normal pushing force at the center of the perturbation, and pulling forces at the periphery of the perturbation (Fig. 5c), that amount to a zero net force when integrated over the deformation area. This contrasts with existing models of filopodia formation, which usually consider bundled actin filaments exerting a net pushing force on the membrane that do not precisely address the force balance within the actin network[6, 17, 18]. Here, we do not *a priori* distinguish the detailed structure of the actin network at the membrane from the one in the protrusion, treating the actin network as a continuum.

A scaling analysis of the Stokes equation, confirmed by our numerical calculation, leads to a normal stress at the center of the perturbation ($x=0$) that scales as $\sigma_{nn} \sim -\eta A^2 b^{-3} v_g$, where η is the viscosity of the actin layer (Supplementary Fig. 10, a and b). An intuitive understanding of this scaling behavior is given in Supplementary Information.

The normal stress σ_{nn} is balanced by the membrane elastic restoring stress[19] $\sigma_{memb} = -\gamma C + \kappa \partial_s^2 C$, where γ is the membrane tension, κ the bending rigidity, C the membrane curvature ($\sim A/b^2$) and ∂_s the curvilinear derivative ($\sim 1/b$). Considering that b is larger than the

characteristic length $\lambda = \sqrt{\kappa/\gamma}$, the stress is dominated by membrane tension. The balance of actin polymerization and membrane stresses defines a threshold amplitude $A^* = \gamma b/(\eta v_g)$. When the amplitude of the perturbation is smaller than this threshold ($A < A^*$) the membrane stress dominates and the perturbation relaxes. Above the threshold ($A > A^*$) the force exerted by the network is dominant and the instability develops. We now evaluate whether such a perturbation could be reached by thermal fluctuations characterized by the Boltzmann constant k_B and the temperature *T*. The average membrane thermal roughness at length scales larger than the actin mesh size ξ, characterized by the average of the gradient of the membrane shape ∇h, is given by $< |\nabla h|^2 > \sim \frac{k_B T}{4\pi\kappa} \log\left(\left(\frac{2\pi\lambda}{\xi}\right)^2 + 1\right)$ [19]. Identifying $< |\nabla h|^2 >$ with $(A/b)^2$ (provided λ and ξ are on the same order), spikes are predicted below a threshold tension: $\gamma^* \approx \eta v_g \sqrt{k_B T/(4\pi\kappa)}$. Evaluating actin network viscosity η as the product of the elastic modulus (*E*) times the viscoelastic relaxation time (τ_{ve}) : $\eta \approx E\tau_{ve} \approx 10^4\ Pa\ s$ (with $E \approx 10^4\ Pa$ [20] and $\tau_{ve} \approx 1\ s$ [14, 15]), $\kappa \approx 10 k_B T$ and $v_g \approx 10^{-9}\ m/s$ (Fig. 3d, note that this velocity is lower than the polymerization of a single actin filament because the network grows under stress[16]), we find $\gamma^* \approx 10^{-6}\ N/m$. This value is in the range of membrane tension for non-deflated liposomes[21], but is larger than the tension of deflated liposomes, leading to the prediction that deflated liposomes are prone to the formation of spikes, in agreement with our experimental results (Fig. 1c). Spike initiation also depends on the structure of the actin network through the value of the network viscosity η. Using the relationship[22]: $\eta \approx k_b T l_p \tau_{ve}/\xi^4$, with $l_p$the persistence length of the actin filament ($\sim 10\ \mu m$)[23], we find the following condition for spike initiation:

$$\gamma \xi^4 < k_B T l_p v_g \tau_{ve} \sqrt{\frac{k_B T}{2\pi\kappa}} \qquad \text{Eq.1}$$

In contrast to "thin" spike-like protrusions[6], the spikes we consider here are formed by the growth of a branched network with a uniform polymerization along the liposome membrane (Fig. 4). The compressive stress resulting from actin polymerization (shown in Fig. 5b) explains that spikes are much wider than the ones previously observed[6], and that they grow faster than the surrounding actin layer (Supplementary Information and Fig. 4).

The initiation of membrane tubes in reference condition requires a pulling force at the tip of the tube larger than $f_{tube} = 2\pi\sqrt{2\kappa\gamma} \sim 2\ pN$ [24, 25] (Fig. 5d with above estimates). The tube radius ($r_{tube} = \sqrt{\kappa/(2\gamma)} \sim 20\ nm$) is smaller than the size of the actin mesh through which it is pulled. This situation differs from spikes where the flow of the actin network is enslaved to the shape of the membrane, thus generating a wider deformation. In our case, tube pulling requires physical attachment of the actin to the membrane through the activator pVCA[26]. The force exerted by the growth of the actin network (moving away from the liposome surface at a velocity v_g) on the filament bound to the tip of the tube (moving at a velocity $\dot{L}$) is equivalent to a friction force (Supplementary Information), which can be crudely estimated using the Stokes law: : $f_{drag} = 6\ \pi\eta r_{tube}(v_g - \dot{L})$ (Fig. 5e). At steady-state, this force has to balance the tube force f_{tube} (Fig. 5f), giving the tube extraction velocity, $\dot{L} = v_g\left(1 - \frac{f_{tube}}{6\ \pi\eta r_{tube} v_g}\right)$. Tube extraction is possible provided $\dot{L} > 0$. This is indeed the case for liposomes under reference conditions ($\gamma \sim 10^{-6}$ N/m), for which $6\ \pi\eta r_{tube} v_g = 6\ \pi\eta(\frac{f_{tube}}{4\pi\gamma})v_g = \frac{3\eta v_g}{2\gamma} f_{tube} \approx 10\ f_{tube}$ (with above estimates). Note that ($\dot{L} \gtrsim 0.9 v_g$) explaining why tubes initiated early during actin growth actually span the entire actin layer. A ten-fold increase of membrane tension could in principle prevent tube formation. Hypo-tonic treatment does not change the occurrence of tubes (Supplementary Fig. 1c), suggesting that the tension does not

reach a sufficiently high level under these conditions. Using the relationship[22]: $\eta \approx k_B T l_p \tau_{ve}/\xi^4$ the condition for tube extraction is :

$$\gamma \xi^4 < \frac{3}{2} k_B T l_p v_g \tau_{ve} \qquad \text{Eq.2}$$

(Supplementary Fig. 10d). Increasing the actin mesh size indeed significantly reduces the occurrence of membrane tubes (Supplementary Fig. 9). Omitting CP, in principle, also decreases network mesh size, and no membrane tubes have been reported in these conditions[6, 27]. In yeast, actin is absolutely required for endocytosis, likely because of the high turgor pressure that opposes inward membrane deformations [28, 29, 30]. The force needed to overcome the turgor pressure can reach 1000 pN [31], almost three orders of magnitude larger than the actin force in our *in-vitro* conditions. Using yeast relevant parameters for actin dynamics (polymerization velocity $v_p = 50nm/s$ [1] and actin network viscosity $\eta = 10^5\ Pa.s$ as estimated from the same scaling law as above and with a Young's modulus $E \approx 10^4\ Pa$, for an actin network in cell extracts[32] and $\tau_{ve} \approx 10\ s$), the drag force generated by the actin network on a tube of radius *r=10nm* is on the *nN* order. It is thus in principle able to overcome the turgor pressure and to trigger membrane deformation leading to endocytosis (Supplementary Information).

The cell is a robust system where redundant mechanisms ensure proper function, which makes detailed cell mechanisms difficult to decipher. This is true for membrane deformations into filopodia [5] or endocytic intermediates [1]. Here, we show that a branched actin network growing at a membrane is able to mimic the initiation of either an endocytosis-like or a dendritic filopodia-like deformation. Our results support recent findings that the initiation of dendritic filopodia and endocytosis primarily relies on the growth of a branched actin network [1, 3, 5].

242 Endocytosis is intimately dependent on the existence of a physical link between the actin
243 network and the plasma membrane in yeast as well as in mammalian cells under high cell
244 tension. Controlled endocytosis is abolished in yeast if this link is suppressed, although
245 already endocytosed vesicles retain their extraordinary capacity to polymerize actin and even
246 undergo actin-based motility [3, 33]. In our reconstituted system, the membrane-pVCA-network
247 linkage is essential to produce tubes, as the absence of one of these links precludes tubular
248 membrane deformation (Supplementary Information, Supplementary Fig. 2a, and Fig. 5d). In
249 fact, the pVCA region interacts with branched actin networks both through the binding of the
250 Arp2/3 complex[26] and through tethering of actin filament free barbed ends[34]. Note that
251 another form of pVCA was shown to induce clustering and phase-separation of lipids in the
252 absence of CP, but not membrane deformations[26]. Here we show that, through our
253 membrane-pVCA-network linkage, actin dynamics alone have the remarkable capacity to
254 initiate endocytosis-like membrane deformations with a width smaller than, or of the order of,
255 the actin mesh size.
256
257 A class of model for filopodia initiation assumes a particular actin organization in the
258 protrusion, typically that of bundled actin filaments [6, 17, 18, 35, 36]. Supported by our dual color
259 actin measurements and by labeling of the Arp2/3 complex and CP, our model for spike
260 initiation assumes that actin polymerization occurs uniformly at the membrane, which
261 indicates that new actin is incorporated all along the conical membrane surface, and not only
262 at the tip of the protrusion as observed in Liu[6]. Moreover, our characterization reveals that
263 the actin network is branched during the entire growth process. Decreasing membrane tension
264 decreases the critical amplitude for spike nucleation and increases the likelihood of spike
265 formation (Fig. 6) oppositely to thin actin filament protrusions[6], thus revealing the very
266 different nature of these two types of protrusions, both in their initiation, and in their

subsequent growth dynamics. Spikes are mimics of filopodia, especially in the case of dendritic filopodia whose formation relies on the Arp2/3 complex-branched network [37].

Our experimental and theoretical results are summarized in Fig. 6, where the threshold for spikes and tube formation (Eq.1 and Eq.2) are shown together with the explored experimental conditions. We conclude that tubes and spikes co-exist at low tension or low mesh size whereas we predict that they do not form at high tension and high mesh size. At intermediate tension and meshsize, only tubes form, but not spikes. We thus highlight how membrane deformations induced by actin polymerization can be modulated by the interplay between membrane tension and actin network mesh size.

Methods

1. Reagents, lipids, proteins

Chemicals are purchased from Sigma Aldrich (St. Louis, MO, USA) unless specified otherwise. L-alpha-phosphatidylcholine (EPC), 1,2-distearoyl-sn-glycero-3-phosphoethanolamine-N-[biotinyl polyethylene glycol 2000] (biotinylated lipids), 1,2-dioleoyl-sn-glycero-3- [[N(5-amino-1-carboxypentyl)iminodiacetic acid]succiny] nickel salt (DOGS-NTA-Ni) are purchased from Avanti polar lipids (Alabaster, USA). Texas Red® 1,2-dipalmitoyl-sn-glycero-3-phosphocholine, triethylammonium salt is from Thermofisher. Actin is purchased from Cytoskeleton (Denver, USA) and used with no further purification. Fluorescent Alexa Fluor 488 actin conjugate and Alexa Fluor 546 actin conjugate are obtained from Molecular Probes (Eugene, Oregon, USA). Porcine Arp2/3 complex is purchased from Cytoskeleton and used with no further purification. Biotin is purchased from Sigma-Aldrich (St. Louis, Missouri, USA), diluted in DMSO. Mouse $\alpha 1\beta 2$ capping protein is purified as in [38]. Untagged human profilin and S-pVCA (where pVCA is the proline rich

292 domain-verprolin homology-central-acidic sequence from human WASP, starting at amino
293 acid Gln150) are purified as in [8] . S-pVCA is fluorescently labeled on the N-terminal amine
294 with Alexa Fluor 546 at pH 6.5 for 2 h at 4°C, desalted and then purified on a Superdex 200
295 column. His-pVCA-GST (GST-pVCA) is purified as for PRD-VCA-WAVE [39] and His-
296 pVCA is essentially the same without the glutathione sepharose step. Mouse α1β2 capping
297 protein is fluorescently labeled with Alexa Fluor 488 C_5-maleimide (ratio of 1:1
298 protein:label) for 1h at room temperature and then at 4°C overnight under agitation. Porcine
299 Arp2/3 complex is fluorescently labeled with Alexa Fluor 488 C_5-maleimide (ratio of 1:10
300 protein:label) at pH 7.2 for 3h on ice and then purified on a PD Minitrap G-25 column.
301 A solution of 30 μM monomeric actin containing 15% of labeled Alexa Fluor 488 actin
302 conjugate is obtained by incubating the actin solution in G-Buffer (2 mM Tris, 0.2 mM
303 $CaCl_2$, 0.2 mM DTT, 0.2 mM ATP, pH 8.0) overnight at 4°C. All proteins (S-pVCA, profilin,
304 CP, actin) are mixed in the isotonic, hypertonic or hypotonic working buffer. The isotonic
305 working buffer contains 25 mM imidazole, 70 mM sucrose, 1 mM Tris, 50 mM KCl, 2 mM
306 $MgCl_2$, 0.1 mM DTT, 1.6 mM ATP, 0.02 mg/mL β-casein, adjusted to pH 7.4. The
307 hypertonic, isotonic, and hypotonic working buffers differ only by their sucrose concentration
308 (hypertonic:320 mM sucrose; isotonic: 70 mM sucrose; hypotonic: no sucrose). Osmolarities
309 of the hypertonic, isotonic, and hypotonic working buffers are respectively 400, 200, and 95
310 mOsmol, as measured with a Vapor Pressure Osmometer (VAPRO 5600). In case of
311 experiments with DOGS-NTA-Ni lipids, all proteins are diluted in a working buffer
312 containing 280 mM glucose, 10 mM HEPES, 0.5 mM DABCO, 100 mM KCl, 4 mM $MgCl_2$,
313 1 mM DTT, 10 mM ATP and 0.05 mg/mL β-casein.
314 **2. Liposome preparation**
315 Liposomes are prepared using the electroformation technique. Briefly, 10 μl of a mixture of
316 EPC lipids, 0.1% biotinylated lipids or 5% DOGS-NTA-Ni lipids, and 0.1% TexasRed lipids

317 with a concentration of 2.5 mg/ml in chloroform/methanol 5:3 (v/v) are spread onto indium
318 tin oxide (ITO)-coated plates under vacuum for 2 h. A chamber is formed using the ITO
319 plates (their conductive sides facing each other) filled with a sucrose buffer (0.2 M sucrose, 2
320 mM Tris adjusted at pH 7.4) and sealed with hematocrit paste (Vitrex Medical, Denmark).
321 Liposomes are formed by applying an alternate current voltage (10 Hz, 1 V) for 2 h.
322 Liposomes are then incubated with an activator of actin polymerization (S-pVCA, 350 nM)
323 via a streptavidin-biotin link for 15 min. Isotonic liposomes are used right away for
324 polymerizing actin in the isotonic working buffer. To obtain deflated or tense liposomes, an
325 extra step is added: they are diluted twice in the hypertonic (400 mOsmol) or hypotonic (95
326 mOsmol) working buffer respectively and incubated for 30 min. The final solution is
327 therefore at 300 mOsmol or 110 mOsmol respectively.

328 **3. Biotin-blocking experiments**

329 S-pVCA labeled with AlexaFluor546 and biotin are diluted in the isotonic working buffer
330 and incubated for 10 min to reach final concentration of 350 nM S-pVCA and various
331 concentrations of biotin (87.5 nM, 175 nM, 262.5 nM, 350 nM). Note that 350 nM of biotin
332 corresponds to a full saturation of the streptavidin sites of S-pVCA. Unlabeled liposomes
333 (99.9% EPC lipids, 0.1% biotinylated lipids) are then diluted twice in this solution and
334 incubated for 15 min. Tubes and spikes are visualized by the fluorescence of S-pVCA.

335 **4. Actin cortices with a branched network**

336 Our condition of reference ("reference condition") corresponds to condition 1 and non-
337 deflated liposomes.

338 Condition 1: Actin polymerization is triggered by diluting the non-deflated, deflated or tense
339 liposomes 6 times in a mix of respectively isotonic, hypertonic, or hypotonic working buffer
340 containing final concentrations of 3 μM monomeric actin (15% fluorescently labeled with
341 Alexa Fluor 488), 3 μM profilin, 37 nM Arp2/3 complex, 25 nM CP. Note that the final

concentrations of salt and ATP in all conditions (isotonic, hypertonic, hypotonic) are 0.3 mM NaCl, 41 mM KCl, 1.6 mM $MgCl_2$, 0.02 mM $CaCl_2$ and 1.5 mM ATP.

Condition 2: Same protocol as in Condition 1 with unlabeled monomeric actin, unlabeled liposomes (99.9% EPC lipids, 0.1% biotinylated lipids) and S-pVCA labeled with Alexa Fluor 546.

In Figure 1, panel c, non-deflated liposomes n=311 are distributed as follows: 215 from 3 experiments in Condition 1 and 96 from 2 experiments in Condition 2. Deflated liposomes n=123 are distributed as follows: 92 from 2 experiments in Condition 1 and 31 from one experiment in Condition 2.

Condition 3: Same protocol as in Condition 1 with unlabeled monomeric actin and Arp2/3 complex labeled with Alexa Fluor 488 C_5-maleimide.

Condition 4: Same protocol as in Condition 1 with unlabeled monomeric actin and capping proteins labeled with Alexa Fluor 488 C_5-maleimide.

5. Actin cortices with a loosened branched network

Actin polymerization is triggered the same way as above (condition 1), except with 15 μM profilin (instead of 3), and during a longer time (overnight instead of 1-2 hours). Reference conditions correspond to non-deflated liposomes in condition 1, except that observation is done 20 hours after the initiation of polymerization.

6. Photo-damage of the actin network

The actin network area to photo-damage is defined with a diaphragm. The area is illuminated for 15 s with a Hg lamp and a FITC filter cube and the illumination is repeated until actin is completely destroyed or at least no longer detectable by eye.

7. Two color experiment

Liposomes are first incubated with 350 nM S-pVCA for 15 min. This solution is then diluted 3-fold into a mix of isotonic buffer containing 3 μM actin (15% Alexa568-labeled, red), 37

nM Arp2/3 complex and 25 nM CP. After 20 min of incubation in these conditions, the solution is diluted 3 times in a mix of same protein concentrations containing 15% Alexa488-labeled actin, green.

8. Free actin filament barbed end labeling

S-pVCA-activated liposomes (labeled membrane) are placed in a mix containing 3 μM unlabeled monomeric actin, 37 nM unlabeled Arp2/3 complex and 25 nM unlabeled CP. After 20 min of incubation in these conditions, the solution is diluted 5 times in the working buffer to stop actin polymerization. This solution is then incubated with 75 nM labeled capping proteins. Image acquisition is done right after the addition of fluorescently labeled capping proteins.

9. Cryo-electron microscopy

To prepare small liposomes, a mixture of EPC lipids and 0.1% biotinylated lipids with a concentration of 1 mg/mL in chloroform/methanol 5:3 (v/v) is dried and resuspended under vortexing in a buffer containing 25 mM imidazole, 1 mM Tris, 50 mM KCl, 2 mM $MgCl_2$, 0.1 mM DTT, 1.6 mM ATP, 0.02 mg/mL β-casein. Liposomes are then incubated with S-pVCA (350 nM) for 15 min and finally flash-frozen for cryo-electron microscopy. Images were recorded under low dose conditions with a Tecnai G2 Lab6 electron microscope operating at 200 kV with a TVIPS F416 4K camera and with a resolution of 0.21 Å/pixel.

10. Observation of liposomes

Observation in 2D: epifluorescence (GFP filter cube, excitation 470 nm, emission 525 nm; Texas red filter cube: excitation 545-580 nm, emission 610 nm-IR), phase contrast and bright-field microscopy are performed using an IX70 Olympus inverted microscope with a 100x or a 60x oil-immersion objective. Images are collected by a charge coupled device CCD camera (CoolSnap, Photometrics, Roper Scientific).

Observation in 3D: confocal and bright-field microscopy are performed using an inverted Confocal Spinning Disk Roper/Nikon with a 100x or a 60x oil-immersion objective and lasers with wavelengths of 491 nm for actin and 561 nm for lipids. A FITC filter cube (excitation filter: 478-495 nm/emission filter: 510-555 nm) and a TxRed filter cube (excitation filter: 560-580 nm/emission filter: 600-650 nm) are used to acquire respectively actin and lipids fluorescence. Images are collected by a charge coupled device CCD camera (CoolSnap HQ2, Photometrics, Roper Scientific).

3D data: Z-stacks are acquired using the software Metamorph on each wavelength with a z-interval of 0.5 μm.

11. Image analyses of liposomes, tubes and spikes

Image analyses are performed with ImageJ software and data are processed on Matlab. The thickness of the actin network and the length of tube membranes is obtained from fluorescence intensity profiles (Fig. 3a). The first peak of the membrane profile determines the liposome surface and the second peak determines the end of the membrane tube. The actin network thickness is the distance between the first peak and the half width at half maximum of the actin fluorescence profile. The length of the membrane tubes is obtained as the peak-to peak distance of the membrane fluorescence profile. The size of spikes (length, width) and actin network is determined by the corresponding positions of the inflexion points. Fluorescence profiles in each case (membrane, actin) are fitted with a polynomial function. The first maximum and the second minimum of the fit derivative, corresponding to inflexion points of the profile, determine the membrane or actin edges. The size is then the distance between the two edges. From actin fluorescence profile, actin network thickness at the base of spike is defined as the distance between the first maximum and first minimum of the fit derivative.

To determine whether shorter tubes are present in addition to the easily visualized long ones, we measure the total fluorescence intensity of the membrane on an arc that is displaced along a radial axis *r* from close to the liposome surface to the external part of the network. We hypothesize that tubes maintain a constant diameter along their length, as is established for pure membrane tubes [24]. In these conditions, if all tubes have the same length, the total intensity should show a plateau as a function of *r*, until falling off to zero at an *r* where there are no more tubes (Supplementary Fig. 4a). Conversely, the total intensity would decrease as a function of *r* if tubes of different lengths were present (Supplementary Fig. 4a).

12. Statistical analyses

All statistical analyses are performed using MedCalc software. N-1 Chi-squared test is used to determine the statistical significance. Differences among samples were considered statistically significant when $p < 0.05$.

13. Theoretical model for spike initiation

To calculate the stress exerted by a viscous network, polymerizing at a curved surface we consider an incompressible Stokes flow, described by force balance and incompressibility, i.e., $\vec{\nabla} \cdot \vec{\sigma} = 0$ and $\vec{\nabla} \cdot \vec{v} = 0$, where $\vec{v}$ is the velocity of the network and $\vec{\sigma}$ is the viscous stress in Cartesian coordinates, given by, $\sigma_{ij} = -p\,\delta_{ij} + \eta\left(\frac{\partial v_i}{\partial x_j} + \frac{\partial v_j}{\partial x_i}\right)$. Polymerization of the actin network is encoded in this model by imposing the velocity of the network, normal to the surface of the curved interface. Moreover, we impose a stress free boundary condition at the outer layer, both for the normal as well as the tangential stress, i.e., $\sigma_{nn} = 0$ and $\sigma_{nt} = 0$. Note that, in the limit we consider, an infinite thick network, this corresponds to a uniform velocity in the z-direction.

We determine the first order correction of the normal stress on a deformed surface characterized by $u(x) = u_0 \exp(iqx)$ along the *x* axis (u_0 is the deformation amplitude and q the wave vector, Fig. 5a, left). We seek a solution for the velocity field within the network of

the form $v_j = v_j(z)\exp(iqx)$, where the index *j* represents the coordinate *x* or *z*, and a pressure field of the form $p = p(z)\exp(iqx)$. Assuming that the network grows normal to the surface, the first order correction of the *x*-component of the velocity field satisfies the boundary condition $\delta v_x(z = 0) = -v_g \partial_x u(x)$ at the interface (*z=0*). We assume here a network of large thickness and require that the first order correction to the velocity vanishes at $z \to \infty$. The first order corrections to the velocity and pressure in the network read $\delta v_x(z) = -iqu_0(1 - qz)v_g \exp(-qz)$,$\delta v_z(z) = -q^2 u_0 v_g z \exp(-qz)$ and $\delta p(z) = -2\,\eta\, q^2 u_0 v_g \exp(-qz)$. At this order the actin normal stress turns out to vanish at any point of the liposome surface: $\sigma_{nn}(x, z = 0) = 2\eta\partial_z v_z - p = 0$. This implies that the membrane is linearly stable against small deformations in the presence of a growing actin network.

The second-order correction for the actin stress is in principle difficult to calculate, as the different modes of deformation are coupled. An analytical estimate can be obtained by expanding the surface normal vector up to second order, which yields the following scaling for the normal stress at the liposome surface, $\sigma_{nn} \propto -\eta q^3 u_0^2 v_g$. This weakly non-linear analysis reveals that there is a non-zero normal stress acting on the membrane, which we will later compare with the membrane contribution to address system stability.

In order to get a numerical solution for the normal stress in a "localized" spike-like perturbation on the interface, as opposed to the periodic one presented above, we use a Finite Element Method from *Mathematica* with default settings. We implement a geometry as described in Fig. 5a (right), where the lower surface is parametrized with a Gaussian deformation as mentioned before, i.e, $u(x, z) = z - A\,\exp{-\left(\frac{x}{b}\right)^2} = 0$ and we choose the height of the system to be much larger that the extend and amplitude of the perturbation ($h = 2\mu m$). Note that here, *b*, the characteristic lateral length of the localized perturbation, is related to the wavenumber $q{\sim}1/b$ used for the linear analysis. To account for a constant

polymerization, perpendicular to the lower surface we impose the velocity on the lower surface, i.e., $\partial v(u(x,z)=0) = v_g(\partial_x u(x,z)\hat{x} + \partial_z u(x,z)\hat{z})$, where v_g is the normalized polymerization velocity and a vanishing normal and tangential stress at the upper boundary $z = h$, i.e., $\sigma_{nn}(z=h) = 0$ and $\sigma_{nt}(z=h) = 0$. Using this approach we could find the same scaling with amplitude and width of the perturbation, as found for the weakly non-linear analysis for a sinusoidal perturbation. Note also that here, by imposing the normal velocity at the interface, a choice that is motivated by the dual color images in Fig. 4a, we do not impose the tangential stress on the membrane, and hence this stress has to be balanced by an in-plane viscous stress in the membrane, which at this stage we do not model. These FEM simulations allow us to visualize the velocity field as well as the pressure throughout the network, indicating the increase in pressure inside the local perturbation caused by the local convergence of the velocity fields (Fig. 5b).

Data availability

The data that support the plots within this paper and other findings of this study are available from the corresponding author upon request.

References

1. Kukulski W, Schorb M, Kaksonen M, Briggs JA. Plasma membrane reshaping during endocytosis is revealed by time-resolved electron tomography. *Cell*, **150**(3)**:** 508-520 (2012).

2. Picco A, Mund M, Ries J, Nedelec F, Kaksonen M. Visualizing the functional architecture of the endocytic machinery. *Elife*, **4:** (2015).

3. Picco A, Kukulski W, Manenschijn HE, Specht T, Briggs JAG, Kaksonen M. The contributions of the actin machinery to endocytic membrane bending and vesicle formation. *Molecular Biology of the Cell*, **29**(11)**:** 1346-1358 (2018).

4. Boulant S, Kural C, Zeeh JC, Ubelmann F, Kirchhausen T. Actin dynamics counteract membrane tension during clathrin-mediated endocytosis. *Nat Cell Biol*, **13**(9)**:** 1124-1131 (2011).

5. Korobova F, Svitkina T. Molecular architecture of synaptic actin cytoskeleton in hippocampal neurons reveals a mechanism of dendritic spine morphogenesis. *Mol Biol Cell*, **21**(1)**:** 165-176 (2010).

6. Liu AP, Richmond DL, Maibaum L, Pronk S, Geissler PL, Fletcher DA. Membrane induced bundling of actin filaments. *Nature Physics*, **4:** 789-793 (2008).

7. van der Gucht J, Paluch E, Plastino J, Sykes C. Stress release drives symmetry breaking for actin-based movement. *Proc Natl Acad Sci U S A*, **102**(22)**:** 7847-7852 (2005).

8. Carvalho K, Lemiere J, Faqir F, Manzi J, Blanchoin L, Plastino J*, et al.* Actin polymerization or myosin contraction: two ways to build up cortical tension for symmetry breaking. *Philos Trans R Soc Lond B Biol Sci*, **368**(1629)**:** 20130005 (2013).

9. Paluch E, Piel M, Prost J, Bornens M, Sykes C. Cortical actomyosin breakage triggers shape oscillations in cells and cell fragments. *Biophys J*, **89**(1)**:** 724-733 (2005).

10. Akin O, Mullins RD. Capping protein increases the rate of actin-based motility by promoting filament nucleation by the Arp2/3 complex. *Cell*, **133**(5)**:** 841-851 (2008).

11. Kawska A, Carvalho K, Manzi J, Boujemaa-Paterski R, Blanchoin L, Martiel JL*, et al.* How actin network dynamics control the onset of actin-based motility. *Proc Natl Acad Sci U S A*, **109**(36)**:** 14440-14445 (2012).

12. J P, S S, A J, B G, MF C. - Profilin Interaction with Actin Filament Barbed End Controls Dynamic Instability. *Dev Cell*, **36**(2)**:** 201-214 (2016).

13. Julicher F, Kruse K, Prost J, Joanny JF. Active behavior of the cytoskeleton. *Physics reports*, **449**(1-3)**:** 3-28 (2007).

14. Gardel ML, Shin JH, MacKintosh FC, Mahadevan L, Matsudaira PA, Weitz DA. Scaling of F-actin network rheology to probe single filament elasticity and dynamics. *Phys Rev Lett*, **93**(18)**:** 188102 (2004).

15. Gardel ML, Kasza KE, Brangwynne CP, Liu J, Weitz DA. Chapter 19: Mechanical response of cytoskeletal networks. *Methods Cell Biol*, **89:** 487-519 (2008).

16. Noireaux V, Golsteyn RM, Friederich E, Prost J, Antony C, Louvard D*, et al.* Growing an actin gel on spherical surfaces. *Biophys J*, **78:** 1643-1654 (2000).

17. Mogilner A, Rubinstein B. The physics of filopodial protrusion. *Biophys J*, **89**(2)**:** 782-795 (2005).

18. Prost J, Barbetta C, Joanny JF. Dynamical control of the shape and size of stereocilia and microvilli. *Biophys J*, **93**(4)**:** 1124-1133 (2007).

19. Deserno M. Fluid lipid membranes: from differential geometry to curvature stresses. *Chem Phys Lipids*, **185:** 11-45 (2015).

20. Marcy Y, Prost J, Carlier M-F, Sykes C. Forces generated during actin-based propulsion: a direct measurement by micromanipulation. *Proc Natl Acad Sci USA*, **101**(16)**:** 5993-5997 (2004).

21. Caorsi V, Lemiere J, Campillo C, Bussonnier M, Manzi J, Betz T*, et al.* Cell-sized liposome doublets reveal active tension build-up driven by acto-myosin dynamics. *Soft Matter*, **12**(29)**:** 6223-6231 (2016).

22. Kroy K, Frey E. Force-Extension Relation and Plateau Modulus for Wormlike Chains. *Phys Rev Lett*, **77**(2)**:** 306-309 (1996).

23. Isambert H, Venier P, Maggs AC, Fattoum A, Kassab R, Pantaloni D*, et al.* Flexibility of actin filaments derived from thermal fluctuations. *J Biol Chem*, **270:** 11437-11444 (1995).

24. Derenyi I, Julicher F, Prost J. Formation and interaction of membrane tubes. *Phys Rev Lett*, **88**(23)**:** 238101 (2002).

25. Roux A, Cuvelier D, Nassoy P, Prost J, Bassereau P, Goud B. Role of curvature and phase transition in lipid sorting and fission of membrane tubules. *Embo J*, **24**(8)**:** 1537-1545 (2005).

26. Smith BA, Padrick SB, Doolittle LK, Daugherty-Clarke K, Correa IR, Jr., Xu MQ*, et al.* Three-color single molecule imaging shows WASP detachment from Arp2/3 complex triggers actin filament branch formation. *Elife*, **2:** e01008 (2013).

27. Liu AP, Fletcher DA. Actin polymerization serves as a membrane domain switch in model lipid bilayers. *Biophys J*, **91**(11)**:** 4064-4070 (2006).

28. Wang X, Carlsson AE. A master equation approach to actin polymerization applied to endocytosis in yeast. *PLoS Comput Biol*, **13**(12)**:** e1005901 (2017).

29. Carlsson AE. Membrane bending by actin polymerization. *Curr Opin Cell Biol*, **50:** 1-7 (2017).

30. Aghamohammadzadeh S, Ayscough KR. Differential requirements for actin during yeast and mammalian endocytosis. *Nat Cell Biol*, **11**(8)**:** 1039-1042 (2009).

31. Dmitrieff S, Nedelec F. Membrane Mechanics of Endocytosis in Cells with Turgor. *PLoS Comput Biol*, **11**(10)**:** e1004538 (2015).

32. Gerbal F, Chaikin P, Rabin Y, Prost J. An Elastic Analysis of *Listeria monocytogenes* Propulsion. *Biophys J*, **79:** 2259 (2000).

33. Sun Y, Leong NT, Jiang T, Tangara A, Darzacq X, Drubin DG. Switch-like Arp2/3 activation upon WASP and WIP recruitment to an apparent threshold level by multivalent linker proteins in vivo. *Elife*, **6:** (2017).

34. Co C, Wong D, Gierke S, Chang V, Taunton J. - Mechanism of actin network attachment to moving membranes: barbed end capture by. *Cell*, **128**(5)**:** 901-913 (2007).

35. Lan Y, Papoian GA. The stochastic dynamics of filopodial growth. *Biophys J*, **94**(10)**:** 3839-3852 (2008).

36. Atilgan E, Wirtz D, Sun SX. Mechanics and dynamics of actin-driven thin membrane protrusions. *Biophys J*, **90**(1)**:** 65-76 (2006).

37. Hotulainen P, Llano O, Smirnov S, Tanhuanpää K, Faix J, Rivera C*, et al.* Defining mechanisms of actin polymerization and depolymerization during dendritic spine morphogenesis. *The Journal of Cell Biology*, **185**(2)**:** 323 (2009).

38. Palmgren S, Ojala PJ, Wear MA, Cooper JA, Lappalainen P. Interactions with PIP2, ADP-actin monomers, and capping protein regulate the activity and localization of yeast twinfilin. *J Cell Biol*, **155**(2)**:** 251-260 (2001).

39. Havrylenko S, Noguera P, Abou-Ghali M, Manzi J, Faqir F, Lamora A*, et al.* WAVE binds Ena/VASP for enhanced Arp2/3 complex–based actin assembly. *Molecular Biology of the Cell*, **26**(1)**:** 55-65 (2015).

Acknowledgments

We acknowledge Dr. Agnieszka Kawska at IlluScientia.com for the Fig.s. We thank Julien Pernier for suggesting the excess profiling experiment for loosening the actin network. This work was supported by the French Agence Nationale pour la Recherche (ANR), grant ANR 09BLAN0283 and ANR 12BSV5001401, by Fondation pour la Recherche Médicale (FRM), grant DEQ20120323737, by the LabEx CelTisPhyBio postdoctoral fellowship (ML), No. ANR-10-LBX-0038 part of the IDEX PSL NANR- 10-IDEX-0001-02 PSL, by Marie Curie Integration Grant PCIG12-GA-2012-334053, “Investissements d'Avenir” LabEx PALM (ANR-10-LABX-0039-PALM), ANR grant ANR-15-CE13-0004-03 and ERC Starting Grant 677532. Our groups belong to the CNRS consortium CellTiss. This work was supported by grants from the French National Research Agency through the “Investments for the Future” (France-BioImaging, ANR-10-INSB-04), the PICT-IBiSA Institut Curie (Paris, France)

Author contributions: CS, RK and VC have equal contributions. CS, VC performed experiments, analyzed data. RK performed the development of theoretical models. AA and MAG, JM, AdC, DL, CC, JP contributed to experimental data, ML and JFJ contributed to the development of the model, PS and CS designed the research. All authors contributed to write the paper.

Author information: request for material should be addressed to PS and CS (pierre.sens@curie.fr and cecile.sykes@curie.fr)

Figures

Figure 1: Experimental system and observations

a, Scheme of the experimental system; proteins not to scale. **b**, Membrane deformations in both non-deflated (three first rows) and deflated conditions (last row). **c**, Top: liposome deflation. Bottom: number of liposomes displaying different indicated behaviors. Non-deflated liposomes, n=311. Deflated liposomes, n=123. (**d**, **e**) Actin network photo-damage (yellow dashed rectangle) on a liposome displaying membrane tubes (**d**) or spikes (**e**). Phase contrast and epifluorescence microscopy of membrane (TexasRed-DHPE, red) and actin network (Actin-Alexa Fluor 488, green). Scale bars, 5µm.

Figure 2: Actin incorporation during tube formation

a, Left: a red actin network is grown for 20 minutes, then an excess of green actin is added, so green regions indicate newly polymerized actin. Right: corresponding polar plots. **b**,Activator of actin polymerization, S-pVCA. False color image and zoom in (white rectangle); the membrane is indicated with a dashed line. (**a**, **b**) Phase contrast and epifluorescence microscopy of the actin network labeled with actin-Alexa Fluor 568 (red) and actin-Alexa Fluor 488 (green) in (**a**), and of S-pVCA-Alexa Fluor 546 in (**b**). **c**, Confocal images of labeled membrane (TexasRed-DHPE, red) and the Arp2/3 complex (Alexa Fluor 488 C_5-maleimide, green) and zoom in (white rectangle). All scale bars, 5µm.

Figure 3: Tube length compared to network thickness

a, Tube length and actin network thickness are measured from fluorescence intensity profiles (yellow dashed box) of the membrane (TexasRed-DHPE, red) and the actin (Alexa Fluor 488, green) channels (Materials and Methods). **b**, Tube length as a function of actin network thickness. White circles: non-deflated liposomes. Grey circles: deflated liposomes. **c**,

667 Dynamics of tube growth (times indicate elapsed time from the start of actin polymerization).
668 **d**, Fluorescence profile of the thick yellow lines shown in (**c**). Membrane and actin
669 fluorescence intensities plotted over time (indicated). Other examples are shown in
670 Supplementary Fig. 4. (**a**, **d**) Epifluorescence microscopy of membrane (TexasRed-DHPE,
671 red) and actin (Alexa Fluor 488, green). All scale bars, 5μm.
672
673 **Figure 4: Actin incorporation in spikes**
674 **a**, Left: Two color experiment: green regions indicate newly polymerized actin. White
675 squares, zooms. Right: fluorescence intensity profiles of spike length (top, thin yellow dashed
676 box on zoomed image) and width (bottom, thick yellow dashed box on zoomed image). **b**,
677 Activator of actin polymerization, S-pVCA. False color and zoom in (white rectangle). (**a**, **b**)
678 Phase contrast and epifluorescence microscopy of the actin network labeled with actin-Alexa
679 Fluor 568 (red) and actin-Alexa Fluor 488 (green) in (**a**), and of S-pVCA-Alexa Fluor 546 in
680 (**b**). **c**, Confocal images of labeled membrane (TexasRed-DHPE, red) and the Arp2/3
681 complex (Alexa Fluor 488 C_5-maleimide, green) and zoom in (white rectangle). **d**,
682 Epifluorescence images of membrane (TexasRed-DHPE, red) and actin (Alexa Fluor 488,
683 green) during spike growth, as a function of time (time indicated after actin polymerization
684 starts). **e**, Spike length and width over time, spike shown in **d**. Other examples in
685 Supplementary Fig. 8. Dashed lines are guides to the eyes. All scale bars, 5 μm.
686
687 **Figure 5: Model for spike initiation and tube formation**
688 **a**, Scheme of the initiation of a periodic and localized membrane deformation by the growth
689 of the actin network. **b**, Velocity field of a viscous network polymerizing over a membrane
690 with a localized (gaussian) perturbation (amplitude $A=0.1\ \mu m$, width $b=0.2\ \mu m$,
691 polymerization velocity $v_g=1\ nm/s$, viscosity $\eta = 10^4\ Pa.s$). Color, pressure in the network
692 layer. **c**, Corresponding distribution of actin and membrane normal stresses (σ_{nn} and σ_{memb}

693 respectively). **d**, Scheme of a membrane tube pulled by the actin network; blue arrows
694 indicate forces within the actin network. **e**, Velocity field of the actin network pulling the
695 membrane tube. We assume a uniform polymerization v_p at the liposome surface and model
696 the presence of the tube as a disc with radius $r_{tube} = 20\ nm$ at a distance from the membrane
697 $h = 100\ nm$. **f**, Force exerted per filament as a function of the distance to the center of the
698 tube, $\bar{r}$, where we have chosen distance between filaments polymerizing on the surface ξ =
699 *30nm*, f_{tube}*= 2pN,* $\gamma = 10^{-6}$ *N/m* and $\nu = 0.4$.
700
701 **Figure 6: Dependence of membrane deformations on membrane tension and actin**
702 **network mesh size.**
703 Representative images of membrane (TexasRed-DHPE) and actin (Alexa Fluor 488) and
704 schematic diagram of membrane deformations as a function of mesh size ξ and membrane
705 tension γ, derived from the theoretical model (Eqs.1 and 2). R corresponds to reference
706 conditions (dense network, non-deflated liposomes, red dot in diagram); a, b, c and d
707 correspond to other experimental conditions with a different mesh size and membrane tension
708 indicated qualitatively in the diagram. Arrows show in which direction membrane tension or
709 mesh size are changed compared to the reference situation (R). Plain arrows indicate a
710 change in membrane tension without affecting the polymerization conditions. Dashed arrows
711 indicate that the conditions of actin polymerization are changed compared to the reference
712 condition. Scale bars, 5 μm.

Figure 1

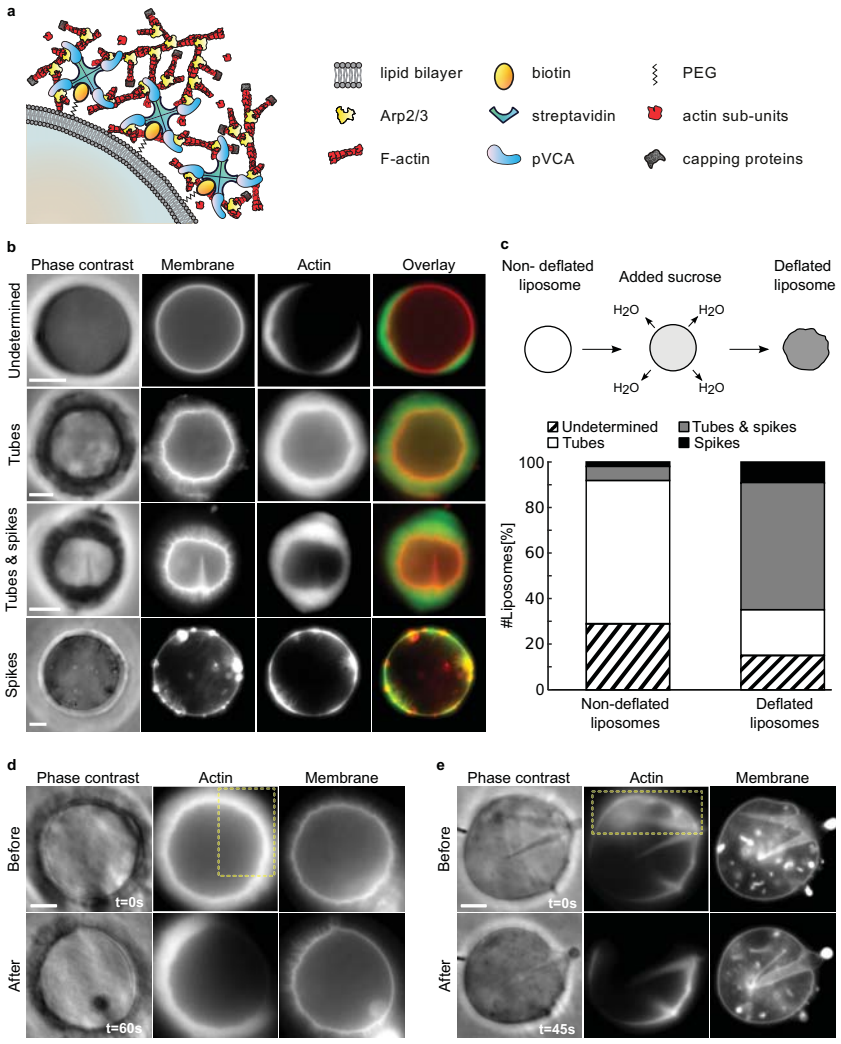
a
lipid bilayer
biotin
PEG
Arp2/3
streptavidin
actin sub-units
F-actin
pVCA
capping proteins
b
Phase contrast
Membrane
Actin
Overlay
Undetermined
Tubes
Tubes & spikes
Spikes
c
Non- deflated liposome
Added sucrose
Deflated liposome
H2O
Undetermined
Tubes
Tubes & spikes
Spikes
#Liposomes[%]
100
80
60
40
20
0
Non-deflated liposomes
Deflated liposomes
d
Phase contrast
Actin
Membrane
Before
After
t=0s
t=60s
e
Phase contrast
Actin
Membrane
Before
After
t=0s
t=45s

Figure 2

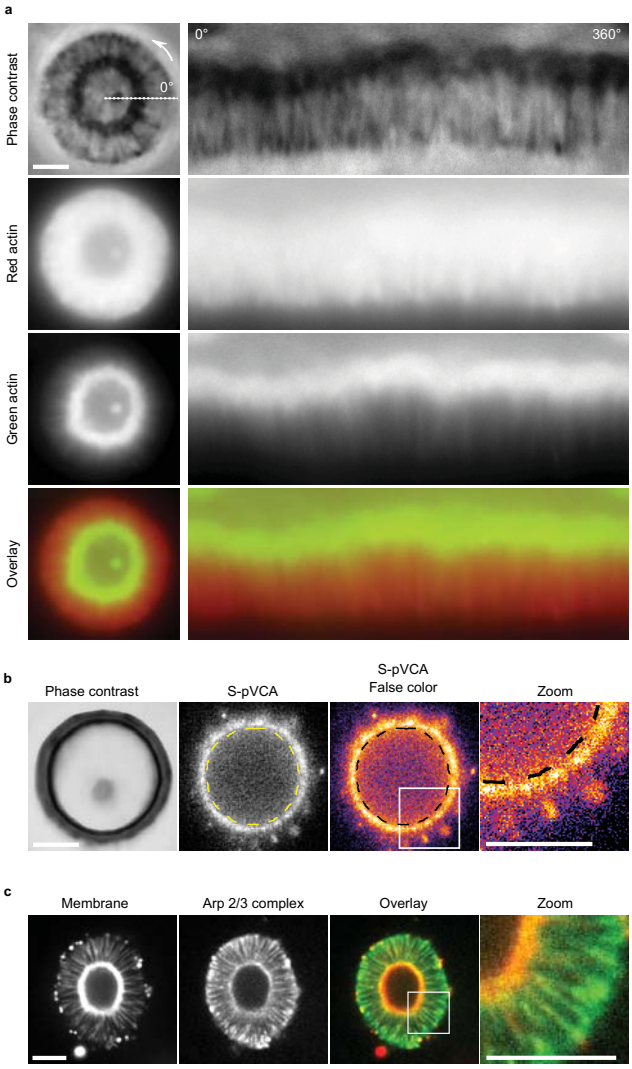
a
Phase contrast
Red actin
Green actin
Overlay
0°
360°
b
Phase contrast
S-pVCA
S-pVCA
False color
Zoom
c
Membrane
Arp 2/3 complex
Overlay
Zoom

Figure 3

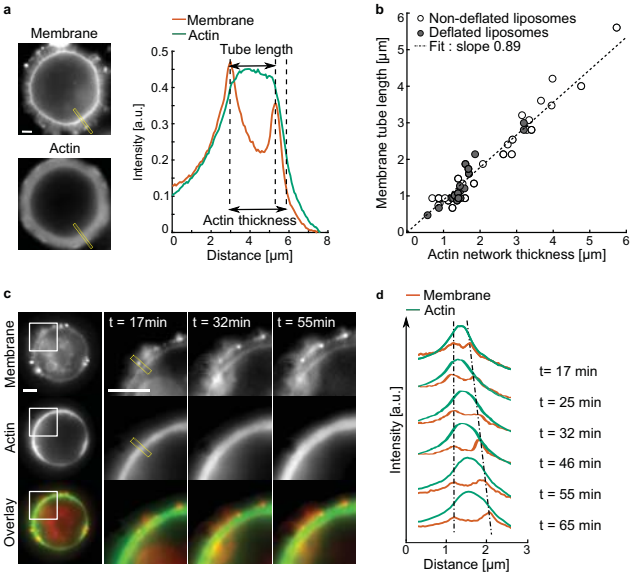
a
Membrane
Actin
Membrane
Actin
Tube length
Actin thickness
Intensity [a.u.]
Distance [µm]
b
Non-deflated liposomes
Deflated liposomes
Fit : slope 0.89
Membrane tube length [µm]
Actin network thickness [µm]
c
Membrane
Actin
Overlay
t = 17min
t = 32min
t = 55min
d
Membrane
Actin
Intensity [a.u.]
Distance [µm]
t= 17 min
t = 25 min
t = 32 min
t = 46 min
t = 55 min
t = 65 min

Figure 4

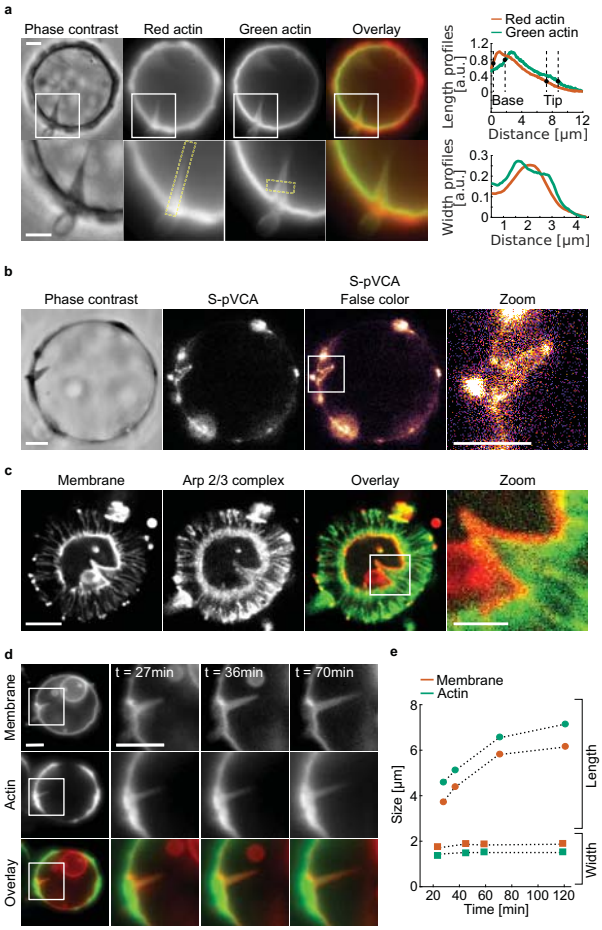
a
Phase contrast
Red actin
Green actin
Overlay
Red actin
Green actin
Length profiles [a.u.]
Base
Tip
Distance [µm]
Width profiles [a.u.]
Distance [µm]
b
Phase contrast
S-pVCA
S-pVCA
False color
Zoom
c
Membrane
Arp 2/3 complex
Overlay
Zoom
d
Membrane
Actin
Overlay
t = 27min
t = 36min
t = 70min
e
Membrane
Actin
Size [µm]
Length
Width
Time [min]

Figure 5

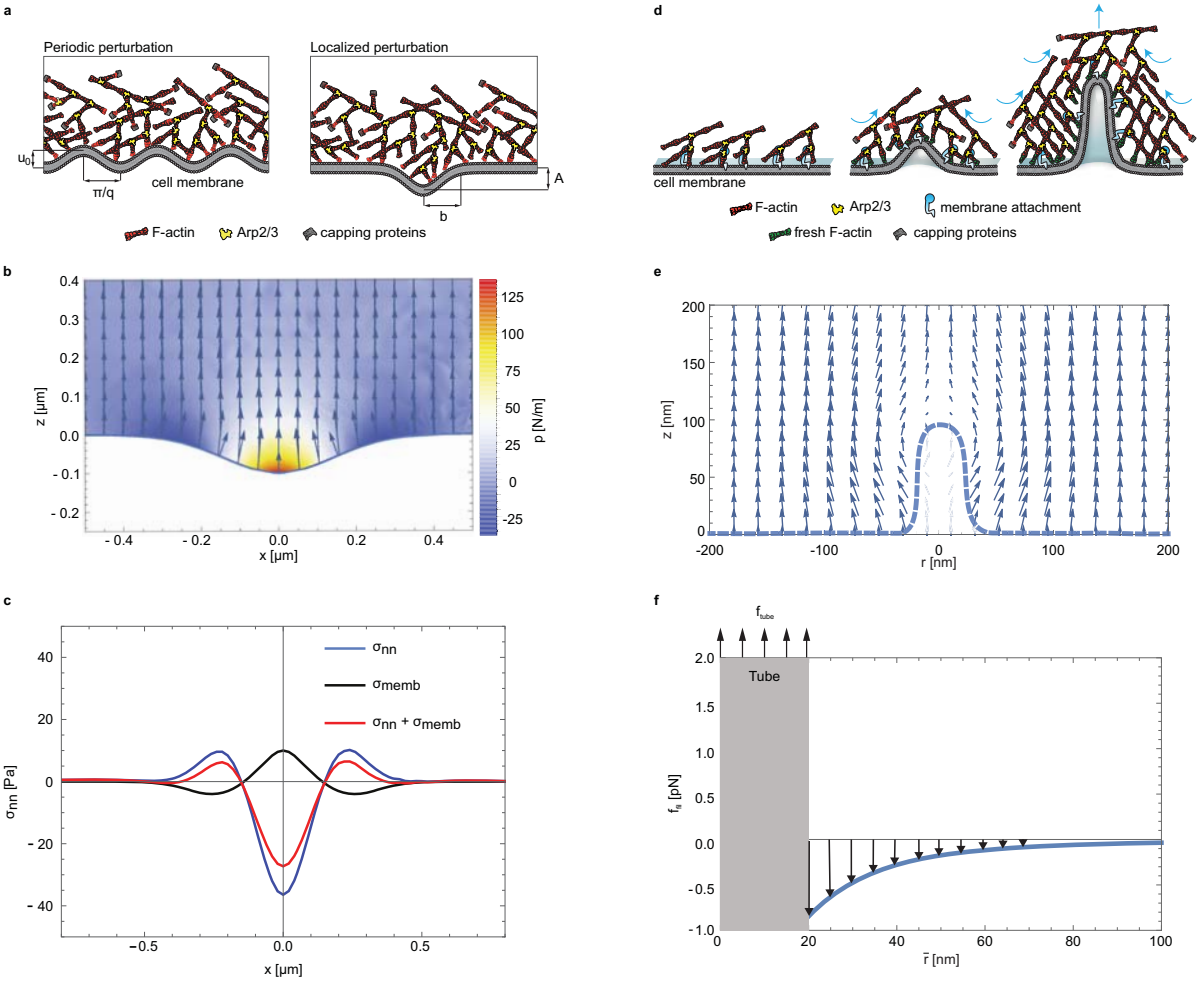
a
Periodic perturbation
Localized perturbation
u0
π/q
cell membrane
A
b
F-actin
Arp2/3
capping proteins
b
z [μm]
x [μm]
p [N/m]
c
σnn [Pa]
x [μm]
σnn
σmemb
σnn + σmemb
d
cell membrane
F-actin
Arp2/3
membrane attachment
fresh F-actin
capping proteins
e
z [nm]
r [nm]
f
f_tube
Tube
f_n [pN]
r̄ [nm]

Figure 6

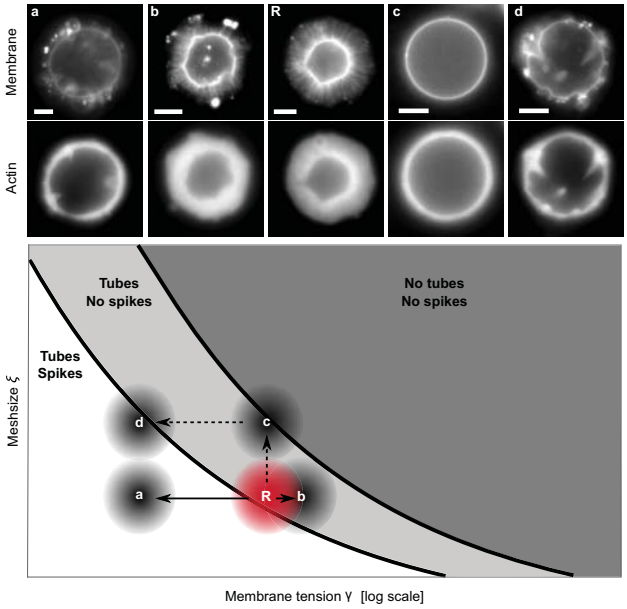
a
b
R
c
d
Membrane
Actin
Tubes
No spikes
No tubes
No spikes
Tubes
Spikes
Meshsize ξ
d
c
a
R
b
Membrane tension γ [log scale]